STRUCTURE BOUND WATER IN NATURAL AND SYNTHETIC QUARTZ, ITS POTENTIAL IMPORTANCE IN NATURAL ROCK DEFORMATION.

BY

Mervyn Edward Jones B.Sc., F.G.S.

March 1978.

A thesis submitted for the degree of Doctor of Philosophy of the University of London and for the Diploma of Imperial College.

Department of Geology,
Imperial College,
London, S.W.7.

STRUCTURE BOUND WATER IN NATURAL AND SYNTHETIC QUARTZ, ITS POTENTIAL IMPORTANCE TO NATURAL ROCK DEFORMATION.

Mervyn Edward Jones.

Abstract.

The method of determining water concentrations in quartz crystals using Infrared Spectroscopy was examined and a satis--factory analytical technique developed to study the concentra--ions and distribution of water in a range of crystals. These analyses showed that most quartz in natural environments contains large concentrations of water, but this is present in fluid inclu--sions and does not weaken the crystal. This was substantiated using a solid confining pressure medium deformation machine con--structed as part of this project. Had this water been dissolved in the structure of the grains, then this quartz might have demon--strated mechanical properties in experiments similar to those inferred for natural quartz deformation.

The growth of fluid inclusions in synthetic quartz by heat treatment at 1atmos. and 10Kbar. confining pressures was studied and a mechanism is suggested in which the inclusions nucleate on the strain fields associated with the grains'microstructure.

Use of the heating stage in the transmission electron micro--scope was developed and experiments using synthetic quartz foils have revealed that this material contains a finely dispersed, as yet unidentified, impurity phase, the density and size of the particles of which are temperature sensitive. These particles act as dislocation sources. Following this, the suggestion is made that the mechanical properties of synthetic quartz be reinterpreted in terms of the theories of precipitation hardening rather than just structural water.

The main conclusions are:-

1). Structural water concentrations are temperature and time depend--ent, so that natural quartz will get stronger with age as it turns milky.

2). Most reported deformation experiments on synthetic quartz were conducted under disequilibrium conditions.

3). The mechanical properties of synthetic quartz may be influenced far more strongly by the solid impurity phase than by structural water.

Acknowledgements.

Firstly I must give my sincere thanks to my supervisor Dr. Ernest Rutter for his continuous support, assistance and encour--agement throughout the duration of this study, and to Dr. Neville Price who first persauded me to enter the field of experimental geology. Next I must thank Dr. Stan White for his generous advice and assistance in the electron microscopy part of this project and for the many long and profitable discussions that we had on the physical and chemical properties of quartz.

For technical assistance I am indebted to Robert Holloway and Ian Morton who were responsible for constructing and maintain--ing the apparatus used in this project as well as assist--ing greatly in the design of much of it and who did an excellent job.

I must also express my gratitude to Dr. J.A.Kitchener in the Mineral Technology Department at Imperial College who gave me unlimited access to his Infrared Spectrometer throughout the period of this study. I also thank the Metallurgy Department at Imperial College who made available time on the Electron Micro--scopes, together with instruction in their use and the necessary technical backup.

Next I must thank all of my colleagues who gave freely of their time in discussions pertinent to this work and who provided some of the specimens analyzed. In particular I thank Rob Kerrich, Rob Knipe, Steve Soldin, Nick Shaw and Ken McClay. I also thank Dr. Angus Skinner who provided encouragement during the writing stage of this project and who read through the final draft of this thesis.

The Natural Environment Research Council financed this research and provided me with a research studentship for my personal maint--enance for which I am duly grateful.

Finally I must thank my wife Jane who encouraged me and provided great moral support throughout the period of this project and who assisted me greatly during the preparation of the final draft of this thesis.

* * * * * * *

CONTENTS.

Contents. Page No.

Contents. Page No.

Contents.

LIST OF FIGURES.

LIST OF PLATES.

LIST OF TABLES.

Chapter One.

INTRODUCTION.

Chapter 1. INTRODUCTION.

1.1. Outline of the Project.

1.2. Structure of the Thesis.

1.3. Published papers and Articles Read at Conferences.

1.1. OUTLINE OF THE PROJECT.

The major aim of this research project was to establish the necessary link between laboratory deformation experiments, showing water weakening of synthetic quartz, and the deformation of quartz in nature. Unfortunately it became apparent as the project progressed that the phenomenon of water weakening of synthetic quartz is far more complex than the ideas presented in the published mechanical studies (see chapter 2 for references to these). A considerable amount of time was therefore devoted to studying these complexities. Because of this my early results, which indicated that much of the quartz found in the natural deformation environments would be water weakened, were not substantiated by mechanical testing. Such quartz always showed strengths in excess of those predicted from its total hydroxyl concentration (according to the model used by Griggs in 1974). This is presumably because much of the water present in these natural crystals is found in molecular form in bubbles, and not as hydroxyl groups bound to the silica tetrahedra. However, the microstructural study of undeformed synthetic quartz revealed a second phase which certainly will exert some influence on the mechanical properties of the material. The composition of this second phase has not yet been identified. Some of the observed differences in the mechanical properties of synthetic and natural quartz may then also be related to the presence of this impurity in the former, but not in the latter.

Within the confines of this study, briefly outlined above, considerable time was devoted to studying the growth of micro-fluid inclusions within the synthetic quartz structure. These are formed through the coalescence of molecules of precipitated water released from the quartz structure at elevated temperatures. The inclusions grown in this way were compared to those responsible for the opal--escence of natural vein quartz, and a similar 'solid state' origin is suggested for both, although the actual mechanisms of growth may differ in detail. These studies,combined with detailed infared spectroscopic work, suggest that quartz may be divided into three broad classes for the purpose of deformation studies. These classes are;

1). Synthetic Quartz.

2). Brazilian (Piezioelectric Grade) and Smokey Quartz.

3). Natural Opalescent Quartz, Natural Quartz (showing areas or patches of mistyness or opalescence), Some Clear Natural Quartz, Amethyst and Citrinous Quartz.

Of these three groups, most of the quartz found deformed in nature falls into group 3, whilst nearly all of the quartz studied in def--ormation experiments is from groups 1 and 2.

* * * *

Ouring the first year of this work I attended a series of lectures and practical classes in Fortran Programming and attended many of the lectures given on the M.Sc.Structural Geology Course, which proved to be very useful during this research.

1.1.1. Experimental Techniques Used During This Project.

Infrared spectroscopy was widely used in this study, for routine analysis, to study variations of the hydroxyl ion concen-tration within single crystals and to quantify the dehydration/precipitation (of water) experiments. Most of the first two years were devoted to developing the technique and to doing this routine analytical work together with the laboratory heating experiments. All the spectroscopic work,conducted during this study, was per-formed on specimens at room temperature. If cryogenic temperatures had been employed it would have been possible to resolve the absorption bands caused by the different hydroxyl bond oscillations, and this would have made it possible to (for example) separate the absorption due to structural water from that caused by molecular water. The cryogenic technique is much slower than the normal rout-ine method and requires a spectrometer of very high frequency resolution. The instrument used in this study was unlikely to satisfy this requirement and as the primary aim was to analyse as many natural quartz crystals as possible cryogenic specimen temp-eratures were not used.

The second important technique used in this study was trans-mission electron microscopy. It proved impossible to start this until the second year when I attended a course organised by the Imperial College metallurgy department, and followed this with solo practice using foils prepared from metal specimens on the 100 K.e.V. E.M.6. instrument in the metallurgy department. Unfortun-ately, obtaining time on the ion beam thinning machine to prepare quartz specimens for this work was initially difficult and it was not until the third year of this study that I started doing the essential electron microscope work. Towards the end of the third year, the use of the 1000 K.e.V. microscope together with a heating stage started to provide some crucial new information on the micro-

-structure of synthetic quartz as well as a new technique for the experimental geologist, this, because of the late start, will have to be the topic of some later project.

It is the combination of the two methods of study, mentioned above, which has led to most of the results presented in this thesis (with the exception of the mechanical data). The number of mechanical deformation tests conducted was restricted for reasons given below, but fortunately many mechanical studies of quartz are reported in the literature and I found that in many instances it was possible to combine this published experimental data with my own, thus aiding greatly the interpretation of my results.

The majority of the reported experimental results come from experiments conducted on Griggs Type solid confining pressure medium deformation machines. One of the original aims of this project was to use a gas pressure medium deformation machine to repeat at much greater accuracy some of these deformation tests. Unfortunately no gas pressure machine existed at Imperial College and plans to build one were subjected to considerable delay. The existing deform--ation machines were completely unsuitable for work on the plastic deformation of quartz. As an interim measure plans were drawn up for a solid medium testing machine which was to be an improvement on the original Griggs design. The construction of this apparatus was also subject to great delay necessitating the abandonment of some of the original experimental aims of the project. A few tests were conducted on this machine but it has never been brought into full operation and at the time of writing still has teething troubles. To some extent the unsuitable Heard style deformation machines served to alleviate the paucity of mechanical test results but they could only be used with the weakest synthetic crystals.

1.2. STRUCTURE OF THIS THESIS.

Instead of a formal introduction I have prepared a general literature survey in chapter 2 which I hope will serve to introduce the reader to the problems associated with water in the quartz structure and to ideas on the water weakening of quartz as they existed at the time of writing. This is followed in chapter 3 by a detailed discussion of the infrared techniques used, and their limitations, something sadly lacking in most published mechanical studies. In chapter 4 the results of the infrared analyses are presented and discussed, and it is shown that much natural quartz has strengths greater than those predicted by the results of the Griggs (1974) deformation experiments and theoretical analysis. Chapter 5 discusses the dehydration of the quartz structure and the growth of micro fluid inclusions and this leads directly into the microstructural data presented in chapter 6. The results of the various directions of this study are then brought together in a general synthesis in chapter 7 under the title "Discussion, Conclusions and Speculations", which also gives suggestions for further study. Details of the computer programs written during this work, sample preparation techniques used and a description of the solid medium deformation machine are given in the appendices.

The first page of each chapter is given over to a detailed breakdown of its contents. I hope this will make the particular aims of each chapter immediately apparent, and make it easier for the reader to go directly to the sections of interest without having to read through large parts of this work which may be of little or no interest to them.

1.3. PUBLISHED ARTICLES AND PAPERS READ AT CONFERENCES.

During the course of this research I have published one

short article entitled "Water Weakening of Quartz and its Application to Natural Rock Deformation" (J.Geol.Soc.Lond.,Vol.131,pp.429-432, July 1975) and have had the discussion that I gave following Dr. Mervym Paterson's paper at the Royal Society meeting,Natural Strain and Geological Structure (April 1975) included in the volume on that meeting.

I have read two papers at Tectonic Studies Group A.G.M.'s, firstly at Birmingham 1975 entitled "Hydroxyl in Quartz- Chemical Aspects of Importance to Deformation Studies", and secondly at Dundee 1976 entitled " The Possible Rheological Significance of Inclusions in Synthetic Quartz". I also provided some of the inform--ation presented in this thesis for a paper read by S.White at the Mineral Studies Group meeting at Durham 1976 called "Micro-fluid Inclusions in Quartz - A Transmission Electron Microscope Study", by S.White, M.Jones and R.Knipe.

— * —

Chapter Two.

LITERATURE REVIEW AND GENERAL INTRODUCTION.

Chapter 2. LITERATURE REVIEW AND THE GENERAL INTRODUCTION.

2.1. Growth of Synthetic Quartz.

2.1.1. Nature of Synthetic Quartz Crystals.
2.1.2. Importance of Impurities in Synthetic Quartz.

2.2. Water in Natural and Synthetic Quartz.

2.3. Water Weakening and the Mechanical Properties of Quartz.

2,4. Electron Microscope and Related Studies on Quartz.

2.1. GROWTH OF SYNTHETIC QUARTZ.

Following the Second World War, the price of natural Brazilian type quartz rose dramatically to the extent that it became economic to consider the synthetic production of high clarity hydrothermal quartz crystals. During the 1950's growth techniques were perfected and crystal production on a commercial scale was started. Very little published information is available on the details of the growth procedure, but it would seem that in all cases the crystals were grown in a strongly alkaline solution (either sodium hydroxide or sodium carbonate) using crushed quartz as a starting material at temperatures between 250°C. and 400°C. and pressures around 2 kilo--bars. Normally the top of the autoclave (within which the crystal seed plates are suspended) was maintained about 50°C. cooler than the bottom(where the source material is placed). The autoclaves used are large, even experimental runs employing a vessel some 3metres high. The growth rates employed are fast (several centimeters per week) but it has generally been found that the purity and anelast--ic quality of the resulting quartz is inversely proportional to the growth rate so that for higher quality crystals a longer growth period is required.

Nearly all the crystals produced in the western world at the present time are grown on Z-cut seed plates at a rate which yields

a product of satisfactory quality for the desired application in the shortest possible time. The Z-cut seed is a thin slice of quartz cut perpendicular to the c-crystallographic axis. Sodium hydroxide solution(often doped with Lithium Hydroxide) is the most widely used growth medium, and coarsely crushed natural quartz is used as the source material. Three companies in particular grow these crystals namely I.T.T. , G.E.C. and the Bell Telephone Labs. Inc. During this project I found G.E.C.uncoperative whereas I.T.T. generously provided me with a large number of crystals,a tour of their plant and a period of discussion with personnel involved in quartz crystal growth. For a good discussion on the growth of synthetic quartz crystals , the reader, is referred to Brown and Thomas (1960).

In Russia other growth techniques have been employed, these produce large very pure crystals which are almost dislocation free. Unfortunately, I have found no discussion of the Russian technique anywhere in the literature.

2.1.1. The Nature of Synthetic Quartz Crystals.

Most synthetic quartz crystals are grown on rectangular seed plates (15cm. X 4cm. X 0.1cm.) cut perpendicular to the c-crystal--lographic axis. The amount of growth on either side of this plate varies according to the desired quality of the crystal and the len--gth of the run, but is normally between 1cm. and 3cm. on each side of the seed. The two growth surfaces, which are never developed in natural quartz crystals; (0001) and $(000\bar{1})$, are not typically smooth crystal faces but are cobbled, this effect apparently being caused by spiral growth around screw dislocations, and competition between distinct growth cells. The nature of this surface has been the topic of several publications , some of which are listed below. Because of the shape of the seed plate, the normal prism faces, seen in natural quartz crystals $\{10\bar{1}0\}$ $\{11\bar{2}0\}$, cannot develop and as a result of this the sides of the crystal are rough. This roughness

is apparently produced by alternating growth, firstly on one and then on the adjacent prism planes. These crenulations along the side of the crystal pass upwards into the cobbles and show on their smooth surfaces the striations parallel to (0001) normally developed on the prism faces of natural quartz crystals. Only at the corners of the rectangular crystal are normal faces developed. These belong to both the rhomb and the pinacoid and are normally of high index. Their development is normally very restricted. Thus the synthetic--ally produced quartz crystals barely resemble their natural equivalent as far as shape is concerned, but this effect is purely superficial resulting only from the confines to crystal growth imposed on the crystal by its unnaturally shaped seed. Figure 2.1. is a sketch of a typical Z-growth synthetic quartz crystal, and plate 2.1.is a photograph of the same.

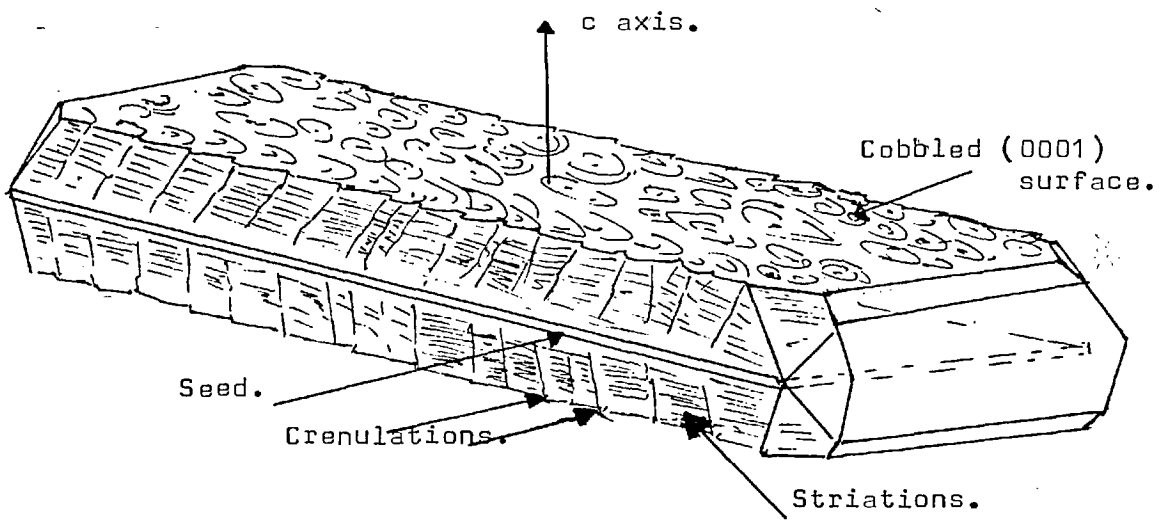

Fig 2.1. Sketch of a typical Z- cut seed synthetic quartz crystal.

A detailed discussion on the shape and nature of the surface of synthetic quartz is given by Augustine and Hale (1960). The microstructure of the cobbled surface is discussed by Lang and

Plate 2.1

A TYPICAL SYNTHETIC QUARTZ CRYSTAL GROWN ON A Z-CUT SEED.

Miuscov (1967) and by Mclaren et al (1971).

2.1.2. The Importance of Impurities in Synthetic Quartz.

A great interest arose in the nature of the impurities in both synthetic and natural quartz during the late 1950's. The reasons for this were mainly economic and the published studies fall into four main groups.

1) The anelastic properties of synthetic quartz crystals manufactured for the electronics industry (where they are used as oscillators, particularly in telecommunications equipment) were observed never to be as good as those recorded from natural Brazillian type quartz crystals. The index of anelastic loss (mechanical Q) was shown to vary with the impurity concentration, in particular with a cluster of absorption bands around three microns wavelength in the quartz absorption spectrum. An excellent discussion of the relationship between the anelastic properties and these infrared absorption bands in the quartz spectrum is given by Dodd and Fraser (1965) and a good bibliography is given with the article by Ballman, Laudise and Rudd (1966).

2) The impurity chemistry of the growth solution affected the growth of synthetic crystals, and it became apparent that studies of the solution chemistry, together with the trace chemistry of both the source material and the new crystals may yield methods of growing synthetic quartz from impure silica source materials. In particular it would have been economically desirable to use natural colloidal silica such as chert or flint as a source material. See Brown and Thomas (1960) for a discussion of this.

3) It was quickly realized that many of the included impurity species, in particular those which substituted for silicon, were associated with lattice defects in the freshly grown crystal. Because the reasonator properties of the crystal were dependant on the degree of perfection of the structure, the use of the trace chemistry to supply information about lattice defects became important. See Wood (1960), Arnold (1960) and Cohen (1960) who all discuss these problems. More important however are the publications by Kats and Haven (1960), Kats, Haven and Stevels (1962) and in particular Kats (1962), whose studies led on to some rather unusual and interesting methods of examining the quartz microstructure using decoration techniques. See White (1968) for a discussion on some of these techniques.

4) Much quartz and fused silica will undergo colour changes when exposed to ionising radiation. This production of colour centres associated with impurity ions and/or structure defects, became a topic of much interest in the late 1950's. Large numbers of papers have been published on this subject and of these I have listed only a few: Primik (1960), Levy (1960), Nelson and Crawford (1960), Cohen (1960) and Arnold (1960). In more recent works, this interest in colour centres has decreased.

During the period when much of this research was conducted, it became known that a number of tetravalent, trivalent and even divalent cations could substitute for silicon in the quartz structure. Within synthetic crystals it was found that the tetravalent cations showed a uniform distribution with respect to the different zones of crystal growth, their concentration not varying in any rational way through the structure. The trivalent

substitutional cations did show a distinct variation in the structure, their concentration being directly and obviously related to the crystallographic direction of the crystal growth. Thus the concentration of trivalent cations,substituting for silicon in synthetic quartz shows a distribution as follows (Cohen and Hodge 1958).

$$(0001) < (0010) < (11\bar{2}1) < (51\bar{6}1)$$

A similar distribution has possibly been recorded for the divalent substitutional cations (Cohen and Hodge (1958), Wood and Ballman (1966)). My work has indicated that the inclusion of hydrogen (as hydroxyl ions) follows a similar scheme, (see section 4.2.3.).

Towards the end of the 1950's, workers started to show an increasing interest in the three micron absorption bands in the quartz spectrum (see Wood (1960) or Dodd and Fraser (1965) for a good review). However much of the work was confused until the studies of Brunner et al (1959,1961), Kats et al (1960,1962a,b) and Bambuer (1961) were published. These papers which represented major steps forward in their field have subsequently become the key towards an understanding of some of the problems of water weakening of quartz. A review of the literature concerned with infrared spect-roscopy of natural and synthetic quartz will be the topic of the next section.

2.2. WATER IN NATURAL AND SYNTHETIC QUARTZ.

Six papers published during the period 1959 to 1962 form the basis of much of our present understanding of hydroxyl ions bound in the structure of natural and synthetic quartz (as against molecular water trapped in fluid inclusions). These,together with

two more recent articles (see below) must then form the basis of the preliminary reading of any worker interested in this field. These articles are in order of appearance, Brunner et al (1959), Kats and Haven (1960), Brunner et al (1961), Bambuer (1961), Kats et al (1962), Kats (1962) Dodd and Fraser (1965) and Dodd and Fraser (1967). These articles show conclusively, from diffusion experiments and spectroscopic considerations that a series of distinct absorption peaks superimposed on to the broad hydroxyl absorption at three microns in the quartz spectrum, are also due to absorption by specifically bonded hydroxyl groups. These groups are present in the quartz structure either hydrolyzing Si - O - Si bridges or as complexes substituting for silicon atoms. In particular these articles describe the infrared technique and the data reduct-ion procedure in detail. It is from these papers and one other (Scholze 1960) that the presently accepted value of 14000 Litre/ mole.cm^2. is taken for the absorption coefficient for hydroxyl ions bound in the quartz structure and absorbing in the vicinity of three microns wavelength. It is important to note however that the relationship used by Bambuer in his data reduction and publish-ed by him (1961) is in error. This equation, which has been widely used, (see all papers by Griggs on hydrolytic weakening) gives concentrations which are too large by a factor of two. This error and the correct form of the relationship are discussed in section 3.6.

Brunner et al (1961) introduced the concept of the silanol bond, ($\equiv$Si - OH : : HO - Si$\equiv$) which although incorrectly interp-reted by Griggs (1967) has formed the basis of all the models for the role of water in aiding dislocation motion in quartz. Brunner(1961) also published the first easily applicable relation-ship based on Beers Law for determining the hydroxyl concentration.

Using this relationship he recorded concentrations in the range 10 to 10000 Hydrogen per million silicon atoms ($H/10^6 Si$) for various types of natural quartz.

> It is important to note these units, often in the more recent publications, results from this relationship have been reported as p.p.m. This is clearly a misuse of these units. P.p.m. implies PARTS PER MILLION BY WEIGHT, not the ratio of one ATOMIC SPECIES TO ANOTHER. Thus by using p.p.m. an error of X 60 is automat--ically introduced into the interpretation of the data (X 92 if silica or quartz is specified rather than silicon).

The work of Kats (particularly his 1962 paper) is more detailed than that of Brunner. He lists distinct associations between defects and different hydroxyl/other impurity ionic groups. He uses these associations to account for the absorption bands which he , like Brunner(1961), recorded at cryogenic temperatures ($77^{o}K.$). Much of Kats (1962) work is based on diffusion experiments and these have enabled him to calculate independently the absorption coefficient for the hydroxyl absorption bands when these bands have a distinct Gaussian form. Comparing concentrations calculated from the same spectrum using both the Brunner (1961) and the Kats (1962) relationships gives excellent agreement, when the peak resolution is sufficiently good.

The paper by Bambuer (1961) shows how the concentrations of Aluminium (3+), Lithium and Sodium ions in samples of Brazilian type vein quartz, from the Swiss Alps are directly related to the hydroxyl ion concentration. This result lends excellent support to

the complex ionic models determined by Kats (1962).

The work of Dodd and Fraser (1965) supports that of Kats (1962) but discusses the properties of the different absorption peaks in the three micron band and reviews the literature leading to their assignment to hydroxyl and hydrogen bond vibrations. They discuss the effects of heat treatment of their crystals more fully than does Kats, and show by spectroscopic means that the milkyness produced by such heat treatment is due to bubbles of precipitated molecular water.Their second paper in 1967 is a discussion of the variation of concentration of hydroxyl ions within the structure of synthetic quartz crystals. In this work they demonstrate conclusively that the concentration of hydroxyl ions bound in the structure of a synthetic quartz crystal is proport--ional to the growth rate of that crystal, and thus the concent--ration of the hydroxyl ions changes throughout the crystal as the growth rate changes.(See chapter 4).

Thus a large pool of information pertaining to the concentra--tion, location and determination of hydroxyl ions in the structure of synthetic and natural Brazilian type quartz was available in the literature by the mid 1960's. To the best of my knowledge, at the time of writing, no more recent major papers on this field have appeared.

2.3. WATER WEAKENING AND THE MECHANICAL PROPERTIES OF QUARTZ.

In 1964, Griggs and Blacic reported that natural Brazilian type quartz,deformed in triaxial compression in a solid confining medium testing machine, became weak at the temperature at which the Talc confining medium dehydrated. They assumed that the hydroxyl ions released from the talc diffused into the quartz crystal and weakened it. Following these experiments, they turned their attent-

-ion to synthetic quartz crystals grown with large concentrations of structure bound hydroxyl groups, and found that they are invar--iably weaker than their'dry' natural equivalents. Figure 2.2.a). shows sets of stress strain curves for two synthetic quartz crystals of differing hydroxyl concentration taken from Griggs(1974). In figure 2.2b). the stepped relaxation behaviour of a number of synthetic quartz crystals is compared. These curves are from Griggs (1967). It is unfortunate that the Griggs laboratory adopted this stepped relaxation test as their standard test on quartz for the interpretation of the results is difficult, if not ambiguous and in many instances a set of stress strain curves demonstrate the weakening to a far better extent. (See the stress strain data in Hobbs et al (1972) for an example of this.) Because the Griggs Laboratory adopted this rather unusual and unsatisfactory technique there are very few published stress strain curves for synthetic quartz crystals which have been widely used not only as experimental material in their own laboratory but also as a standard in many other laboratories around the world. (The stepped relaxation technique will be discussed more fully in section 4.6.)

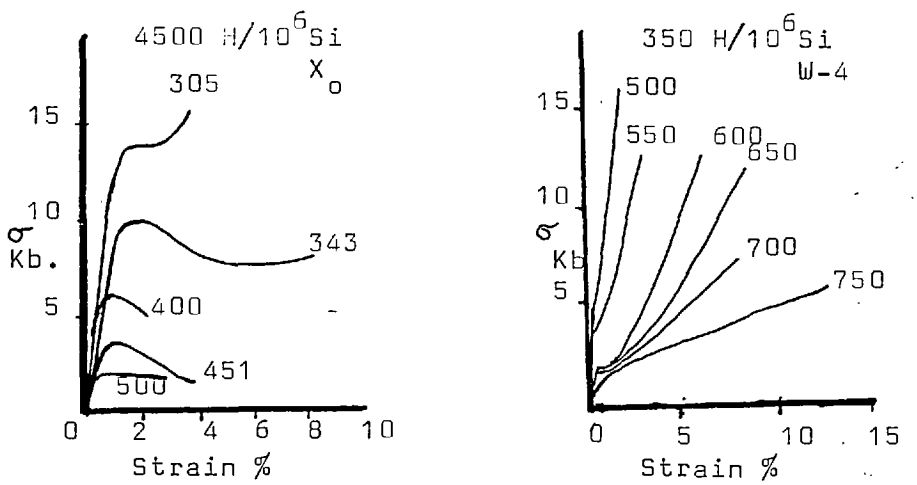

Fig2.2a. Stress/strain curves for synthetic crystals X_o and W-4 with 4500 and 350 H/10^6Si. Numbers against curves are temperature in degrees centigrade. From Griggs (1974).

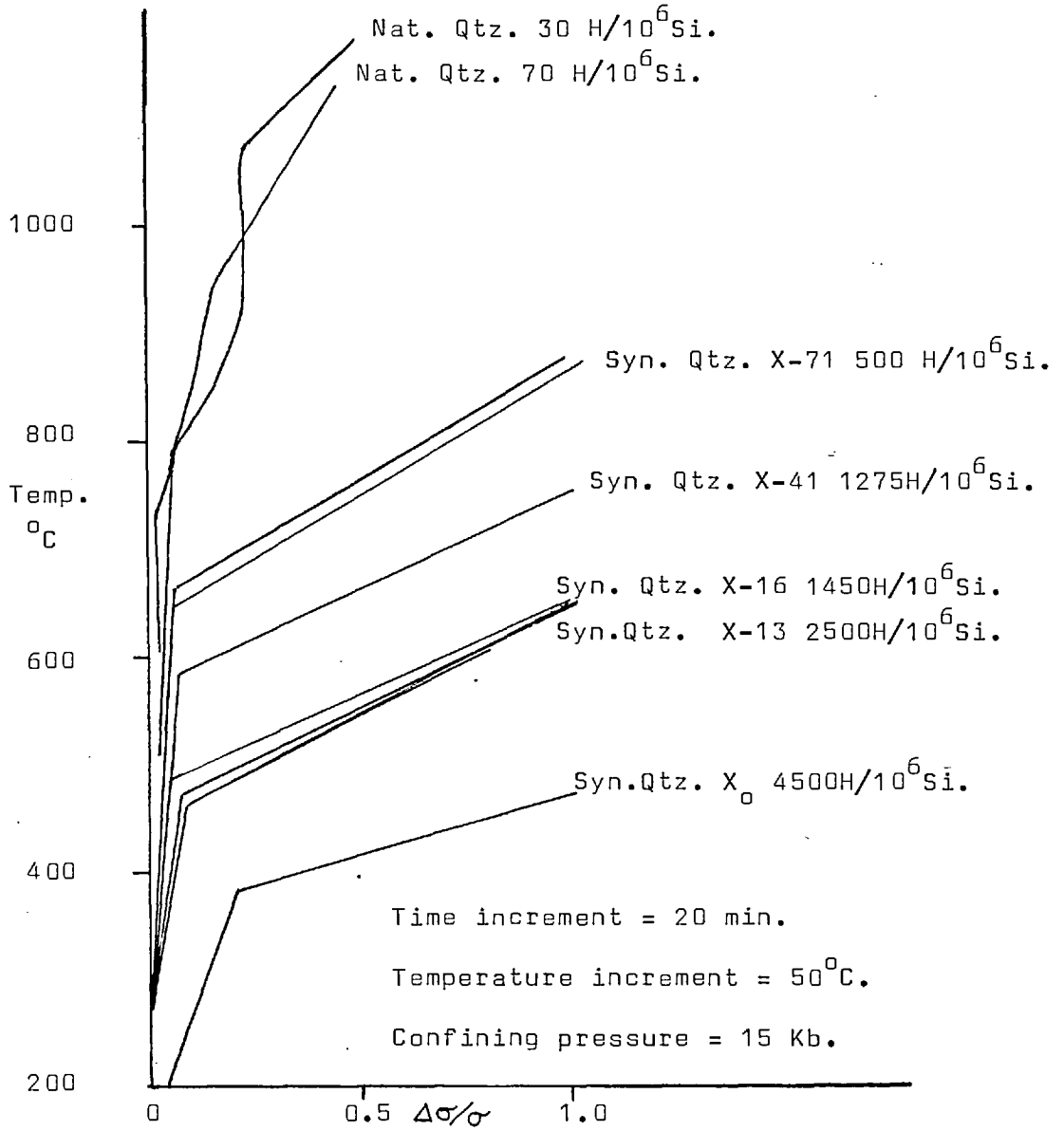

Fig. 2.2b. Relaxation plots of typical natural and synthetic quartz single crystals. From Griggs (1967) data points omitted.

Mechanical testing of these synthetic crystals revealed that yield points could be identified at lower temperatures in those crystals with the higher water concentrations, and that at some temperature above this value, the crystal became very weak. Both the lowest temperature at which yield could be identified,

and the weakening temperature are thus inversely related to the hydroxyl concentration. Between the lowest yield temperature, and the weakening temperature, the stress strain curves show extreme work hardening, the degree of which decreases somewhat with increas-ing temperature until the weakening temperature is reached. Above the weakening temperature the stress/strain curves show little or no work hardening, and certainly during some of the tests conducted as part of this project show strain softening. At temp-eratures close to the lowest recorded yield temperature, when the yield stress is very large, the slope of the plastic section of the stress/strain curve is almost identical to that of the elastic section. This is because the rate of work hardening is so very extreme at these 'low' temperatures.

Griggs and Blacic in a series of publications (e.g. 1965, 1967) correlated these results with the infrared absorption (at three microns wavelength) and assumed that the mechanical properties were being controlled by the amount of water dissolved in the structure of their individual crystals. Unfortunately their spectro-scopic analyses, as reported, left much to be desired. In particular they apparently only analyzed each crystal once and used Bambuers relationship (see chapter 3) so that each analysis was too large by a factor of two. They also made the unwarranted assumption that molecular water would diffuse into the crystal structure under the high pressures and temperatures that prevailed during their deformation tests. In the publications, which appeared in 1965 and 1967, they developed a model for the weakening process which came to be termed the 'Frank-Griggs Mechanism for Hydrolytic Weakening'. In this it was assumed that the hydroxyl groups within the structure diffused to the dislocation line, and there hydro-lyzed Si - O - Si bridges. The resulting hydrogen bonds being weaker than the silicon oxygen bonds which they replaced, thereby

facilitated the easy glide motion of the dislocations. A model of this type is elegant in its simplicity but fails to take acc--ount of the far more complex atomic models suggested by Kats (1962). It also fails to explain the shape changes which occur in the stress/strain curves as the temperatures are increased. These shape changes suggest that an initial high density of dislocation sources is rendered increasingly ineffective as the temperature is raised. In the 1967 publication the Frank-Griggs Model was applied to the plastic deformation of all the major rock forming silicate minerals, a presumption which is now known to be both incorrect and unnecessary (see for example Weertman 1970).

This original model of Griggs is clearly unsatisfactory and was superceded by the work of Mclaren et al (1969,1970) who suggested that the major role of the structure bound hydroxyl groups was in aiding recovery. Thus the weakening temperature was seen as a temperature at which rapid recovery, presumably as a result of cross slip and sub grain formation, occurred. The suggestion was that the more water that there was present in the structure, the lower would be the temperature at which recov--ery could occur. This model is presumably correct in part because it satisfactorily accounts for the large stress drop at constant strain as the temperature is increased. Unfortunately it fails to explain the very rapid work hardening which occurs at temperatures below the weakening temperature and which would appear to require a very high initial dislocation density, or a very large number of dislocation sources operative at the yield point.

In 1972 Hobbs, Mclaren and Paterson produced a large paper showing mechanical results for a different set of quartz crystals to those originally used by Griggs. These results were in good agreement with the original Griggs data. Hobbs et al adopted a different approach and applied the microdynamical yield theory of Alexander and Haasen (1968) to the problem of the interpretation. This theory, framed for dislocations in the diamond structure, enabled several of the problems to be overcome, and although attractive from the microdynamical standpoint (it described the yield behaviour of the crystals very well)it did not explain the fundamental role of the hydroxyl impurity.

Griggs (1974), using the mechanical data of Baldermann (1974), produced a revamped version of the theory as presented by Hobbs et al. This was mathematically more sophistocated, providing a series of equations with 12 independent variables, which presumably could be made to describe the yield behaviour of any material not only that of synthetic quartz. It is in this most recent paper that Griggs produced an equation predicting the weakening temper--ature from the hydroxyl concentration.

$$\bar{c}\,(H/Si) = 7.4 \times 10^{-8} \exp(15700/R\,T_c) \qquad \ldots\ldots 2.1.$$

where $\bar{c}$ is the hydroxyl concentration,

T_c the weakening temperature,

and R the gas constant.

After modifying the pre exponential constant to correct for the errors in Griggs spectroscopic technique (see section 3.6.5.), I found that this satisfactorily predicted the weakening temperature

for synthetic quartz crystals but fails to give even vaguely reasonable values for natural quartz crystals with large hyd--roxyl concentrations. This is presumably because in natural crystals much of the infrared absorption is due to molecular water in bubbles, not to the structure bound hydroxyl groups.

In 1975 Blacic published a paper which reviewed the devel--opment of the water weakening theory, concentrating on the role of water in the process. He again refers to experiments in which the talc confining medium has dehydrated, and in which the released water diffuses into the quartz sample weakening it. Unfortunately these experiments have never been successfully repeated (despite repeated attempts by several workers) (M.S. Paterson personal communication) and the results of Kats (1962) suggest that the diffusion of water into the quartz structure may be a slow and difficult process. One which is hardly likely to occur during a short deformation test. Experiments conducted as part of this project certainly tend to support this view. Blacic (1975) reports that the appearance of micro fluid inclus--ions in his samples,recovered from these tests,are evidence that this inward diffusion of water into the quartz structure has occur--red. In chapter 5 I will show quite conclusively that this inter--pretation is incorrect.

The most recent major article is that of Morrison-Smith, Paterson and Hobbs (1976). In this paper the authors combine detail--ed electron microscope observations with infrared spectroscopic analysis and the results of mechanical deformation experiments. They describe an impurity phase not previously reported in the microstructure of synthetic quartz. In chapters 6 and 7 I will try to show that many of the unusual mechanical properties of

of synthetic quartz may be explained by reference to the presence of this impurity phase rather than to structural water alone.

Another set of apparently good experimental results are those of Baeta and Ashbee (1968, 1969a,b, 1970a,b, 1973). These authors have concentrated on the microdynamical approach and provide a wealth of useful quantitative data on the slip systems operative in deforming single crystals of quartz.

Whilst preparing the final draft of this thesis an article by Ayensu and Ashbee was published (1977). This article discusses the results of a number of triaxial compression and extension tests on helices cut from single crystals of synthetic and natural quartz. At the end of the article these authors use a theoretical analysis to arrive at a maximum confining pressure under which bubbles of precipitated molecular water will nucleate and grow in the structure of a synthetic quartz crystal. Their result of 1 Kilobar is unreasonable as I will show using the results of exp--eriments reported in chapter 5. The error in their analysis appears to have resulted from a failure to appreciate fully the Pressure, Temperature and Volume relationships that will govern the size,shape and growth of a bubble of water in the quartz structure.

There are many other papers on the deformation of both wet and dry,natural and synthetic quartz, which have appeared between 1964 and 1977,of which Hobbs et al (1966), Hobbs (1968), and Heard and Carter (1968) are useful. In some of the more recent publications, ideas on water weakening have often been combined with studies of natural quartz deformation and texture formation, (Tullis et al 1973). In the present rather confused state of ideas on water weakening, this may be a little premature.

2.4. ELECTRON MICROSCOPE STUDIES OF QUARTZ.

The first worker to study quartz in the transmission electron microscope was Mclaren, who, with co-workers, published papers on the microstructure of synthetic and natural quartz between 1965 and 1972 (a complete list of references to these is given in the bibliography). Of these articles, the paper on bubbles in Citrine and Amethyst quartz (1966) is of the utmost importance to the present study, and I have referred to it freq--uently. In this article Mclaren et al use the transmission elect--ron microscope to study the changes that occur in the microstruct--ure and the growth of micro-fluid inclusions in specimens of citrine and amethyst which had been heat treated in the laboratory. They compare the results of this study with observations of micro--fluid inclusions in natural milky quartz. More recently White (1973) reported a solid state origin for fluid inclusions in natur--al milky quartz, this conclusion also resulting from a transmission electron microscope study. In this present study I support the view of White with further experimental evidence and conclude that a solid state origin for these inclusions in natural quartz is absolutely essential if the natural deformation of quartz is to be satisfactorily explained.

S. White has produced numerous publications on the natural deformation of quartz during the period 1968 to 1977. These papers, the majority of which are transmission electron microscope studies, are listed in full in the bibliography. These articles are of imp--ortance to the experimentalist because they accurately describe the microstructures resulting from different natural deformations, and because they demonstrate to good effect the use of the high voltage electron microscope for studying the microstructure of natural materials. White has pioneered the use of this instrument

on naturally deformed quartz rocks and it is from such studies that the experimentalist can check the validity of his ideas. Much of the electron microscopy reported in chapter 6 was cond--ucted on the high voltage electron microscope in the Metallurgy Department at Imperial College in close collaboration with S. White.

* * * * *

The bibliography briefly reviewed in this chapter covers a range of the major publications pertaining to the physical and chemical properties of natural and synthetic quartz, and to the water weakening of quartz, as known to me at the time of writing. This list is far from complete, but should, if used in conjunction with the bibliographies included in the papers referred to, provide access to almost all of the articles of interest. I hope that the brief discussions, contained in this chapter, have served as an introduction to the water weakening of quartz and helped to familiarize the reader with some of the more important problems which will be discussed at length in the remainder of this thesis.

— * —

Chapter Three.

MEASUREMENT OF THE STRUCTURE BOUND WATER CONCENTRATION.

Chapter 3. MEASUREMENT OF THE STRUCTURE BOUND WATER CONCENTRATION.

3.1. Available Methods for the Direct Measurement of H^+ and OH^-.

- 3.1.1. Mass Spectroscopy.
- 3.1.2. Ion Beam Spectrochemical Analysis.
- 3.1.3. Infrared Spectroscopy.
- 3.1.4. Other Methods.

3.2. The Infrared Spectrometer.

3.3. Samples Used in the Analysis.

3.4. Recording the Spectrum.

3.5. Quantitative Analysis.

- 3.5.1. The Beer-Lambert Law.
- 3.5.2. The Absorption Coefficient.
- 3.5.3. Deviations from the Beer-Lambert Law.
  - a) Chemical.
  - b) False Measurement of the Absorption Band by the Spectrometer.
- 3.5.4. The Integral Intensity.

3.6. The Analysis of the Quartz Spectra.

- 3.6.1. The Quartz Absorption Coefficient.
- 3.6.2. Measuring I and I_o.
- 3.6.3. Measuring the Cell Length (b).
- 3.6.4. Determining the Concentration.
- 3.6.5. Bambuers Error.

3.7. Other Quantitative Procedures.

- 3.7.1. The Kats Method.
- 3.7.2. The Simplification used by Dodd and Fraser.

3.8. The Effect of Orientation.

3.9. The Absorption due to Molecular Water.

3.10. The Shape of the Quartz 3500cm.$^{-1}$ Absorption Band.

- 3.10.1. Brazilian Type Quartz.
- 3.10.2. Synthetic Quartz.
- 3.10.3. Other Natural Quartz, Including Opalescent Vein Quartz.

3.11. Concluding Summary.

3.1. AVAILABLE METHODS FOR THE DIRECT MEASUREMENT OF H^+ AND OH^-.

The concentrations of structure bound water in both natural and synthetic quartz are extremely small and cannot be determined by wet chemical analysis. It is thus necessary to utilise a spectroscopic technique for this analysis, but the techniques available are few and each has severe limitations. Niether X ray fluorescence spectroscopy nor electron probe micro-analysis, which have been the most used analytical techniques in petrology,can detect these ions, so they are overlooked in most quartz analyses. Three methods for this determination have been used and reported in the literature, and these, together with a number of more 'exotic' techniques are,

1) Mass Spectroscopy (Baker and Sommer 1974).
2) Ion Beam Spectrochemical Analysis (Tsong,Mclaren and Hobbs 1976).
3) Infrared Spectroscopy (Brunner et al 1959,1961).
4) Other Techniques.

3.1.1. Mass Spectroscopy.

Mass Spectroscopy was used by Barker and Sommer (1974) to determine the relative concentrations of water released from a finely crushed quartz specimen in an evacuated reaction tube at elevated temperatures, the temperature being increased stepwise to beyound the melting point of the sample. This technique shows that water is released from quartz at a distinct series of temp-eratures, and that each such temperature is related to the dehy-dration of a different structural location. The technique is however severely limited in so much that the absolute concentrat-ions are unknown, and the distribution of any one type of struct-

-ural water throughout the crystal cannot easily be determined. Further, it gives no indication of how the water changes its structural sites during the heat treatment prior to its ultimate release from the crystal. Because this technique employs a finely ground sample from which the water is released to be analyzed, it cannot be used to provide information on the heating of a large crystal sample which has not been ground, i.e. when the structural water mobilized by the heat treatment cannot easily reach a free crystal surface.

3.1.2. Ion Beam Spectrochemical Analysis.

This is a new technique being developed for silicates by Tsong, Mclaren and Hobbs (1976) and may become an important method for the determination of hydrogen in silicates, particularly as the analysis may eventually be conducted whilst ion beam thinning the specimen for electron microscopy. The technique does however have one serious drawback in so much that only the total hydrogen concentration of the crystal can be measured, so that it is imp--ossible to distinguish between H^+, OH^- and H_2O which is import--ant when hydrolytic weakening is being considered.

3.1.3. Infrared Spectroscopy.

This is the most widely established method for measuring H^+, OH^- and H_2O concentrations in silicates, using the intensity of the absorption band(s) around $3500cm^{-1}$. If the analyses are conducted at cryogenic temperatures, it is also possible to dist--ingush quantitatively between the ionized and molecular water. Using this technique, the specimen is analyzed at or below room temperature and thus the concentration, ionic state, distribution, and location of the water in the specimen is not significantly modified during the analysis. Infrared spectroscopy has been adopt--ed during this study, and although it suffers from the limitations

discussed at length below (this chapter), has produced results which at the least have a strong relative value. These results should be comparable to those presented in other published work (loc cit), if adequate precautions are taken. The rest of this chapter is devoted to a discussion of the technique and appara-tus used, paying particular attention to their limitations. This discussion also outlines the precautions that should be taken when comparing this data to that from other studies (loc cit).

3.1.4. Other Techniques.

Hydrogen may also be determined by Differential Thermal Analysis and Thermo-gravimetric Analysis, but the result of these techniques are only aproximate. Other published analyses have used M.eV. electron beams to cause nuclear reactions or proton scattering (Cohen et al 1972, Leich et al 1973 and Ligeon et al 1974) but such procedures are hardly suitable for routine labora-tory work. Recently the possibility of using the ion microprobe mass analyser has been demonstrated by Hinthorne and Anderson (1975) and this may become a useful technique. It is unfortunate that at present the ion beam spectrochemical analyser has had to rely on standard samples for calibration in which the hydrogen concentration has been determined by D.T.A. , T.G.A. or ignition loss. Often these standards are micas and the analysis necessarily assumes stoichiometry. Thus the calibration may introduce signifi-cant errors, reducing greatly the usefulness of this potentially accurate technique.

3.2. THE INFRARED SPECTROMETER.

The concentration of water in a silicate sample may be easily determined with any of the commercially available infrared spectrometers fitted with a sample cell operating at or below room

temperature. The accuracy of any such analysis will however vary greatly, depending on the operating parameters of the instrument chosen. In undertaking a spectroscopic study of this type, it is therefore advantageous to identify clearly the objectives of the study before selecting the type of spectrometer to use. In this study, where numbers of analyses were a premium a simple double beam instrument of the type widely used in routine analysis was employed. This was operated at room temperature.

The infrared spectrometer is basically simple, a hot black body reflector emits infrared radiation over a range of frequenies at almost constant intensity. It is this range which limits the operating frequency range of the spectrometer. The beam is split into two paths one of which passes through the sample being analyzed whilst the other passes through a reference sample, often simply a material which is transparent at the frequencies of interest. These paths are sampled alternately (at 10 cycles per second in the Grubb Parsons instrument used in this study) and passed through a monochromator (consisting of either a diffraction grating or an alkali halide prism or some combination of the two) which is scanning slowly across a selected range of frequencies. The radiation leaving the monochromator is then sensed by a photocell or thermocouple (depending on the manufacture of instru--ment used). If the intensity of the two beams differs at the detector, a signal is generated which is proportional in sign and strength to the difference in intensity. This signal is used to operate a servo controlled V-toothed comb which is either driven into or pulled out of the reference beam (normally called the attenuator comb) either increasing or decreasing its intensity as required to keep the energy in the two beams constant. It is

the relative displacement of this servo system which is recorded on the strip chart, giving a plot of intensity versus frequency. Some instruments are designed to operate with a single beam. In these the reference beam and servo system can be switched off and the detector linked directly to the chart recorder. Generally however double beam operation is simpler, more accurate, and more reliable because the paired beams serve to average and negate the effects of contamination in the laboratory atmosphere so that radiation absorption from such effects is not recorded on the chart recorder. Careful choice of the reference sample can remove the effects of most contaminants from the recorded spectrum.

Figure 3.1 is a simplified diagram of the spectrometer used in this study. This instrument was a Grubb Parsons Spectromaster (Plate 3.1) which was operated throughout in accord with the manufacturers published instructions. The spectromaster uses a Nernst filament radiation source at a temperature of about 1200^{o}K, fired by a current of 0.9 amps. This instrument is double beam, and employs a combined diffraction grating and alkali halide prism monochromator. The radiation detector is a thermo-couple which enables the instrument to operate over a wide range of wavelengths. This range from 0.6 microns to 25 microns is split into three sections by the diffraction grating employed. These are 5 to 25 microns using a first order grating of 1500 lines per inch, 1 to 5 microns using a first order grating of 7500 lines per inch and 0.6 to 2 microns using a second order grating of 7500 lines per inch. The entrance and exit slits of the monochr-omator unit can be manually set or operated by an automatic program which maintains optinium slit width across a full wavelength span. By altering the slit program, the resolution can be doubled but with a 75% energy loss.

Plate 3.1

THE GRUBB PARSONS SPECTROMASTER INFRARED SPECTROMETER USED FOR THE WATER ANALYSES IN THIS STUDY.

Figure 3.1. A simplified diagram of the Grubb Parsons Spectromaster Infrared Spectrometer showing the major optical components, the ray path and demonstrating the principle of operation. The key to this diagram is given overleaf.

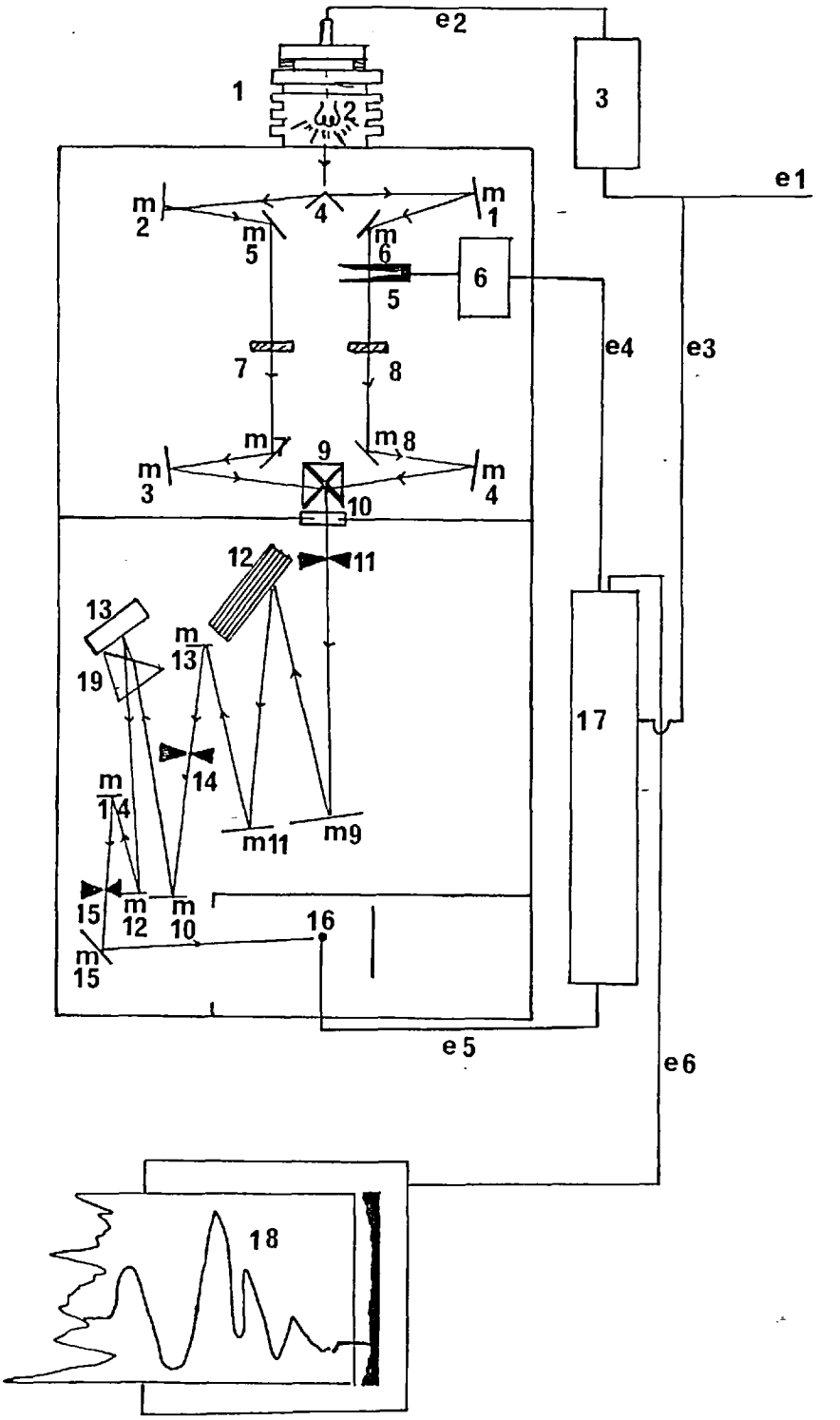

Figure 3.1 Key.

1. Nernst Filament Housing. (Note air cooling fins).
2. Nernst Filament.
3. 0.9 Ampere Current Stabilizer. (Three 0.3 amp Barreter Lamps).
4. Pair of Plane Mirrors dividing the beam.
5. Attenuator Comb.
6. Servo Motor.
7. Sample.
8. Reference Sample.
9. Reciprocating Mirror System. (Alternately samples the beams).
10. Teflon Window to Monochromator.
11. Monochromator entrance slit. (Variable).
12. Diffraction Gratings.
13. Littrow Mirror.
14. Monochromator central slit (Variable).
15. Monochromator exit slit (variable).
16. Thermocouple detector.
17. Servo Amplifier (variable gain).
18. Strip chart recorder.
19. Potassium Bromide Prism. (Single Crystal).

e1. 240 volt A.C. supply.

e2. 240 Volt, 0.9 amp stabilized current supply to the Nernst Filament.

e3. Power supply to the servo amplifier and chart recorder.

e4. Energising supply for the servo motor.

e5. Signal lead from thermocouple to the servo amplifier.

e6. Signal lead from the servo amplifier to the chart recorder. (Power for the chart recorders own amplifier and motors is supplied from the servo amplifier.)

m1 - m4. Spherical Mirrors.

Figure 3.1 Key contin.

m5 - m8. Plane Mirrors.

m9 and m10. Collimating Mirrors.

m11 and m12. Focusing Mirrors.

m13 to m15. Plane Mirrors.

3.3. DESCRIPTION OF THE SAMPLES USED IN THIS WORK.

The Grubb Parsons Spectromaster used in this work was equipped with a double beam sample holder designed to contain two solid disc shaped samples, which can be up to 0.5cm thick with a diameter of 1.5cm. The beam passes through the vertical diameter of these discs but is only 0.1cm wide so that it is possible to use a smaller sample with a surface area of 1.5 X 0.2cm in the plane of incidence. Such samples could be fitted into the standard sample holder using an opaque packing material (plasticene). Because the transmitted beam intensity decreases linearly with increasing sample thickness it is also necessary to maintain the thickness at a minimum but this also leads to a decrease in the number of absorbing ions of the species being analyzed, within the area covered by the beam. It is thus nec-essary to compromise between a large background absorption with a large absorption band and a small background absorption with a small absorption band. This compromise varies with every sample, those with small hydroxyl concentrations being necessarily thicker than those with large. I found that normally a thickness of 0.1cm was ideal, as a starting point when studying a crystal for the first time.

Two types of sample were devised to fit this holder. When single crystals of sufficiently large size were being studied (which was normally the case), plates were cut from the crystals, these were disc shaped with a diameter of 1.5 cm.and with thick--nesses varying between 0.08 and 0.5 cm.to suit the conditions. Such samples were easily prepared from large synthetic and natural Brazilian type quartz crystals, but clearly were of little use when finer grained quartz rocks were being studied. For the less coarsely crystalline material, pressed discs of the finely powdered sample in a potassium bromide matrix were used. Potassium bromide is transparent throughout the near infrared. Full details of the preparation of these samples including grinding times and media, and precautions against contamination by hydrous minerals and water absorbed from the atmosphere are given in appendix 1. The cutting and grinding procedure for the single crystal plate samples is also described in that section.

Where the distribution of structure bound water in a crystal was being investigated, it was convenient to use a larger speci--men, generally a slice cut across a single crystal or polycryst--aline vein. These slices were mounted in a clamp which hung in the sample beam in the same position as that normally occupied by the specimen. With this procedure plates up to 5 X 5 X 0.5cm could be analysed. A standard reference sample was used.

The reference samples were either cut from synthetic or brazilian type quartz crystals with small hydroxyl concentrations, or were pressed discs of pure infrared grade potassium bromide. (This high purity potassium bromide is manufactured by B.D.H. Poole Dorset.) If transparent (optically) single crystal plates were being analyzed, then either a dry quartz plate of similar thickness or a thin potassium bromide disc was used in the refer--ence beam. Natural opalescent quartz crystals were always com-

-pared to thick potassium bromide discs to negate the absorption caused by light scattering on the surfaces of the many small fluid inclusions in these samples. The pressed disc quartz samples were compared to potassium bromide discs of similar weight to the potassium bromide in the quartz sample.

3.4. RECORDING A SPECTRUM.

All the spectra recorded during this study were measured at room temperature, because the frequency resolution on the Grubb Parsons Spectromaster is not very high. Because of this the use of a cryogenic cell would have produced only a small improvement in the resolution. A marginal improvement in frequ -ency resolution was therefore sacrificed for a much faster analytical procedure. It is important to note that if, as was done during this study, the spectra are analyzed using the integral intensity procedure (see sections 3.5 and 3.6) then the recorded concentration is almost independent of the freq--uency resolving power of the spectrometer. The use of a high resolution spectrometer in conjunction with a cryogenic cell would have yielded much more detailed structural information. However, at the preliminary level of investigation which this study represents I was interested in the total amount of water, or structure bound water, in a large number of samples rather than the details of the actual bonding arrangements, most of which have been satisfactorily worked out by Kats (1962). The influence of sample temperature on the shape of the 3500 $cm.^{-1}$ absorption band for hydroxyl in the quartz structure, has been documented by Brunner *et al* (1961), figure 3.2. is taken from this study and clearly shows the effect of sample temperature on the frequency resolution.

Figure 3.2. The effect of sample temperature on the frequency resolution for the 3500cm.$^{-1}$ absorption band caused by hydroxyl ions in the quartz structure. This is taken from Brunner, Wondratschek and Laves (1961).

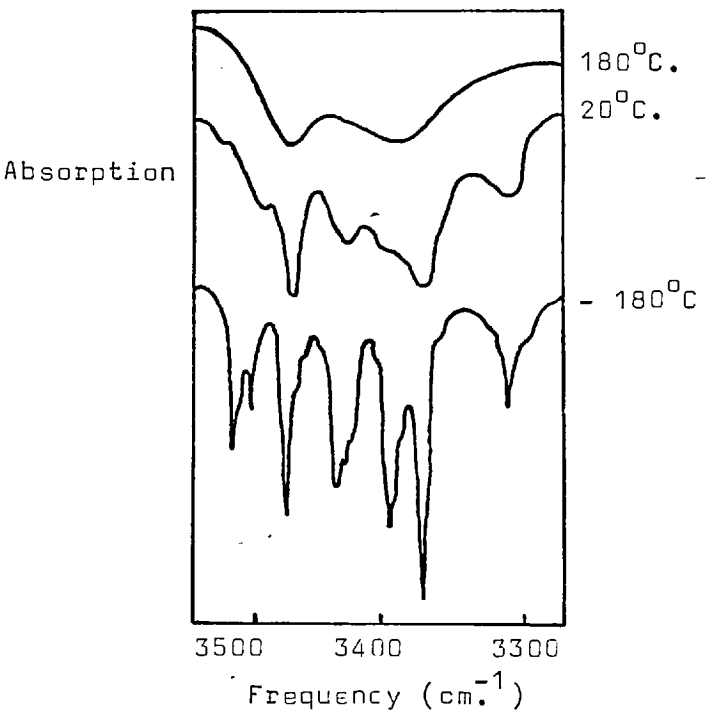

Before recording a spectrum, a check was made on the frequency resolution of the spectrometer using a thin film of polystyrene recorded against air in the reference beam. Figure 3.3. is an example of the spectrum recorded from this material when the spectrometer was opereting at its maximum resolution. The instrument was always adjusted to reproduce this spectrum before any analyses were conducted. Following this resolution check, the amplifier gain was adjusted in accord with the pub--lished instructions provided in the manual supplied with the spectrometer and then a sample of synthetic quartz (cut from crystal AX1) was run to check that the recorded intensity was the maximum. The spectrum for this sample (designated C3) is

shown in figure 3.4. and as with the polystyrene spectrum, the spectrometer was always adjusted to reproduce this curve before analytical work proceeded.These two checks together with the standard adjustments described in the spectrometer instruction booklet (see bibliography) served to maintain a good standard of reproducibility throughout this work.

The spectrometer was designed to provide three ranges of frequency scan (each linked to different diffraction gratings in the monochromator). These are 0.5 to 2 microns, 1 to 5 microns and 4 to 24 microns. The range 1 to 5 microns is the only one of interest in this work although the full range (0.5 to 24 microns) was occasionally scanned. In normal routine work the range was restricted to scanning from 2 to 4 microns which was sufficient to cover completely the group of hydroxyl absorptions.

Figure 3.3. The infrared spectrum of Polystyrene in the region around three microns wavelength.

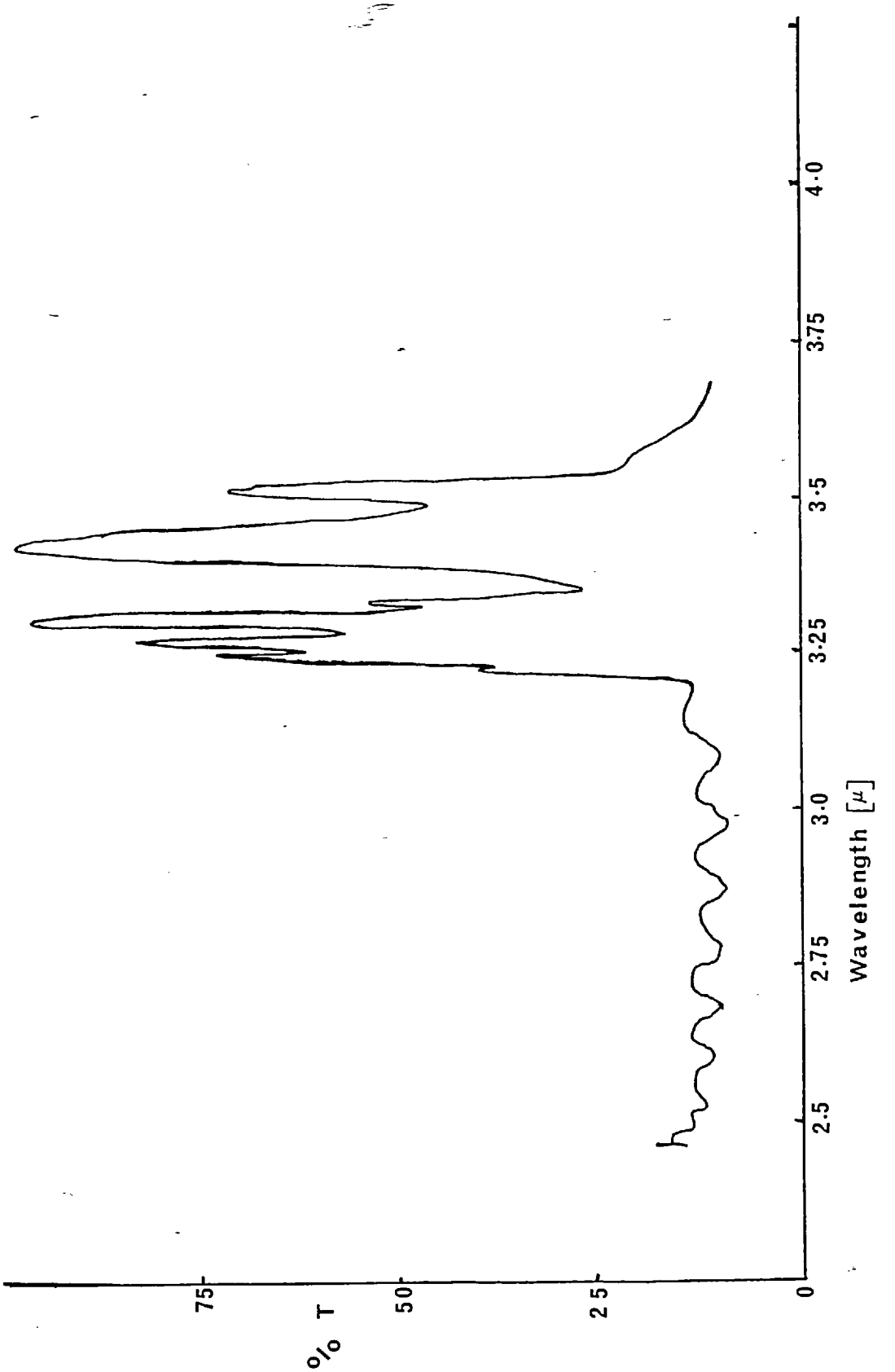

Figure 3.4. The infrared spectrum of sample C3 cut from synthetic quartz crystal AX1.

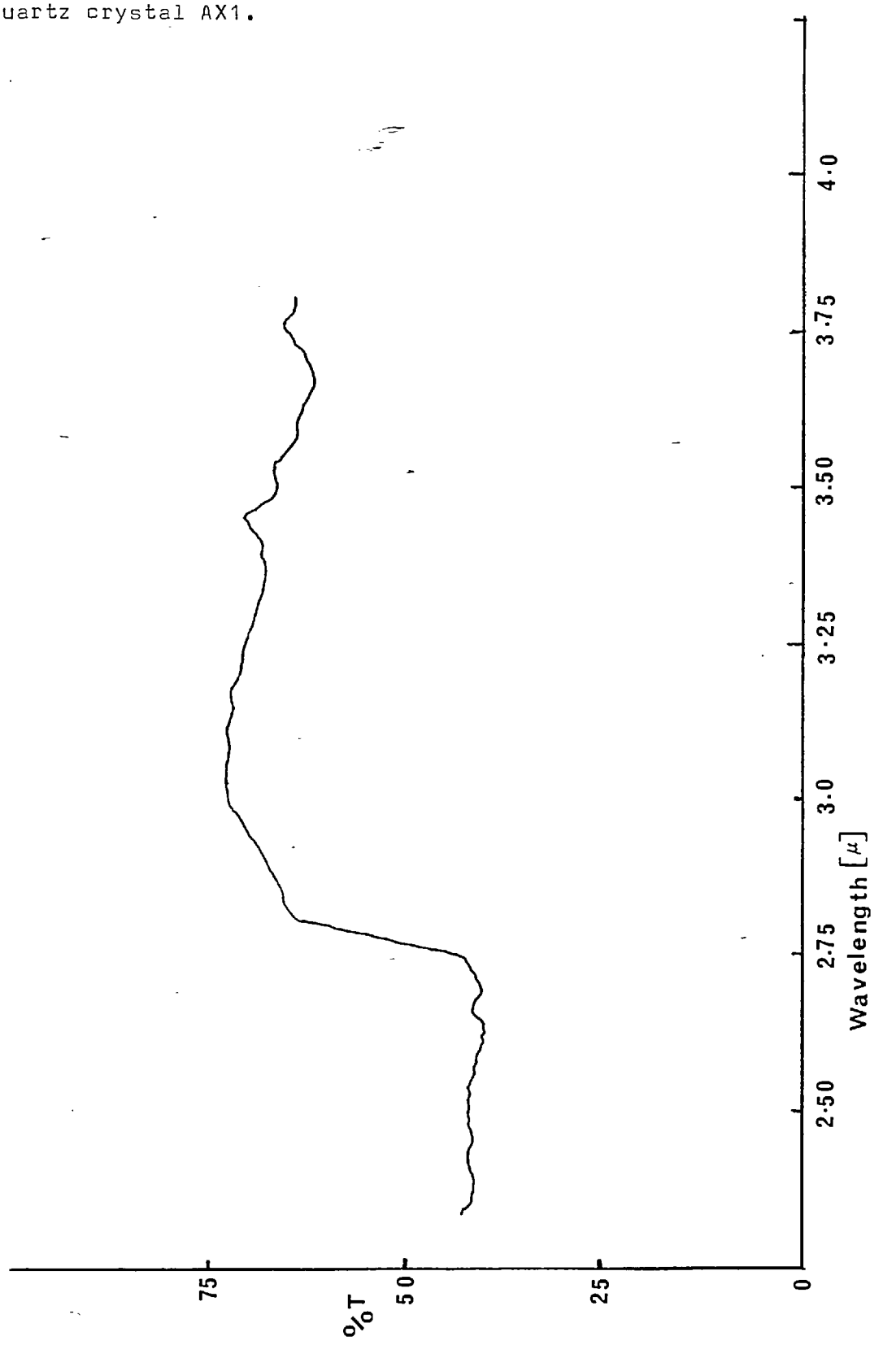

3.5. QUANTITATIVE ANALYSIS.

The intensity of an absorption band in the spectrum of a substance is related to the concentration of the absorbing ion by the Beer-Lambert Law (see below). Accurate quantitative analysis requires independant calibration to provide a proport--ionality constant called the absorption coefficient which relates the concentration to the intensity in the Beer-Lambert Law. Unfort--unately, no suitably accurate analytical technique is available to provide a calibration for the determination of the hydroxyl concentration in quartz crystals so that a value has to be assumed. This provides an unavoidable degree of uncertainty in all but the work of Kats (loc cit) who used an electro-chemical diffusion experiment to exchange H^+ ions for Li^+ and Na^+ ions in a synthetic quartz crystal. From this experiment he was able to determine a value for the absorption coefficient but even this was depend--ent on the assumption that the absorption bands had a simple shape (either Lorentzian or Gaussian curves). A second possible source of error in the interpretation of the spectra results from deviations from the simple Beer-Lambert relationship, and care must always be exercised in choosing a numerical technique in the analysis which minimises such effects.

3.5.1. The Beer - Lambert Law.

The Beer-Lambert Law states that the logarithm of the inten--sity of the absorption band is directly proportional to the concentration of absorbing molecules in the volume of sample penetrated by the beam. Thus, assuming the cross sectional area of the beam to be constant (which it is in all practical situ--ations),the absorbance is dependent only on the concentration of absorbing molecules, the frequency and the absorbing path length.

Figure 3.5. The passage of a number of monochromatic light quanta through an absorbing sample, the basis of the Beer - Lambert Law.

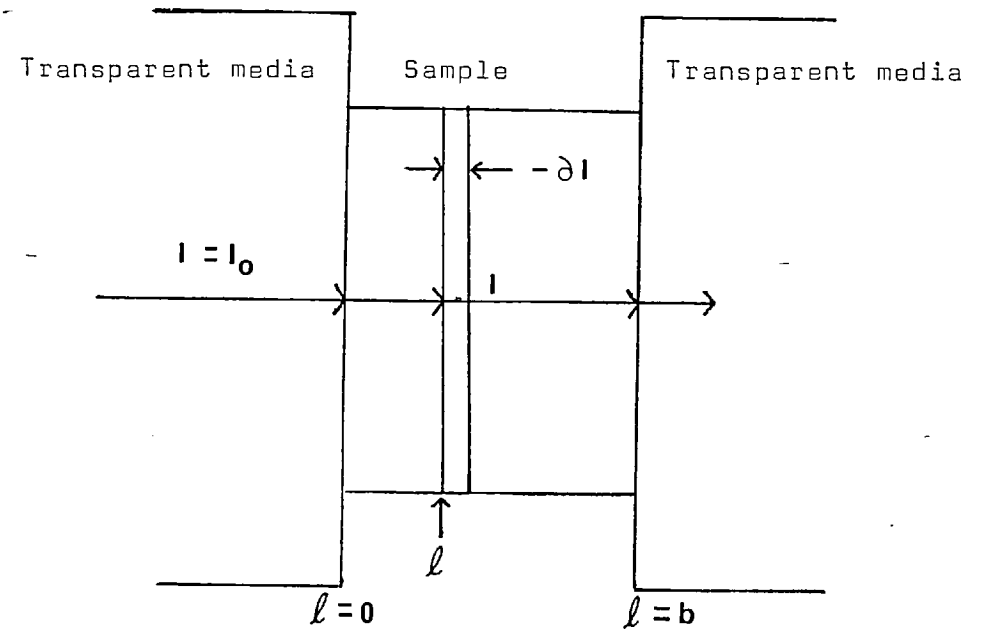

Taking the slice through the volume containing the absorbing molecules (figure 3.5) the number of monochromatic light quanta incident on the sample is I_0 and at some distance ℓ into the sample this is decreased in the differential slice at ℓ by $-\partial I$ (which has the units number of quanta $sec^{-1}cm^{-2}$). The number of quanta leaving the differential slice at ℓ is I and is proportional to I_0 , ℓ , $-\partial I$ and the concentration of absorbing molecules c . Thus :-

$$-\partial I = a'_A I c \partial \ell \qquad \cdot \qquad \cdot \qquad \cdot \qquad 3.1.$$

where a'_A is a constant of proportionality whose magnitude depends on the units of c and ℓ , and is a constant for a given molecule at a given frequency.

Integrating equation 3.1. gives the total decrease in intensity across the absorbing path $\ell = b$.

$$\int_{I_o}^{I} \frac{dI}{I} = -\int_{0}^{b} a' c \, d\ell = -a' c \int_{0}^{b} d\ell \quad . \quad . \quad 3.2.$$

thus $$\log_e \frac{I}{I_o} = -a' b c \quad . \quad . \quad . \quad . \quad .3. 3.$$

and converting to $\log_{10}$ by changing the magnitude of a' to a, we obtain

$$\log_{10} \frac{I}{I_o} = -abc \cdot \quad . \quad . \quad . \quad . \quad 3.4.$$

which is the normal presentation of the Beer-Lambert Law. The absorbance A, is defined as

$$A = \log_{10} \frac{I_o}{I} \cdot \quad . \quad . \quad . \quad . \quad 3.5.$$

3.5.2. The Absorption Coefficient.

The proportionality constant a is known variously as the absorption coefficient, extinction coefficient or absorpivity, sometimes symbolized e , and may be defined from equation 3.4,

$$a = \frac{1}{bc} \log_{10} \frac{I_o}{I} \cdot \quad . \quad . \quad . \quad . \quad .3.6.$$

clearly this is a constant for any molecule at any particular frequency. However in the literature the use of the term has be--come confused. Brunner (1961) discusses an 'extinction coefficient' which is defined as

$$e = \frac{1}{b} \log_{10} \frac{I_o}{I} \cdot \quad . \quad . \quad . \quad . \quad 3.7.$$

which is obviously a variable whose magnitude is proportional to the concentration of the absorbing ion. Dodd and Fraser (1967) have adopted this use but have called the variable the absorption coefficient. Throughout this study I have used the term absorption coefficient strictly in accord with the definition in equation 3.6.

This confusion extends beyond the literature pertaining to infrared studies of minerals e.g. Biggs (1975a,b),working on hydrogen filled cavities in MgO crystals,defines the absorp-tion coefficient in accord with equation 3.7 and this double usage of the term seems widespread in the materials science lit-erature.

In most analytical work, the absorption coefficient is cal-culated by calibrating the spectrometer using standards of known compositions, or the concentration is derived directly by solving equation 3.4 simultaneously for both the standard and the unknown sample and eliminating **a** . As samples of known composition are not available for the calibration of the spectrometer for struct-ural water in quartz determinations, a value for the absorption coefficient has to be assumed, this is discussed in section 3.6.1.

3.5.3. Deviations from Beers Law.

It should not always be assumed that the absorbance is a linear function of the product of cell length and concentration. Deviations from the Beer-Lambert Law do occur and result from two principal causes.

a). Chemical effects leading to variations in the shape and frequency of the absorption band, often due to reaction or association of molecules of the absorbing species with those of the transparent base or solvent carrying the absorbing molecules. The effect may be pronounced in the case of hydroxyl absorption in the quartz spectrum because of the differences between OH^- and hydrogen bonded OH^- absorption bands. This effect is prob-ably partially responsible for the convergence of the individual absorption bands recorded at 77^oK. when the temperature is increas-ed (Brunner et al 1961). In studies of hydroxyl ions in min-erals it is almost impossible to allow for such effects and they are generally ignored. Kats (1962) showed that even at 77^oK.

chemical effects caused convergence in some of the absorption bands, which may be regarded as representing a chemical deviation from the law, for in such cases the Gaussian (or Lorentzian) description of the peak shape fails, leading to a change in the absorption coefficient (see section 3.7.1.). Potts (1963) dis--cusses chemical deviations from Beers Law using OH^- and H bonded OH^- in phenols and alcohols as an example.

b). False measurement of the absorption band by the spect--rometer. This always occurs to some extent unless the frequency distribution of the radiation passed by the monochromator exit slit is considerably narrower than the absorption band. This can in part be overcome by the use of integrated intensities in Beers Law (section 3.5.4.). Although Potts (1963) discusses these spectrometer effects at length, I have summarized them in this section because they are pertinent to the choice of method used in reducing the spectroscopic data and in evaluating other publ--ished infrared results.

It can be shown (Potts 1963) that over a single symmetrical absorption, a as a function of frequency w is closely given by

$$a_{(w)} = \frac{\bar{K} \quad \mathcal{E}}{\Pi \ (w-w_o)^2 + \ \mathcal{E}^2} \quad . \quad . \quad . \quad . \quad 3.8$$

where $\bar{K}$ is the integrated intensity coefficient (see section 3.5.4.), w_o is the frequency at the band maximum and $\mathcal{E}$ is the halfwidth of the band, $2\mathcal{E}$ being the width of the band in cm^{-1}. measured at half the total absorbance. $\mathcal{E}$ is theoretically independent of the inherent strength of the absorption band. The absorption band described by equation 3.8 is Lorentzian and may be expressed in terms of transmission using equation 3.4.

$$\frac{I}{I_o}(w) = \exp\left[- \frac{\bar{K}\, b\, c \quad \mathcal{E}}{\Pi (w - w_o)^2 + \mathcal{E}^2} 2.3025 \right] . \quad . \quad . \quad 3.9$$

The solid curves in figure 3.6. show the form of this function for a selected range of values of the producted $b \cdot c$ for an arbitary half width δ .

A finite spectral slit width[1] allows a range of frequencies to pass through the monochromator and reach the detector when the spectrometer is set at a fixed frequency. Certainly the nature of the slit function is such that it will peak more or less sharply at w_o (as the slits are made narrow or wide respectively) and will fall to a small value at frequencies far removed from w_o. Thus the Gaussian or Error function may be taken to be a close approximation to the actual slit function.

$$P_{(w)} = P_o \exp\left[- \frac{(w - w_o)^2}{(\Delta w)^2} \right] \quad . \quad . \quad . \quad . \quad 3.10.$$

where $P_{(w)}$ is the monochromator output power at frequency w , P_o is the output power at w_o and Δw is the spectral slit width[1]. The dashed curves in figure 3.6 represent this function. In figure 3.6a. the curves suggest that a plot of absorbance versus the product $b \cdot c$ will be essentially linear, i.e. the spectrometer will closely obey Beers Law. This is hardly the case in figure 3.6c., whilst figure3.6b. will be an intermediate case.

Footnote 1.

The spectral slit width of an infrared spectrometer is defined according to the optical system employed by the monochromator. For a grating instrument similar to the Grubb Parsons Spectromaster, this gives:-

$$\Delta w = w^2 \frac{d \cos\theta}{2n} \frac{s}{f} + F_{[s]} \frac{w}{Mn}$$

where n = The diffraction grating order.
d = The diffraction grating constant.
θ = The angle of incidence or diffraction (essentially small).
M = The total number of lines on the grating.
$F_{[s]}$ = A function of the slit width the exact nature of which is still in doubt, but sometimes taken to be in the range 0.9 to 0.5 for narrow and wide slits respectively.
w = The frequency in cm^{-1}.
s = The slit width.
f = The focal length of the collimator.

Figure 3.6. Bandwidths and slit widths compared for various values of $\frac{\Delta W}{\mathscr{E}}$. From Potts (1963) page 178.

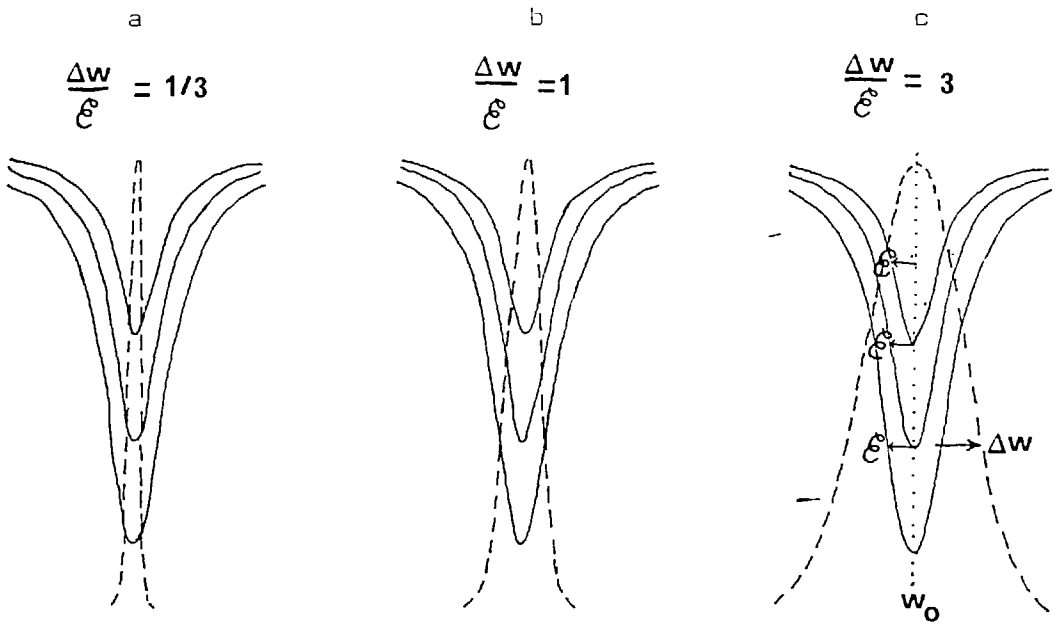

In order to determine the exact nature of the deviations from Beers Law produced by this situation, it is necessary to calculate the total amount of radiant energy per unit time (power) that will reach the detector when a monochromator of finite spect--ral slit width is set at w_o and a material having a Lorentzian shaped absorption band at w_o is placed in the beam. The power at any frequency w will be the product of equations 3,9 and 3.10.

$$P_{(w)}\left(\frac{I}{I_o}\right)_{(w)} = P_o \exp\left[-\frac{(w - w_o)^2}{(\Delta w)^2}\right] \exp\left[-\frac{\bar{K}bc \quad \mathscr{E}}{\Pi(w-w_o)^2+\mathscr{E}^2} 2.3025\right] \quad 3.11$$

The total power reaching the detector is this function integrated over the frequency range in which the recorded power level is great--er than the Johnson noise level[2]. The transmission measured by

Footnote 2.

The source of noise recorded by the spectrometer is due to the Johnson noise voltage produced in the detector circuit by random thermal drift of electrons in the conductors. The Johnson noise voltage is given by:- $E_j^2 = 4kTR(\Delta f).10^{-7}$
where E_j = The Johnson noise voltage, K = Bolzmanns Constant, T = The absolute ambient temperature, R = The resistance of the detector, Δf = The band pass of the amplifier (this is inversely proportional to the time constant) and the factor 10^{-7} converts ergs to joules. The Johnson noise is the limiting feature for intensity

the spectrometer is this integral divided by the total power that would reach the detector if no absorbing material were placed in the beam.

$$\left(\frac{\bar{I}}{I_0}\right)_{(w_0)} = \frac{\int P_0 \exp\left[-\frac{(w - w_0)^2}{(\Delta w)^2}\right] \exp\left[-\frac{\bar{K} b c \quad \mathcal{E}}{\Pi (w - w_0)^2 + \mathcal{E}^2} 2.3025\right] \cdot dw}{\int P_0 \exp\left[-\frac{(w - w_0)^2}{(\Delta w)^2}\right] \cdot dw} \quad 3.1$$

The integrals in equation 3.12 have been numerically evaluated (Potts 1963) and are plotted in figure 3.7 as a function of $A \left(= \log_{10}\left(\frac{\bar{I}_0}{I}\right)_{(w_0)}\right)$ versus the product $\mathbf{b} \cdot \mathbf{c}$. The dashed straight line results from an infinitesimal value of $\Delta w / \mathcal{E}$ (this is the ideal situation never obtained) the other curves are for values of $\Delta w / \mathcal{E}$ ranging from 0.1 to 10.0. It should be noted that not only is the correct value for the absorption coefficient not measured (= the slope of the line) but the curves increasingly depart from linearity as $\Delta w / \mathcal{E}$ increases.

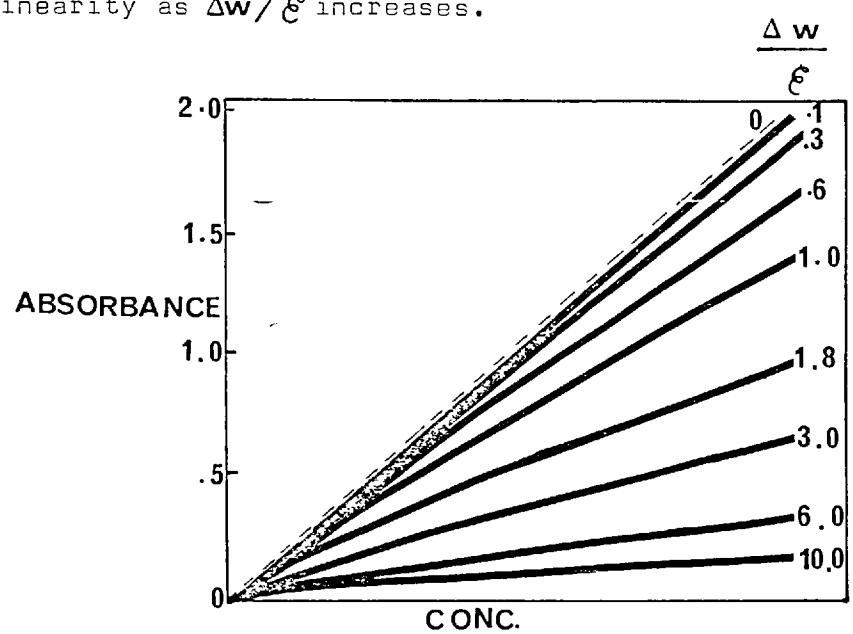

Figure 3.7. The effect of spectral slit width on absorbivity and the Beers Law relation. From Potts (1963) page 180.

Footnote 2 continued.
resolution in the spectrometer, and is generally seen as an oscilla-
-tion on the output chart. This oscillation must be minimised bef-
-ore recording a spectrum.

Because the relationship between absorbance and concentration is nearly linear over short ranges, it is possible, providing the analytical application is over a sufficiently small range of conc--entration, to use an absorption coefficient proportional to the average slope in that range. Under such circumstances, Beers Law will apply with only a very small error. However it is obvious from figure 3.7 that the absorption coefficient is strongly dep--endant on the spectral slit function of the spectrometer. Clearly a value for the absorption coefficient can only be applied to instruments with identical slit functions. Unfortunately it is not possible, for manufacturing reasons, to produce spectrometers with identical slit functions and thus the absorption coefficient for any band must be unique to the instrument on which it was determined. Only when $\Delta w / \varepsilon$ assumes a small value is it safe to assume that the absorption coefficient has a value that is close to the theor--etical maximum, and conversely, it is not safe to use the theoret--ical absorption coefficient unless this function has a very small value. Figure 3.8 shows the effect of changing the monochromator slit width (this is proportional to the spectral slit width[1]) on the spectromaster for a sample of piezoelectric grade natural quartz.

As the optimum monochromator slit width changes with frequency,[3] the spectromaster is fitted with a cam system which alters the slit width continually during a spectral scan. In normal routine analysis, use was made of this automatic program. Figure 3.8b shows a spectrum for the same piezoelectric grade crystal recorded using this program but with the amplifier gain set high to demonstrate the Johnson Noise[2].

Footnote 3.

The output power of an infrared source varies with frequency. This frequency dependance effects both the brightness and the radiant power and is compensated for mechanically by altering the monochromator slit width as the frequency is changed. This is done most simply by using an automatic cam system linked to the grating drive mechanism.

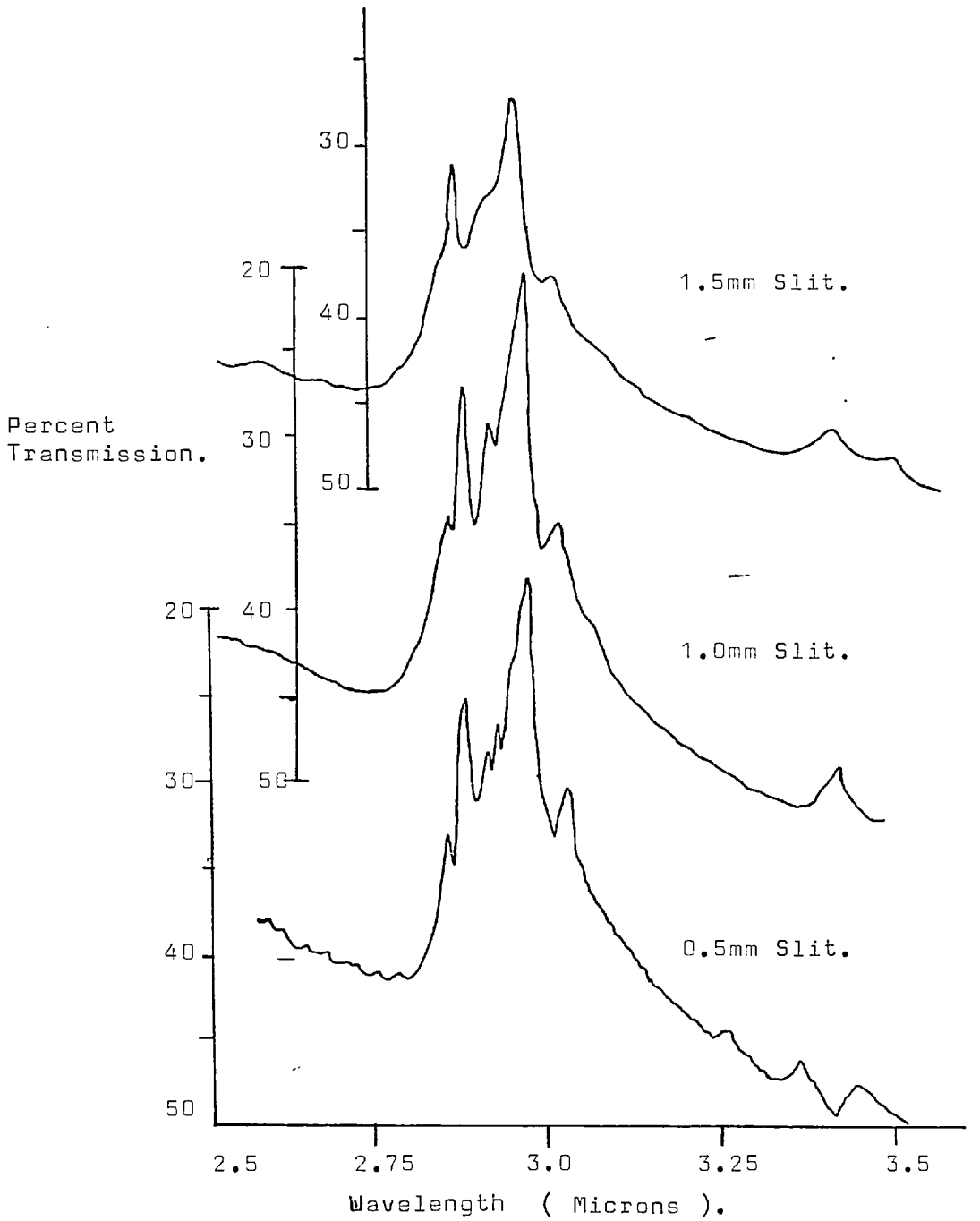

Figure 3.8a. The influence of the monochromator exit slit width on the frequency resolution. Crystal sample M1. The same plate was used for all three spectra.

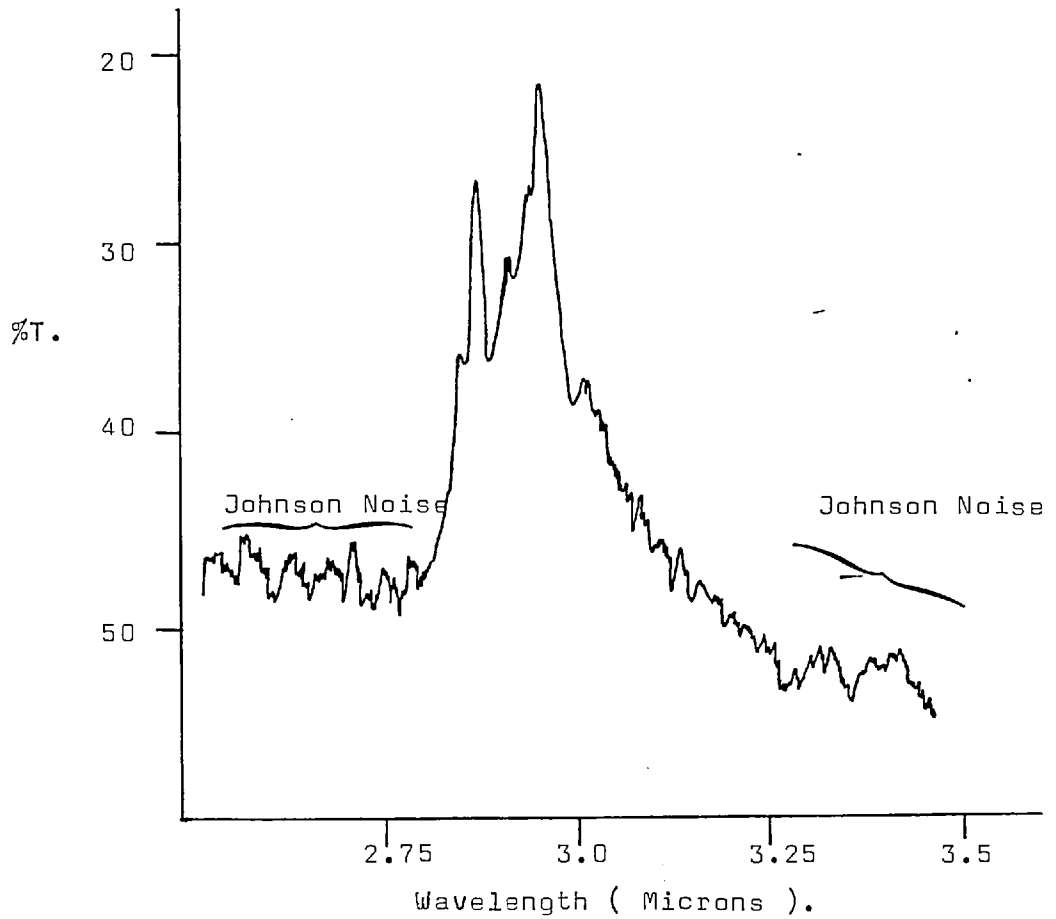

Figure 3.8b. The spectrum of the same sample from crystal M1 as shown in figure 3.8a. but recorded using the automatic slit program (program 10). In this instance the amplifier gain was increased slightly to demonstrate the Johnson Noise signal. This is clearly seen at the higher transmission values.

The Grubb Parsons Spectromaster is equipped with a variable slit program adjuster. This control is calibrated from 0 to 10 and alters the resolution of the instrument when it is operated with the automatic slit drive mechanism engaged. Decreasing the setting from 10 to 0 gives double the resolution, but the energy arriving at the detector is reduced to $\frac{1}{4}$ of its value at program 10. This necessitates increasing the amplifier gain which inturn gives a higher Johnson noise voltage. Thus in routine use, program 10 was used.

3.5.4. The Integral Intensity.

The absorption coefficient **a** has been shown to deviate from Beers Law, and to be particularly sensitive to the spectral slit function of the spectrometer. Further to this, **a** is dependent purely on peak height and does not distingush between narrow and broad absorption bands of similar height, even though a broad band represents a greater absorption than a narrow one. The inte--grated intensity of an absorption band is a number equivalent to the absorption coefficient at the band maximum but which considers the total absorption of the band and thus has a greater theoretical significance. The first integral intensity $\bar{K}$ is defined:-

$$\bar{K} = \int_{band} a_{(w)} \cdot dw \qquad . \qquad . \qquad . \qquad . \qquad 3.13$$

This is also called the true integral intensity and is defined by equation 3.13 when $a_{(w)}$ is the theoretical value obtained from a spectrometer with a spectral slit width which approaches zero. When the spectrum is recorded on a spectrometer with a finite spectral slit width, the second integrated intensity **K** is deter--mined according to:-

$$\bar{K} = \int_{band} a_{(w)} \cdot dw \qquad \geq \qquad K = \frac{1}{b.c} \int_{band} \log_{10}\left(\frac{I_o}{I_{(w)}}\right) \cdot dw \qquad 3.14$$

Departure of **K** from $\bar{K}$ increases as $\Delta W / \mathcal{E}$ becomes larger, but it has been shown (Kostkowski and Bass 1956) that the departure of **K** from $\bar{K}$ is much less severe at high values of $\Delta W / \mathcal{E}$ than shown in figure 3.7 for $a_{(W)}$. For example, if $\Delta W / \mathcal{E} = 1.0$ at an absorb--ance of 0.3 then **K** is only 2% less than the theoretical value whilst $a_{(W)}$ is 25% lower. In figure 3.9 the products **K.b.c** and $\bar{K} \cdot b \cdot c$ are plotted against the product $b \cdot c$. The resulting curves are analogous to those in figure 3.7 but show the closer approx--imation to the theoretical value when integrated intensities are used.

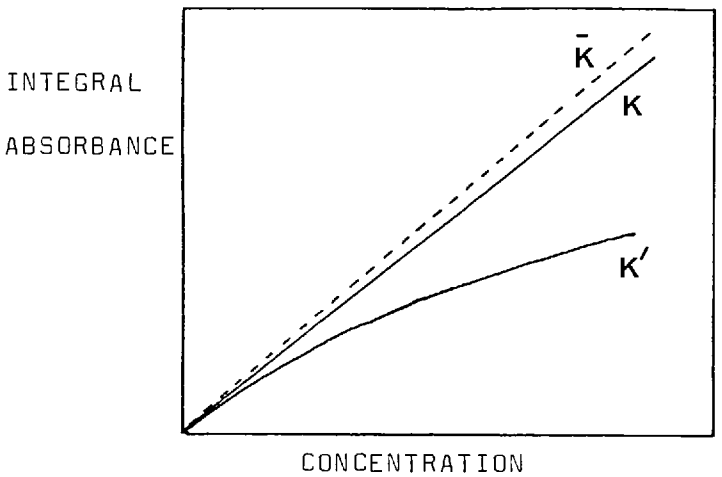

Figure 3.9. Plots of Integral absorbance versus concentration for the three types of integral intensity coefficient in use. The curves for K and K' are constructed for a spectrometer with $\Delta W/\mathcal{E} = 1.0$.

A third type of integrated intensity K' is given by equation 3.15 and although easily determined experimentally was not used in this study. This function is non-linear over the full concen-tration range and the absorption coefficient has to be computed for each value of the absorbance.

$$K' = \frac{1}{bc}\int_{band}\left(1-\left(\frac{I}{I_o}\right)_{(W)}\right).dW \qquad 3.15$$

This function is also plotted in figure 3.9 which shows clearly its strong departure from linearity. This curve does however have a known analytical form given by:-

$$K'bc = X e^{-X}\left(I_j(X) + I_k(X)\right) \qquad 3.16$$

where

$$X = \bar{K}bc/2\Pi\mathcal{E} \qquad 3.17$$

and $I_j(X)$ and $I_k(X)$ are Bessal functions with all terms positive. This type of analysis is only of use when standards are available to calculate one point on the curve K' in figure 3.9 from

which $\bar{K}$ can be obtained using equations 3.16 and 3.17.

3.6. THE ANALYSIS OF QUARTZ SPECTRA

Having discussed Beers Law and its limitations it is now possible to apply it directly to the evaluation of the 3500cm^{-1} absorption band for quartz,but with one major reservation conc--erning the value of the absorption coefficient.

3.6.1. The Quartz Absorption Coefficent for the 3500cm^{-1} Band.

Studies of the concentration of structure bound water in quartz crystals are seriously hampered by the complete absence of suitable standard samples for calibration. It is thus neces--sary to make certain assumptions and use a standard value. Clearly from section 3.5.2. this cannot be a value for $a_{(w)}$ because this would only be valid for one spectrometer in one laboratory. Further the absorption band at 3500cm^{-1} in synthetic quartz is very broad (in many cases differences in concentration are reflected more by changes in band width than in the peak height) so $a_{(w)}$ would not act as a true measure of the absorbance. It is thus essential to use the integrated intensity.

Scholze (1960) evaluated an integral absorption coefficient for molecular water, mica and silica glass (table 3.1.) and it is from these results that Brunner et al (1961) took a value of 14000 litre/gram atm. H / mole in his studies on hydrogen in quartz. This value has subsequently been widely used by other workers (Bambuer 1961, Griggs and Blacic 1965, 1967, Hobbs et al 1972, Jones 1975, this study) and has become the standard value. It has been used throughout this study.

From table 3.1. it is seen that $\overset{c}{\underset{\lambda}{S}}$holze(1960) quotes a value of 22000 litre/ mole cm^2 for the integral absorption coefficient for molecular water. It would thus appear that if the structure bound water in a quartz crystal were precipitated as molecular

water (see chapter 5) then the infrared absorption would be increased by a factor of 1.57. However molecular water contains two hydrogen - oxygen bonds in each molecule whereas the hydroxyl in quartz contains only one such bond per ion. Thus dehydration of the quartz structure will yield only half the number of water molecules as there were originally hydroxyl ions and this in turn will lead to a reduction in infrared absorption by a fact-or of 1.27. I have independently calculated the absorption coefficient for molecular water on the Grubb Parsons Spectromaster and have found that a five fold reduction in intensity of absorp-tion would occur if the structural water in a quartz crystal were precipitated out in molecular form (see section 3.9).

Table 3.1. Values of the integral intensity **K** (litre/mole cm^2), the absorption coefficient at the band maximum $a_{(w)}$ and the frequency of the band maximum **W** (cm^{-1}). From Scholze (1960).

SUBSTANCE	W	$a_{(W)}$	K
Water	3389	55	22000
Silica Glass	3508	70	27000
Muscovite Mica	3610	170	11000

3.6.2. Measuring I and I_0 .

The Grubb Parsons Spectromaster presents the spectrum as a curve of I against the frequency, and it is therefore only nece-ssary to recognise the band to read off values of I directly, across the frequency range of the band. Values for I_0 are also read directly from the recorded spectrum but in this case it is necessary to fit a baseline to the absorption peak because as a general rule the incident intensity cannot be taken to be 100% transmission. The construction of this baseline is subjective

and for some specimens (particularly synthetic quartz or crystals with very small values of the absorbance) can be very difficult to fix with any reliability. Figure 3.10 gives examples of base-lines fitted to different quartz absorption bands and demonstrates the difficulties which may be encountered in some analyses.

A further problem that may seriously affect the accuracy of the analysis is that a baseline fixed in this manner assumes that the percentage of incident radiation is constant, or varies lin--early with frequency. It is probable that for quartz this is not the case. Figure 3.10e shows a spectrum to which a curved baseline could be fitted rather than the straight line approximation that is used. Unfortunately it is possible that the baseline is even more complex so that the added problems of assuming a curved base--line will probably not provide any greater degree of accuracy and will impair the reproducibility of the technique. For this reason straight baselines were used throughout this study.

Differences in the choice of baseline can lead to very significant differences in concentrations recorded by workers in different laboratories analyzing the same material. This is dem--onstrated in table 3.2 which compares the analyses conducted by Griggs with those performed during this study on the same crystals. The differences in recorded concentration may be attributed to both differences in the chosen baseline and the systematic variat--ion in the water concentration in the crystals, (a variation app--arently not recognized by Griggs when he sent samples to other laboratories to calibrate their spectrometers).

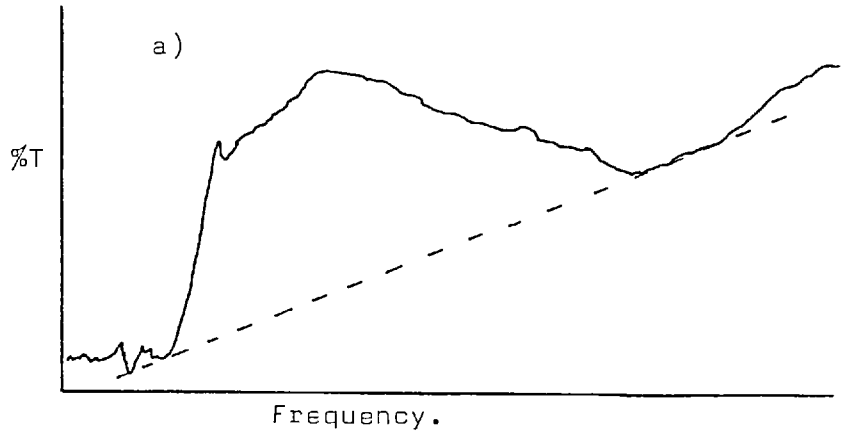

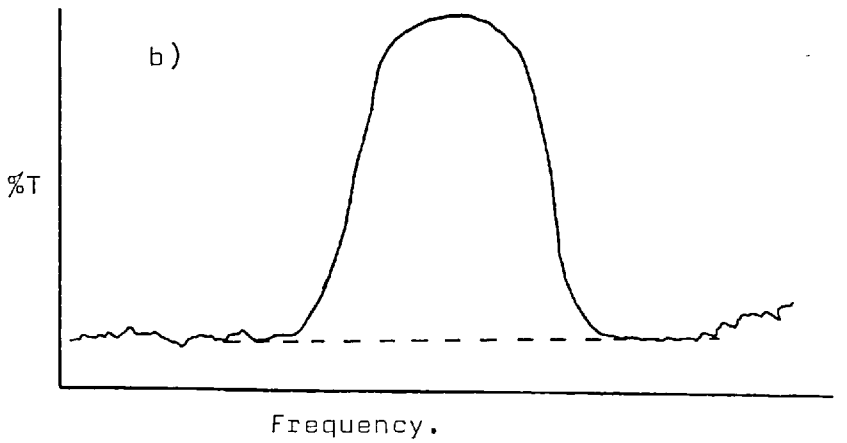

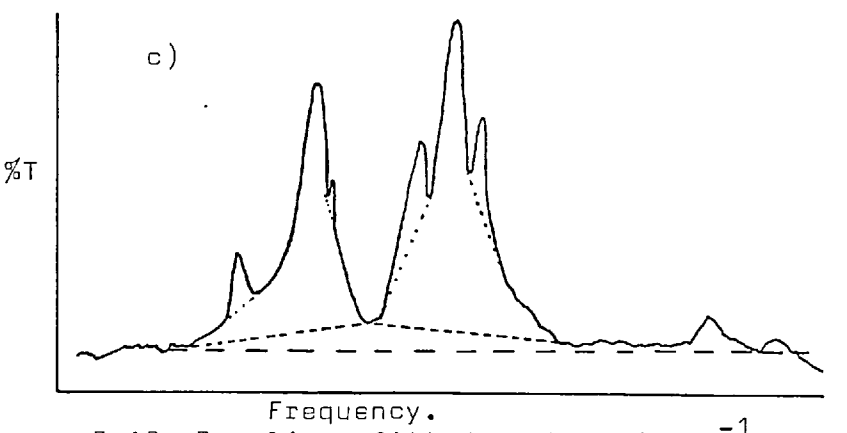

Figure 3.10. Baselines fitted to the 3500cm^{-1} absorption bands for a) a wet synthetic crystal, b) a wet natural crystal and c) a Brazilian type natural crystal.

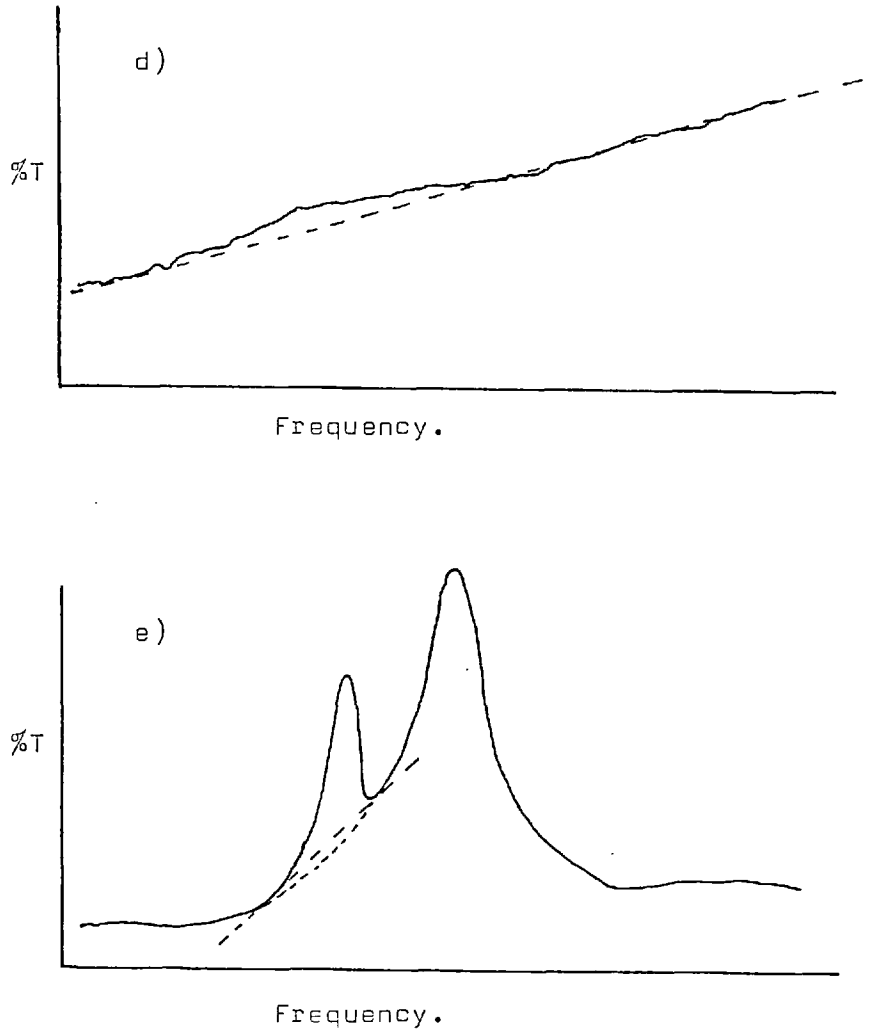

Figure 3.10 continued. d). Baseline fitted to the spectrum of a dry synthetic quartz crystal, and e). A situation where a curved baselines could possibly be used, simplified spectrum of a Brazilian type natural quartz crystal.

Table 3.2. A comparison of the hydroxyl concentrations originally measured by Griggs (loc cit)and subsequently modified by Blacic (1975), with those determined from the same crystals during this study. The differences can be attributed to differences in the choice of baseline in all but crystal X13. For this crystal it is thought that the sample supplied was cut from a dry growth band (Dodd and Fraser 1967, this study chapter 4). Crystals Xo, X13 and X43 are synthetic, A1 is a natural crystal from Brazil. Concentrations are given as $H/10^6 Si$.

Sample No.	Griggs original determination	Griggs Revised determination	This study
Xo	8000	4350	2750
X13	5000	2575	525
X43	3000	1425	1125
A1	20	10	45

3.6.3. Measuring the Cell Length **b**.

For samples cut from single crystals, the cell length was easily determined, it being simply the thickness of the quartz plate, measured parallel to the direction of propagation of the infrared beam. This measurement is made with a micrometer, but care must be exercised when making the measurement because the determined concentration is linearly dependent on the value of **b**. In this study measurements were made with a one inch micro--meter screw to an accuracy of better than 0.001 inches. This is converted to centimeters in the data reduction program (appen--dix 2).

When pressed disc samples were used, the determination of *b* is more difficult and far less accurate, this is reflected in the poorer reproducibility of spectra from pressed disc samples. Differences in compressibility and compaction between the potas--sium bromide and the mineral sample results in the contribution of the KBr to the thickness of the disc being greatly reduced from the original concentration ratio. This ratio cannot then be used as a dilution factor. Also the path taken by a quantum of radia--tion passing through the disc is lengthened by reflection and refraction effects from the surfaces of the finely powered min--eral grains. Thus the path length cannot be simply related to the thickness of the disc, nor to the original ratio of concent--rations. This problem was overcome by calibrating the spectrom--eter using discs made from quartz samples of previously known structure bound water concentration (prepared from analyzed single crystal plates). This calibration was performed by plotting the concentration as determined using the total thickness of the disc against the ratio of quartz to KBr in the sample and it was found that a disc prepared from a ratio of 5 KBr to 1 quartz gave a concentration which was very close to (but always less than) the

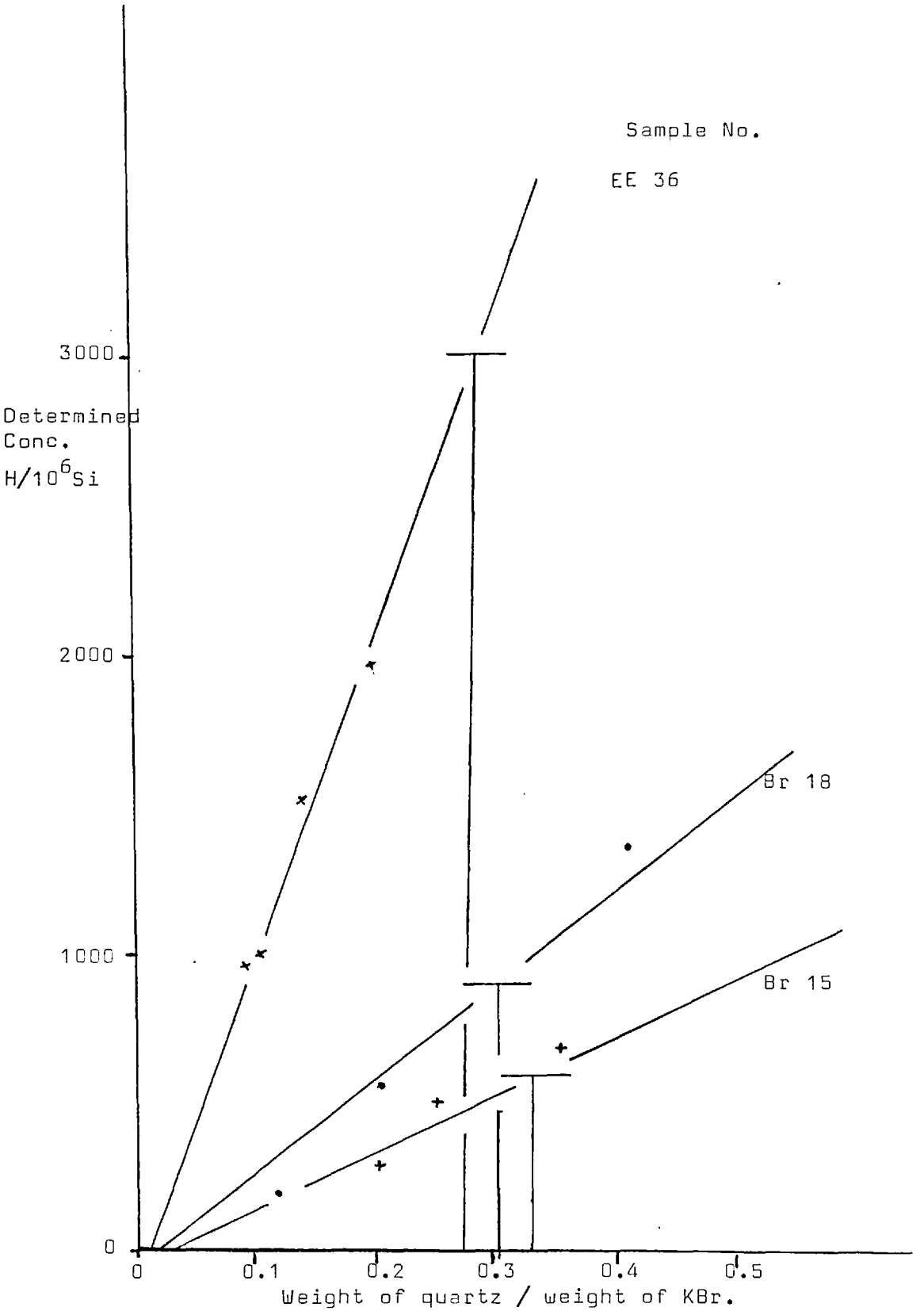

Figure 3.11 Pressed disc samples thickness calibration.

actual concentration determined using a single crystal plate. Discs were always prepared using this ratio of weights (0.2 on the graph) and the grinding procedure outlined in appendix 1 was strictly adhered to. Figure 3.11 shows these calibration curves for pressed disc samples. Because of the ratio taken it is known that all the recorded concentrations err on the low side for pressed disc samples and can be safely assumed to be minimum values.

Because of the problems of measuring **b** in pressed disc samples, they were used as infrequently as possible, but it proved necessary to resort to them if fine or medium grain size quartz rocks were to be considered, generally however only large crystals from veins which could be cut into plates were used. The reliability of analyses from pressed disc samples is reduced still further if the quartz and KBr are poorly mixed prior to pressing, or if the mixture is unevenly distributed in the die, for both will lead to an irregular distribution of the mineral in the disc.

3.6.4. Determining the Concentration.

As stated in section 3.6.1. an assumed value has to be used for the integral intensity, substituting this into equation 3.14 and rewriting to give the concentration directly gives:-

$$c = \left(\int_{band} \log_{10}\left(\frac{I_o}{I}\right)_{[W]} \cdot dW \right) \Big/ 14000.b \qquad 3.18$$

To account for the anisotropic nature of the hydroxyl stretching vibration in quartz (see sections 3.7.1 and 3.8) Brunner et al (1961) multiplied the right hand side of equation 3.18 by 2/3.

$$c = 2\left(\int_{band} \log_{10}\left(\frac{I_o}{I}\right)_{[W]} \cdot dW \right) \Big/ 3.14000.b \left[Gr.Atm.H/Litre\, Si\, O_2 \right] \qquad 3.19$$

Traditionally following the work of Bambuer (1961) (see section 3.6.5.), structure bound water concentrations have been presented in the units hydrogen atoms per million silicon atoms ($H/10^6 Si$).

This is done by multiplying equation 3.19 by $m.10/\rho$ where m is the molecular weight (~60 for quartz) and ρ is the density (2.66 for quartz) giving:-

$$c = 2\left(\int_{band} \log_{10}\left(\frac{I_o}{I}\right).dW\right)\left(m.10^3\right)\Big/ 3.14000.\rho\left[H/10^6 Si\right] \qquad 3.20$$

Simplifying equation 3.20 by changing the units of the integral intensity gives a value of 0.617 $H^{-1}.10^6 Si.cm^{-2}$ for this cons--tant and multiplying through by 2/3 gives

$$c = \left(\int_{band} \log_{10}\left(\frac{I_o}{I}\right).dW\right)\Big/ 0.926b\left[H/10^6 Si\right] \qquad 3.21$$

which is the relationship used throughout this study. The integral in this equation can easily be evaluated numerically using Simpsons rule :-

$$\int_{i=1}^{m} F_i.di \simeq \frac{m/n}{3}\left\{F_o + F_n + 4\left(F_1 + F_3 - - - - - + F_{n-1}\right) + 2\left(F_2 + F_4 - - - - - + F_{n-2}\right)\right\} \qquad 3.22$$

and a fortran computer program has been written to facilitate data reduction (see Appendix 2).

3.6.5. Bambuers Error.

As stated in section 3.6.4. Bambuer (1961) was the first worker to use the units $H/10^6 Si$ and this practice was subsequently adopted by Griggs et al (loc cit) and used by all workers inter--ested in hydrolytic weakening. Unfortunately the conversion factor used by Bambuer is incorrect. Bambuer started from equation 3.19 and multiplied by $\rho/m.10^6$ to effect the conversion giving:-

$$c = 2\left(\int_{band} \log_{10}\left(\frac{I_o}{I}\right).dW\right)\left[\rho/m.10^6\right]\Big/ 3.b.14000 \qquad 3.23$$

A consideration of the units employed in this conversion demon--strates that the factor used by Bambuer is incorrect giving results which are too large by a factor of 2. The necessary units for the integral absorption coefficient are $10^6 Si/H/cm^2$; where the unit cm^{-2} is necessary to satisfy both the frequency term and the cell

path lemgth term in equation 3.19. The original units of this term are litre SiO_2/Gram Atom H/cm^2 and this has been given the value of 14000 in the original Brunner equation (3.19 in this chapter). Writing 14000cm^2= **N** for simplicity the conversion can be written in the form:-

$$\mathbf{N}'\left[10^6 Si/H\right] \quad = \quad \mathbf{N}\left[\text{Litre/Gram atom H}\right] \times \mathbf{A}$$

where **A** is the conversion factor. Multiplying the right hand side by 1000 changes its units to 1000$cm^3 SiO_2$/ Gram Atom H and this means that an absorption of strength **N** X 1000 $cm^3 SiO_2$ is caused by 1 Avogadros number of hydrogen atoms, the atomic weight of a single hydrogen atom being 1 (= 6.023 X 10^{23} hydrogen atoms). So:-

$$\frac{\mathbf{N} \times 1000\left[cm^3 SiO_2\right] \times \mathbf{A}}{6.023 \times 10^{23}\left[\text{H atoms}\right]} \quad = \quad \mathbf{N}'\left[10^6 Si/H\right]$$

1 mole of quartz weighs 60.09 grams and each mole contains 6.023 x 10^{23} SiO_2 molecules. 2.65 gram of quartz has a volume of 1c.c. Thus 1000 cm^3 SiO_2 contains:-

$$\frac{6.023 \times 10^{23} \times 2.65 \times 1000}{60.09} \quad = \quad 2.6561 \times 10^{25}\left[\frac{\text{molecules}}{SiO_2}\right]$$

The absorption due to 2.6561 X 10^{25} molecules of SiO_2 containing 6.023 X 10^{23} hydrogen atoms is 14000 (in the original units) and from this the absorption due to 1 hydrogen atom in 2.6561 X 10^{25} silica molecules will be:-

$$\frac{14000}{6.023 \times 10^{23}} \quad = \quad 2.344 \times 10^{-20}$$

The absorption due to 1 hydrogen atom in 10^6 silicon atoms is then:-

$$\frac{2.3244 \times 10^{-20} \times 2.6561 \times 10^{25}}{10^6} \quad = \quad 0.617.$$

Dividing the recorded value for the integral absorption by this value will give a solution in the units H/10^6Si. The conversion factor being:-

$$\frac{\rho \times 10^3}{m \times 10^6} \quad = \quad \frac{\rho}{m \times 10^3}$$

where ρ is the density of quartz,

and m is the molecular weight.

Griggs (loc cit) used equation 3.23 when reducing his spect--roscopic data and the resulting error remained in his published data until corrected by Blacic (1975). This error presumably went unnoticed for so long because after the initial analyses of the Griggs synthetic crystals were conducted, the recorded values were taken as fact and the analyses never repeated. Samples from the Griggs crystals were used for calibration in the work of Mclaren (1965b,1966a, 1969) and Hobbs (1968, 1972) so that the hydroxyl concentrations reported in every major American and Australian publication on hydrolytic weakening prior to 1975 are too large by a factor of two. The possibility that Griggs never repeated his spectroscopic work and that he apparently failed to check it properly for reproducibility by using more than one sample for infrared analysis from the same crystal is indicated by the fact that he did not detect the presence of growth bands in his synthetic crystals. These growth bands are present in all synthetic crystals and are responsible for a systematic large variation in concentration throughout the crystal structure (Dodd and Fraser 1967, this study chapter 4).

3.7. OTHER QUANTITATIVE PROCEDURES.

Two relationships other than equation 3.21 have been used to determine the concentration of structure bound water from the quartz 3500cm^{-1} absorption band. The first, that of Kats (1962) is extremely accurate, but can only be used in the analysis of high resolution spectra in which the absorption bands assume a Gaussian or Lorentzian shape. The second, used by Dodd and Fraser (1967) is a very poor approximation which they were forced to use by the nature of the experiments they were conducting.

3.7.1. The Kats Method

Kats (1962) in his high resolution study of the hydroxyl and O D vibrations in the quartz spectrum, was able to restrict his work to absorption bands of strictly gaussian form and be - -cause of this he was able to derive an expression for the conc- -entration directly from quantum mechanical considerations. This analysis is repeated below.

Assuming that the OH and OD stretching vibrations may be described as harmonic oscillators Crawford (1950) has shown that the quantum mechanical relation:-

$$\bar{K} = \left(8\,\Pi^3 NW/3hc\right)\left(\left[M\right]^{n,m}\right)^2 \qquad 3.24$$

is valid for this model where N = the number of molecules per cm^3,

c = the velocity of light,

h = Planks constant,

$\bar{K}$ and W have their usual meanings

and $\left[M\right]^{n,m}$ is the electric transition dipole moment between the states n and m such that:-

$$\left[M\right]^{n,m} = \int \psi_n \psi_m^{*} M.d\tau \qquad 3.25$$

where ψ_n ψ_m are the time dependent eigen functions of the system in the states n and m. The transition between n and m is proport- -ional to the square of this factor which has been expanded by Waldron (1955) for the transition dipole of an isotropic oscillator in a power series in the normal coordinate r.

$$\left[M\right]^{n,m} = M_o\int \psi_n \psi_m^{*}\, d\tau + \left(dM/dr\right)\int \psi_n r\, \psi_m^{*} d\tau + \frac{1}{2}\left(d^2M/dr^2\right)\int \psi_n r^2 \psi_m\, d\tau + \ldots \qquad 3.26$$

The first term vanishes and the third term is zero for harmonic vibrations, whilst terms higher than quadratic may be neglected. Now for harmonic oscillators, the integral:-

$$r^{01} = \int \psi_n \, r \, \psi_m^* \, d\tau = \left(\frac{1}{2}a\right)^{1/4} \qquad 3.27$$

where **a**, the polarizability, is given by:-

$$a = 4\Pi^2 \, m.c.w/h \qquad 3.28$$

and **m** is the reduced mass. Thus equation 3.26 simplifies to

$$\left[M\right]^{n,m} = \left(\frac{1}{2}a\right)^{1/4} \frac{dM}{dr} \qquad 3.29$$

because

$$\left\{\left[M\right]^{n,m}\right\}^2 = \left(\frac{1}{2}a\right)\left(\frac{dM}{dr}\right)^2 = \left(h/8\Pi^2 m.c.w\right)\left(\frac{dM}{dr}\right)^2 \qquad 3.30$$

and equation 3.24 now becomes

$$\bar{K} = \left(N\Pi/3m.c^2\right)\left(\frac{dM}{dr}\right)^2 \qquad 3.31$$

Equation 3.31 is only applicable to the gaseous state and must be corrected for molecular vibrations in crystals. These corrections are difficult to specify and Kats (1962) overcame the problem by introducing the effective charge for the vibrating ion in which all the corrections due to polarizability of the medium and other factors are contained. The relative effective charge **p** is defined by:-

$$e = p\,e_o = \frac{dM}{dr} \qquad 3.32$$

where e_o is the elementary charge on the electron. Substituting into equation 3.21 gives:-

$$\bar{K} = N\Pi e_o^2 p^2/3mc^2 \qquad 3.33$$

This is valid for an isotropic oscillator with three degrees of freedom represented by the factor $\frac{1}{3}$, but Kats (1962) showed that OH and OD vibrations in quartz act as anisotropic oscillators and that the component of the dipole parallel to the c crystallographic axis has only one degree of freedom, thus equation 3.33 may be

rewritten as:-

$$\bar{K} = N\Pi e_o^2 p^2 / mc^2 \qquad 3.34$$

The absorption spectra recorded by Kats (1962) for OH and OD vibra--tions could be represented by Gaussian curves described by the relation

$$a_{(w)} = a_{(m)} \exp\left\{-\left(4 \ln 2 / \mathcal{E}^2\right) h^2 w^2\right\} \qquad 3.35$$

where a_m is the absorption coefficient at the peak of the absorption band and $\mathcal{E}$ is the halfwidth of the band. The integral intensity $\bar{K}$ is then given by:-

$$\bar{K} = \int_{band} a_{(w)} \cdot dw = \left\{\left(\Pi^{1/2}/2\left(\ln 2\right)^{1/2}\right)\mathcal{E} a_{(m)}\right\} = 1.0645\, a_{(m)} = 1.0645K \qquad 3.36$$

substituting into equation 3.33 gives the expression for p^2.

$$p^2 = 1.0645\, m.c^2 K / N\Pi e_o^2 \qquad 3.37$$

where m is the reduced mass of the oscillator defined as

$$1/m = 1/m_H + 1/m_o \quad \text{or} \quad 1/m = 1/m_D + 1/m_o \qquad 3.38$$

and from this the reduced mass of the OH and OD oscillators can be calculated

$$m_{OH} = 1.5167.10^{-24}\ g$$

and

$$m_{OD} = 2.8636.10^{-24}\ g$$

and as $c = 2.9979.10^{10}$ cm sec. and $e_o^2 = 2.3068.10^{-19}$ abs. e.s.u , then $p^2 = 2.001.10^{15}\, K/N$ for the dipoles of OH vibrations parallel to the optic axis and $3.779.10^{15}\, K/N$ for OD vibrations. Measuring with light polarized perpendicular to the optic axis, dipoles orientated perpendicular to the optic axis have two degrees of freedom in which case p^2 takes values of $4.003.10^{15}\ K/N$ or $7.558.10^{15}\ K/N$ for OH and OD vibrations respectively. Measuring

with unpolarized light, the dipole with a direction perpendicular to the optic axis, the intensity of the absorption of the infrared beam incident parallel to the optic axis is exactly twice as large as when the infrared beam is incident perpendicular to the optic axis. Thus if the dipole is perpendicular to the optic axis values of $4.003.10^{15} K/N$ or $7.558.10^{15} K/N$ are valid for measuring the absorption of unpolarized light incident parallel to the optic axis for OH and OD vibrations respectively. In the case where the unpolarized light is incident perpendicular to the optic axis these constants must be choosen twice as large. Kats(1962) deter--mined values for **K** and **N** using a diffusion exchange experiment, the only recorded exact calibration of a spectrometer for the analysis of hydroxyl in quartz, and this gave the relative effect--ive charge for the hydrogen ion **p** as 0.43. If however a lorentzian approximation is used for the shape of the absorption band the constant in equation 3.36 becomes $\Pi/2$ and in this case **p** =0.52. From these calculated values for hydrogen Kats (1962) was able to calculate using D/H echange experiments the ratio $\bar{K}_D / \bar{K}_H = 0.38$ which gave values for **p** for duetrinium of 0.37 and 0.45 for the gaussian and lorentzian approximations respectively. From this it is easy to obtain direct relationships between **K** and the concentration **N** which for the gaussian approximation are:-

$$N_H = 2.16.10^{16} K \left[H.atms\, cm^{-3} SiO_2 \right] \qquad 3.39$$

and

$$N_D = 5.52.10^{16} K \left[D.atms\, cm^{-3} SiO_2 \right] \qquad 3.40$$

For the OH and OD vibrations respectively, measured with unpolarized light incident in the direction of the c crystallographic axis.

3.7.2. The Simplification used by Dodd and Fraser (1966)

Dodd and Fraser (1967) set up a spectrometer to scan at constant frequency across a crystal plate so to observe the variation in hydroxyl concentration. The output from the spectrometer in this case is the absorbance at constant frequency (they used 3500cm^{-1}) verses distance or time so that the complete absorption band cannot be measured. To equate the measured absorbance with the actual concentration they used a relationship

$$c = 0.01\, a_{3500}\left[\text{Wt }\%_{o}\text{ H bonded OH}\right] \qquad 3.41$$

where a_{3500} is defined in accord with the work of Brunner ($= \frac{1}{b}\log_{10}\left(\frac{I_o}{I}\right)_{3500}$) and incorrectly termed the absorption coefficient at 3500cm^{-1}. This relationship is subject to all the problems discussed in section 3.5.3b because it does not use the integral intensity and hence is probably not directly transferrable between spectrometers it is thus of little analytical use. Dodd and Fraser (1967) do not derive the expression nor do they show where the constant 0.01 comes from, it is probable that it is an assumed value which may have been accurate on their instrument but which proved to be greatly in error when used on the spectromaster and compared with concentrations determined by the integral intensity method.

3.8. THE EFFECT OF ORIENTATION.

The detailed study of Kats (1962) (section 3.7.1) shows that the magnitude of the integral intensity is strongly sensitive to the crystallographic orientation of the sample with respect to the beam direction. The intensity of the absorption being modified by as much as a factor of 2. This however is established working at high resolution and considering the absorption caused by a single vibration dipole in a particular direction. In the spectra recorded in this study, the resolution is low and the

recorded band in most instances results from the overlap of the effects of all the dipoles favourably orientated to absorb. Thus when the broad absorption band of a synthetic quartz crystal is analyzed, the recorded concentration is almost independent of the orientation (care must be taken not to confuse any systematic growth variation with such orientation effects see chapter 4), most certainly any orientation effects are contained within the limits of reproducibility of the results recorded from this spect--rometer (see appendix 1). Table 3.3 gives the effect of changing the direction of beam incidence from parallel to c to normal to c in several samples of quartz and figure 3.12 shows the effect on the shape of the absorption band.

Table 3.3 The effect of orientation on the recorded hydroxyl concentration.

Crystal.	Incidence Parallel to c. $H/10^6 Si$	Incidence Normal to c. $H/10^6 Si$
AX1	1000	950
ITT4	175	180
ITT6	275	300
M1	420	350
Br5	25	-

Crystals AX1, ITT4 and ITT6 are synthetic crystals showing broad low resolution absorption bands. Crystals M1 and Br5 are natural Brazilian type quartz crystals and exhibit much higher frequency resolution in their recorded spectra, note that it is these crystals which show an orientation effect.

In the relationship used by Brunner et al (1961) and adopted in this study (eq 3.19) a factor 2/3 appears, this is related to the orientation effects discussed by Kats (1962). It would appear that this term is related both to the number of degrees of free-

Figure
3.12
Caption
over leaf

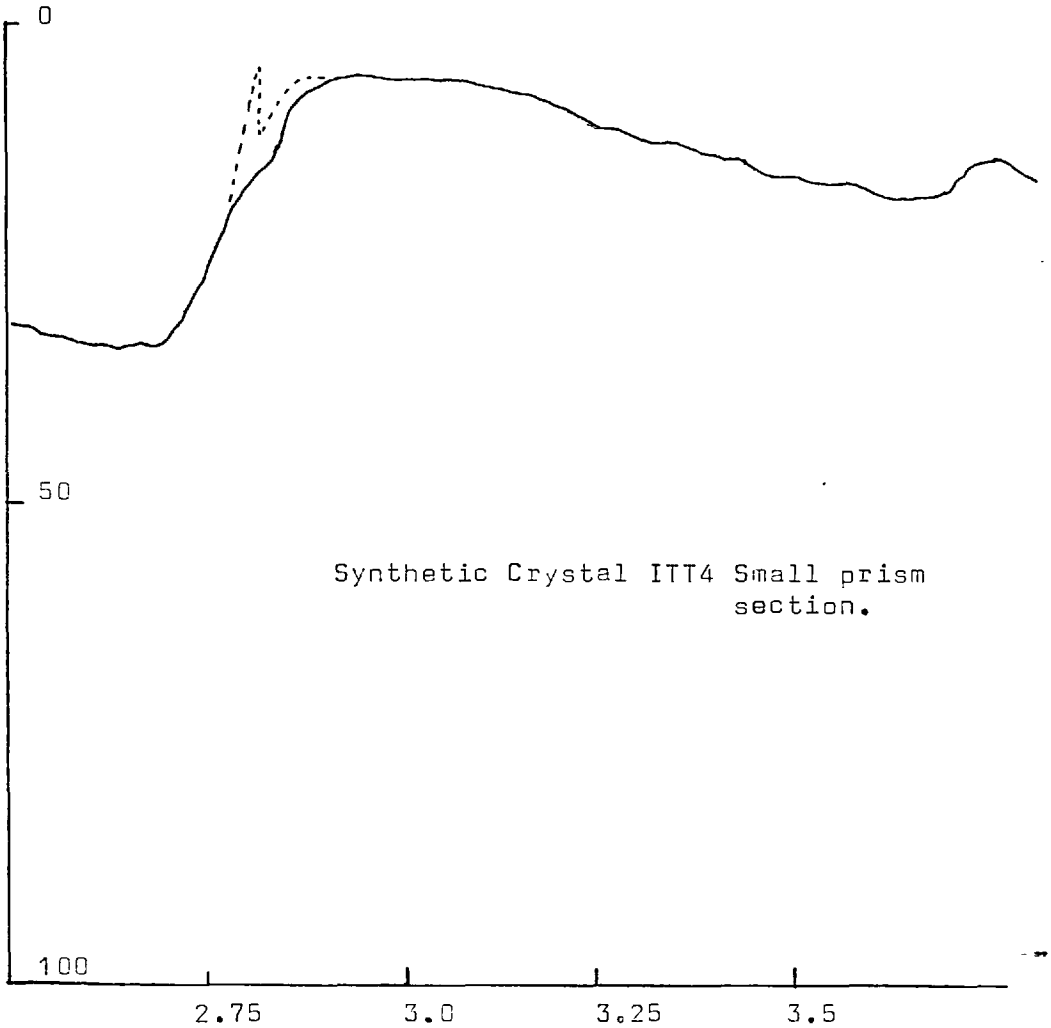

Synthetic Crystal ITT4 Small prism section.

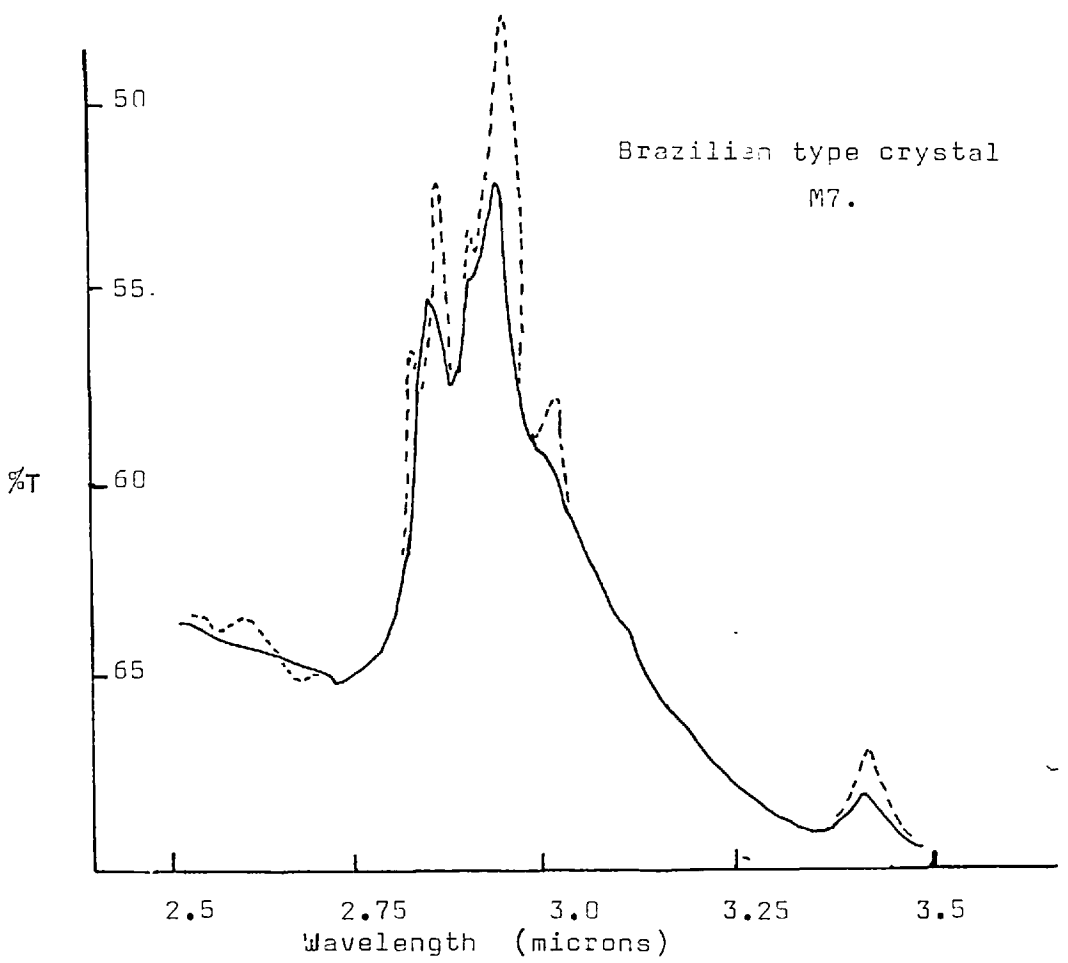

Brazilian type crystal M7.

Figure 3.12 Caption.

Typical examples of the effect of crystallographic orientation on the infrared absorption of a wet synthetic crystal (upper curve) and a Brazilian type natural crystal (lower curve). The solid line is the absorption for a beam incident normal to the c axis and the broken line for a beam incident parallel to the c axis. These curves show how a serious orientation effect only occurs in high resolution spectra.

-dom of the oscillator in the planes favourably orientated to cause absorption and to the change in intensity with crystallographic direction. Brunner et al (1961) however fails to give clear reason-ing for the adoption of this constant, but it gives results which compare favourably with those obtained from high resolution spectra using equation 3.39. It is because of this and the fact that it has been widely used by other workers (loc cit) that I have adopted it in this work. (See chapter 4 for the comparison of these techniques.) Where individual absorption bands were resolved as in Brazilian type quartz spectra (see section 3.10.1) the analyses were always conducted with the direction of beam incidence parallel to the c crystallographic axis.

The lower grade natural quartz with its large densities of aqueous fluid inclusions gives a spectrum which is very similar to that of molecular water. This similarity results from the fact that the greater proportion of the absorption is due to molecular water in these inclusions and not to structure bound water. This molecular water, being isolated from the quartz structure in bubbles does not show the orientation effect seen in natural Brazilian quartz spectra, and as such most natural quartz will not show orientation effects in its spectra.

3.9. THE ABSORPTION DUE TO MOLECULAR WATER

It is an unfortunate fact that ordinary molecular water shows a strong absorption band across the same range of freq--uencies as do the hydroxyl groups within the quartz structure (Bonner and Curry 1970). It is necessary to evaluate and compare the strengths of these absorptions, both to aid the interpretat--ion of the spectrum of opalescent quartz and to demonstrate the dehydration of the synthetic quartz structure. It is obvious that the dehydration (see chapter 5) can only be satisfactorily demon--strated if one of these absorptions is appreciably stronger than the other.

The comparison can be simply made by dividing the measured integral absorption by the actual number of absorbing molecules in the sample beam. Doing this for both a sample of molecular water and for a sample of synthetic quartz, with no bubbles pres--ent in its structure, enables the comparison to be made.

1). The sample of molecular water.

A thin film, 0.015cm thick, was prepared between two thin glass plates and placed in the sample beam of the spectrometer. Two identical glass plates without the aqueous film were then placed in the reference beam and the absorption across the three micron region recorded. The resulting spectrum is shown in figure 3.13a and compares favourably with the water spectrum recorded by Bonner and Curry (1970) which is shown in figure 3.13b. The absorption in this band was integrated between 4540cm^{-1} and 2560cm^{-1} using the 100%T line as a baseline. This gave an integral absorption of 18810cm^{-1}, a value which can be taken to be the absolute maximum for the recorded band.

Using Avogadros Number, 1cm^{3} of molecular water contains 6.023 X 10^{23} / 18 molecules at N.T.P. (the density of pure water = 1). Assuming the sample was at N.T.P. then the number of molecules

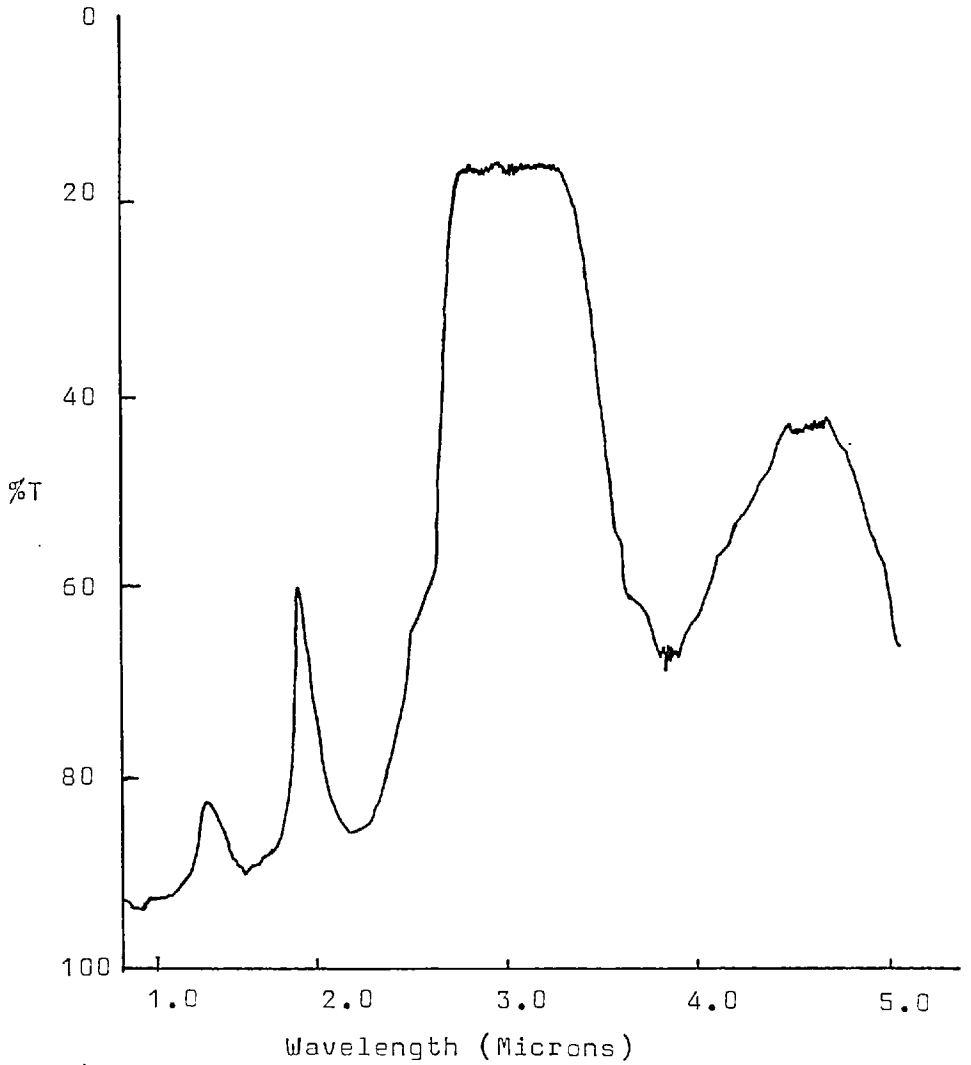

Figure 3.13a) The spectrum of molecular water used for the determination in section3.9.

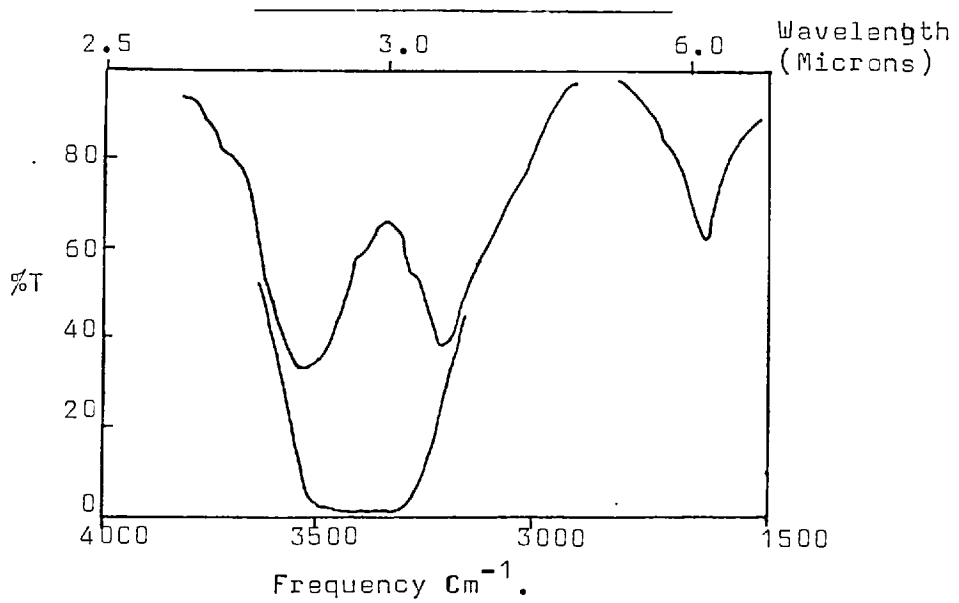

Figure 3.13b) The infrared spectrum of pure water from Bonner and Curry (1970).

sensed in the spectrometer beam is:-

$0.06\ cm^3$ (Vol. of water in the beam) X $\frac{6 \times 10^{23}}{18}$

giving 1.9×10^{20} molecules of water. Dividing the integral absorp-tion by this and rounding upwards gives a maximum possible value for the absorption due to 1 water molecule as $1 \times 10^{-16} cm^{-1}$ per molecule. Each water molecule contains two hydrogen atoms, so that the absorption due to each hydrogen atom in a sample of molecular water is:-

$$\underline{0.5 \times 10^{-16} cm^{-1}.}$$

This is the maximum possible value, for the absorption of water in the spectrum recorded (figure 3.13a) and in reality the base-line will occur at values of transmission less than 100% so that the actual value could be much less.

2). The Quartz Sample.

A sample of synthetic quartz with an integral absorption of 361.5 cm^{-1} (integrating between 3703 cm^{-1} and 2777 cm^{-1}),giving a concentration of 3903 $H/10^6 Si$,when the absorption is integrated to the baseline shown in figure 3.14, was used for this calculat-ion.

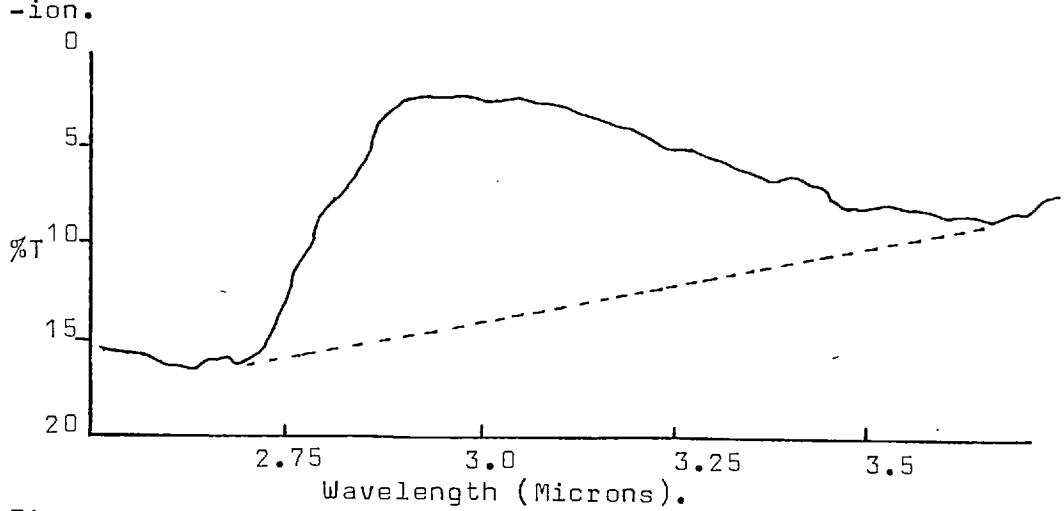

Figure 3.14. The spectrum of synthetic quartz crystal ITT4 which was used in the analysis showing the actual baseline which was adopted.

The specimen was 0.1 cm thick which using a similar analysis to that used for molecular water above gives:-

$$\frac{6.023 \times 10^{23}}{60.09} \times 0.04 = 4 \times 10^{20} \text{ molecules of quartz}$$

in the sample beam. This number of quartz molecules contain

$$\frac{4.0 \times 10^{20}}{10^{6}} \times 3903 = 1.5 \times 10^{18} \text{ atoms of hydrogen (or hydroxyl groups).}$$

So the absorption due to one hydrogen atom bound in the quartz structure will be:-

$$\frac{361.5}{1.5 \times 10^{18}} = \text{(approx) } \underline{2.5 \times 10^{-16} \text{cm}^{-1} \text{ per atom of hydrogen.}}$$

Thus the absorption due to a single hydroxyl group or hydrogen atom bound in the quartz crystal structure is at least five times as strong as the absorption due to a single hydrogen atom in the water molecule. It is possible that this difference may be significantly larger. I demonstrated in section 3.6.1. that the absorption coefficients determined by Scholze (1960) suggested that the infrared absorption would be reduced by a factor of 1.27. It is difficult to account exactly for the difference in this factor between the work of Scholze (1960) and my study but it presumably results from the differences in spectrometer response as outlined in section 3.5. This difference must then also suggest that the widely excepted value of 14000 litre/gram atm H /mole for the integral absorption coefficient for hydroxyl in quartz is not so readily transferrable between spect--rometers as has previously been presumed.

It is because of this difference in the relative strengths of the absorptions of hydrogen in molecular water and in quartz that the dehydration of the quartz structure (involving the combination of ionic hydroxyl groups to produce water molecules which are precipitated in bubbles) can be recorded by spectroscopic means. This is the subject of chapter 5.

3.10. THE SHAPE OF THE QUARTZ 3500cm^{-1} ABSORPTION BAND.

The purpose of this section is to introduce briefly the shape of the absorption bands recorded from different quartz types. The origin of these shape differences will be discussed at length in chapter 4, but for the present purpose a subdiv-ision into Brazilian type, Synthetic and other natural quartz including opalescent (milky) quartz is useful.-

3.10.1. Brazilian Type Quartz.

The spectra of good quality transparent (clear or coloured) piezioelectric grade quartz crystals have a distinct and reprod-ucible form, consisting of a broad background absorption onto which is superimposed a set of gaussian absorption peaks. (These peaks may be analyzed using equation 3.39). An example of this type of spectrum is shown in figure 3.15a. As the concentration of the absorbing groups becomes less, the peaks become smaller and the background flattens out, this is shown in figure 3.15b.

Figure 3.15a (caption). The absorption spectrum of crystal M1. This is a transparent, colourless piezioelectric crystal from a vein in Madagascar. A typical baseline is fitted to this spectrum.

Figure 3.15b (caption). The absorption spectrum of a dry Brazilian type crystal from Brazil. This crystal has a pale smokey colouration.

Figure 3.15a

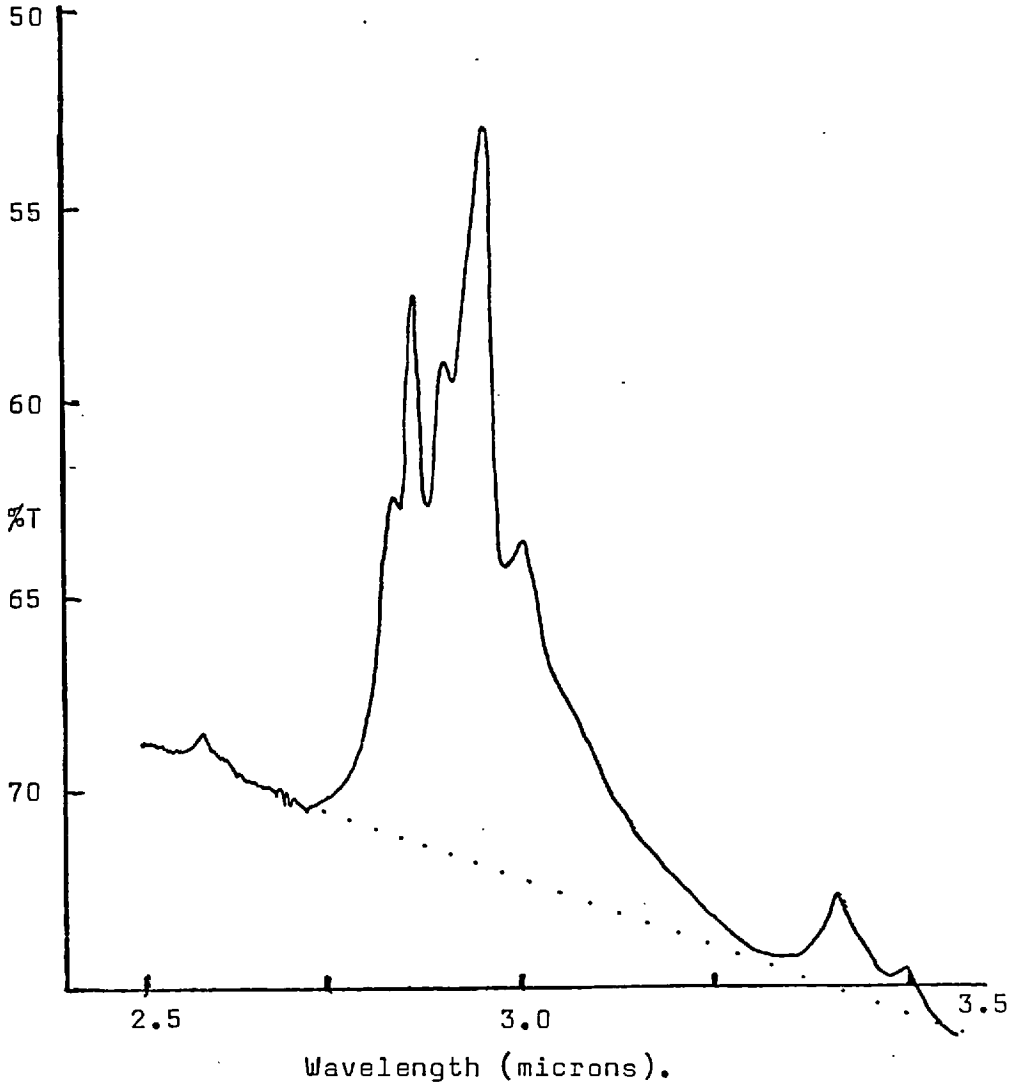

Figure 3.15b

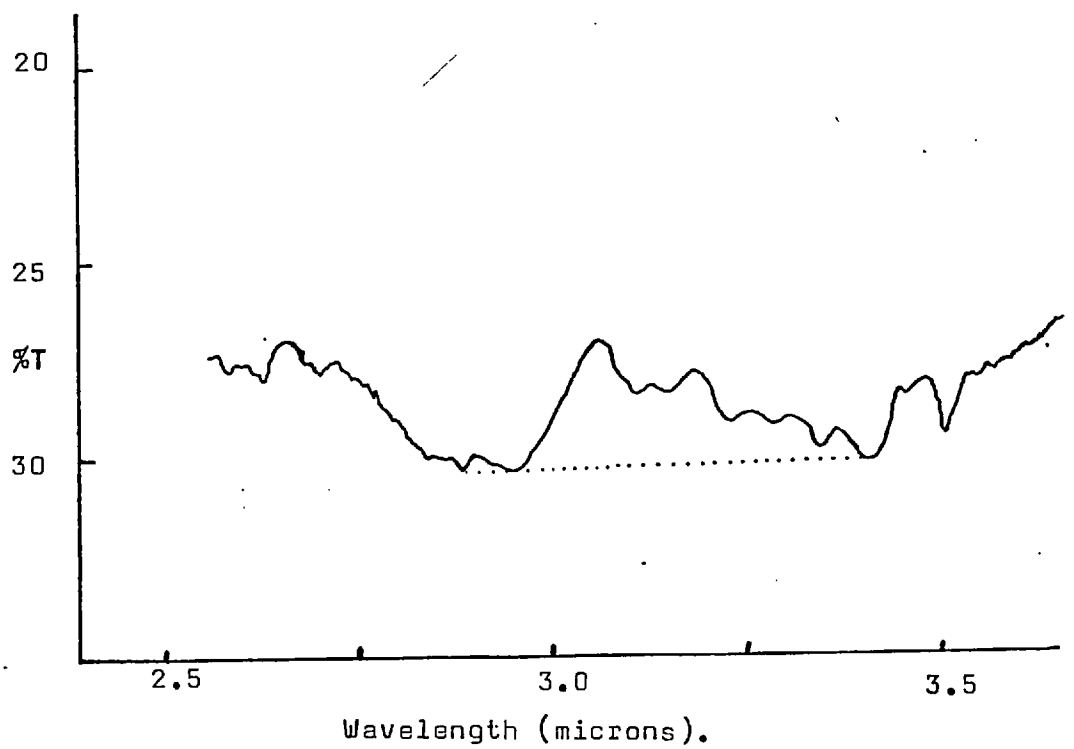

3.11.2. Synthetic Quartz.

Synthetic quartz crystals with large concentrations of structure bound hydroxyl groups exhibit a single large absorp--tion band of a strongly asymmetric nature, as shown in figure 3.16a. Only when the concentration becomes small does this over--all shape change into two poorly developed peaks on a slight background (figure 3.16b). Synthetic quartz crystals with spectra intermediate between the two extremes shown in figure 3.16 are generally rare, simply because the quartz crystal industry prod--uces quartz with these two different water concentrations (approx.) for different electronic applications, and generally has no call to produce intermediate crystals. In this study one crystal intermediate between these extremes (ITT4) was examined, this showed a single absorption band of similar shape to that in figure 3.16a but with a reduced intensity. The crystals used by Griggs (loc cit) span a wider range of concentrations and show the cont--inuous decrease in intensity of the single asymmetric absorption band to good effect (see chapter 4).

Figure 3.16a (caption). The infrared absorption band of a wet synthetic crystal (Griggs crystal Xo)recorded as part of this study.

Figure 3.16b (caption). The infrared absorption band of a dry synthetic quartz crystal (ITT8).

Figure 3.16a

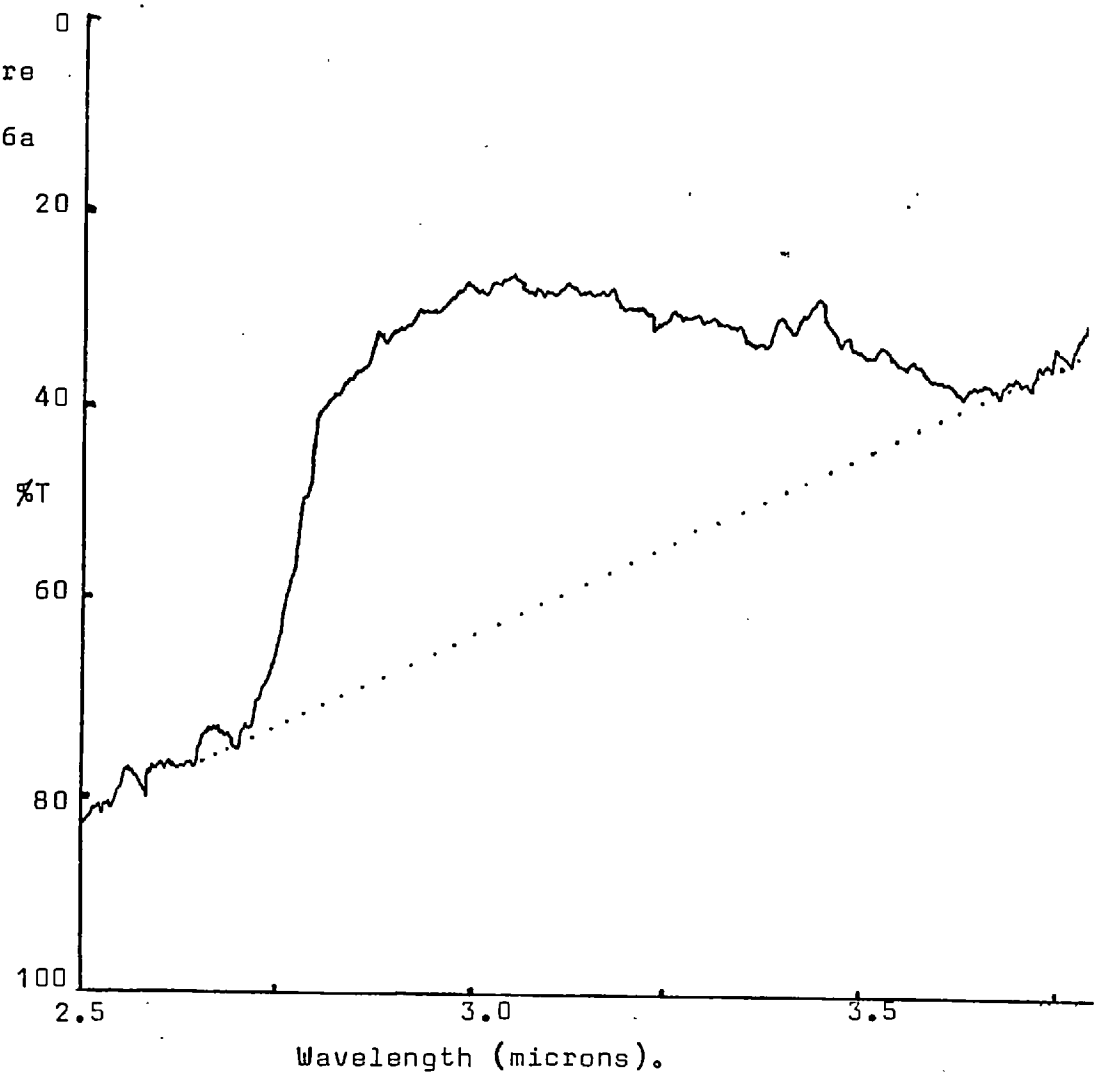

Figure 3.16b

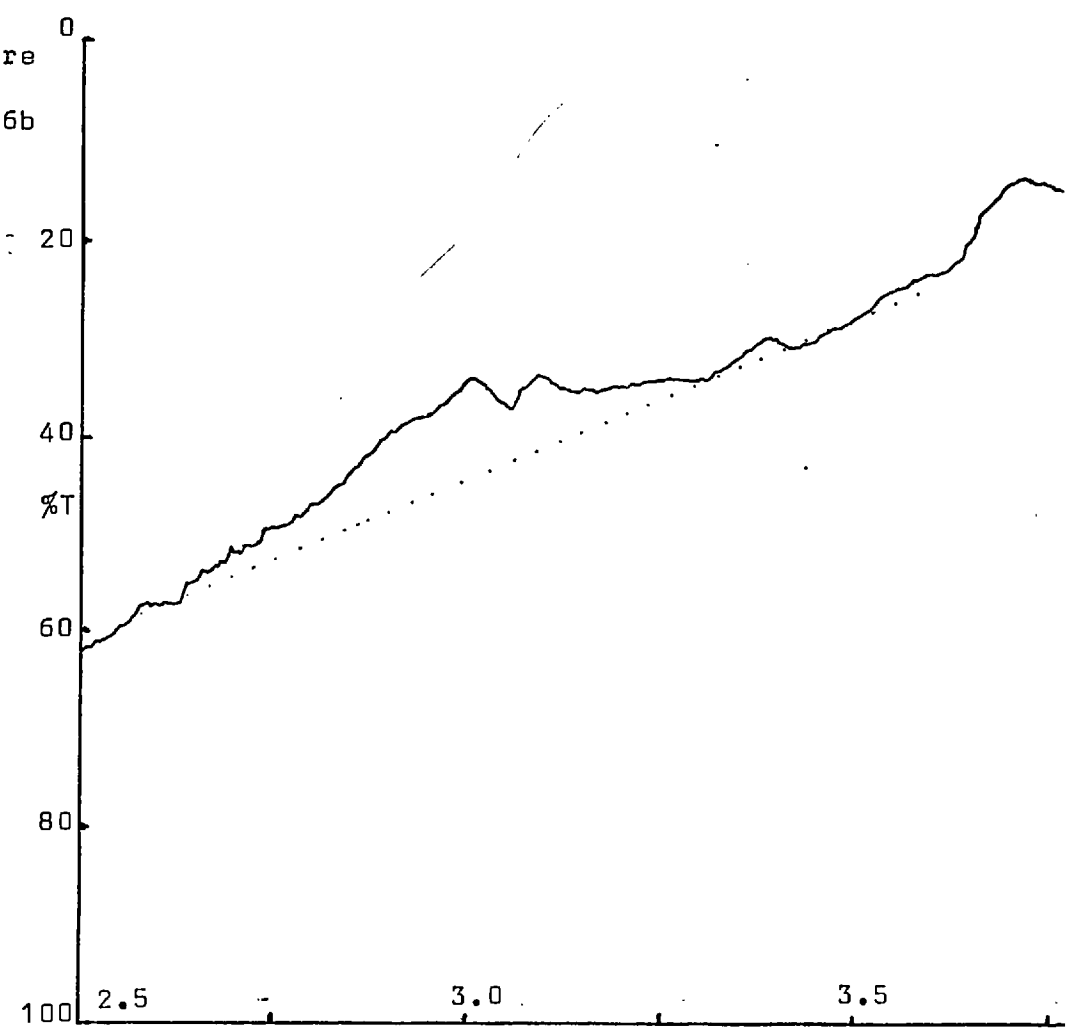

3.10.3. Other Natural Quartz (Vein Quartz).

Most naturally occuring quartz is not typified by the spectra in figure 3.15 but shows a single large symmetrical absorption band with a nearly horizontal baseline (see figure 3.17). Often if the sample is opalescent, this absorption is pushed into the upper section of the chart, and only if very thin samples are used can it be extended across the full chart width, as shown in figure 3.17. The large background recorded through much of the frequency range (1 to 24 microns) for nat--ural quartz of this type is probably due to Rayleigh scattering from the high density of inclusions and fluid filled voids.

This absorption band is very similar to that recorded for thin films of molecular water at room temperature, and knowing that molecular water is present in the inclusions, is very difficult to interpret. Part of the absorption will certainly be due to structural hydroxyl groups, but it is impossible to seperate out the contribution that this structural water makes to the absorption at room temperature. Because the absorption by structural hydroxyl groups is five times stronger than that for hydrogen in molecular water, it is impossible to calculate the absolute concentration for either the hydroxyl or the mole--cular part of the total water concentration of the sample, or for that matter the total water concentration, for most natural quartz. It is however possible to show that at some stage in the crystal's history,all of the water contained in the grain was dissolved in the structure as structural bound water and that a proportion (alas unknown) has been precipitated. However,if it is assumed that all the water were still as structural bound groups and the absorption coefficient for such groups applied to the solution of the spectrum, a minimum value(in $H/10^6Si$) for the total water concentration of the grain is recorded. This

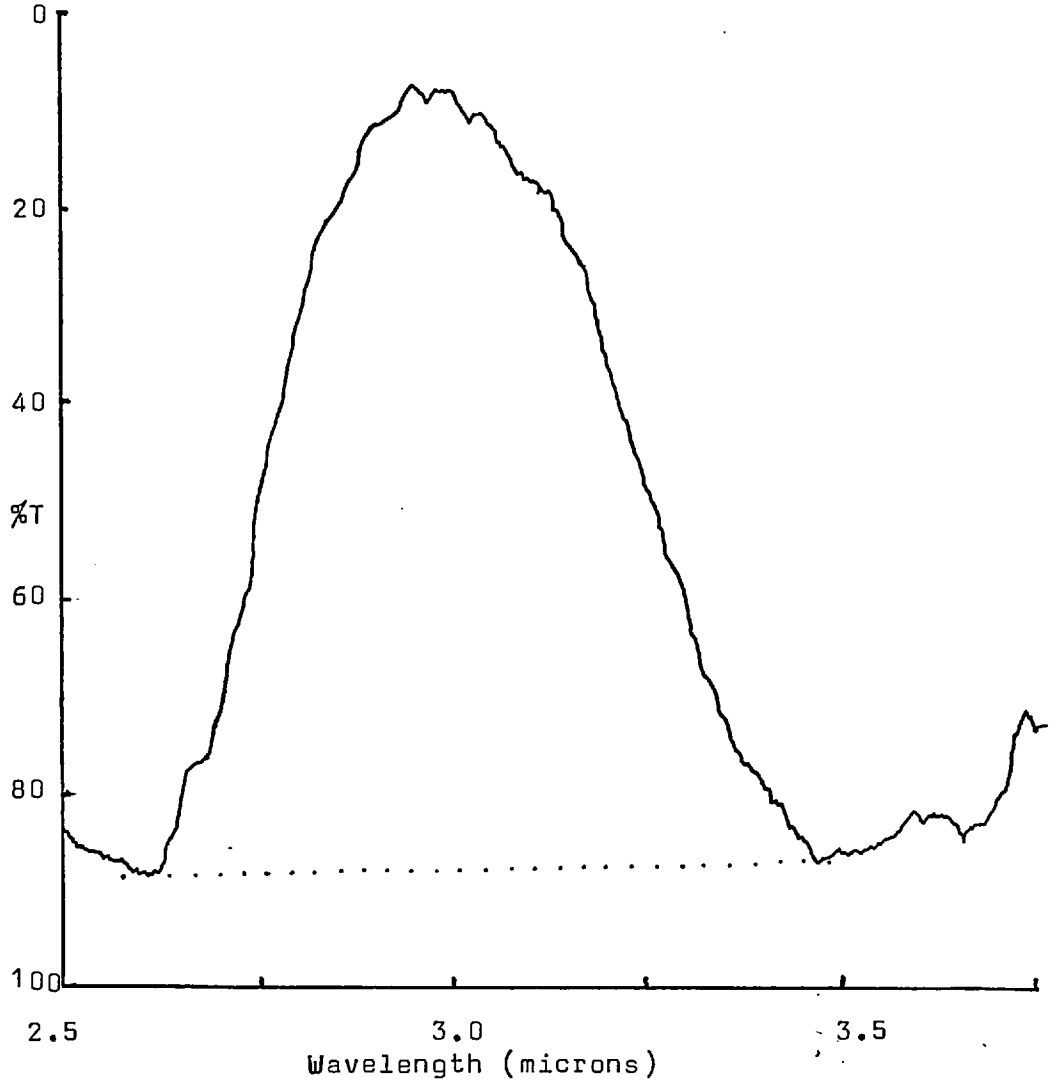

Figure 3.17. The spectrum of a natural milky quartz crystal from a vein deformed with the glaucophane schists on Anglesey. Note the close similarity of shape of this absorption band with that of molecular water.

figure may be an under estimate by as much as a factor of five.

3.11. CONCLUDING SUMMARY.

In this chapter I have attempted to describe in detail the method selected for the determination of the concentration of structure bound water in my quartz samples. Much of the dis--cus ion concerning Beers Law can be found in standard texts on

on quantitative infrared spectroscopy (most of the discussion presented here is based on that of Potts (1963)) but I feel that the inclusion of such discussion is important in putting this and other published spectroscopic data in the correct context. Similarly I have included almost directly the very detailed treatment of Kats (1962) (see section 3.7.1) because this dem-onstrates the physical interpretation of the Beer-Lambert Law, and provides what is probably the most accurate method of analy-zing the 3500cm^{-1} absorption bands for structure bound water, providing the spectra are of sufficiently high resolution and the absorption bands satisfy either the Gaussian or the Lorent-zian approximation. The work of Kats also serves to emphasise the possible errors and complications that may be caused by orient-ation effects, a problem which has generally been ignored (with some justification see section 3.8) in studies on the hydrolytic weakening of quartz (loc cit). I have deliberately discussed at length both the derivation of equation 3.21, and how the variables are measured so that in any subsequent study this information, which is only poorly described and rather widely scattered in the literature, is readily available. This is particularly important because of the erroneous form of this relationship which has been widely used in previous studies (see section 3.6.5).

I hope that I have left the reader with the impression that determining the hydroxyl concentration using the 3500cm^{-1} absorption band in the quartz spectrum, is not as simple or as straight forward a proposition as that implied by many of the published papers on water weakening of quartz (loc cit)in which hydroxyl concentrations are not only often incorrect due to Bam -buers error, but also possibly of poor reproducibility due to lack of adequate attention to the spectroscopic technique itself.

The work presented here has not been conducted at cryogenic temperatures, but as high frequency resolution is not at a premium, or for that matter really possible on the spectromaster, this should not be important, particularly when the quantitative procedures employed in this work are considered. The reader is referred to appendix 1 for sample preparation procedures, and steps taken to eliminate errors due to contamination, and to appendix 2 for the computer programs written to aid data processing.

* * *

Chapter Four.

WATER IN SYNTHETIC AND NATURAL QUARTZ, AND ITS INFLUENCE ON THE MECHANICAL PROPERTIES.

Chapter 4. WATER IN SYNTHETIC AND NATURAL QUARTZ, AND ITS INFLUENCE ON THE MECHANICAL PROPERTIES.

4.1. Introduction.

4.2. Water in Synthetic Quartz.

- 4.2.1. The Range of Concentrations Recorded.
- 4.2.2. Growth Banding in Synthetic Quartz.
- 4.2.3. The Effect of Orientation of the Growth Surface on the Included Concentration.
- 4.2.4. The use of Bubbles to Highlight the Hydroxyl Distribution.

4.3. The Inclusion of Structure Bound Water in Synthetic Quartz.

4.4. Water in Natural Quartz.

- 4.4.1. Concentrations of Water in Natural Quartz Recorded in Other Studies.
- 4.4.2. The Concentration of Structure Bound Water in Brazilian Type Quartz (This Study).
- 4.4.3. The Interpretation of the Brazilian Quartz Spectrum.
- 4.4.4. The Absorption Peaks at 2920cm^{-1} and 2840cm^{-1}.
- 4.4.5. The Concentrations of Water Recorded from Commonly Occuring Natural Quartz, Representative of a Range of Geological Environments.
- 4.4.6. Interpretation of the Spectra Recorded from Natural Low Quality Quartz.

4.5. The Subdivision of Quartz into Three Classes According to the Shape of its 3500cm^{-1} Absorption Band.

4.6. The Influence of Structure Bound Water on the Mechanical Properties of Natural Quartz.

- 4.6.1. The Predicted Water Weakening of Group 2 Quartz.
- 4.6.2. The Recorded Weakening Effect of Water in Group 2 Quartz.

4.7. The Usefulness of the Solid Confing Pressure Medium Deformation Machine.

4.8. Concluding Statement.

4.1. INTRODUCTION.

The range of concentrations of structure bound water for natural and synthetic quartz from this and other studies is presented in this chapter. This information is used to replace the often assumed subdivision of quartz into 'dry' natural quartz and 'wet' synthetic quartz with a threefold subdivision which shows natural Brazilian type quartz to be abnormal (with respect to its structure bound water concentration) when compared with other natural and synthetic crystals. This subdivision is supported by the molecular interpretation of synthetic and Brazilian type quartz spectra, and it is shown that the wet natural crystals are more closely akin to synthetic than to Brazilian type quartz when their spectra are interpreted. The possible mechanical effects of these large concentrations of water in natural quartz are discussed, but the low strengths predicted by the water weakening theory are not realised in experiments, it is therefore concluded that some fundamental difference exists between wet synthetic and wet natural crystals.

4.2. WATER IN SYNTHETIC QUARTZ.

All the synthetic crystals grown on Z-cut seeds in the western world show concentrations of structure bound water which are normally greater than 50 $H/10^6Si$ and which may be as large as 4500 $H/10^6Si$ (Griggs crystal Xo). It is this range of conc--entrations, and the distribution of the water within the crystals which is discussed in this section. Certain synthetic quartz crystals grown in Russia have attained far higher purities and extremely low defect concentrations, but these are not readily available in the west and are very expensive because of the slow growth rate which has to be employed in their production. Baeta and Ashbee (1970) have studied such a crystal which they suggest

is dislocation free, with a hydroxyl concentration of only "47 ppm" hydrogen bonded hydroxyl groups. Unfortunately they fail to state whether the 47 ppm is by weight (a very large concentration) or by numbers of atoms (a very small concentration), their published mechanical data when compared with that of Griggs (loc cit)does not conclusively support either interpretation.

4.2.1. The Range of Concentrations Recorded.

The wet Griggs crystal Xo (4500H/10^6Si) and the very pure Russian crystals described above, form the extremes of the record--ed concentrations of structure bound water in synthetic quartz crystals. Between these two extremes lie the concentrations for all the synthetic quartz crystals examined during this study. These are listed in table 4.1, and examples of synthetic quartz spectra are shown in figure 4.1. Because the concentration is dependent on the crystallographic orientation of the growth sector it is necessary to adopt a rigorous system of orientations for the spectrometer beam during the analysis so as to produce repro--ducible and comparable results, the four orientations used in this work are shown in figure 4.2.

Figure 4.1.a (caption) The infrared absorption for the three growth regions of crystal ITT4. The actual concentrations deter--mined from these spectra are Small Prism = 1465 H/10^6Si, Seed= 311 H/10^6Si and Sym. Normal seed = 173 H/10^6Si.

Figure 4.1.b (caption) The infrared absorption of the three growth regions of synthetic crystal A2. Small Prism = 3000 H/10^6Si, Seed = 100 H/10^6Si and Asym.Normal Seed = 315 H/10^6Si.

Figure 4.1a.

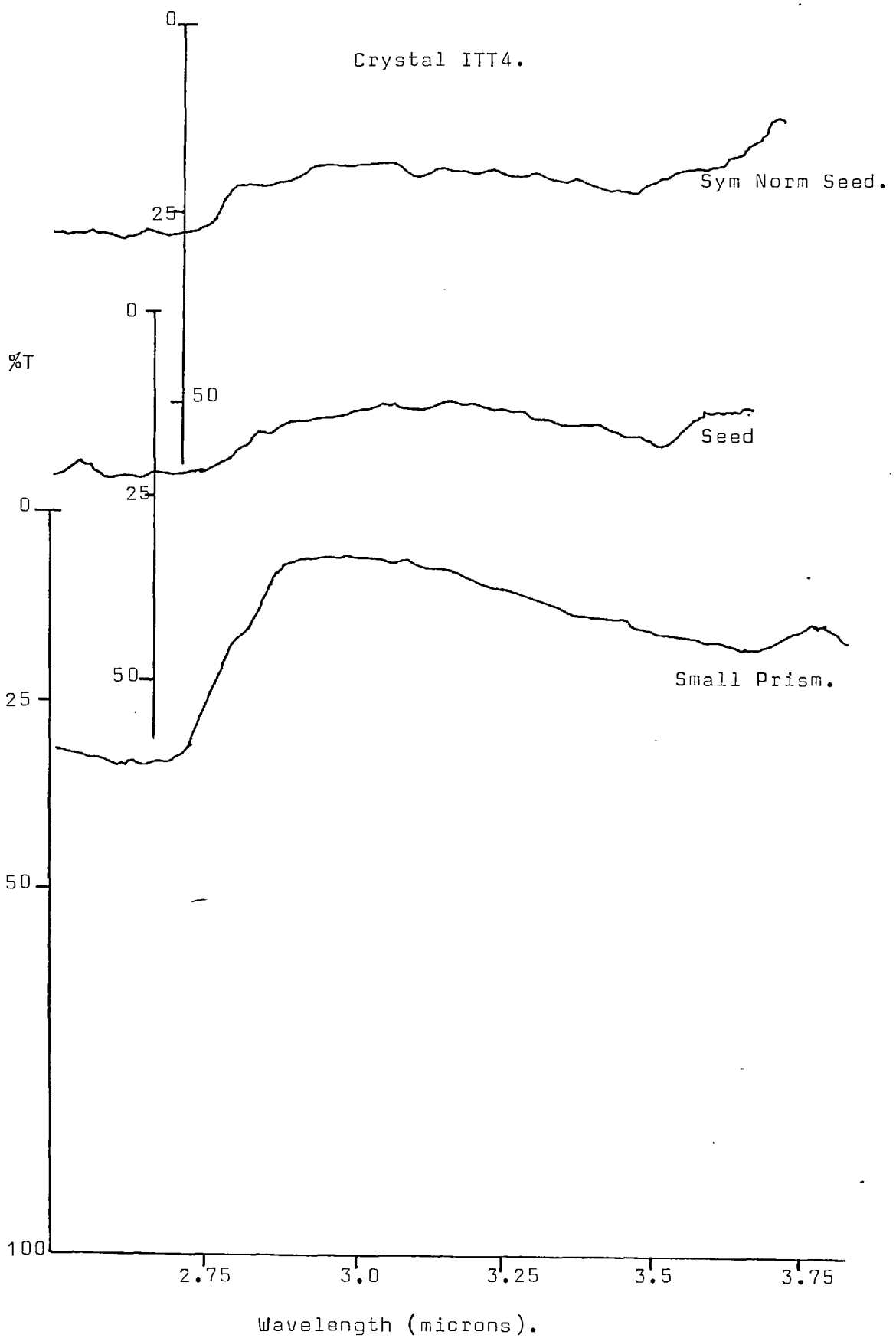
Crystal ITT4.
Sym Norm Seed.
Seed
Small Prism.
%T
0
25
0
50
0
25
50
25
50
100
2.75
3.0
3.25
3.5
3.75
Wavelength (microns).

Figure 4.1b.

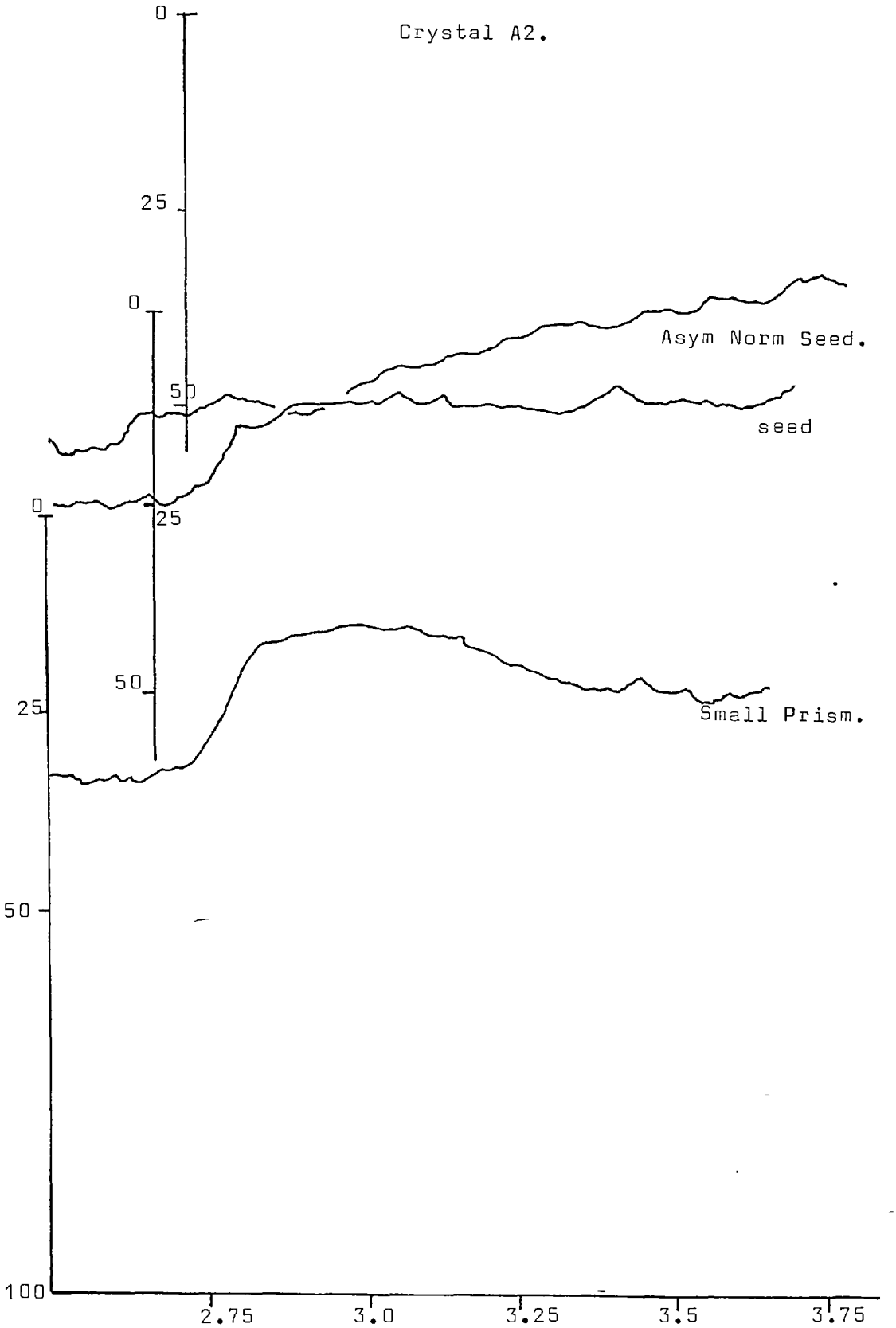
Crystal A2.
0
25
0
50
0
25
50
25
50
100
Asym Norm Seed.
seed
Small Prism.
2.75
3.0
3.25
3.5
3.75

Table 4.1. Concentrations of Structure Bound Water in Synthetic Quartz Crystal.

Sample	Orientation	Source	Concentration $H/10^6$ Si.
ITT1	Seed	This Study	190
"	Asym norm seed	" "	95
ITT2	Asym norm seed	" "	100
"	Seed	" "	200
ITT3	Asym norm seed	" "	75
"	Seed	" "	210
ITT4	sym norm seed	" "	173
"	Seed	" "	311
"	Small prism	" "	1465
ITT5	Asym norm seed	" "	30
"	Seed	" "	170
ITT6	Asym norm seed	" "	300
"	seed	" "	185
ITT7	Asym norm seed	" "	80
"	Seed	" "	200
ITT8	Asym norm seed	" "	55
"	Seed	" "	210
ITT9	Asym norm seed	" "	120
"	Seed	" "	115
ITT10	Asym norm seed	" "	150
"	Seed	" "	250
ITT11	Asym norm seed	" "	170
"	Seed	" "	250
ITT12	Asym norm seed	" "	57
"	Seed	" "	100
41	Z	Kats 1962	90
51	Z	" "	50
88	Rhomb	" "	10
27	Z	" "	70
99	Z	" "	60
57	Z	" "	90
42	Z	" "	230
31	Z	" "	60
Mossbach Inst.	//c	" "	50
Bell Tele. Labs.	//c	" "	70
AX1	Range from Z growth.	This Study	780 - 1000
A2	Asym norm seed	" "	315
"	Small prism	" "	3000
"	Seed	" "	100
A3	Sym norm seed	" "	150
Xo	?	Blacic 1975	4350
"	?	This study	2750
X13	?	Blacic 1975	2575
"	?	This study	525
X43	?	Blacic 1975	1425
"	?	This study	1125
X16	?	Blacic 1975	1440
X41	?	" "	810
X72	?	" "	430
X71	?	" "	170
OX-1	?	" "	90
X-125	?	" "	70
X-2	?	" "	40
S1	?	Hobbs et al (1972) corrected	3050
W1	?	for the error in the original	925
W2	?	Xo determination.	800
W4	?	" "	365

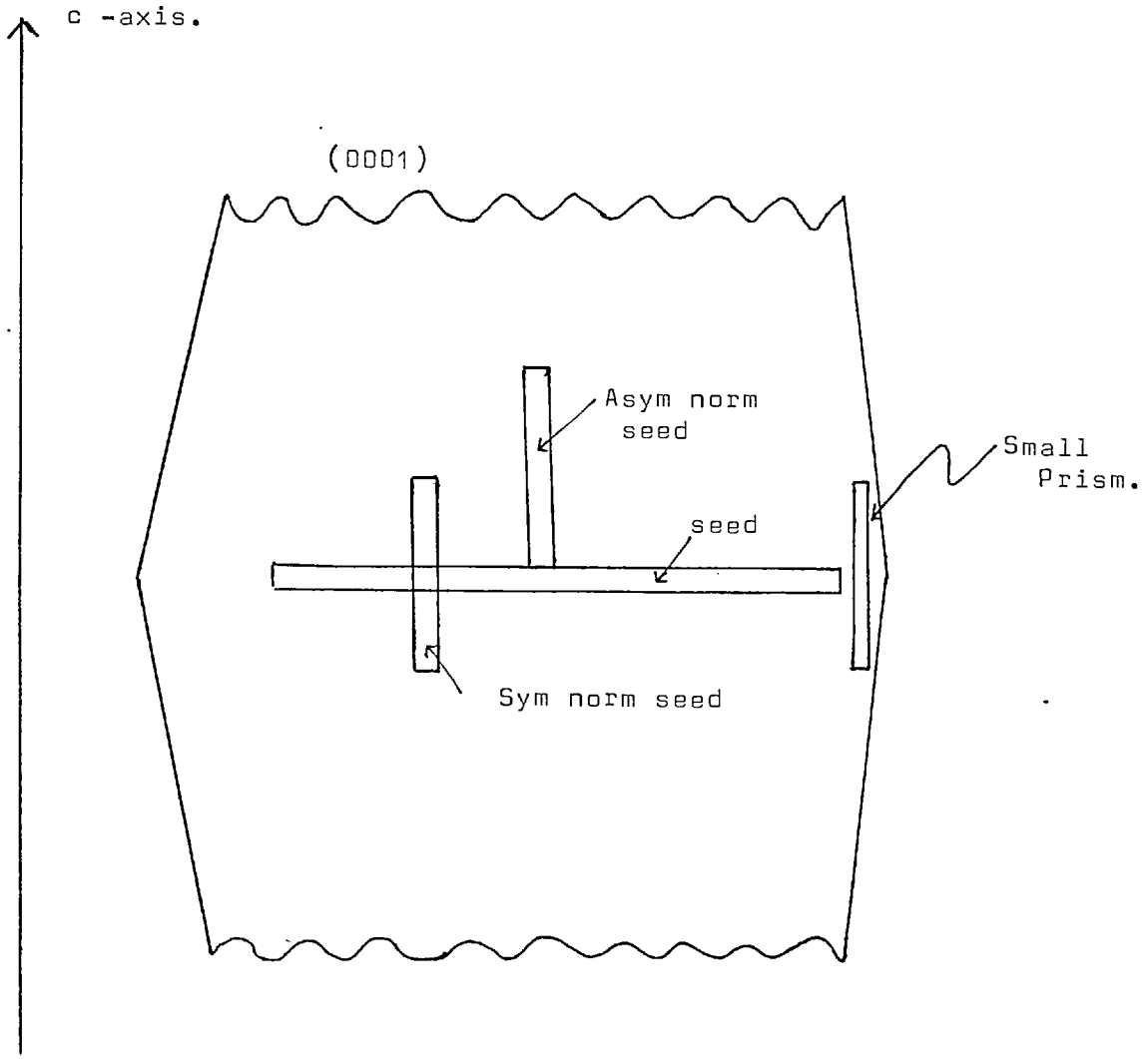

Figure 4.2. Cross section of a synthetic quartz crystal showing the three orientations used during this study. The small prism and seed regions show fairly constant water contents because the regions are small with respect to the cross-sectional area of the I.R.beam. The two orientations normal to the seed sample a range of growth bands of differing hydroxyl concentration.

4.2.2. Growth Banding in Synthetic Quartz.

The existence of closely spaced bands of variable hydroxyl concentration parallel to the growth surfaces in synthetic quartz crystals was first recognized and discussed by Dodd and Fraser (1967). They scanned the spectrometer across the crystal in diff--erent crystallographic directions at constant frequency ($3500cm^{-1}$) using the relation discussed in section 3.7.2. to obtain the concentration. Figure 4.3 is an example of their results. This work has generally been ignored in studies on the hydrolytic weakening of quartz (loc cit), although it is of paramount importance to the interpretation of such features as the def--ormation bands reported by Griggs in his deformed synthetic quartz samples.

In this study it has not been possible to use the contin--uous scan method used by Dodd and Fraser but some idea of the growth band distribution in many of the synthetic crystals, was obtained by taking closely spaced spectra across a crystal plate cut from the crystal in the desired orientation. The results of this analysis are given in figure 4.4 (a-l). These results show that in all synthetic crystals (except possibly the Russian ones) considerable variation in hydroxyl concentration occurs in planes parallel to the growth surface as the scan proceeds along the c-crystallographic axis. It is also important to note that this variation is exactly symmetrically mirrored across the seed indi--cating that this is a feature associated with changing conditions at the crystal/solvent interface during growth. This symmetry is shown to better effect in the continuous scan data of Dodd and Fraser than it is in the repeated spectra data of this study, because of the difficulties in placing the beam exactly equi-distant from the seed on both sides of the seed plate. The decoration technique for revealing the distribution of hydroxyl ions, which

is discussed below, provides still better evidence of the symmet-
-rical nature of this banding.

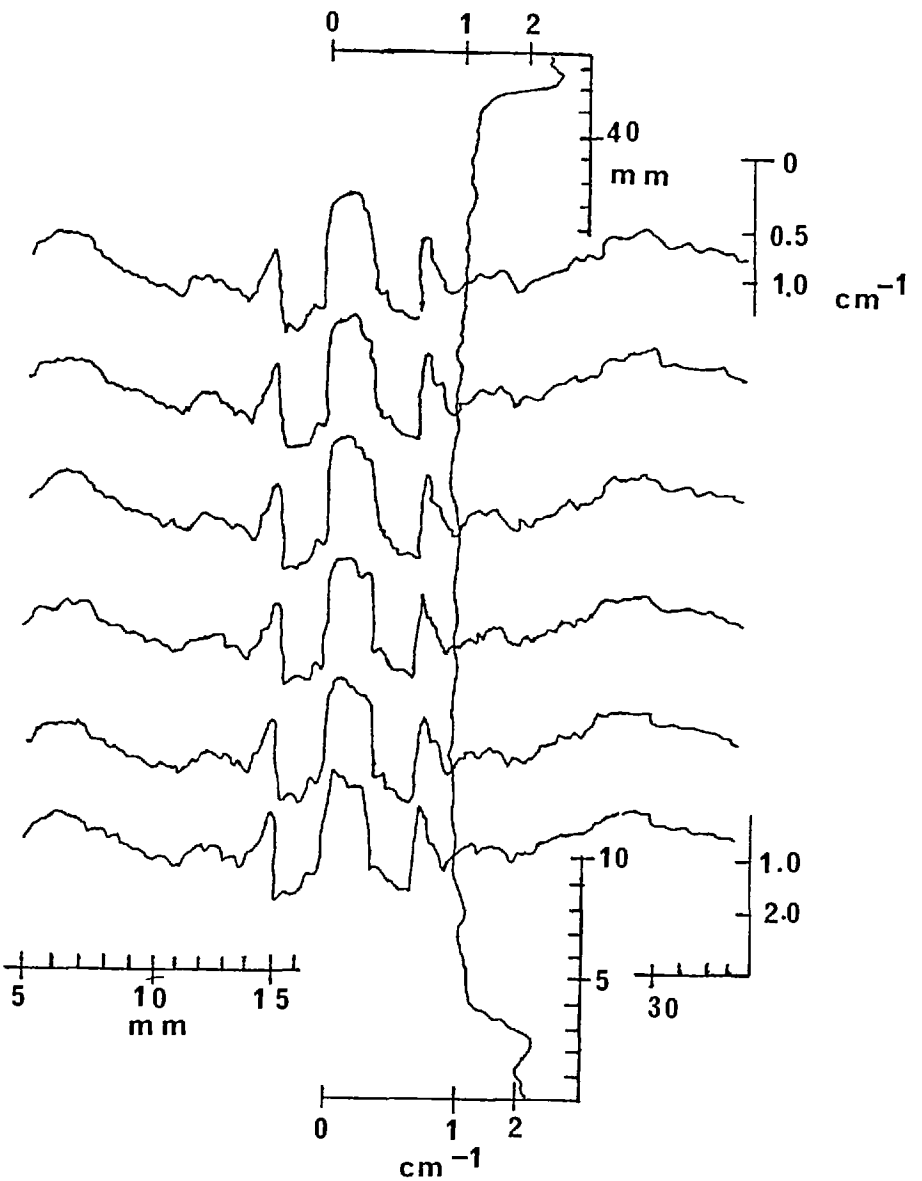

Figure 4.3. The variation in intensity of Infrared absorption within a synthetic quartz crystal. From Dodd and Fraser (1967). The plot is of $\alpha_{3500} = \frac{1}{b}\log_{10}\left(\frac{I_o}{I}\right)_{3500}$ versus distance across the crystal.

Figure 4.4. The variation in hydroxyl concentration in some of the synthetic quartz crystals examined during this study. The curves are plots of hydroxyl concentration versus distance from the seed along the c-crystallographic axis.

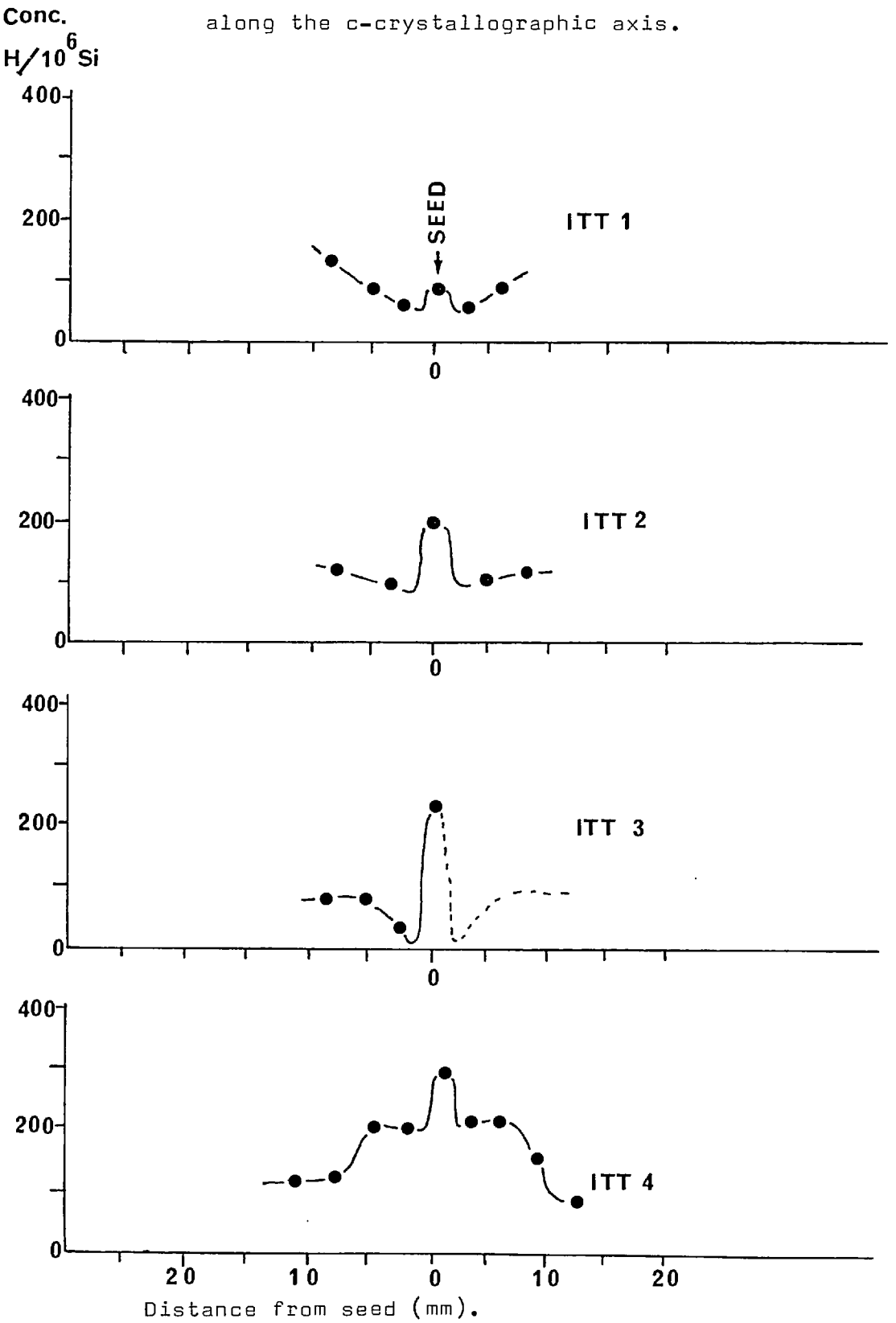

Figure 4.4 contin.

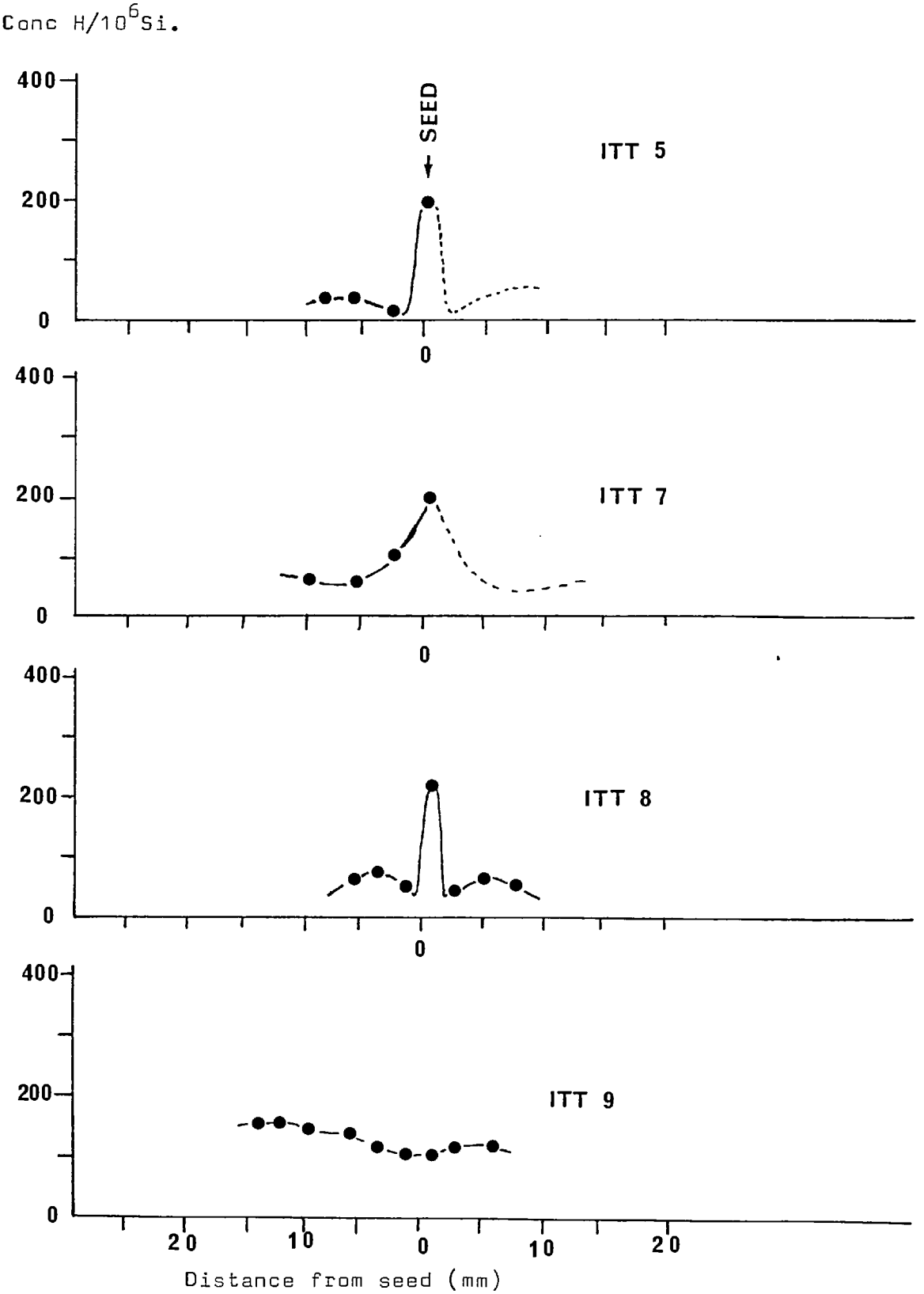

Figure 4.4 contin.

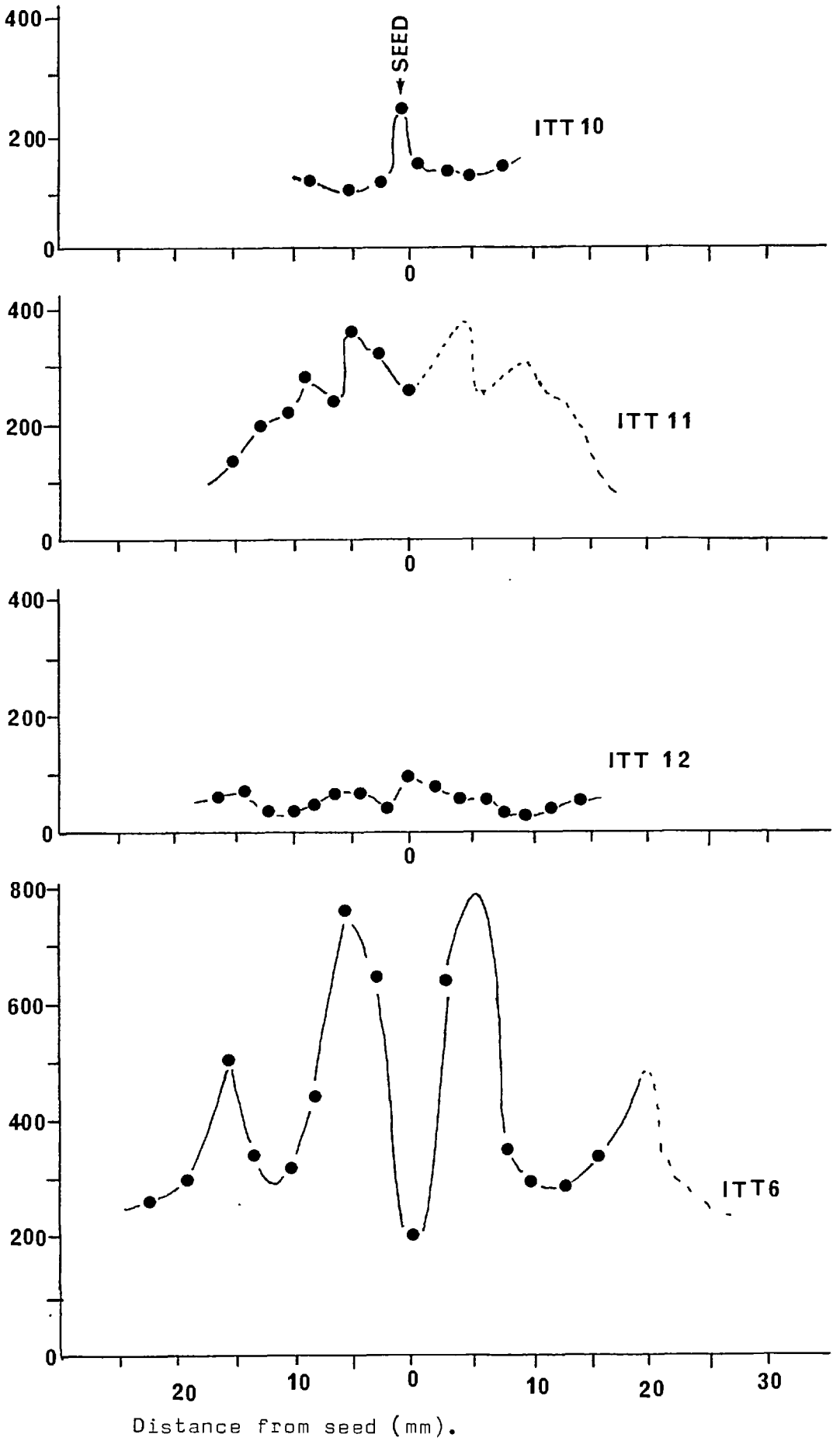

4.2.3. The Effect of Orientation of the Growth Surface on the Included Concentration.

Figure 4.5. is a cross section of an idealized synthetic quartz crystal showing the seed, Z-growth regions and the two regions of asymetrical prism growth. The growth bands can be traced at constant concentration from one Z-growth region through the larger prism into the other Z-growth region.

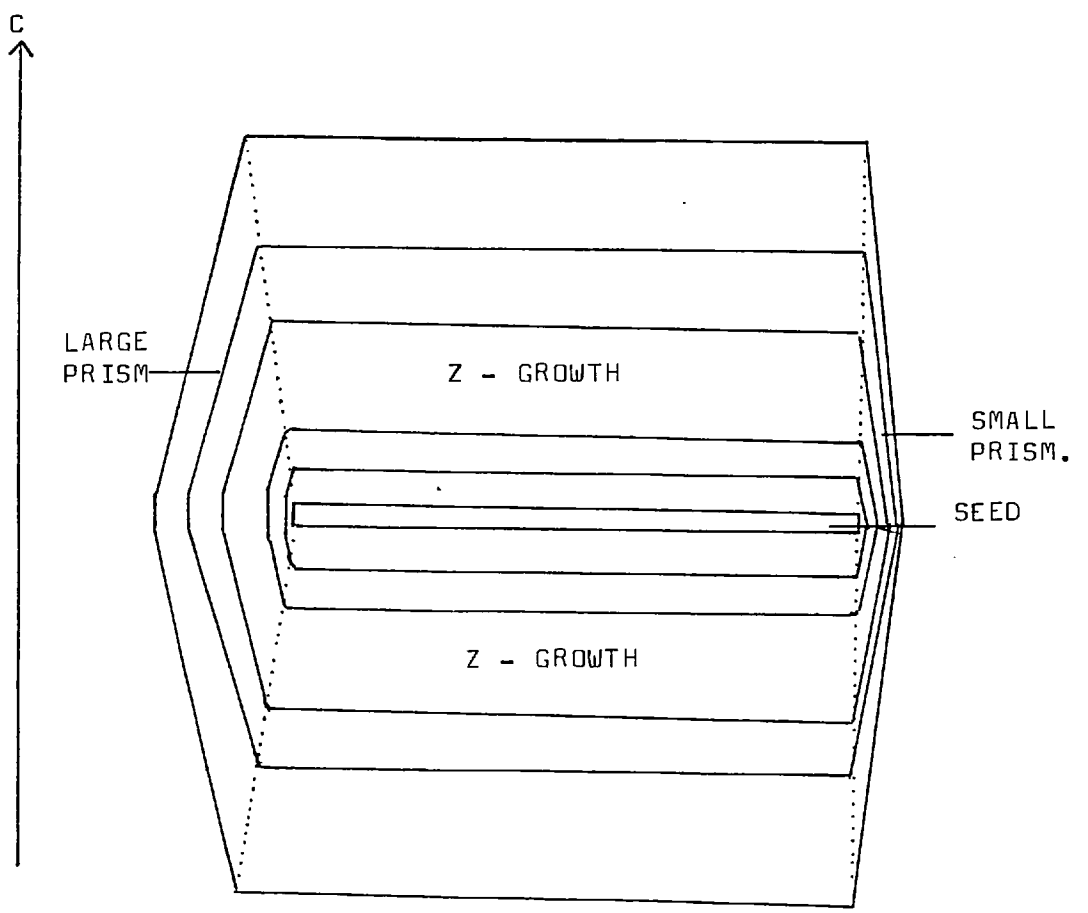

Figure 4.5 Cross section of an idealized synthetic quartz crystal showing how the growth bands can be traced around the seed plate. The actual concentration in the small prism region is about 5 times greater than that in the remainder of the crystal.

However when they are traced into the smaller prism region the recorded concentration is seen to increase by a factor of about 5. Table 4.1 lists the hydroxyl concentration for this small prism region for the synthetic crystals ITT4 and A2 as well as the concentration for the seed and Z-growth region. It would seem that this dependence of the concent--ration on the orientation of the growth surface occurs in all synthetic crystals, and should be accounted for, when preparing orientated cores for deformation experiments. This growth direction dependence of the concentration of monovalent hydrogen or hydroxyl ions has not to my knowledge been present--ed elsewhere, but a similar effect has been demonstrated for trivalent (Cohen and Hodge 1958) and possibly divalent ions (Cohen and Hodge 1958, Wood and Ballman 1966) substituting for silicon in the structure. Tetravalent substitutional impu--rities show a uniform distribution (Cohen and Hodge 1958). The order of inclusion recorded for the trivalent impurities is :-

$$(0001) < (0010) < (11\bar{2}1) < (51\bar{6}1)$$

and it would seem that the inclusion of hydrogen is governed by a similar scheme.

4.2.4. <u>The Use of Bubbles to Highlight the Hydroxyl Distribution.</u>

If synthetic quartz crystals with moderate to large conc--entrations of structure bound water are heated, the hydroxyl groups are precipitated as molecular water in bubbles, imparting a milkyness to the crystal. This effect is the topic of the next chapter where it is discussed in more detail. For the present it is sufficient to mention that the intensity of the opales--cence (milkyness), which is dependent on the size and density of the bubbles, is proportional to the original structure bound water concentration. It is thus possible by heating a plate

cut across a synthetic quartz crystal at sufficiently high temperatures for sufficiently long periods of time (850°C. and 24 hours) to precipitate the water and observe the origin--al distribution of water in the structure as a result of both growth banding and orientation effects. By adjusting the heating time or temperature it is possible to pick out the wettest growth bands etc. so that a few simple heating exo--eriments will provide invaluable information on the distribution of water in the crystal without much time consuming spectros--copy. It would seem to be sensible to make such a heating test a necessary ore-requisite to coring samples from a synthetic crystal for deformation experiments. Unfortunately this tech--nique does not yield quantitative data, but could be made to do so with suitable calibration using a combination of heating tests and infrared spectroscopy on a number of different syn--thetic quartz crystals.

A major outcome of this technique has been to reveal that the growth banding occurs on a far finer scale to that detected by taking adjacent infrared spectra across the crystal. This lat--ter technique revealing only relatively wet or dry areas caused by clusters of bands. From these heating experiments, the den--sity of growth bands can be seen to vary from a uniform distri--bution with the concentration remaining constant throughout the Z-growth region to extreme examples with as many as 5 bands per millimeter. Unfortunately the contrast of these bands is very low so they cannot be satisfactorily photographed. Dodd and Fraser (1967) used schlieren photographs to produce a photographic plate showing the same distribution as described here with bubbles, and this technique can be applied to the crystal without having to first precipitate the water into bubbles.

4.3. THE INCLUSION OF STRUCTURE BOUND WATER IN SYNTHETIC QUARTZ.

The concentration of structure bound water in synthetic quartz is generally found to be proportional to the growth rate of the crystal (Dodd and Fraser 1967)although, to the authors knowledge, little quantitative data on this relation--ship has been published. The growth banding discussed in sect--ion 4.2.2. probably reflects nothing more than variations in the growth rate of the crystal as the concentration of impur--ities in the hydrothermal fluid in the autoclave should always be constant or varying only slowly. It is thus necessary to account for this dependence in any model for the inclusion of water in the quartz structure. However, as shown in section 4. 2.3. the highest concentrations of structure bound water occur in the slowest growing region of the crystal. Thus the establish--ed axiom of the concentration being proportional to the growth rate must be modified to include the effect of the orientation of the growth surface.

The shape of the synthetic quartz spectrum with its single large absorption band suggests that most of the hydroxyl ions are present as hydrogen bonded groups (Dodd and Fraser 1965,1967) and not as the more complex groups identified by Kats (1962) for Brazilian type and the dryest synthetic crystals. Thus the typ--ical synthetic quartz spectrum is different to that studied by Kats and not really suitable for comparison. These hydrogen bonded groups are the silanol groups (Brunner 1961) and were suggested by Brunner to have the formula:-

$$\equiv Si - OH \quad HO - Si \equiv$$

which may be interpreted as two silicon tetrahedra joined by a pair of hydrogen bonds.

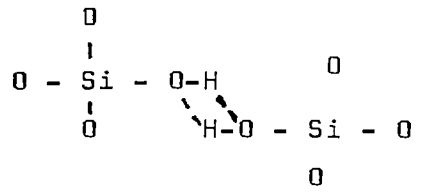

It is important to note that Griggs (1967) interpreted the Brunner formula in the form :-

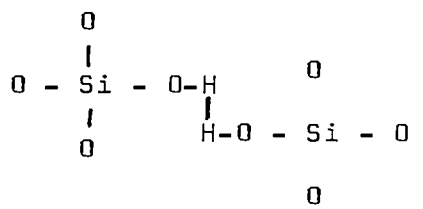

putting the hydrogen bond between the two hydrogen atoms which is obviously in correct (cf Campbell 1970, Bell 1959).

Silica in solution is normally present as $H_4Si\ O_4$ (Krauskopf 1967) which has a tetrahedral form and may be considered to be a single silica tetrahedra with its free negative charges satisfied by Hydrogen atoms. Similarly the surface of a growing quartz crystal in contact with its hydrothermal growth solution will have its free negative charges compensated by hydrogen ions. Growth proceeds by the hydrolyzed silica tetrahedra in the solut-ion arriving at the crystal liquid interface and reacting with the hydrolyzed silica at that interface to produce a normal silicon - oxygen - silicon bridge and water.

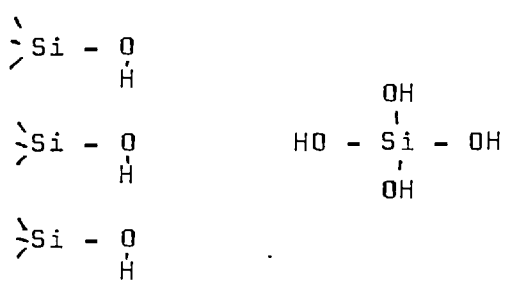

Crystal. Growth Solution.

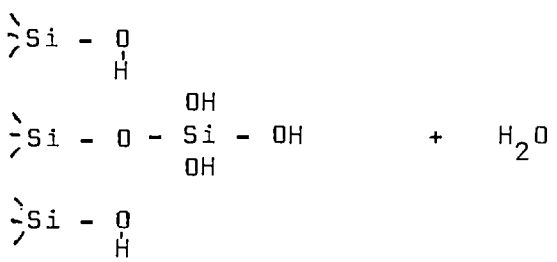

The actual mechanics of this reaction are controlled by the pH of the growth solution.

Obviously some of the hydrolyzed silica tetrahedra will arrive at the surface of the growing crystal suitably orientated to form hydrogen bonds with the hydroxyl on the surface (the tetrahedra may also hydrogen bond together in the solution) which will be sufficiently stable not to breakdown to water and silica immediately. If the number of tetrahedra arriving at the surface is large (causing a rapid growth rate) then some of these hydro--gen bonded groups will become inbedded in the structure. The faster the growth rate the greater the probability that a hydro--gen bonded group will become trapped and thus the larger the included hydroxyl concentration. This effect will obviously depend critically on the orientation of the growth surface so that certain directions will incorporate more hydroxyl groups than others. This model gives rise to hydroxyl groups which are paired, this is implicit in Brunners' silanol bond and necessary to explain the dehydration behaviour discussed in the next chapt--er. Clearly, modifying the chemistry of the growth surface or the growth solution will modify this up take of water. Ballmann et al (1966) showed that the addition of other ions, notably Li^+ to the growth solution would improve the anelastic properties of the crystal. A large anelastic response being undesirable in crystals grown for use in the manufacture of oscillators. This improvement in mechanical Q was presumably accomplished by reducing the hydroxyl concentration in the structure direct--ly by reducing its up take during crystal growth. The incorp--oration of hydroxyl ions into the silica structure as silanol bonds is summarized diagrammatically overleaf.

Growing Crystal Hydrothermal Growth Solution.

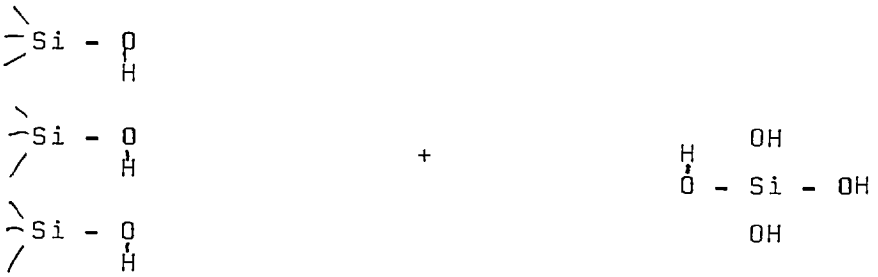

A tetrahedral group in the solution approaches the growth surface favourably orientated to form a pair of hydrogen bonds.

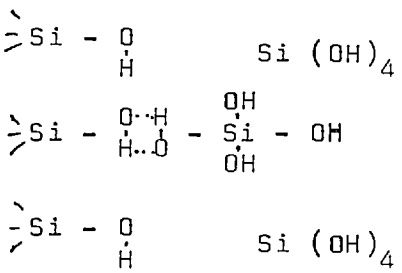

The first group arrives at the growth surface and because of its orientation hydrogen bonds to the hydroxyl group on the growth surface. Two other groups are now approaching this part of the growth surface and are orientated to form normal bonds.

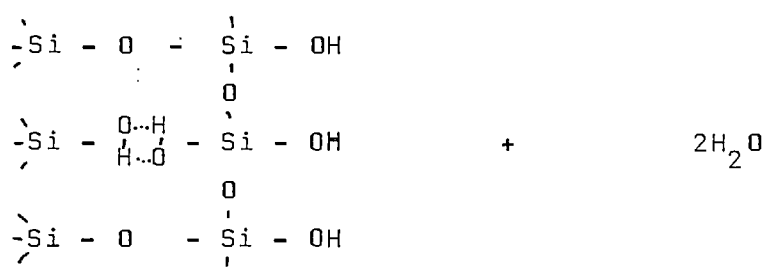

These other groups react with the surface and form a continuation of the normal silica structure. The pair of hydrogen bonded hyd--droxyl groups are now left trapped in the crystal. The structural diagrams shown above are schematic and not meant to portray a true two diamensional representation of the silica structure.

It is important to stress that this model for the incorp-
-oration of hydroxyl ions into the structure of quartz during
crystal growth is qualitative (based on discussions with members of the Min.Tech department), and almost certainly a drastic oversimplification, it is of course a model and not an inter-
-pretation of experimental data. This model is set up to acc-
-ount for the silanol bond suggested by Brunner (1961) and implicit in the Griggs models of hydrolytic weakening. Almost certainly in reality trivalent ions are important in controll-
-ing the up take of water by the crystal for it has been shown by Cohen and Hodge (1958) that these impurities substituting for tetravalent silicon show a distribution in the crystal which is the same as that reported here for hydroxyl groups. Part of the hydroxyl must then be simply acting as a charge compensator and this part of the concentration will be depend-
-ent on the number of tri and di valent substitutional impurities.

This section is necessarily vague because of the almost total lack of information in the literature on the inclusion of water in the synthetic quartz structure, although the crystal growing industry will almost certainly have investigated it. It is to be hoped that at some stage the hydrothermal growth of quartz will be investigated accademically for any such study would certainly provide much useful information and fill in many of the gaps in the very scattered and often rather trivial literature on the growth of synthetic quartz.

4.4. WATER IN NATURAL QUARTZ.

If water weakening is to have any application to natural quartz deformation it is necessary to establish that naturally occurring quartz can support sufficiently large concentrations of structure bound water to be mechanically weakened.

4.4.1. Concentrations for Natural Quartz Recorded from other Studies

Nearly all the infrared studies of hydroxyl in natural quartz have been restricted to high purity piezoelectric grade, Brazilian type, quartz single crystals. These have generally shown very small concentrations of structure bound water, giving spectra with distinct Gaussian absorption bands superimposed on a broad background absorption. Bambuer (1961) records concentrat--ions for his Alpine quartz up to 1000H/10^6Si, but these results have been shown in chapter 3 to be too large by a factor of two. Table 4.2. lists the results of other workers analyses (converted to the units H/10^6Si) together with their source, and clearly shows that Brazilian (and other good quality natural quartz) has, as a rule, small concentrations of structure bound hydroxyl groups. Studies of the mechanical properties of natural quartz have generally concentrated on these good quality natural crystals with the result that an axiom has been established in which it is assumed that natural quartz is typified by the Brazilian type crystals and is both dry and strong, whilst synthetic quartz can be both wet and weak. Obviously if this is true, water weakening need not concern structural geologists.

Mclaren (1966a), working on amethysts and citrines, record--ed high concentrations of structure bound water, and showed that this could be precipitated in bubbles on heating. Many subsequent workers have assumed in their studies of naturally deformed quartz (cf. White 1971 a,b,c,d, 1973) that large concentrations of structure bound hydroxyl groups must have been present during the deformation to enable flow to occur. This has lead to a situation where the experimentalists have generally ignored natural quartz as being too strong and hence difficult to work with, whilst students of naturally deformed quartz have often interpreted their results in terms of the data gleaned

from'weak' synthetic quartz crystals. Obviously the question must be asked are they both referring to the same material by the label "natural quartz". Much of the rest of this chapter will be spent establishing that they are not.

White(1973) working on the microstructure of natural quartz from low grade tectonic veins has shown that many of the fluid inclusions lie along dislocations (and concluded that they were precipitated there). In later work Knipe and White (1978) have recorded interactions between the dislocation microstructure and small fluid inclusions and have shown that small fluid inclusions already existing before the dislocation microstruct--ure can pin dislocations. It is implicit in both of these studies that the low grade natural quartz considered had contained at some stage during its history a large concentration of structure bound water and that this had been precipitated leading to the solid state growth of fluid filled voids. This solid state growth of fluid inclusions (a phenomenom often ignored by geologists) has been demonstrated by Mclaren for'wet'amethyst and is extens--ively investigated as part of this study for synthetic quartz (chapters 5 and 6). Thus it may be possible to interpret the high density of fluid inclusions responsible for the opalesc--ence in much natural quartz as resulting from the dehydration of an initially 'wet structure and not from the inclusion of molecular water in bubbles during crystal growth. (See Knipe, a study to be presented as a PhD thesis Univ. of Lond. 1977,for a detailed discussion of the sedimentological and microstructural evidence etc.) The actual concentration of water in a range of natural quartz crystals representing different natural envir--onments is presented in sections 4.4.2. and 4.4.4.

Table 4.2. Concentrations of Structure Bound Water in Natural Quartz from Previous Studies.

SAMPLE	SOURCE	CONCENTRATION $H/10^6 Si$
?	Brunner 1961	2
?	" "	10
?	" "	100
?	" "	200
Amethyst	" "	10000
Brazilian(Clear)	Kats 1962	500
Brazilian(Smokey)	" "	30
Smokey and clear	Bambuer 1961	2.25
Brazilian type quartz	(corrected for	1.75
from late Alpine veins.	the error in	3.25
"	his results)	3.5
"	" "	9
"	" "	3.25
"	" "	8
"	" "	2.25
"	" "	10
"	" "	27.25
"	" "	27.5
"	" "	10
"	" "	15
"	" "	6.5
"	" "	0.5
"	" "	3
"	" "	0.75
"	" "	14.5
"	" "	9.5
"	" "	3
"	" "	1.5
"	" "	65
"	" "	600
"	" "	340
"	" "	220
"	" "	80
"	" "	115
"	" "	17.5
"	" "	32.5
"	" "	45
"	" "	217.5
"	" "	155
"	" "	230
"	" "	585
"	" "	4.5
"	" "	3.5
"	" "	3
"	" "	3.5
"	" "	1.75
"	" "	4.75
"	" "	7.5
"	" "	3
"	" "	3.5
"	" "	1.5
"	" "	2.5
"	" "	1.5
"	" "	3.5
"	" "	2.75
"	" "	5.5
"	" "	4.5

Table 4.2 Contin.

SAMPLE	SOURCE	CONCENTRATION
Smokey and Clear	Bambuer 1961	1
Brazilian Type	(corrected)	11
Quartz.	" "	6
"	" "	3
"	" "	3.75
X-1	Blacic 1975	45
H-1	" "	10
A-1	" "	10
Amethyst	Mclaren 1965 (corrected)	15000

Table 4.3. Concentrations of Structure Bound Water in Natural Brazilian Type Quartz recorded during this Study.

SAMPLE	DESCRIPTION AND LOCALITY	CONCENTRATION $H/10^6Si$
Br1	High purity colourless transparent quartz Brazil	50
Br2	"	400
Br3	"	100
Br4	"	450
Br5	"	25
Br6	"	325
Br7	"	410
BrB	"	275
Br9	"	90
Br10	"	110
Br11	"	180
Br12	Gem Quality Smokey Quartz from Brazil	350
Br13	"	30
Br14	"	60
Br15	"	120
Br16	"	90
Br17	"	40
Br18	Deep green gem quality citrine from Brazil	850
Br19	Gem Quality smokey quartz from Brazil	150
Br20	"	40
Br21	"	20
Br23	"	300
M1	Small high clarity rock crystals from Madagascar	420
M2	"	250
M3	"	225
M4	"	370
M5	"	270
M6	"	500
M7	"	390
NV1	Brazilian type rock crystal locality unknown.	25
NV2	"	75
NV3	"	140
NV6	"	190

4.4.2. The Concentration of Structure Bound Water in Brazilian Quartz.

Thirty five different Brazilian type quartz crystals were analyzed during this study, and these results are listed in table 4.3. This table shows that these crystals have concentrations less than 450 $H/10^6Si$ in all but one instance (Br18), which is in good agreement with the concentrations recorded from earlier studies (see table 4.2).

The spectra of these crystals always show distinct absorpt--ion bands superimposed on a broad background absorption except in cases where the concentration is very small and the resolution consequently poor. Figure 4.6 shows examples of these Brazilian quartz spectra.

It is possible to analyze the superimposed peaks in these absorption bands using the gaussian approximation of Kats (1962) discussed in chapter 3. By summing the results of this analysis it is possible to compare it with the concentration as recorded for the complete band using the normal Brunner relationship. In all cases a difference proportional to the magnitude of the back--ground absorption is recorded. Table 4.4 lists these results for comparison.

Table 4.4. Comparison of concentrations determined by the Kats and Brunner methods. Concentrations in $H/10^6Si$.

Sample.	Total Conc. (Brunner)	Peaks Conc.(Kats)	Background (Brunner)
M2	250	100	160
M4	370	290	85
Br4	450	310	140
Br14	60	15	50

Figure 4.6.

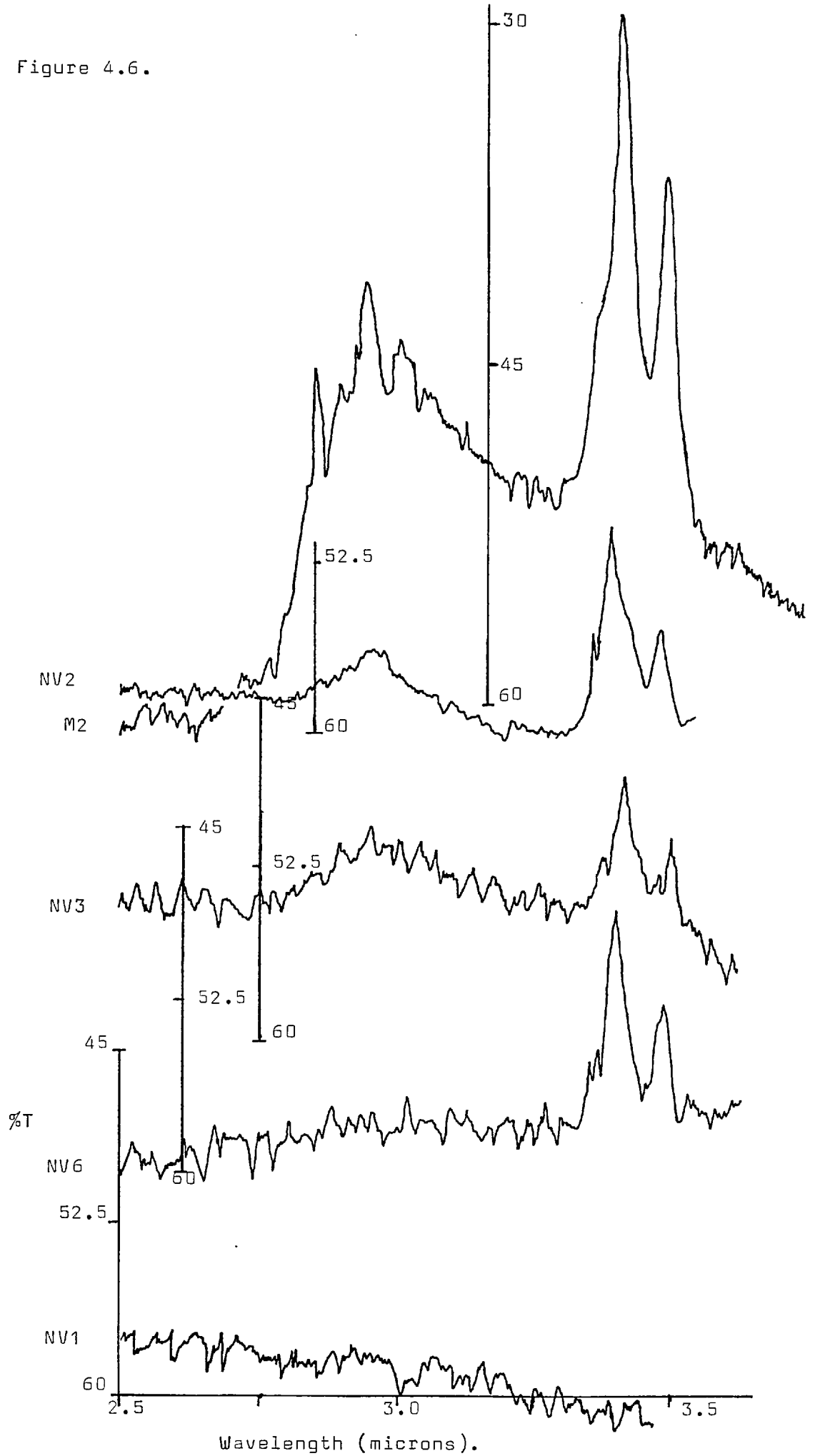
30
45
52.5
60
NV2
M2
45
60
45
52.5
NV3
52.5
60
45
%T
NV6
60
52.5
NV1
60
2.5
3.0
3.5
Wavelength (microns).

Figure 4.6 Caption. The absorption spectra of a number of Brazilian type quartz crystals choosen to show the abnormal absorption maxima at 3.41 and 3.53 microns (2925 and 2825 cm^{-1}).

4.4.3. The Interpretation of the Brazilian Quartz Spectrum.

The superimposed absorption peaks have distinct and repro-ducible frequencies which correspond to the frequencies of the more dominant (or groups of more dominant) bands recorded and identified by Kats (1962). These assignments recorded by Kats have been presented in a table by Dodd and Fraser (1965) and from this it is possible to assign all the reproducible frequencies recorded during this work, with the exception of two, with the minimum of ambiguity. This assignment is presented in table 4.5 , in which only those frequencies identified in this study are listed, the reader is referred to Dodd and Fraser (1965) for the complete assignment, and to Kats (1962) for the reasoning behind it. This table clearly shows the importance of hydroxyl in assoc-iation with lithium and sodium ions as well as that associated with hydrogen, in causing this absorption. The broad background band is almost certainly caused by hydrogen bonded hydroxyl groups, (silanol bonds) (Dodd and Fraser 1965, 1967).

In many of the Brazilian type natural crystals, two further strong absorption bands are often, but not always found at 2925 and 2840 cm^{-1} respectively. The intensity of these peaks is app-arently independent of the background and other absorption peaks in the three micron band (see figure 4.6) and they may be present even when the absorption due to identified hydroxyl vibrations is at a minimum. These absorptions and their assignment are dis-cussed in section 4.4.3a. Figures 4.7 and 4.8 are examples of typical Brazilian type quartz spectra.

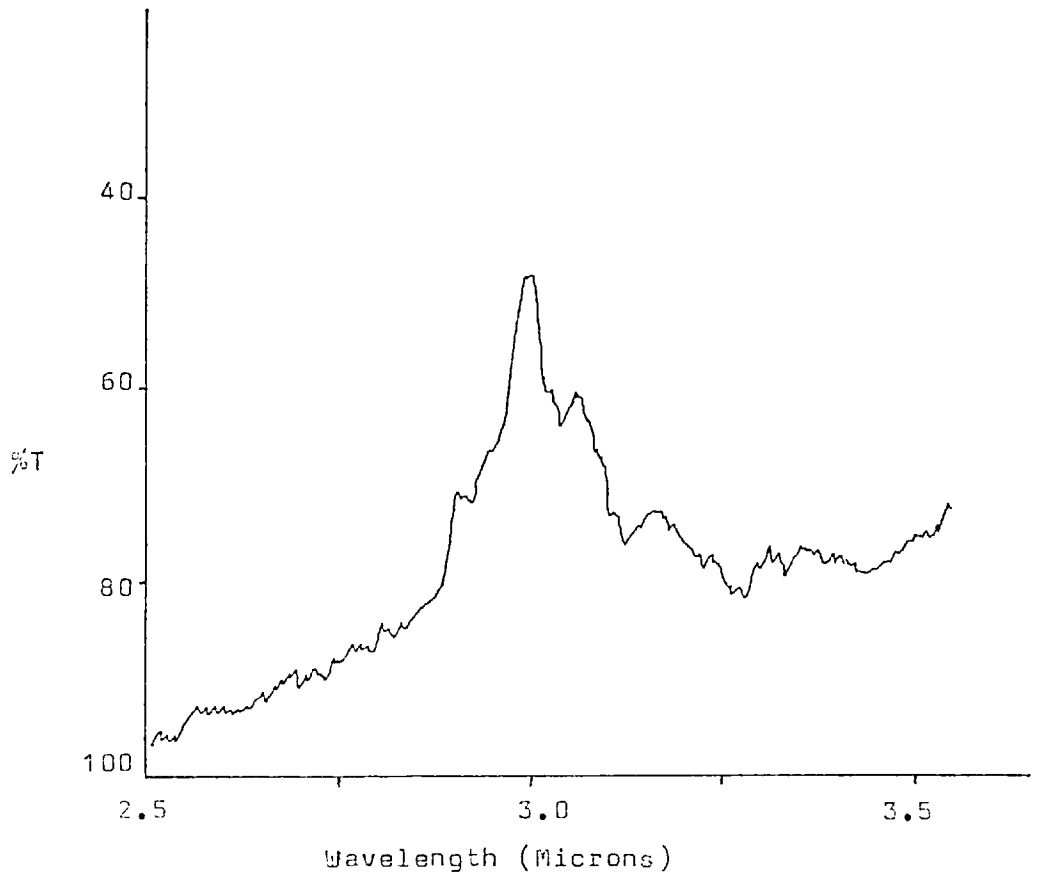

Figure 4.7.

The Infrared spectrum of a thick single crystal slice samole prepared from Brazilian Crystal Br23. This crystal is a smokey quartz crystal from Brazil. The slice was prepared from the centre of this large crystal. (About 5 cm. from the nearest crystal face.)

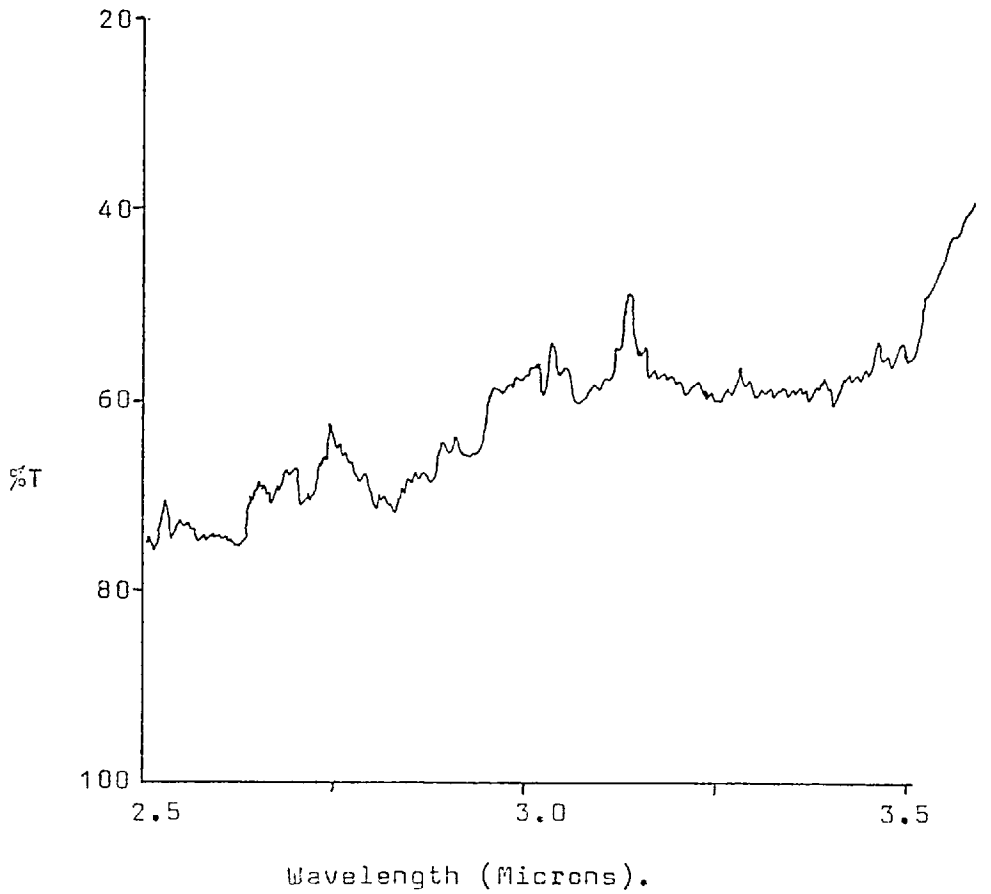

Figure 4.8.

The infrared spectrum of a thick single crystal plate prepared from the Brazilian type quartz crystal Br8. This crystal is a perfect transparent and colourless crystal from Brazil. This crystal is very large, and the sample plate was cut from the centre, some 8 cm. from the nearest crystal face.

Table 4.5. Assignment of the peaks found in the 3500cm^{-1} absorption band for sample M1 in accord with the work of Dodd and Fraser (1965) and Kats (1962). Values in parenthesis are the actual frequencies of the peak maxima in cm.$^{-1}$ deter-mined at 77^{o}K.

Frequency cm^{-1}	OH^- associated with	other.
3512	Li^+(3510) Na^+(3513)	
3485	H^+ (3485)	
3440	Li^+(3440)	
3381	H^+ (3380) Na^+(3382)	
3311	H^+ (3311)	
3200 - 3240	H^+ (3240) H^+ (3222)	Overtone or combination band of Si-O vibration. (3204)
2925	H^+ -	
2825	H^+ -	

Kats (1962) lists a number of possible structural inter-pretations to account for the more complex ionic impurities which he identified in his study of the three micron band. These generally are based on the substitution of a trivalent cation for Si^{4+} (most commonly Al^{3+} and Fe^{3+}) with the hydrogen, lithium and sodium acting as charge compensators. Figure 4.9 shows several possible groupings of this type. This relationship between Al^{3+}, Na^+ and Li^+ in natural Brazilian type quartz has been in-vestigated by Bambuer (1961) who found linear relationships between groups of these ions and hydrogen in analyses of a range of these crystals. His work is summarized in figure 4.10. However the units in Bambuers figures have only qualitative significance because of the error in his data reduction technique for the

structure bound hydroxyl concentration, and the figures can only be used for comparative purposes.

Figure 4.9 Complex ionic groupings suggested for the inclusion of impurities in the Brazilian quartz structure by Kats (1962)

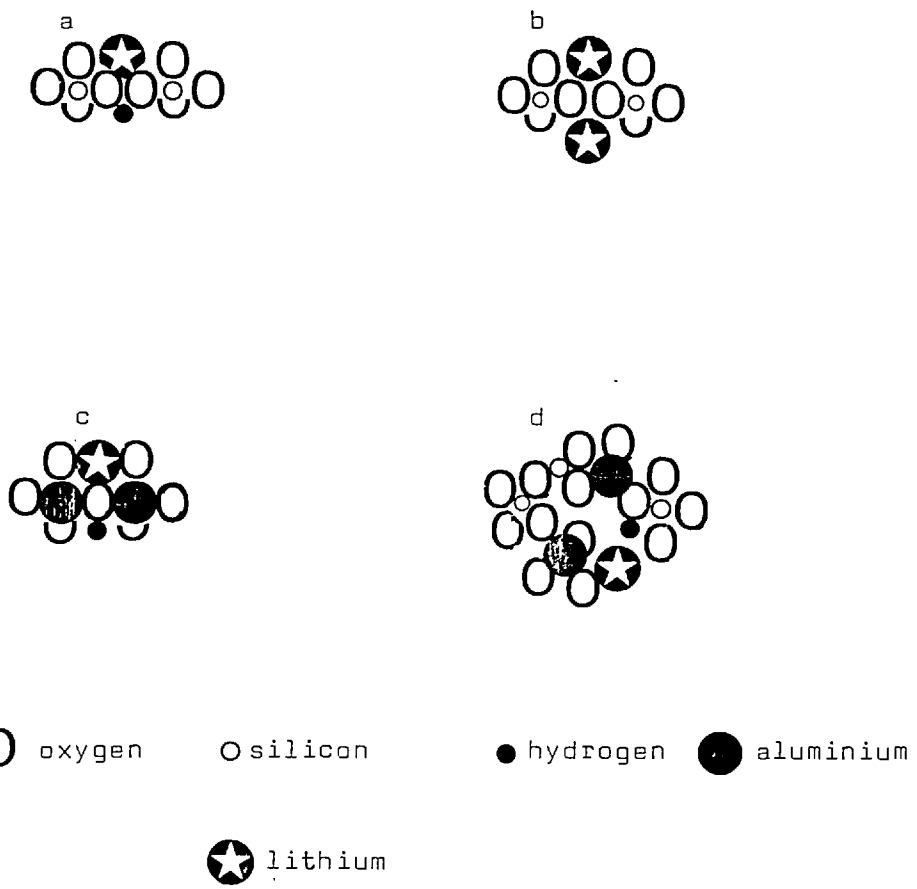

a). A lithium and a hydrogen ion bonded to two non bridging oxygens ions between two silicon ions.

b). Two Li^+ and one H^+ ion bonded to two non bridging oxygen ions between a silicon and an aluminium ion.

c). A Li^+ and a H^+ ion bonded to a bridging oxygen ion between two aluminium ions.

d). A Li^+ and a H^+ ion bonded to oxygen ions of two different tetrahedra in which silicon ions are replaced for aluminium ions and which are located in a c-axis tunnel.

(from Kats 1962).

Figure 4.10.

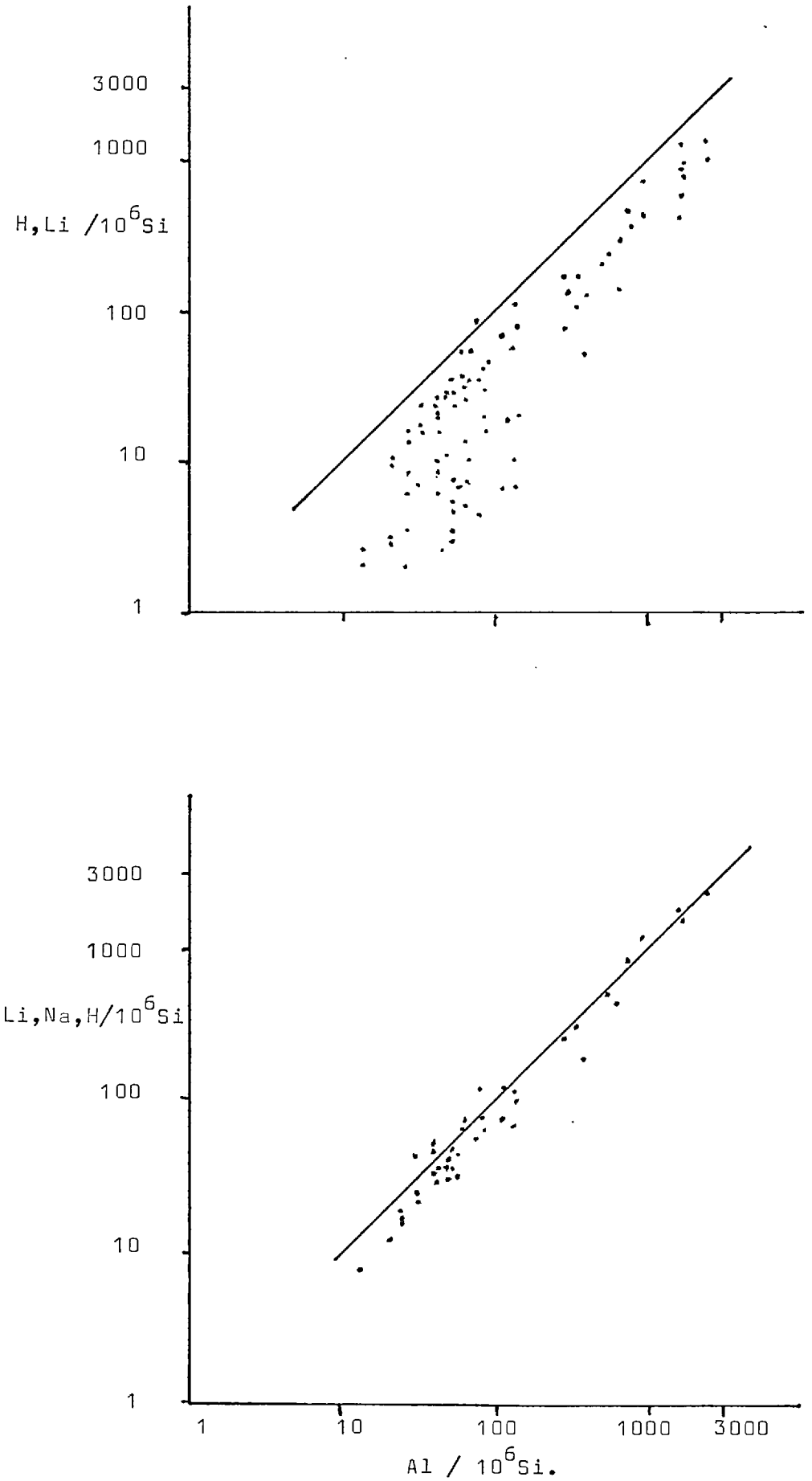
3000
1000
H,Li /10^6Si
100
10
1
3000
1000
Li,Na,H/10^6Si
100
10
1
1
10
100
1000
3000
Al / 10^6Si.

Figure 4.10 Caption.

Plots of the concentration of Al^{3+} versus $Li^+ + H^+$ and $Li^+ + Na^+ + H^+$ concentrations in Brazilian type quartz crystals from alpine veins. From Bambuer 1961.

4.4.3a. The Absorption Peaks at 2920 and 2840cm^{-1}.

These absorption bands at 2920 and 2840 cm^{-1} are not present in the spectra of all Brazilian type quartz crystals (they were not recognized by Kats 1962 or Dodd and Fraser 1965) and thus cannot be assigned to a fundamental SiO_2 vibration nor to its combination or overtone absorptions. Their magnitude is, however, sufficiently great as to make their assignment to some impurity or lattice defect important if reliable hydroxyl analyses are to be calculated from these spectra. Considering the spectra for wet synthetic quartz, the same bands are often present, superimposed on the background absorption at frequencies around 2920cm^{-1} and 2840cm^{-1} which almost certainly result from the same vibration. I found that when reducing the data from the dehydration tests (see chapter 5) that sets of synthetic quartz spectra from the same crystal at different heat treatment temperatures would only produce meaningful results if these peaks were calculated as hydroxyl. In those instances in which the peaks were not present a similar relationship was found. It would thus appear that the peaks are the result of yet another different vibration mode for hydroxyl in the quartz structure. It is possible that this mode is unstable with respect to the others. There are two reasons for this, firstly the dehydration tests indicated that the appearence of these two absorption peaks for any given crystal at any given temperature appeared to be independent of whether they were present in the unheated crystal. Secondly the appear-ence of the peaks were independent of the temperature of the

treatment. Thus although inconclusive it would seem that some other factor such as the rate of cooling controlled their pres--ence in the spectrum. The possibility that the presence of deutrinium in the crystal was responsible for the appearence of these bands was considered but rejected for three reasons. Firstly because of the apparent exchange with known hydroxyl vibrations, secondly because the concentration was much too large and thirdly because Kats (1962) showed that the highest OD^- absorption freq--uency occurs around 2678 cm^{-1} which is considerably lower than the absorption frequencies in question. Thus I conclude that these two bands are related to hydroxyl in the quartz structure.

4.4.4. The Range of Concentrations of Water in Natural Quartz From Various Geological Environments.

The data presented thus far in this chapter has been restr--icted to quartz crystals in which there are very few or no fluid inclusions containing precipitated molecular water. Unfortunately, this is not the case when much of the commonly occuring natural quartz is considered. The three micron band in the spectrum of most commonly occuring natural quartz crystals is nearly always compound, being partially due to absorption by molecular water and partially due to absorption by the structure bound hydroxyl groups. The absence of an accurate independent method of deter--mining the concentration of either of these components at room temperature restricts the usefulness of the spectroscopic data and makes quantitative determination of the concentration imp--ossible.

Presenting the results of these analyses in a meaningful way is thus made difficult. However, as I will show later, it is possible to assume that all of the water found in micro fluid inclusions in natural quartz crystals was originally dissolved in the structure as structure bound water. As one of the major

aims of this chapter is to develop some idea of the concent--rations of structure bound water which may have existed at some time during the history of natural quartz crystals (not necessarily that which exists now) it is possible to put this data to good use. The absorption due to one molecule of water is only one fifth of that caused by one structure bound hydroxyl group, so if the absorption band is analyzed using the absorption coefficient for structure bound water, a conc--entration will be determined which is a minimum value for the concentration of structure bound water which existed in the grain at some time during its history. Obviously such concentrations may be too small by a factor of five, depending on how much of the original structure bound hydroxyl concentration has been precipitated as molecular water.

The data summarized in table 4.6 and figure 4.11 are the results of a survey of the total water concentrations in natural quartz, presented as minimum original structure bound water concentration. The samples represent a range of different geological environments. These results show that contary to previous opinion much of the quartz commonly occuring in nature, in veins or as a rock forming mineral, contains, or has contained at some time, during its history, a large concentration of structure bound water. This would seem to include even that quartz which crystal--lized at, or has subsequently been subjected to, the highest metamorphic grades.

The three quartzite samples studied, 7304, 7327 and Q1 were all analyzed by X ray diffraction to check for substantial contamination by hydrous impurities such as mica. The X.R.D. traces for these samples are given in figure 4.12 and show that both 7304 and 7327 may contain trace concentrations of muscovite, but that Q1 would appear to be almost pure quartz. As only 1%

mica is sufficient to account for all of the water recorded in these analyses, the recorded concentrations for the quartzites 7304 and 7327 must be regarded with care as they may be seriously in error. The result for sample Q1 would however appear to be more reliable.

Table 4.6. Analyses of the water concentrations in natural quartz samples. Those analyses marked with a D were determined from pressed disc samples, all others were from crystal plates. The concentrations are given as structural H /10^6Si, subject to the assumptions discussed in section 4.4.4. which would suggest they are minimum values.

SAMPLE	DESCRIPTION	CONC.
NV4	Crystal with opalescent prism passing into a clear termination.	2075
NV5	Opalescent aggregate of rose quartz from a granite pegmatite, Connecticutt, U.S.A.	650
Q1	Pure Quartz ganister with sedimentary SiO_2 cement.	7500 D
7304	Undeformed pipe rock quartzite) Scotland	3400 D
7327	Deformed pipe rock quartzite)	2750 D
Dev1	Milky Quartz from the Culm, North Devon.	6500
Dev2	" "	3200
Dev3	" "	8900
Dev4	" "	5250
Dev5	" "	11750
Dev6	" "	4300
Dev7	" "	2500
Dev8	" "	7000
Dev9	" "	5250
Dev10	" "	9500
Dev11	" "	13650
Dev12	" "	12150
Dev13	" "	4900
Dev14	" "	9950
Dev15	" "	8100
Dev16	" "	2550
Dev17	" "	6750
Dev18	" "	10870
Dev19	" "	14050
Dev20	" "	6350
Dev21	" "	7900
Dev22	" "	8550
Dev23	" "	4750
Dev24	" "	7150
Dev25	" "	3790
Dev26	" "	5230
Dev27	" "	11340
Dev28	" "	5700
Dev29	" "	2800

Table 4.6 Contin.

SAMPLE	DESCRIPTION	CONC.
K1	Tectonic Vein , North Wales Slate Belt	3100
K2	" "	1500
K3	" "	2750
K4	" "	2000
K5	" "	1750
K6	" "	1500
K7	North Wales tectonic vein cut by later hydrothermal vein which has modified the hydroxyl concentration.	TV =850 HV =600
An1	Transparent quartz from the Anglesey Blueschists, may be pretectonic.	525
An2	Syntectonic milky quartz vein from the Anglesey blueschists.	2500
An3	" "	3500
P3	Intensely deformed vein from the Parys mountain copper mine Anglesey.	2000
EE36	Milky vein quartz, Outer Isles thrust belt Scotland	3000
SS1	Laxfordian Pegmatite quartz Scotland.	2450 D
SS2	" "	900 D
SS211	Intensely deformed quartz vein Laxfordian.	950 D
SS219	Recrystallized quartz mylonite,Laxfordian or Outer Isles thrust belt.	400 D
469JW	Laxfordian pegmatite quartz, Scotland.	5000 D
157JW	Quartz rich metasediment,retrogressed Scourian to Laxfordian, Scotland.	1800 D
158JW	Pegmatites from a late Scourian suite intrud-	2250
242JW	-ed into rocks undergoing charnockite meta-	950 D
460JW	-morphism. 700°C and 7Kbar were the approx- -imate conditions at the time of intrusion North west Scotland.	1600 D
Gra1	Quartz from the west of England Granite.	2100 D

TV = Tectonic Vein. HV = Hydrothermal Vein.

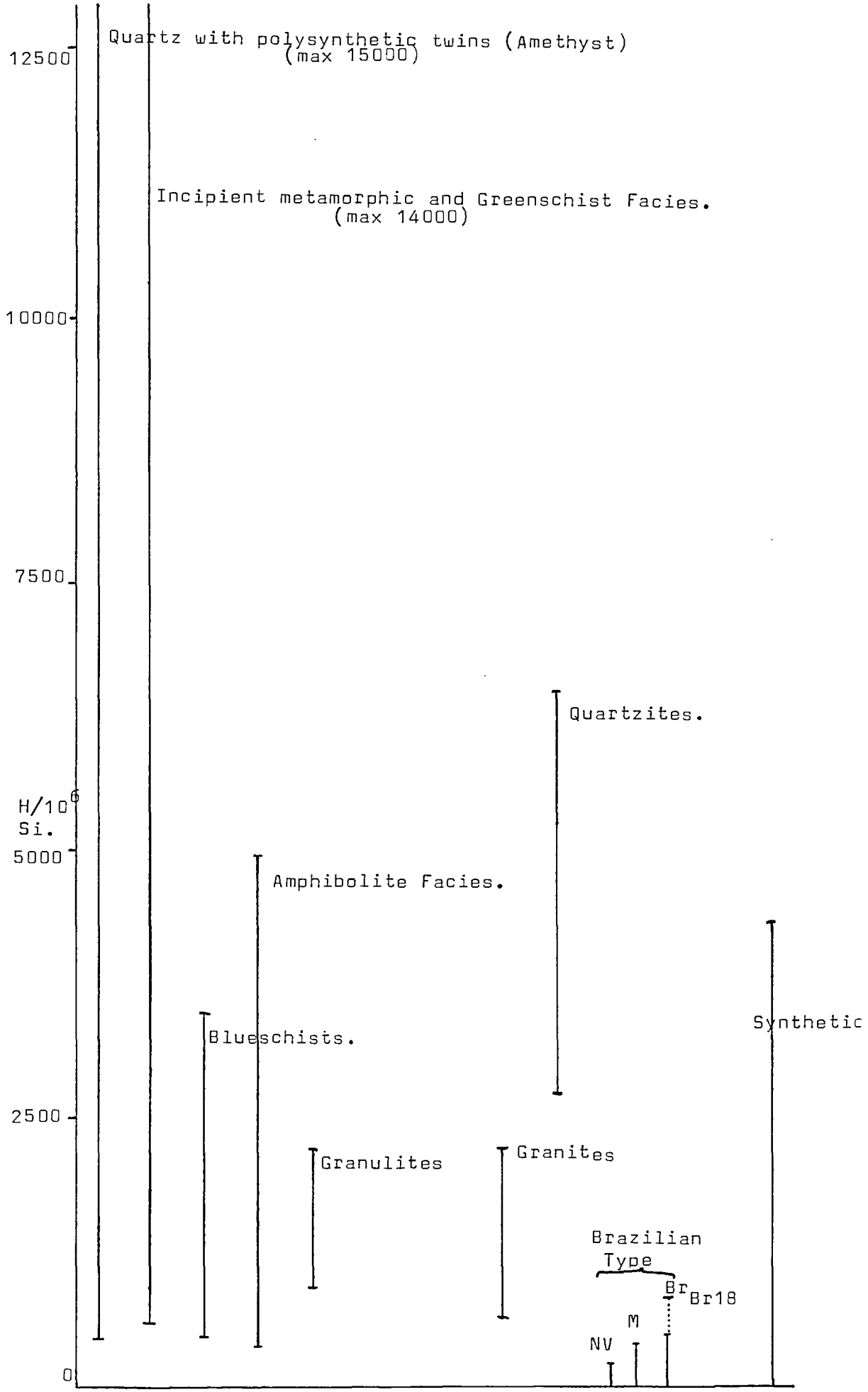

Figure 4.11. The range of concentrations of water, calculated as minimum structure bound water concentration which existed prior to the precipitation of molecular water in the grains, in natural quartz from a number of different environments.

Figure 4.12a Caption. The X ray diffraction trace of quartzite Q1. All the peaks correspond to reflections from the quartz structure so it can be assumed that the hydroxyl absorption for this quartzite does correspond to the actual water con--tent of the quartz grains and there overgrowths.

Figure 4.12b Caption. A similar trace of a sample from quartz--ite 7304 from the pipe rock quartzite in Scotland. Comparing this trace with that in figure 4.12a indicates that some other reflections are present. These reflections correspond to a hydrous phase probably muscovite. Thus the infrared absorption band at 3 microns for this quartzite does not necessarily ind--icate the concentration of structure bound water present in the grains.

Figure 4.12c Caption. The X.R.D. trace for quartzite 7327. This is very similar to the trace for quartzite 7304 and shows the other reflections corresponding to the same hydrous phase. Consequently the structure bound water concentration for this crystal cannot be reliably determined.

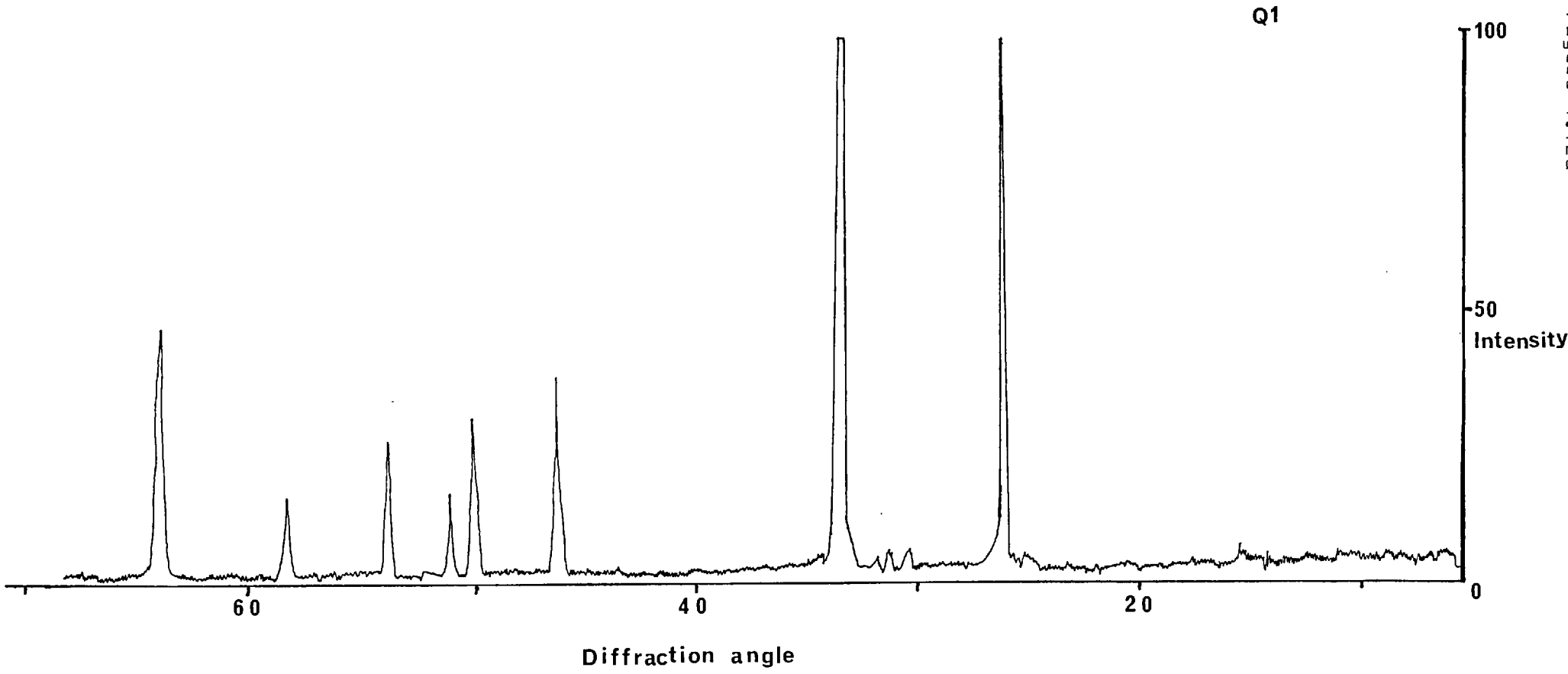

Figure 4.12a

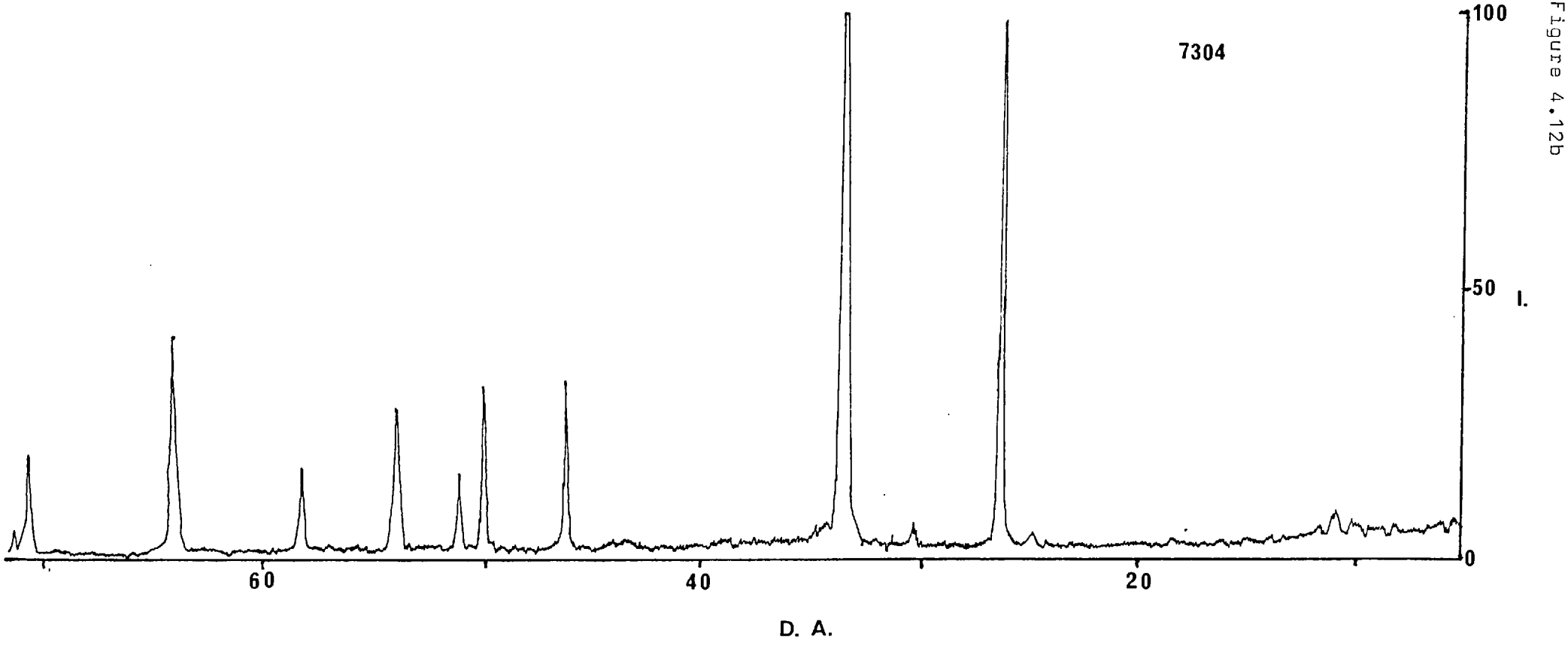

Figure 4.12b

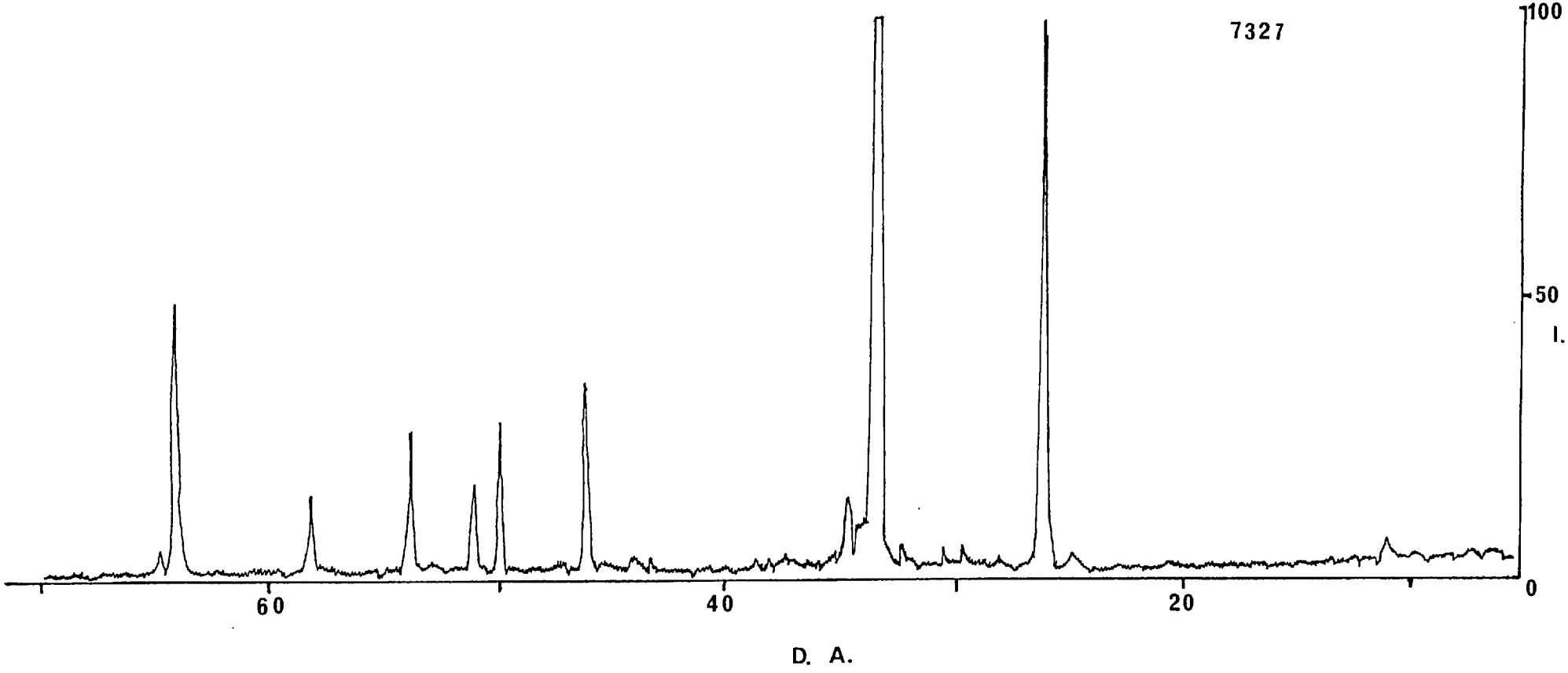

Figure 4.12c.

4.4.5. Interpretation of the Spectra of Natural Low Quality Quartz.

The spectra in figure 4.13 are typical of those recorded for natural quartz with large concentrations of water. These show the nearly horizontal baseline, typical of Brazilian type quartz spectra, and often have a shape similar to that of the three micron band for molecular water. It would thus seem that molecular water together with silanol bonds is the primary cause pf this absorption, and not the more complex ionic groups resp--onsible for the absorption in Brazilian quartz spectra. (See section 4.5). This wet natural quartz also shows differences when its absorption band is compared to that of wet synthetic quartz and it is thus possible to separate the two. These differences in the spectra presumably result from the more comp--lex microstructure in the wet natural quartz (which is twinned, contain fluid inclusions and variable but often large dislocat--ion densities) which will provide special sites for silanol bonds to form, together with the major difference that the wet natural quartz contains a significant proportion of free molec--ular water which the synthetic quartz does not. Another diff--erence may be related to the presence of an impurity phase in the structure of synthetic quartz. This phase, as yet unidentified, is not found at all in natural quartz structures and may account for many of the differences between natural and synthetic quartz, it is the topic of chapter 6.

Figure 4.13

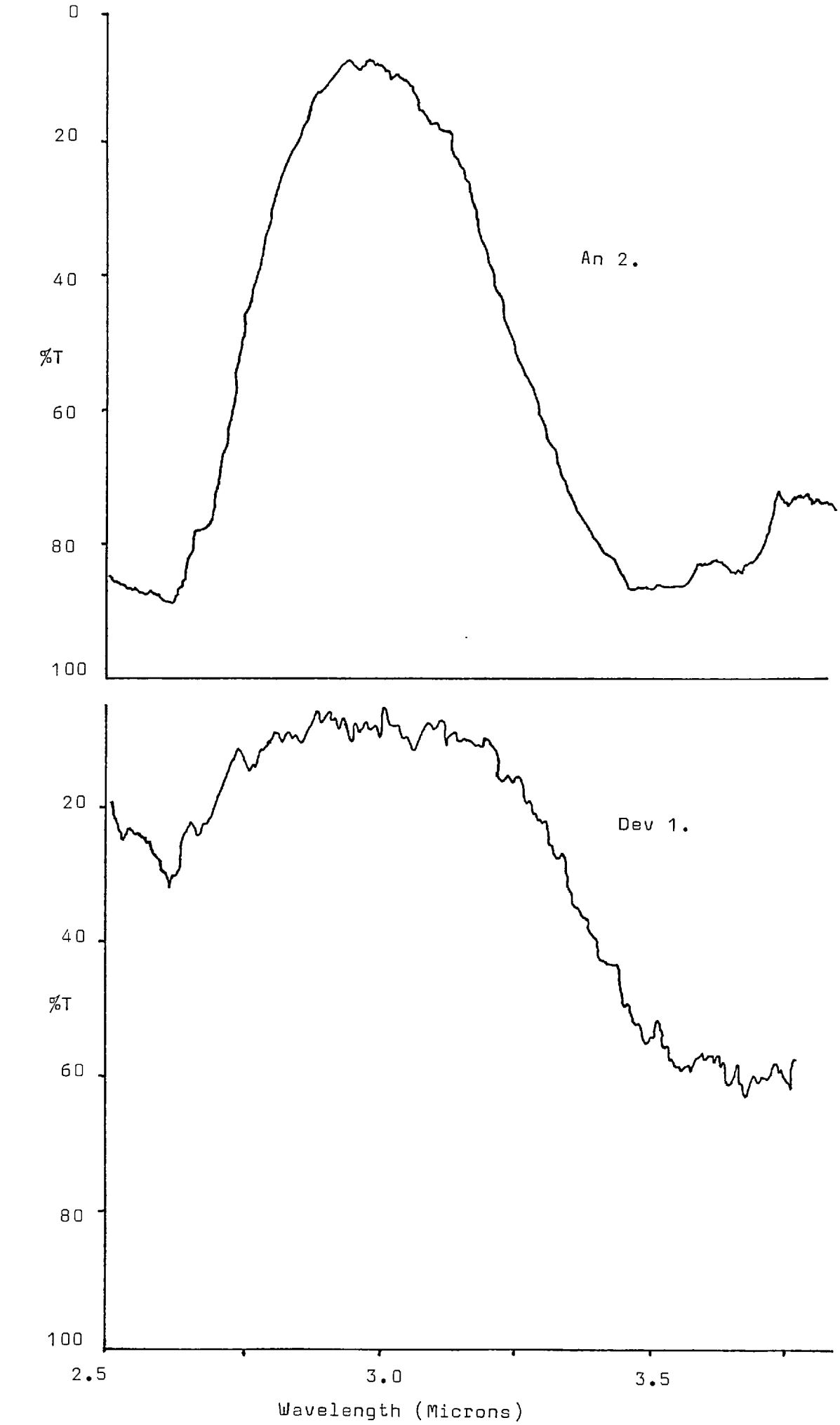
0
20
40
%T
60
80
100
An 2.
20
40
%T
60
80
100
Dev 1.
2.5
3.0
3.5
Wavelength (Microns)

Figure 4.13.

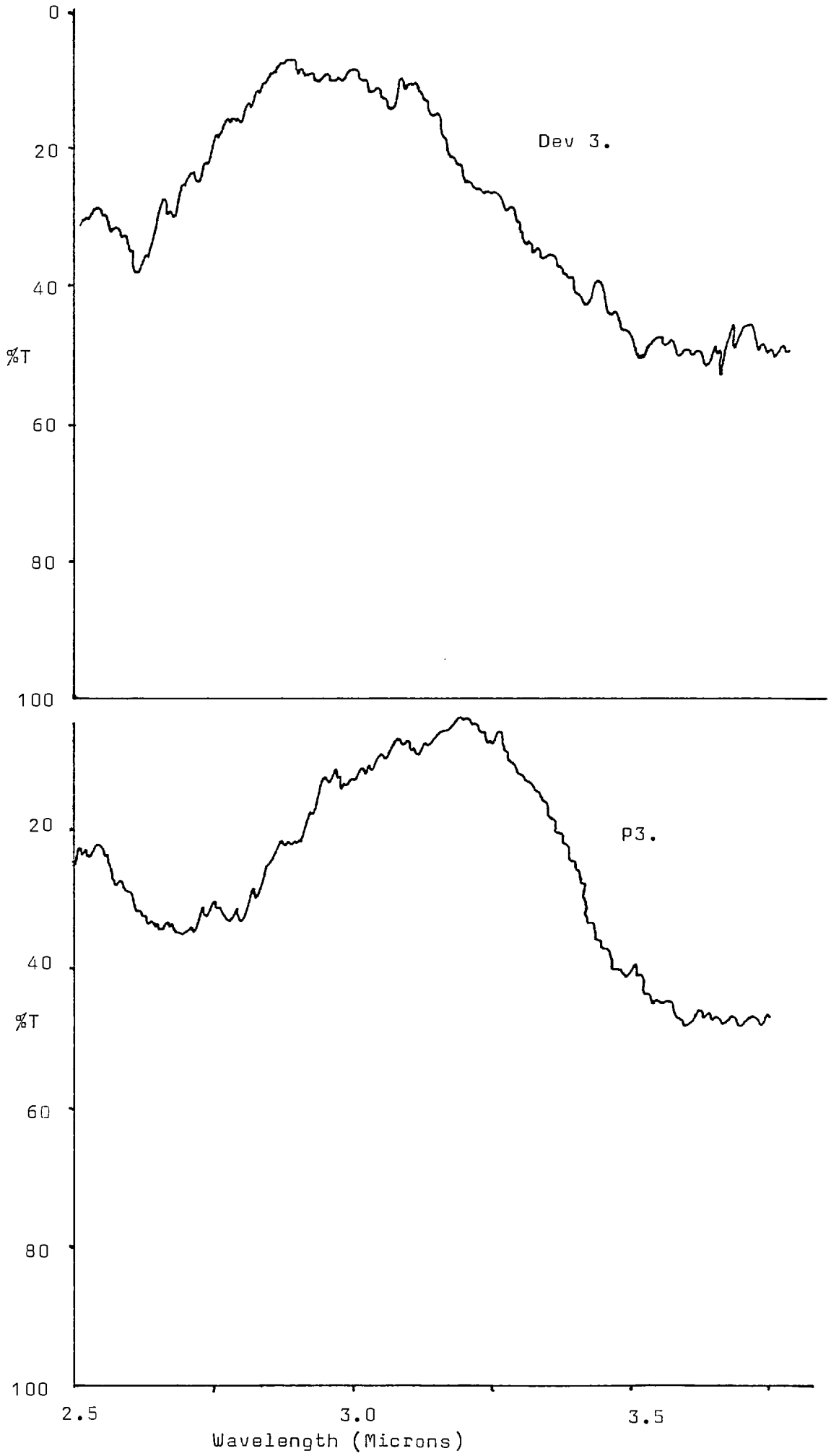
0
20
40
%T
60
80
100
Dev 3.
20
40
%T
60
80
100
P3.
2.5
3.0
3.5
Wavelength (Microns)

Figure 4.13.

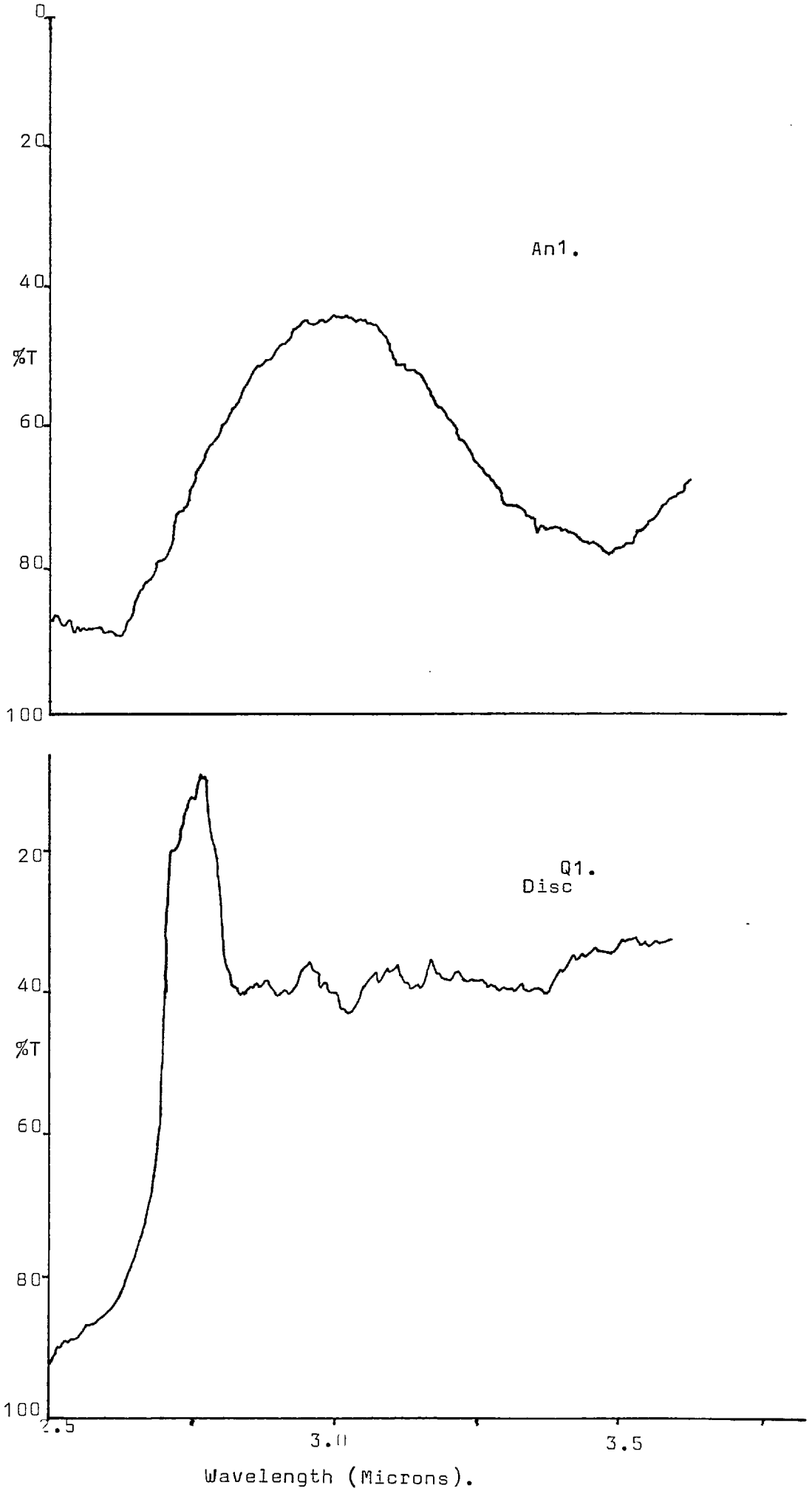
0
20
40
%T
60
80
100
An1.
20
40
%T
60
80
100
Q1.
Disc
2.5
3.0
3.5
Wavelength (Microns).

Figure 4.13

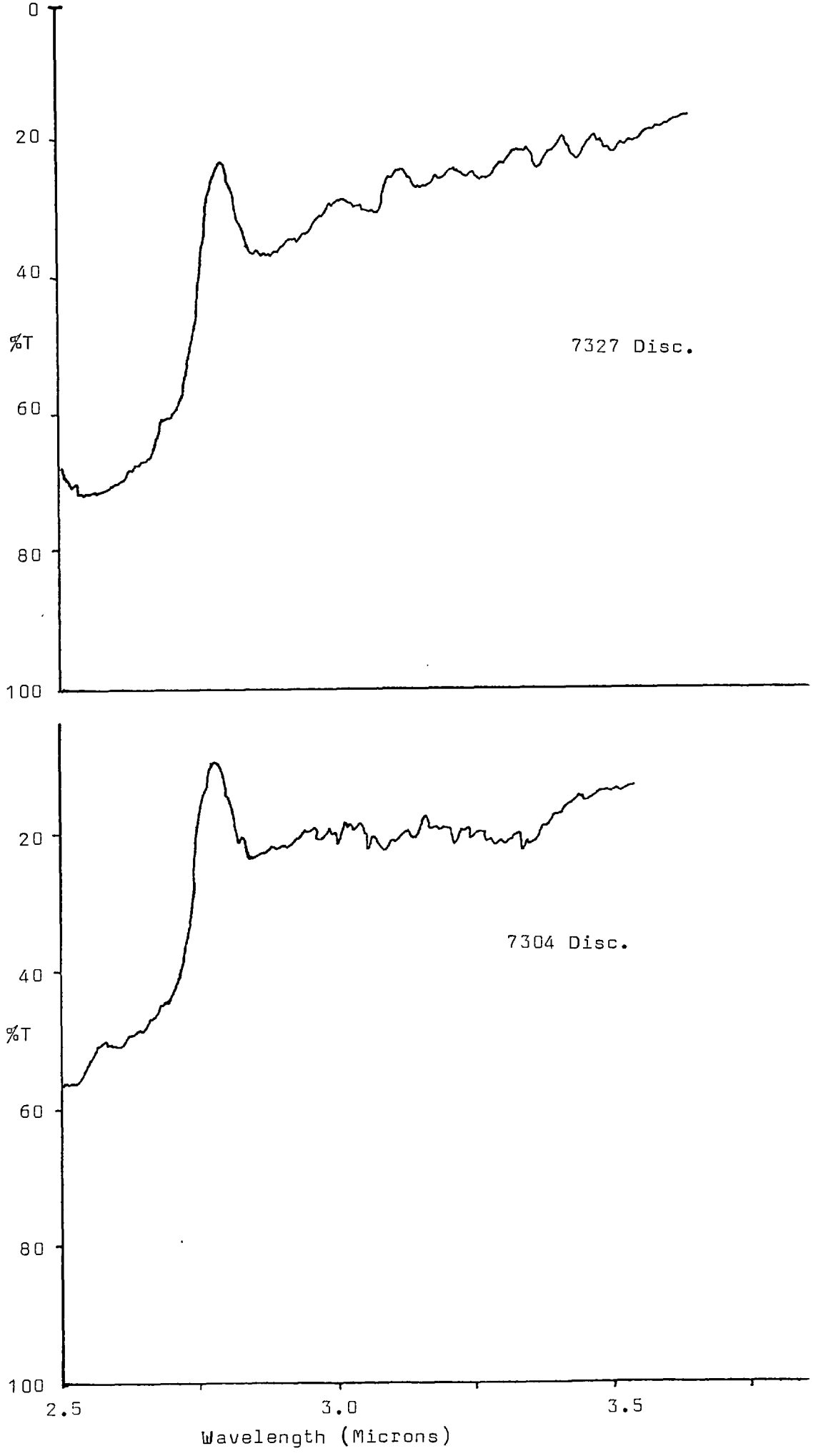
0
20
40
%T
60
80
100
7327 Disc.
20
40
%T
60
80
100
7304 Disc.
2.5
3.0
3.5
Wavelength (Microns)

Figure 4.13.

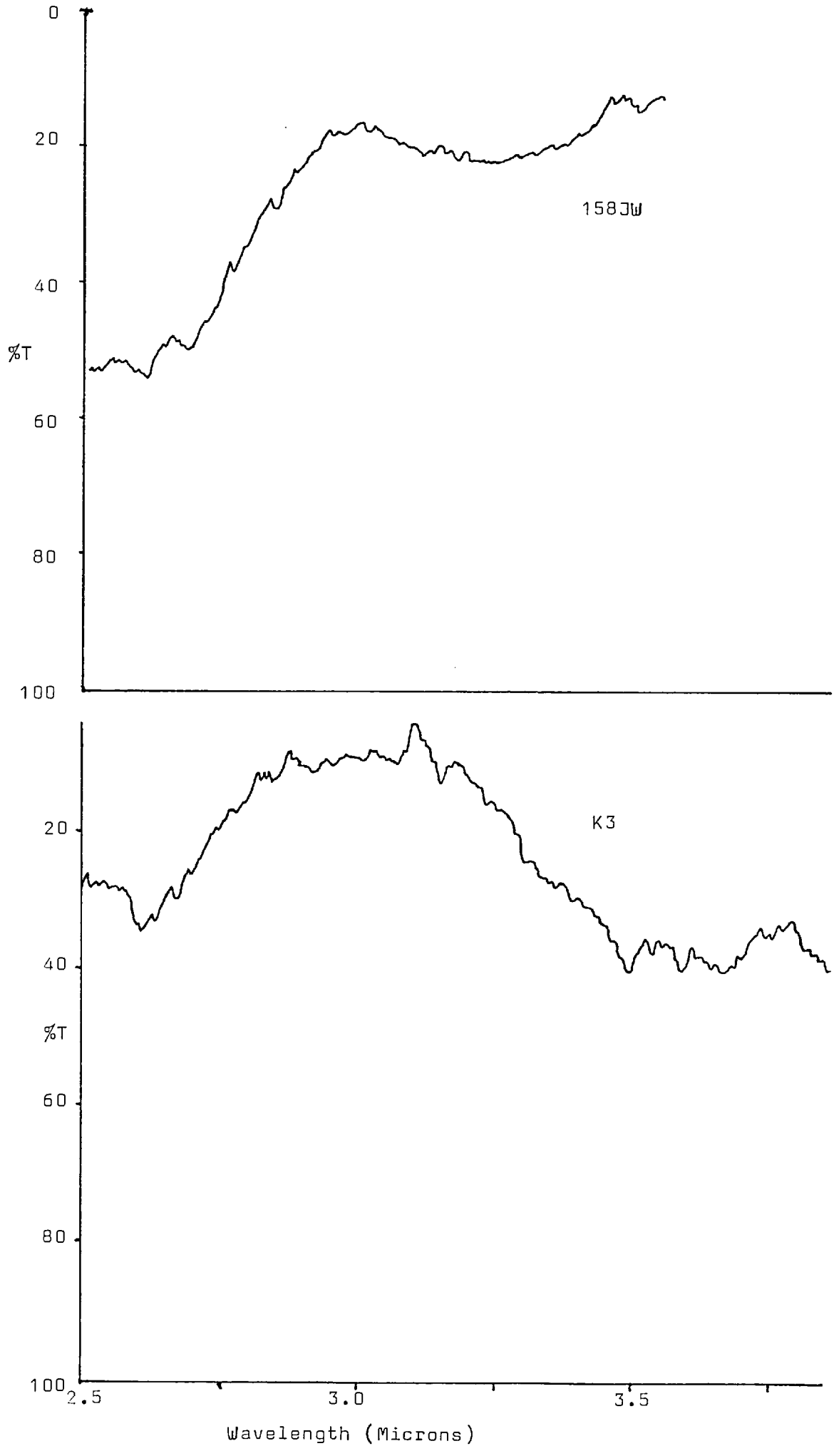
0
20
40
%T
60
80
100
158JW
20
40
%T
60
80
100
K3
2.5
3.0
3.5
Wavelength (Microns)

Figure 4.13 Caption.

Examples of the three micron absorption band for a number of different natural quartz crystals typical of those commonly found in natural quartz environments. These spectra are very different from those normally presented for natural quartz which are taken from Brazilian type quartz crystals.

The three quartzite spectra (Q1, 7304 and 7327) are interesting in so much that they demonstrate a single large absorption superimposed on the background. This single band was not present in the spectra recorded from other disc samples so that it cannot be a result of the sample preparation technique. It must therefore be a feature of the infrared absorption of quartzites which separates them from single crystal samples. This band is probably related to the water bound in the quartz grain overgrowths suggesting yet another mode of bonding. The possibility that the band results from other hydrous silicate phases can be discounted because X.R.D. analysis has shown that the concentration of such impurities in sample Q1 is too small to significantly influence the shape of the three micron absorption band in this sample.

4.5. THE SUBDIVISION OF QUARTZ INTO THREE CLASSES ACCORDING TO THE SHAPE OF ITS 3500 cm^{-1} ABSORPTION BAND.

A study of the literature pertaining to hydroxyl groups in the quartz structure shows that three different molecular structural interpretations have been placed on the spectra. Firstly Brunner (1961) introduced the concept of the silanol group (see section 4.3) in which a Si - O - Si bridge is hydrolyzed by a single molecule of water. Continuity of the structure is maintained by a pair of hydrogen bonds but its strength is greatly reduced, the hydrogen bond being several orders of magnitude weaker than the Si - O bond it replaces.

Secondly Kats (1962) in his detailed study of the 3500 cm^{-1} absorption band in good quality natural and dry synthetic quartz, showed from diffusion experiments that certain of the absorption peaks in this band were due to more complex groups involving hydr--oxyl related to other impurities, notably aluminium, lithium and sodium. Workers studying the relationship between the 3500 cm^{-1} absorption and the anelastic properties of synthetic quartz have concentrated on these bands (Dodd and Fraser 1965, Ballmann *et al* 1966). Bambuer (1962) records direct relationships between the concentrations of these ions in Brazilian type quartz from late alpine veins, and Wood *et al* (1966) record the up take of Fe^{3+} by synthetic quartz, producing an amethyst coloured mineral. The only structural geologist to have considered the possible role of these other impurities in the weakening of quartz is White(1971).

Griggs (*loc cit*) introduced the third model for the location of hydroxyl in the quartz structure when he first published the Frank-Griggs Model of Hydolytic Weakening. In this model (and its subsequent modifications *loc cit*) it is assumed that the hydroxyl in the form of silanol groups is concentrated along the dislocat--ion cores, either relieving tension on the stretched bonds at the

core of screw dislocations or acting as charge compensators at the end of the extra half plane in edge dislocations. Figure 4.14 shows the Frank Griggs model for the inclusion of hydroxyl in the quartz structure.

Figure 4.14

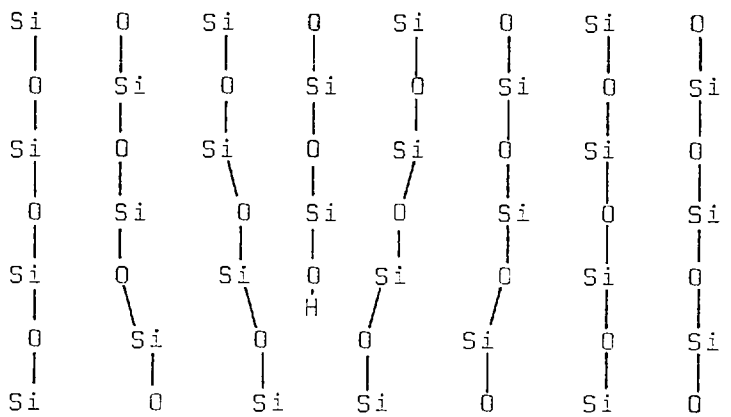

The simplified diagram of an edge dislocation in synthetic quartz in which a hydroxyl ion acts as a charge compensator on the extra half plane as suggested by Griggs (1967). In reality the structure of an edge dislocation in quartz will be far more complex but the idea that water will be concentrated in the dislocation core is almost certainly valid.

I suggest that in any one crystal all three types of structural water will be present to greater or lesser extent, namely:-

1) Hydrating Si - O - Si bridges.

2) Forming complex groups with Na^{+}, Li^{+}, Al^{3+} and Fe^{3+} ions.

3) As silanol bonds or the more complex groups bound up in the dislocation microstructure of the crystal, together with precipitated molecular water contained in fluid inclusions. It being the relative concentrations of each of these three groups

which influences the final shape of the 3500 cm^{-1} absorption band in the absorption spectrum of any quartz crystal.

An examination of Tables 4.2, 4.3, and 4.6, and Figure 4.11 shows that natural quartz can be divided into two types according to the hydroxyl concentration. 1). The high quality, transparent, colourless and smokey[1] Brazilian type quartz crystals with small hydroxyl concentrations, generally less than 500 $H/10^6Si$. 2). The opalescent and other natural crystals not included in group 1 which have hydroxyl concentrations in excess of 500 $H/10^6Si$ and which may exceed $10^4H/10^6Si$. In these natural crystals molecular water makes a contribution to this determined hydroxyl concentration. This subdivision may be equally effectively made if the shape of the absorption band is taken, group 1 having a complex absorption band with superimposed absorption peaks, typical of Brazilian quartz, whilst group 2 always shows a single broad absorption peak with a horizontal baseline similar to that for molecular water. Previous infrared studies have concentrated on quartz of type 1 (as have mechanical studies of natural quartz single crystals) whilst it is obvious that it is quartz of type 2 that it is typical in nature (see figure 4.11). This is in contrast to previous ideas.

Kats (1962) demonstrated that amethyst and its naturally bleached equivalent citrine have spectra similar to those of his dry synthetic quartz (this is however wetter than the Brazilian quartz he studied) and Mclaren and Phakey(1966) have demonstrated that quartz with polysynthetic twin lamellae may show hydroxyl

---

Footnote 1. The term smokey quartz is used here to group all black, brown and green natural quartz which has a small hydroxyl concentration, akin to that found in natural,transparent, colour--less Brazilian type quartz. Quartz in this group does not turn milky on heating. The term Brazilian citrine (Kats 1962) could be used for this quartz but citrine has been shown to have similar properties to amythest (Kats 1962, Mclaren 1966) which is more akin to synthetic quartz than to the material presented under the label Brazilian type quartz in this study.

concentrations up to and exceeding those for wet synthetic quartz. Thus citrine and amethyst may be included in group 2 above, restricting group 1 to Brazilian type colourless and smokey crystals, a distinction which should be used to define Brazilian type quartz.

All synthetic quartz may be classed together as a third group. This group (group 3) would be restricted to all quartz which shows a 3500cm^{-1} absorption band with a distinctly sloping baseline, such that the less the frequency the smaller the value of Io. Obviously from the spectra illustrated in this and the preceeding chapter, most quartz shows a baseline with a slight slope but it is seen that only the synthetic crystals show steeply sloping baselines. Such quartz also turns milky when heated for long periods at high temperatures (assuming sufficient hydroxyl in the structure) (see chapter 5) and contains large concentrations of solid impurity particles which do not affect the clarity of freshly grown samples and can only be detected in the transmission electron microscope (see chapter 6).

Thus it is possible to state that most of the quartz occuring in nature (group 2) is fairly similar to synthetic hydrothermally grown quartz which has been heat treated to precipitate some of its structural water in molecular form in voids. However, the presence of an impurity phase unique to the structure of synthetic quartz, together with differences in the shape of their spectra, separate synthetic quartz into a third group. The group 1 natural quartz which has often been taken by experimentalists to represent all natural quartz, is distinctly different and may be considered in a class of its own.

Examples of each of these three classes of quartz are shown in plates 4.1 and 4.2.

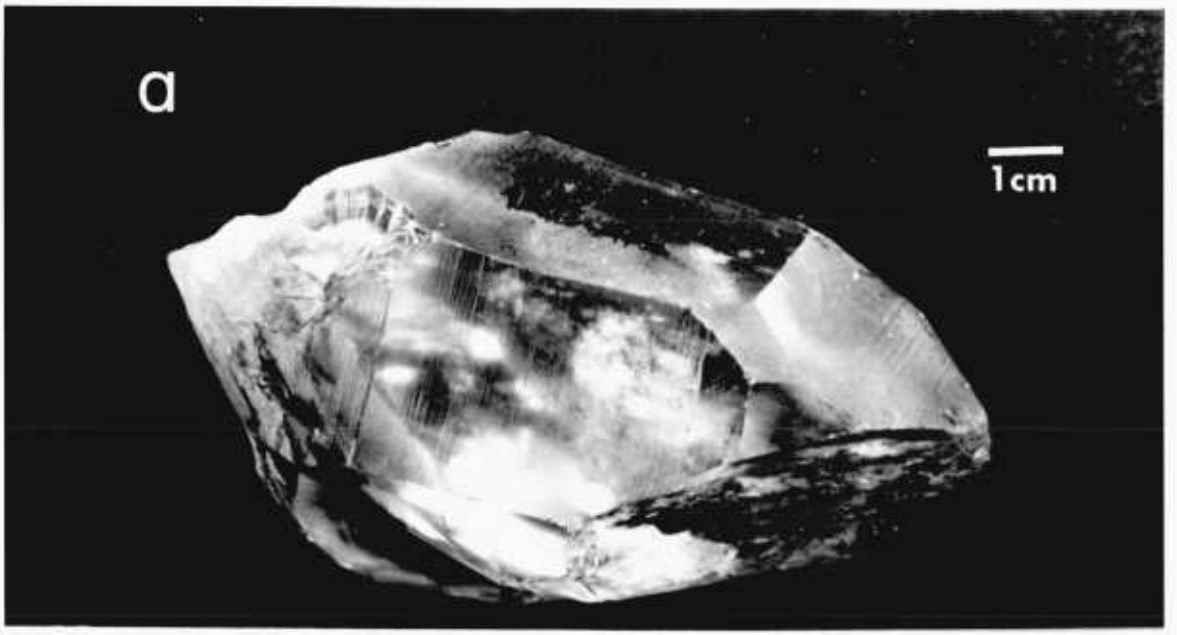

Plate 4.1a

A BRAZILIAN TYPE QUARTZ CRYSTAL.

Plate 4.1b

A NATURAL MILKY QUARTZ CRYSTAL.

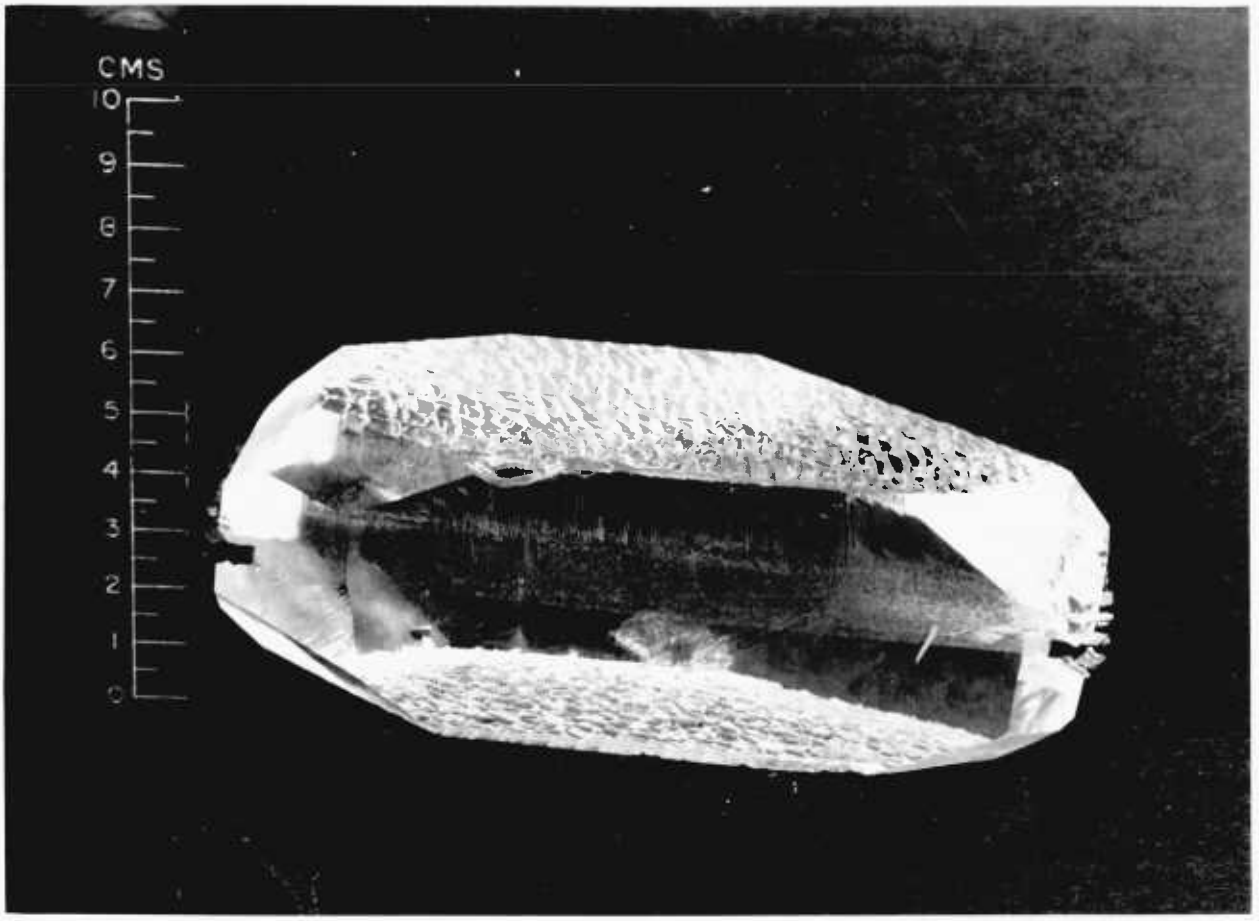

Plate 4.2

A TYPICAL SYNTHETIC QUARTZ CRYSTAL.

4.6. WATER WEAKENING OF NATURAL QUARTZ.

4.6.1. Predicted Weakening of Group 2 Quartz.

Griggs (1974) relates the weakening temperature **Tc** with the hydroxyl concentration according to the relationship :-

$$\bar{c}\left[H/Si\right] = 7.4 \times 10^{-8} \exp\left(15700/R\,Tc\right) \qquad 4.1.$$

where **R** is the gas constant. This relationship is incorrect in its present form, because of the error in the Griggs hydroxyl determinations. It can be simply corrected however by halving the pre-exponential term giving it a value of 3.7×10^{-8}. Using the value of 0.007 H/Si for the sandstone Q1 gives a weakening temperature of $310^{o}C$ for deformation at laboratory strain rates, whilst the amethyst reported by Mclaren with 0.015 H/Si will be weak at an even lower temperature. This of course assumes that the water currently contained in the fluid inclusions was orig--inally dissolved in the structure, and if this assumption is correct it means that most natural quartz was potentially very weak at some stage during its history.

Mclaren (1966) used the relationship :-

$$\Pi\, d^2 n = 3NkT/2\gamma \qquad 4.2.$$

in which **d** = the diameter of the bubbles,

k = Boltzmanns constant,

N = the number of gas molecules,

n = the density of the bubbles.

T = the absolute temperature of bubble formation,

and γ = the surface energy of quartz.

to develop an idea of the structure bound water concentration responsible for a given bubble density, (assuming that the water behaves as an ideal gas).For a typical coalescent vein quartz crystal, with a bubble density of around $10^{14} cm^{-3}$ (this is the

most commonly recorded bubble density from electron micrographs of milky quartz), a temperature of formation of 200°C, an average bubble diameter of 1000Å and taking the surface energy of quartz as 1000 erg cm^{-2} (Mclaren 1966, Brace and Walsh 1962) this gives an original structure bound water concentration of 3000C H/10^6Si. Increasing the bubble density to $10^{15}cm^{-3}$ increases this value by an order of magnitude to 300000H/10^6Si: bubble densities of this order are commonly recorded locally within milky quartz grains. The weakening temperature for milky quartz which contained this amount of water in its structure would be around 225°C for deform--ation at laboratory strain rates. This is in good agreement with the inferred temperatures (from fluid inclusion studies) and obser--ved features (from electron micrographs) of naturally deformed vein quartz. Thus it would seem possible to use the mechanical data for synthetic quartz to account for the observed microstructure in natural, low grade metamorphic, deformed quartz rocks and veins.

Using this rather simple relationship from Mclaren (1966) and comparing the predicted water concentrations with those deter--mined by Infrared spectroscopy is interesting. Typically low grade vein quartz,gives concentrations of around 5000 H/10^6Si when its spectrum is analyzed using the absorption coefficient for structure bound water. As some fraction of this absorption is infact due to molecular water, this concentration may be up to five times greater. Typically, from the Mclaren relationship, natural vein quartz will have about 30000 H/10^6Si contained within its bubble population, and as this value compares closely with the inferred value of 25000 H/10^6Si, it would seem to suggest that most if not all of the water is trapped in bubbles. The implied error stems from four sources, firstly,the water does not behave as an ideal gas (so that somewhat more water is contained in the bubbles than predicted). Secondly, from the experiment to compare the absorption

of structure bound and molecular water (see chapter 3) the ratio of five to one is a minimum and may in practice be closer to ten to one giving the measured concentration a value of 50000H/10^6Si, if it is entirely precipitated in bubbles. Thirdly the assumed value of 1000 erg cm^{-2} may not be correct. Finally in counting the bubbles in the electron micrographs, the third diamension parallel to the direction of beam propogation is ignored and the bubble density calculated as if the micrographs were two dimensional. This will give a slight over estimate in the value of n in equation 4.2. Allowing for these sources of error it would seem probable that most of the structure bound water in this natural quartz has been precipitated in the fluid inclus--ions and that the structure is nearly dry, perhaps with concent--rations of structural water closely akin to those reported for Brazilian quartz.In the next section I shall demonstrate that structural water which has been precipitated in molecular form in bubbles can no longer weaken its host grain.

4.6.2. The Weakening Effect of Water in Natural Quartz.

Natural milky quartz crystals are a more difficult material to work with than are the good Brazilian or synthetic crystals. This is because specimens cut from natural samples, especially vein quartz samples, often contain rather random arrays of grain boundaries and healed fractures which cause serious planes of weakness in specimens cored for deformation experiments. The quantitative nature of the effect of the large densities of fluid inclusions is also unknown but these must influence the mechanical properties. However, in an attempt to determine whether molecular water in microfluid inclusions could influence the mechanical properties in a way similar to that reported by Griggs (loc cit) for structural water, a few experiments were conducted on natural milky quartz crystals.

The object of these experiments was to establish if natural milky quartz showed a weakening temperature using a similar relax--ation experiment to that used by Griggs and Blacic (loc cit) to define their weakening temperature in synthetic quartz crystals (see figure 4.15). These experiments were conducted on a new solid medium deformation apparatus which was designed and built as part of this project (see appendix 3). Specimens were cut from the nat--ural quartz sample P3 from the Parys Mountain copper mine on Anglesey. This was selected because it had a large uniform grain size, a uniform milkyness suggesting a uniform bubble density and an apparent lack of colouration due to contamination by other minerals, as well as a low density of vugs and voids.

Figure 4.15.

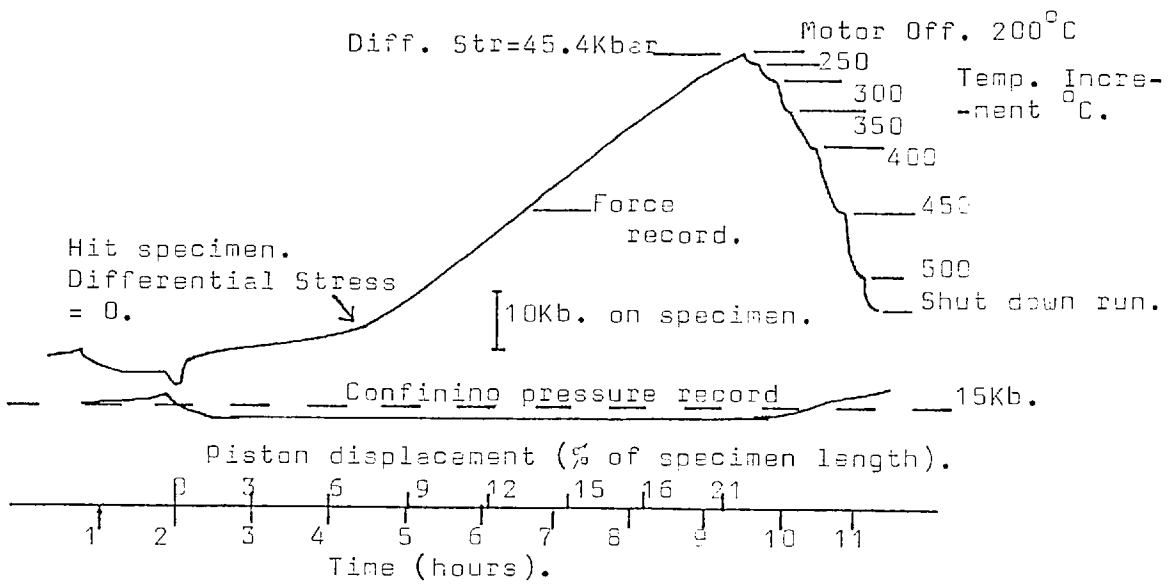

The relaxation experiment used by Griggs (1967) to demonstrate the weakening temperature for synthetic crystal Xo, the weakening occuring at the change of slope (400°C). A similar technique was employed in this study to look for a weakening temperature in natural quartz.

The experimental procedure was that used by Griggs and Blacic (loc cit), namely the sample was taken to a large differential stress (30 Kilobars) at a comparatively low temperature (250°C) and the motor was then stopped. The temperature was then increased in 50°C steps at 20 minute intervals until some high value (1000°C) was reached. Figure 4.16 illustrates the output from such an exp--eriment, being a plot of stress supported by the specimen against time, with the temperature of each relaxation increment marked in, and plate 4.3 shows an electron micrograph of the finally recrys--tallized specimen compared with the undeformed material.This specimen becomes very weak at high temperature, but does not show the single weakening temperature reported by Griggs for his syn--thetic material. Figure 4.17 is a plot of $\log_e$stress versus the reciprocal temperature, and shows two breaks in slope. This speci--men gives a minimum water concentration of 2000 H/10^6Si which if calculated as molecular water would be of the order of 10000 H/10^6Si. It would seem possible that the high stress change in slope is associated with the onset of weakening in the wettest parts of the structure (possibly the quartz adjacent to the bubble surfaces) and that the lower stress change in slope is caused by the more general weakening associated with the remaining structural water or with the onset of recrystallization. From plate 4.3 it can be clearly seen that the specimen has recrystallized and that the water originally in the bubbles has been transferred to voids in the grain boundaries, leaving a bubble free structure. The high stress change in slope occurs at 350°C and the low stress change in slope at 520°C., these corresponding to weakening caused by 10500 H/10^6Si and 740 H/10^6Si respectively (following equation 4.1.). However this stepped relaxation experimental technique

Figure 4.16.

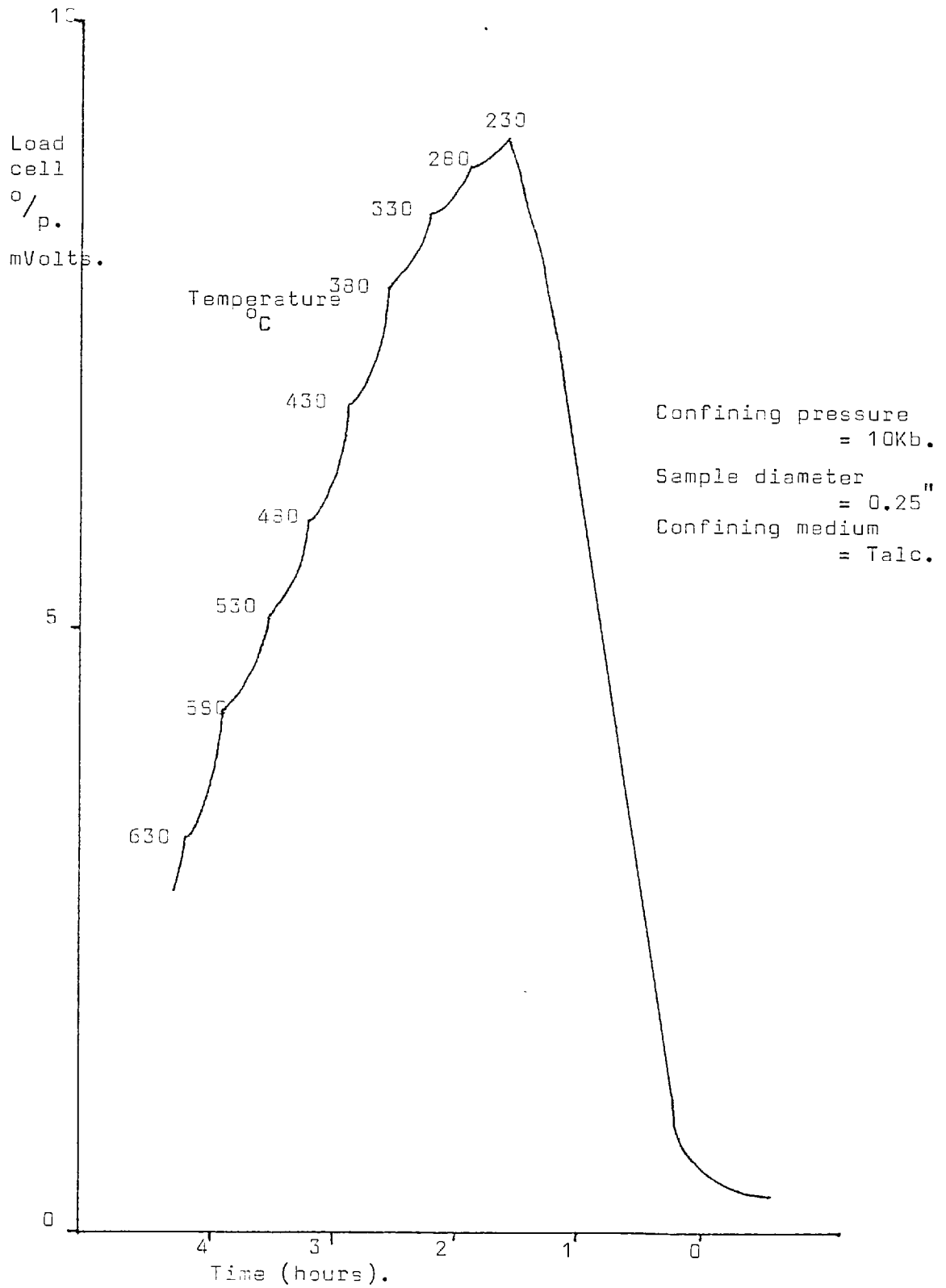

The loading history of a specimen cut from the natural quartz sample P3.

Figure 4.17.

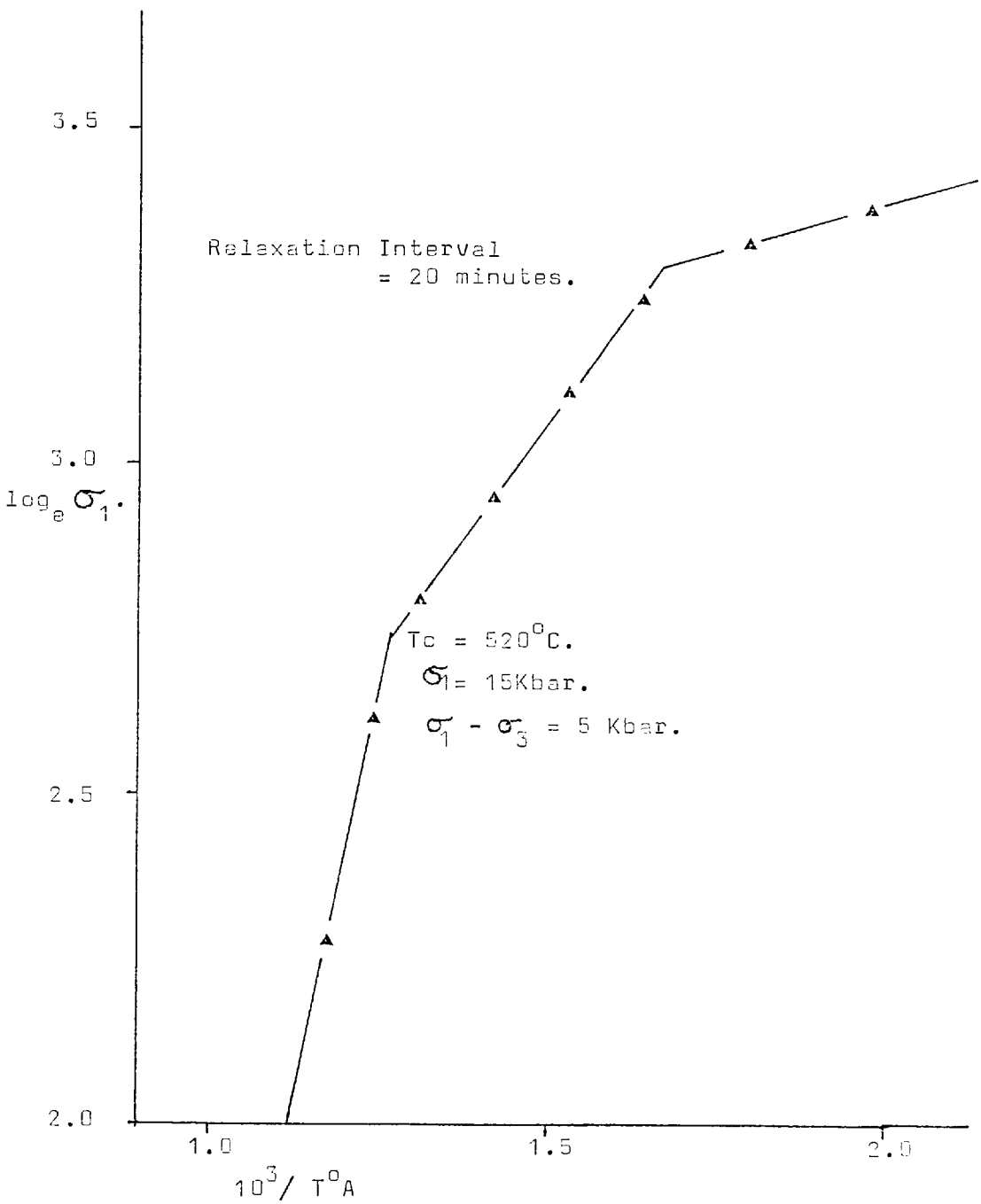

The temperature dependence of the flow stress from a stepped relaxation experiment on a specimen cut from samole P3.

Figure 4.17b.

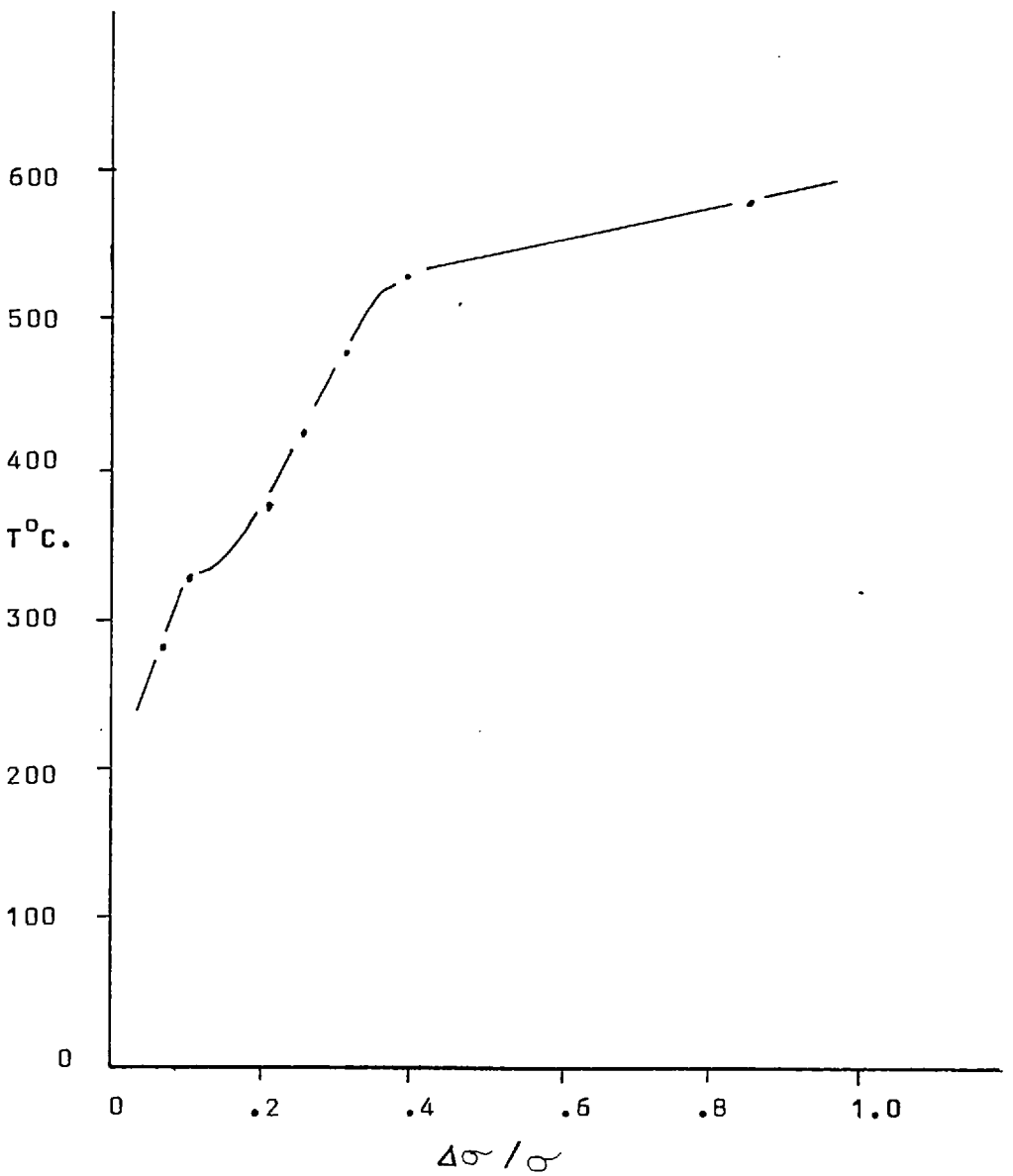

The data in figure 4.17a replotted on the same axis as that used by Griggs, see figure 2.3, and comparing this curve with those in figure 2.3 shows that this natural milky quartz crystal behaves in a manner intermediate between the wet synthetic and the dry natural crystals studied by Griggs.

is very unreliable so that the data in figure 4.17. may be show--ing an apparent rather than a true effect. It would thus seem probable that natural milky quartz is weakened by the proportion of the water remaining bound in the structure but that the water precipitated in the fluid inclusions does not play any signifi--cant role in this weakening of the structure. This is not how--ever to say that the synthetic quartz data is completely appli--cable to making predictions of the weakening to be expected in natural quartz deformation. Synthetic quartz contains an impurity phase which will significantly effect its mechanical properties, and these effects may have been confused with those of the struct--ure bound water. This impurity does not appear to occur in natural quartz so that its effects are probably not felt in natural quartz deformation. See chapters 6 and 7 for a discussion of the role of this impurity in synthetic quartz deformation.

4.7. THE USEFULNESS OF THE SOLID CONFINING PRESSURE MEDIUM DEFORMATION MACHINE.

The experiments by which Griggs and Blacic (loc cit) defined the weakening temperatures for their synthetic quartz samples were conducted using a solid confining pressure medium deformation mach--ine. Infact the majority of the deformation experiments conducted on quartz specimens have utilized deformation rigs of this type. The solid medium deformation machine constructed as part of this study was based on the original Griggs design (see appendix 3) but with an improved design for the inside of the vessel.

Whilst using this deformation machine to heat treat quartz at 850^{o}C and 10 kbar. confining pressure I noticed that the speci--mens of synthetic quartz contained a well developed microstructure similar to that observed in much naturally deformed quartz. Compar-

-ing this microstructure to that of an identical specimen, with the same orientation, from the same growth bands of the same crystal heat treated at 850°C and 1 atmosphere, revealed that this microstructure developed in rèsponse to shear stresses gener--ated in the solid confining medium deformation rig. Knowing the mechanical properties of this crystal it was apparent that these stresses must have been in excess of 1 kilobar to have instigated the observed deformation at this temperature. Plate 4.4. shows examples of the microstructures generated in each of the heat treated specimens.

As a result of these experiments I feel that the solid medium deformation machine is not a suitable design for use in detailed deformation studies. Certainly doubts must be cast on many of the published mechanical results for quartz deformation (loc cit). In view of this I would suggest that in future deformation studies a gas confining pressure medium deformation machine be used rather than the solid medium machine. Existing studies of the mechanical properties of quartz which have utilized the gas pressure machine have amply demonstrated the superiority of the mechanical data gleaned from this apparatus (Hobbs et al 1972, Morrison-Smith et al 1976).

4.8. CONCLUDING STATEMENT.

The data presented in this chapter indicates that much of the quartz found in the natural deformation environment contains large concentrations of water and as such is more closely akin to heat treated synthetic quartz than to natural Brazilian type quartz crystals. This natural quartz normally shows a large concentration of molecular water in voids as well as some, normally small, conc--entration of structure bound water. This molecular water was orig--inally dissolved in the crystal structure and as such probably

played a significant role in the weakening of this natural quartz. Following its precipitation in voids, the effective structure bound water concentration is thus reduced and the crystals strength increased. This water which, by analogy with the experimentally observed water exsolution behaviour of synthetic and natural quartz, was originally dissolved in the structure probably played a very important role in the deformation histories of most meta - quartzites and tectonic veins.

The deformation of natural quartz cannot be explained by direct analogy to the water weakening of synthetic quartz, although the theory in its broadest terms may apply. This occurs for two reasons, firstly because the water, once precipitated in voids, cannot weaken the structure and thus does not assist in the deformation. Secondly because an impurity phase which probably modifies the mechanical properties of all synthetic quartz crystals is not present in natural quartz and thus cannot alter its mechanical properties The mechanical properties of synthetic quartz are thus modified by the combined influences of structural water and the solid impurity phase whilst those of most natural quartz were originally influenced by structural water which has been precipitated in fluid inclusions during the period of geological time following the formation of the grain.

* * * * *

Chapter 4.

ELECTRON MICROGRAPHS.

Plate 4.3. Caption.

4.3a). The microstructure of natural milky quartz crystal P3 prior to deformation in the solid confining medium machine. Note the widely and irregularly distributed dislocations and bubbles.This specimen shows a typical natural quartz microstructure.

4.3b). The effect of deformation on the microstructure of sample P3. Note the new grains, which have a low dislocation density and the movement of water into the new grain boundaries.

4.3c). A larger region of the deformed specimen P3 showing the uniform grainsize of the new grains, straight grain boundaries and triple junctions.

Plate 4.4. Caption.

4.4a). The microstructure produced by the heat treatment of a synthetic quartz specimen at 850^{o}C and atmospheric pressure for 24 hours. Note the large bubble density and small number of disl--ocations.

4.4b). The microstructure produced by the heat treatment of a synthetic quartz specimen at 850^{o}C and 10 Kbars. 'apparently' hydrostatic pressure in the solid confining medium deformation rig. Clearly the applied pressure was far from hydrostatic in its action on the sample. Note the subgrain forming in the centre of the area.

4.4c). As 4.4b. but a different area of the foil.

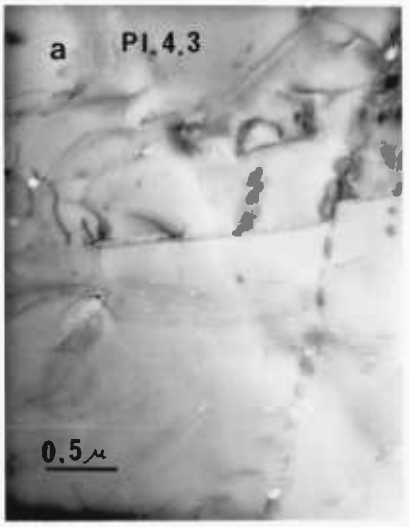
a
Pl. 4.3
0.5μ

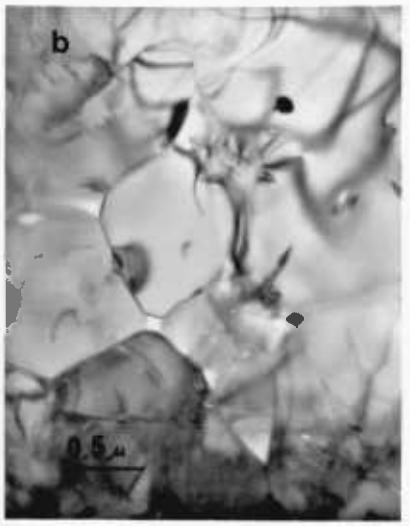
b
0.5μ

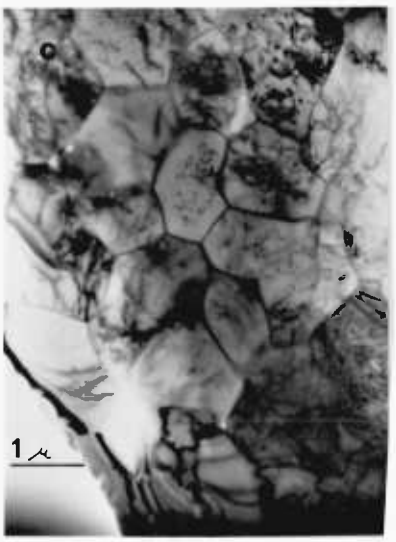
c
1μ

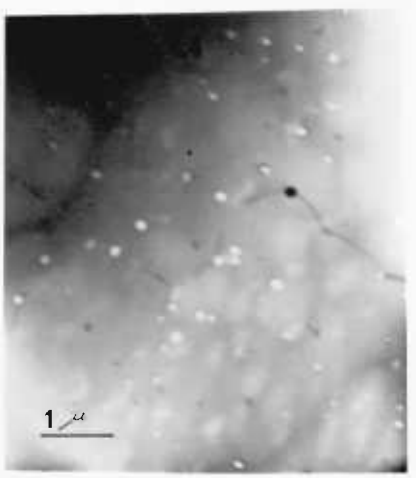
1μ

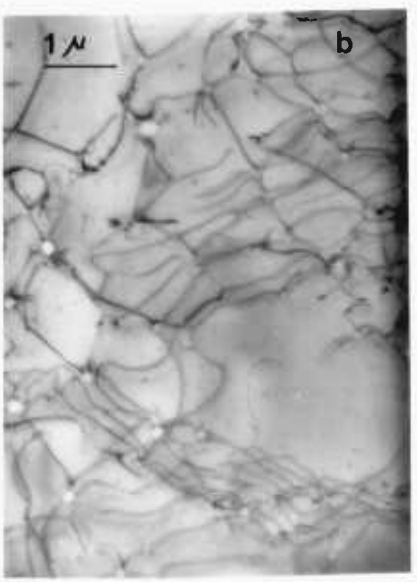
1μ
b

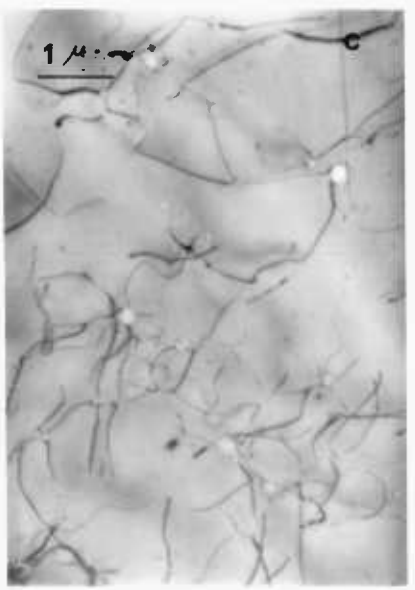
1μ
c

Chapter Five.

DEHYDRATION OF THE QUARTZ STRUCTURE.

Chapter 5. DEHYDRATION OF THE QUARTZ STRUCTURE.

5.1. INTRODUCTION

In experimental studies on the hydrolytic weakening of quartz (loc cit) it has always been assumed that the hydroxyl concentration determined in the laboratory before the start of a deformation test, is the same as that which existed in the sample throughout the duration of the test. The only widely mentioned exception to this assumption being the isolated examples in which it has been claimed that hydroxyl ions have diffused into the sample from the confining pressure medium (Griggs, Blacic, loc cit, Tullis et al 1973). This assumption, as to the constant hydroxyl concentration in the crystal at elevated temperatures has never been verified by experiment, or predicted from theoretical considerations, but it is critical to the interpretation of quartz deformation test results.

A study of the literature on hydroxyl in synthetic quartz (loc cit) suggests that this assumption may be far from correct, and it is because of this that I started to investigate the influence of temperature on the hydroxyl concentration, finding that the concentration is greatly reduced at elevated temperatures, and consequently that the assumption is incorrect.

5.1.1. Literature Survey

Many of the studies of hydroxyl in synthetic quartz refers to a milkyness which develops when synthetic crystals with large hydroxyl concentrations are heated. The precipitated phase responsible for this milkyness has been variously interpreted as either a complex aluminium silicate, or molecular water, before being finally proven to be molecular water by Dodd and Fraser (1965, see this paper for a review of these interpretations). The appearance of bubbles of molecular water within the hitherto perfect continuous structure of

synthetic quartz crystals that have been heat treated, strongly suggests that the structure bound hydroxyl concentration is being reduced, i.e. the silanol bonds are being broken down to Si-O-Si bridges and molecular water.

Kats (1962) reported that the magnitude of certain of the absorption maxima in the 3 micron region of the quartz spectrum are reduced if the crystal is heated prior to analysis, Dodd and Fraser (1965) report a similar effect. This reduction in intensity of absorption occurred in both natural (Brazilian type) and synthetic quartz.

Dodd and Fraser (1967) correlated the spectroscopic and observational evidence finding excellent correlation between the wettest growth bands in the unheated sample, and those regions in the heated sample (from the same crystal in the same orientation) which show maximum milkyness (due to Rayleigh scattering) and hence the maximum bubble density. On the strength of this evidence it can be positively concluded that hydroxyl is precipitated out of the structure as molecular water when the crystal is maintained at elevated temperatures and atmospheric pressure.

McLaren (1966) studied amethyst in the electron microscope. He found that,if he heat treated his samples prior to microscopic analysis, they were full of small bubbles and that if the heating period was long enough the bubbles assumed an equilibrium shape as negative crystals (from which he calculated a very reasonable value for the surface energy). Even this study however failed to cause any reappraisal of the original Griggs and Blacic studies (loc cit) and it became generally accepted (for no apparent reason other than convenience) that this dehydration was completely suppressed by small increases in pressure and did not occur at pressures of interest to geologists, a view still apparently

held by Christic and co workers (1977).

Published electron micrographs of experimentally deformed synthetic quartz (Ayensu and Ashbee 1977) often show bubbles (voids) similar to those reported by Mclaren from his amethyst. These have never been acknowledged as resulting from dehydration of the structure in work predating Ayensu and Ashbee (1977), and Blacic (1975) interprets such bubbles as evidence for the dehydration of the talc confining pressure medium, and the subsequent diffusion of the released water into the quartz sample. I hope to establish that this latter reaction is highly improbable.

5.1.2. Scope of this Chapter

As a result of this confusion in the literature, I undertook a detailed study of the dehydration reaction for natural (Brazilian type) and synthetic quartz crystal structures. It is the results of these experiments which are presented in this chapter. Most of this work was conducted at 1 atmosphere (and if no pressure is mentioned 1 atmosphere can be assumed) but sufficient high pressure runs were conducted to show that hydrostatic pressures up to 10 kbar do not greatly alter this reaction. These high pressure runs also show Blacic's (loc cit) assumption of water diffusing from the talc into the quartz at the talc dehydration temperature to be incorrect.

This study shows that there is room for considerable reinterpretation of the original deformation experiments on synthetic quartz and raises serious doubts as to the validity of the constant used in theoretical models of the hydrolytic weakening phenomenon. Further these results show that the hydroxyl concentration of every crystal and even different parts of the same crystal show completely different temperature sensitivities. These sensitivities vary sufficiently to

make it suprising that reproducible sets of mechanical data related simply to the room temperature hydroxyl concentration could be collected from deformation experiments if the assumption that the mechanical properties are directly dependent on the hydroxyl concentration is correct.

5.2. EXPERIMENTAL TECHNIQUE

The design of experiments to investigate the influence of temperature on the structure bound water concentration in quartz crystals is extremely simple. Samples of suitable shape and size for infrared spectroscopic analysis are cut from the crystal, taking care that each set of samples is cut from a homogeneous area (especially with synthetic quartz where the orientations shown in figure 4.2 were rigorously adhered to). These samples are then placed in furnaces and each heated to a different temperature for the desired period of time. The "time at temperature" for quantitative analysis of the results was taken to be the period from switching on the furnace, to the start of the cooling down period. In practice the period during which the sample was at some temperature other than the desired value was always very small compared with the time of the desired temperature and hence would not significantly modify the equilibrium obtained.

5.2.1. The Apparatus Used

The furnaces used in these experiments were small tubular types purpose made in the laboratory. The central tube was of crystallized alumina wound with 'Kanthol' high resistance wire. This was coated in 'Pyruma' refractory cement and baked in an oven at 100°C for 24 hours. This central tube unit was supported between asbestos discs and packed with 'Kao Wool' to provide good thermal insulation. This

whole unit was then cased in stainless steel. Figure 5.1 is an actual size diagram of such a furnace.

The temperature was monitored using a standard stainless steel sheathed Chromel-Alumel thermocouple connected either to a digital volt meter or to a chart recorder. The cold junction was a similar thermocouple maintained at $20^{o}C$. The single cold junction was arranged to be used in conjunction with any number of recording thermocouples and reading/display devices. (See figure 5.2.a.).

Power to the furnaces was supplied as stabilized mains current held constant at 240 volts A.C. stepped down using a "Variac" variable transformer to give a range of voltages across the windings from 0 to 260 volts A.C. In earlier heating experiments an Ether "Transitrol" temperature controller or a digital comparator were used to control the temperature, but this was found to be unncecessarily accurate and extravagant on equipment. So that in the majority of the experiments the temperature was regulated simply by setting the variac from a calibration curve and adjusting it twice a day. I found that this simple procedure enabled the temperature to be maintained within plus or minus $10^{o}C$ for periods in excess of a week. This simple power supply arrangement is given in figure 5.2b.

5.2.3. The Dehydration Reaction

The dehydration reaction will be of the general form

$$Si\text{-}OH\ HO\text{-}Si \underset{\text{cooling?}}{\overset{\text{heating}}{\rightleftharpoons}} Si\text{-}O\text{-}Si + H_2O$$

although probably more complex in detail. This reaction poses difficulties for its determination by spectroscopic means. This is because both the hydroxyl ions on the left hand side and the molecular water on the right hand side show infrared absorption at similar

Figure 5.1. Actual size cross section of one of the cylindrical Furnaces used in the heating experiments.

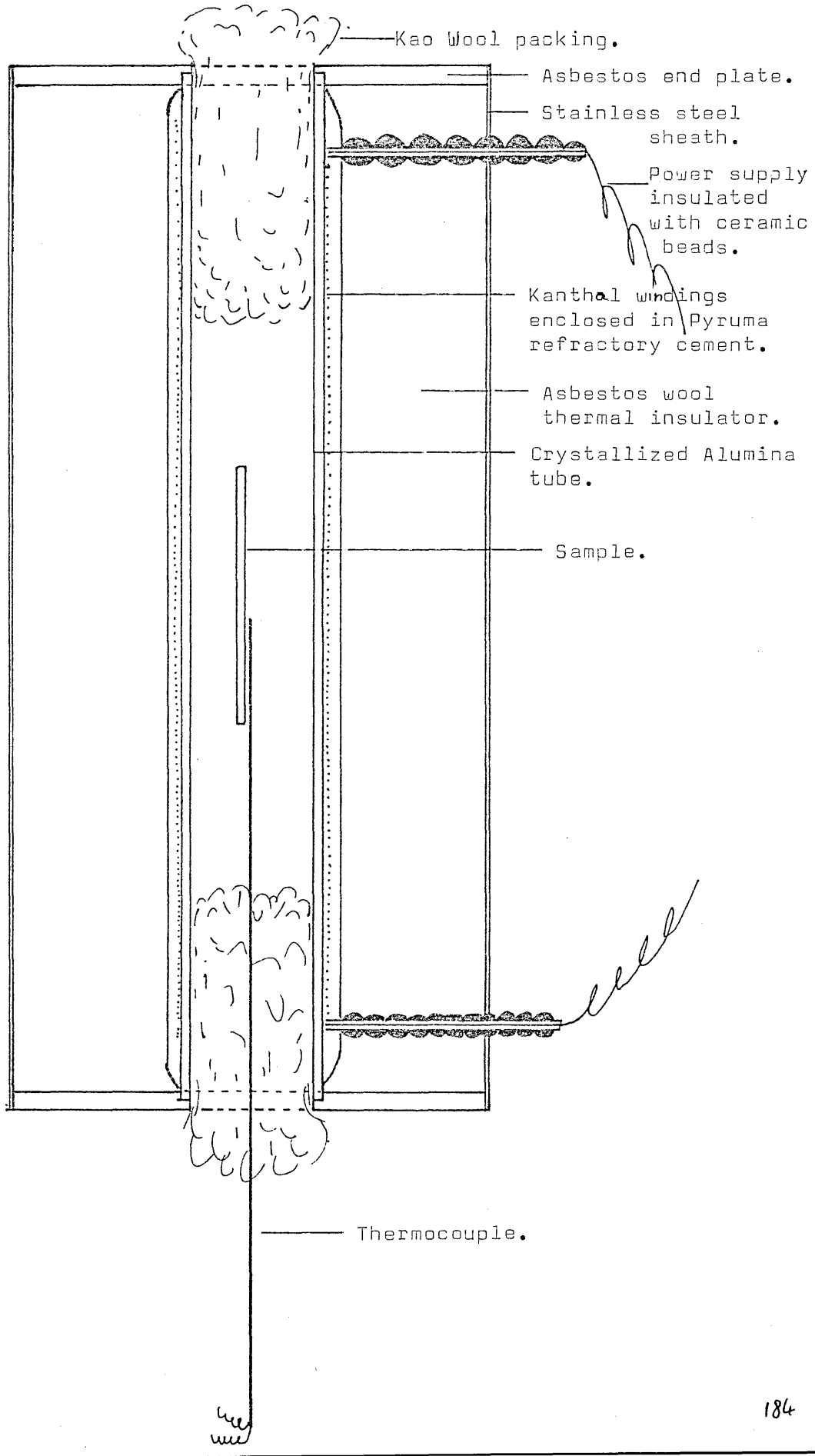

Figure 5.2a. The arrangement for using a number of thermocouples with a single reference junction at 20°C (or any other preset temp.).

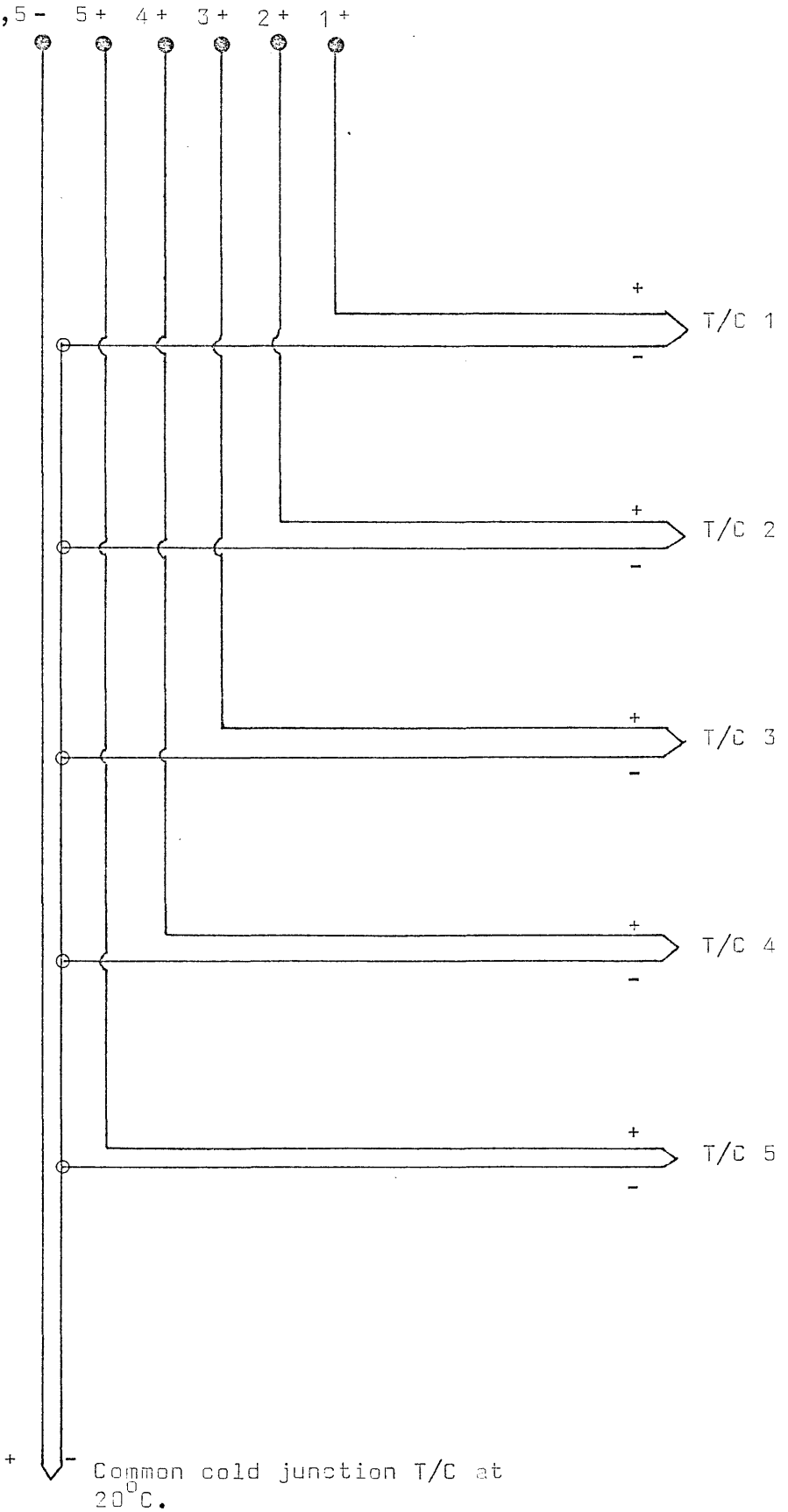

Figure 5.2b. The power supply circuit for the furnaces.

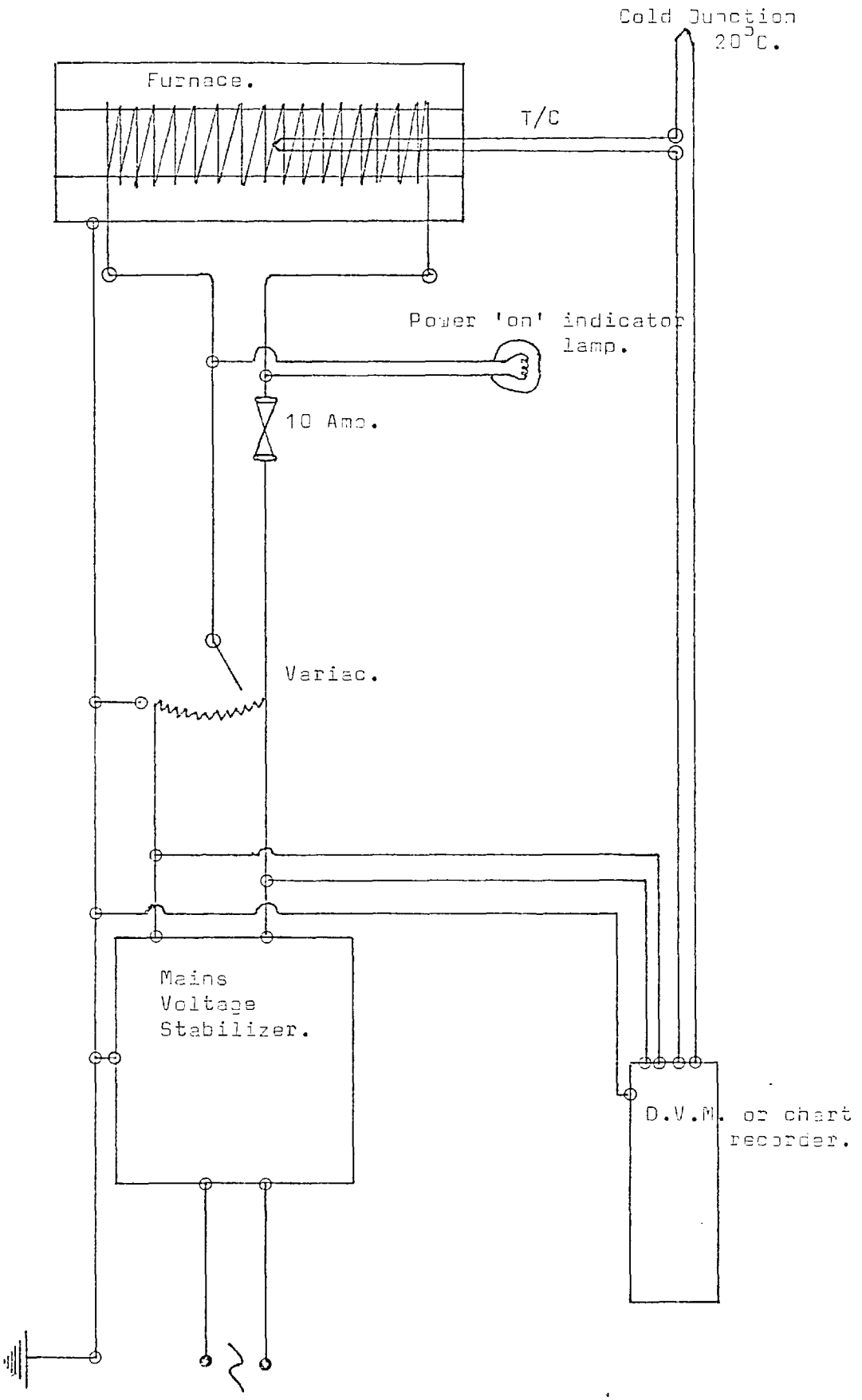

frequencies. Fortunately however the absorption on the left hand side of the equation is 5 times stronger than that on the right (see Chapter 3). This means that the infrared absorption should decrease with increasing temperature.

If it is assumed that all of the original structure bound water concentration will eventually be converted to molecular water if a sufficiently great temperature is reached, then the measured infrared absorption should be reduced to 1/5 of its room temperature value. Thus if the infrared absorption at some elevated temperature (I) is subtracted from the room temperature absorption (A) and this difference is increased by 1/5 to give a new value for the absorption at the elevated temperature (I') this should be equal to the absorption due to the remaining structure bound hydroxyl groups, simply:-

$$I' = I - \frac{(A - I)}{5} \qquad 5.1$$

and then the new concentration N is given by

$$N = I'/0.926 \qquad 5.2$$

All the dehydration data recorded for the synthetic quartz crystals was treated in this manner. In the data for the dehydration of Brazilian type quartz (in which the initial concentration was small) the error in the value of the denominator in equation 5.1 becomes significant so in this case the absorption due to hydroxyl groups was taken to be the measured absorption. This should introduce no significant error into the results.

5.2.3. Conducting the Experiment

It is obviously necessary as a starting point to establish the period of time required at a given temperature to cause the dehydration

reaction to approach equilibrium. This being the minimum time for heating the sample in any of the sets of experiments leading to the temperature versus concentration plot which is the aim of these tests. These preliminary experiments indicated that a period of 5 hours was the minimum time allowable if equilibrium was to be approached (see section 5.5) and as a result of this I adopted a minimum heating time of 24 hours to err well on the side of accuracy. That each set of points for a given crystal did show the equilibrium condition was cross checked by selecting a temperature in each set of tests and maintaining the sample at this temperature for much longer than the normal 24 hour period (seven days). When constructing the temperature versus concentration plot I always found that this point fitted the curve constructed through the 24 hour points i.e. equilibrium was closely obtained.

In each experiment the quartz sample, normally wrapped in a high temperature metal foil of the type widely used to wrap steel for tempering was placed in the furnace tube adjacent to the thermocouple, and the furnace ends plugged with Kao Wool as far as the ends of the sample plate. The temperature was then taken up quickly to the desired value (if below 573^{o}C). If above this, the α/β transition temperature (which was more often the case) the heating was stopped when a temperature in the range 525 to 550^{o}C was reached and then advanced slowly by increasing the variac setting by small increments until a temperature of between 600 and 625^{o}C was reached. The maximum rate of temperature increase across this range was of the order of 1 to 2^{o}C per minute, and when the upper value was reached I found it advisable to wait at least 10 minutes before rapidly taking the temperature up to the desired value. On

cooling this procedure had to be reversed. The reason for this rather tedious procedure is to ensure that thermal stresses developed during the phase change are dissipated before reaching sufficient magnitude to cause fracturing of the sample. If these precautions are not observed, the sample recovered at the end of the test is often so severely fractured as to be completely unsuitable for spectroscopic analysis.

The maximum temperature available from these furnaces is 1350°C using a thermocouple with a high temperature rating, above this temperature, or after long periods at this temperature, the Kanthal wire reacts with the alumina tube and the pyrume cement, thereby destroying the furnace. This reaction often occurs at a point where the thermocouple touches the furnace tube and spreads outwards from this point, care must thus be taken to prevent the thermocouple coming into contact with the tube in high temperature runs.

5.3. DEHYDRATION OF BRAZILIAN TYPE QUARTZ

The dehydration of the structure of natural Brazilian Type quartz will be treated in two sections. Firstly the reduction in intensity of the superimposed peaks in the 3 micron absorption band will be discussed using crystal M1, and secondly the reduction in intensity of the complete band will be dealt with using crystal M6.

5.3.1. The Superimposed Peaks

The four major superimposed absorption maxima in the 3 micron band of the spectrum of crystal M1, have been studied for the influence of temperature on the hydroxyl concentration represented by each band. The results of this work are shown in figure 5.3. the bands being

Figure 5.3a. Dehydration of the component peaks of the spectrum of the Brazilian type crystal M1. Peak maxima frequencies (cm^{-1}) are given above each curve.

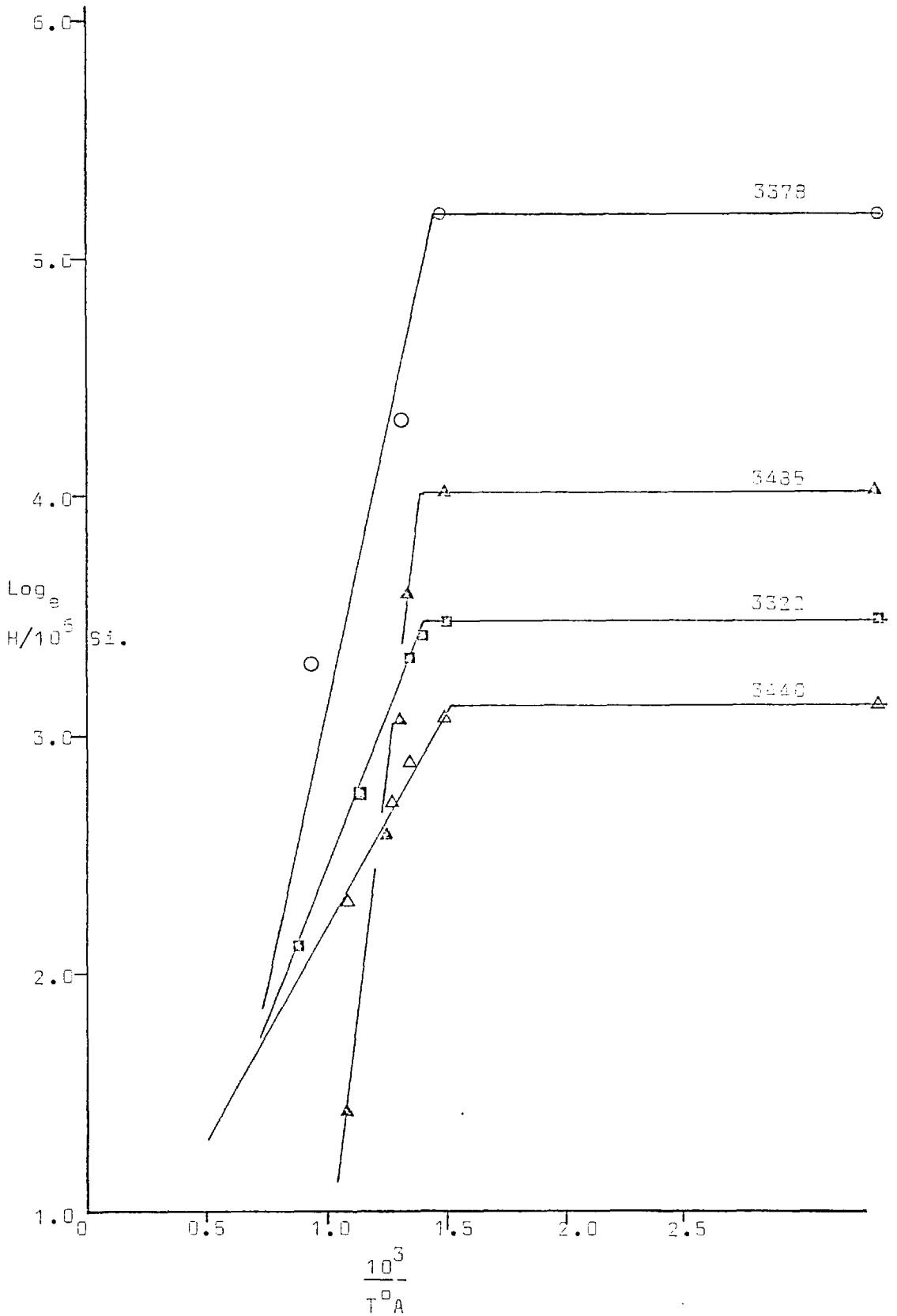

Figure 5.3b. The dehydration of the total absorption band (3 microns) in the spectrum of Brazilian type crystal M1.

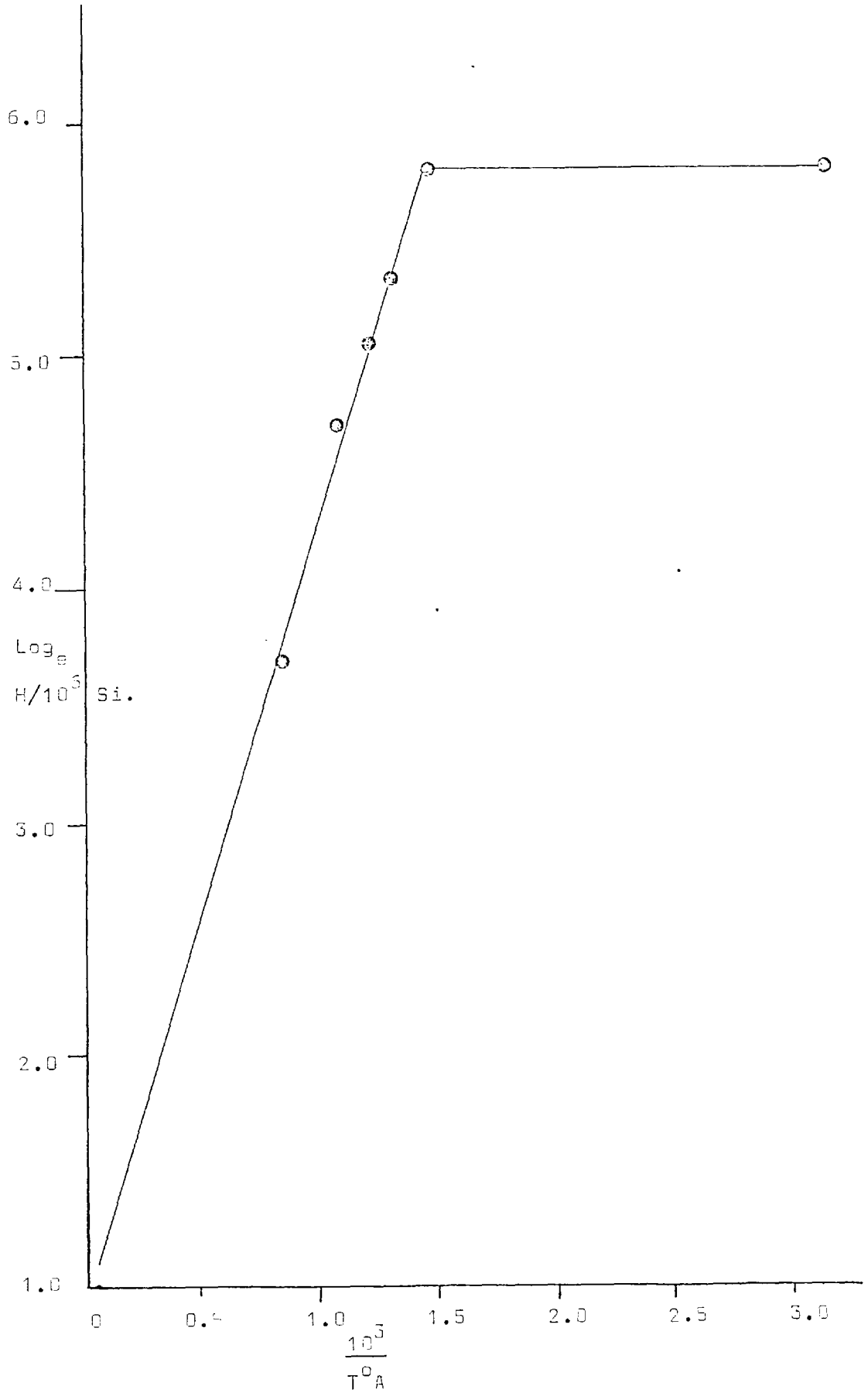

identified by their frequency (3485, 3440, 3378 and 3322 cm^{-1} respectively) together with a curve for all the superimposed peaks in the 3 micron band of this crystals spectrum. The data is presented as a plot of natural log concentration against reciprocal absolute temperature, which produces a straight line graph. The interpretation of this will be discussed in a later section.

Clearly the hydroxyl concentration responsible for each of the peaks in the spectrum decreases with increasing temperature above some threshold value which for this crystal is between 400 and 450°C. It is important to note that each peak (representing a differently bonded group, or a different vibration mode for a particular bonded group) shows a different temperature sensitivity, in this crystal the 3485 cm^{-1} band being the most sensitive. It is possible that differences in the intensity of these different peaks in different crystals spectra (differences in the distribution of different bond types for hydroxyl in the structure) may account for the differences in behaviour observed when the dehydration of different crystals is compared.

5.3.2. The Peaks plus Background

Figure 5.4 is the total structure bound hydroxyl versus temperature curve (on the same axes as figure 5.3 which are used throughout this chapter) for crystal M6. This has a similar form to the curves for crystal M1 but shows a far greater temperature sensitivity, which is almost certainly related to the far greater proportion of the total hydroxyl concentration bound in the 3485 cm^{-1} vibrational mode, than that recorded for crystal M1.

The threshold temperature is 376°C, very close to that recorded for crystal M1, which, as these crystals are from the same environment, may be related to the pressure and temperature conditions which existed

Figure 5.4. The dehydration of the 3micron absorption band for Brazilian type crystal M6.

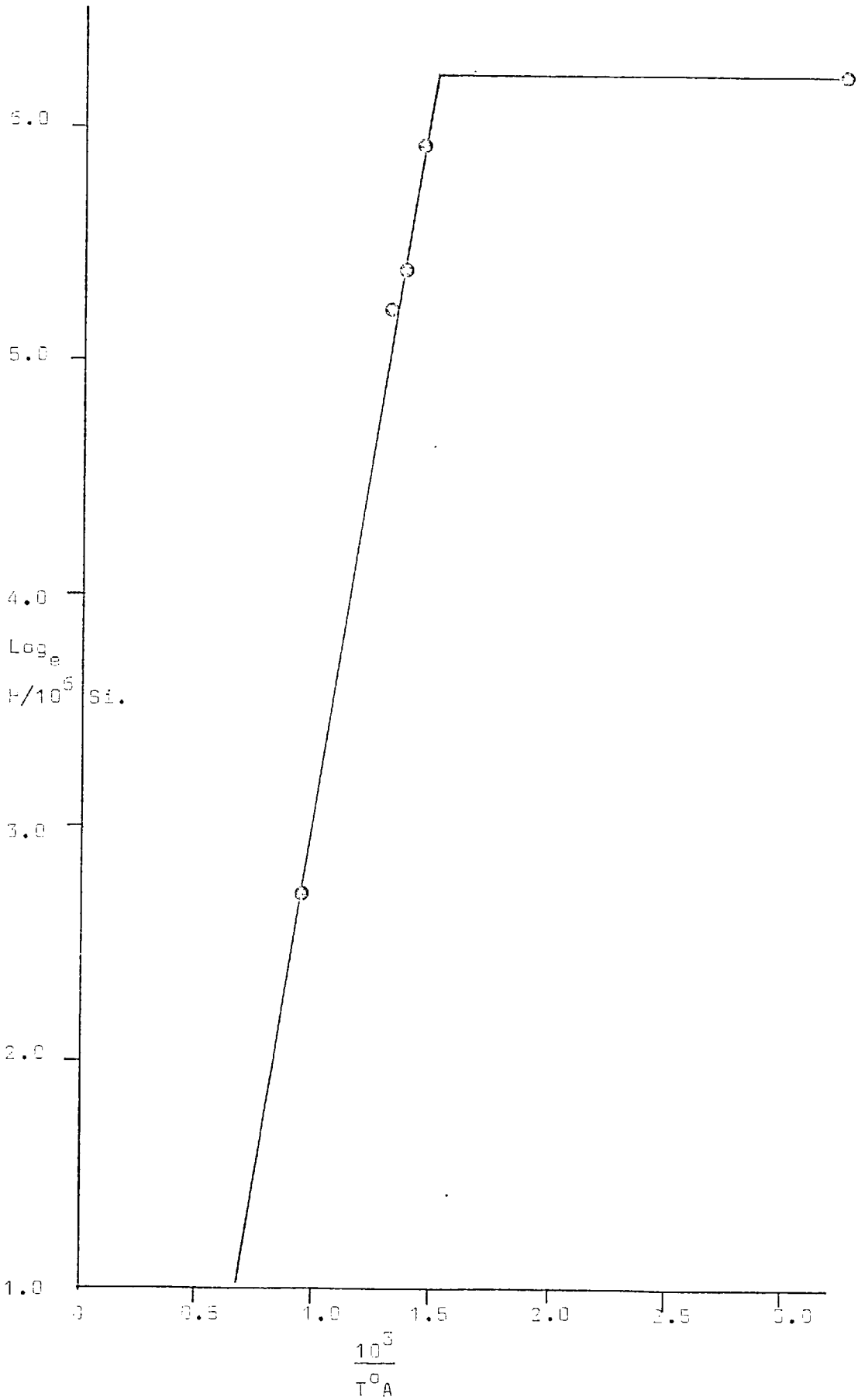

at the time of crystallization. However as will be shown below different parts of the same synthetic crystals show widely differing threshold temperatures, so it may also be orientation controlled.

5.3.3. Description of the Dehydration Curves for Natural Brazilian Type Quartz

An inspection of the dehydration curves for both the total hydroxyl and the individual superimposed peaks in figures 5.3 and 5.4 shows that the dehydration behaviour is described by a simple solubility relationship.

$$C = Co \exp \Delta H/RT \qquad 5.3$$

where

C = the concentration at absolute temperature T

Co = the extrapolated concentration at T = ∞ which is a constant for each dehydration curve

ΔH = the heat of solution

R = the Gas Constant

Values for Co and ΔH for the Brazilian Type crystals studied are given in Table 5.1.

The dehydration reaction can then be considered to be the result of the decreasing solubility of hydroxyl in the quartz structure with increasing temperature.

5.4. DEHYDRATION OF SYNTHETIC QUARTZ

As demonstrated in Chapter 4, synthetic quartz crystals show a single absorption band in the 3 micron region of their spectra, so that only the complete hydroxyl concentration need be considered and not its component bonding groups.

Table 5.1. Values of C_o and ΔH for the dehydration of Brazilian Type Quartz. These values are calculated from the dehydration curves for these crystals.

Crystal	Frequency cm^{-1}	C_o $H/10^6 Si$	ΔH cal $mole^{-1}$
M1	Total	2.7	6533
M1	3485	1.85×10^{-6}	25168.6
M1	3440	0.38	5490
M1	3378	2.0137	5961
M1	3322	1.173	4620
M6	Total	0.019	13358.9

However as also shown in Chapter 4 three different regions for spectroscopic analysis can be identified in all synthetic quartz crystals, the small prism, the seed and the z growth region. The dehydration behaviour of these three regions will be shown to vary using data for crystal ITT4 and then this crystal compared with data for the z growth regions of two other synthetic crystals AX1 and A2.

5.4.1. Comparison of the Three Growth Regions

Figure 5.5 shows the dehydration curves for the three regions of crystal ITT4 each curve being for the total hydroxyl concentration in that region. The shape of these curves is the same as that recorded for the Brazilian Type crystals, but the three curves differ greatly in detail from one another, not only showing the different initial concentrations, but differing temperature sensitivities, and threshold temperatures, the latter ranging from 288 to 460^{o}C for the small prism and seed respectively.

Obviously the z-growth and small prism regions grew under similar conditions of pressure temperature and solution chemistry, so that threshold temperature must be influenced by some other factor as well. It could possibly be related to the initial hydroxyl concentration, which is greater in the small prism region where the threshold temperature is least.

From the results of this comparison of these three regions in synthetic quartz crystals it would seem that not only does the seed differ from the rest of the crystal (as might be expected as it is initially cut from some other crystal), but the z growth and small prism regions also differ greatly. This poses the question as to whether each growth band in the z growth region with its individual hydroxyl concentration is also unique in its dehydration behaviour.

Figure 5.5. Dehydration of the three growth regions of synthetic quartz crystal ITT4. (Results corrected for molecular water).

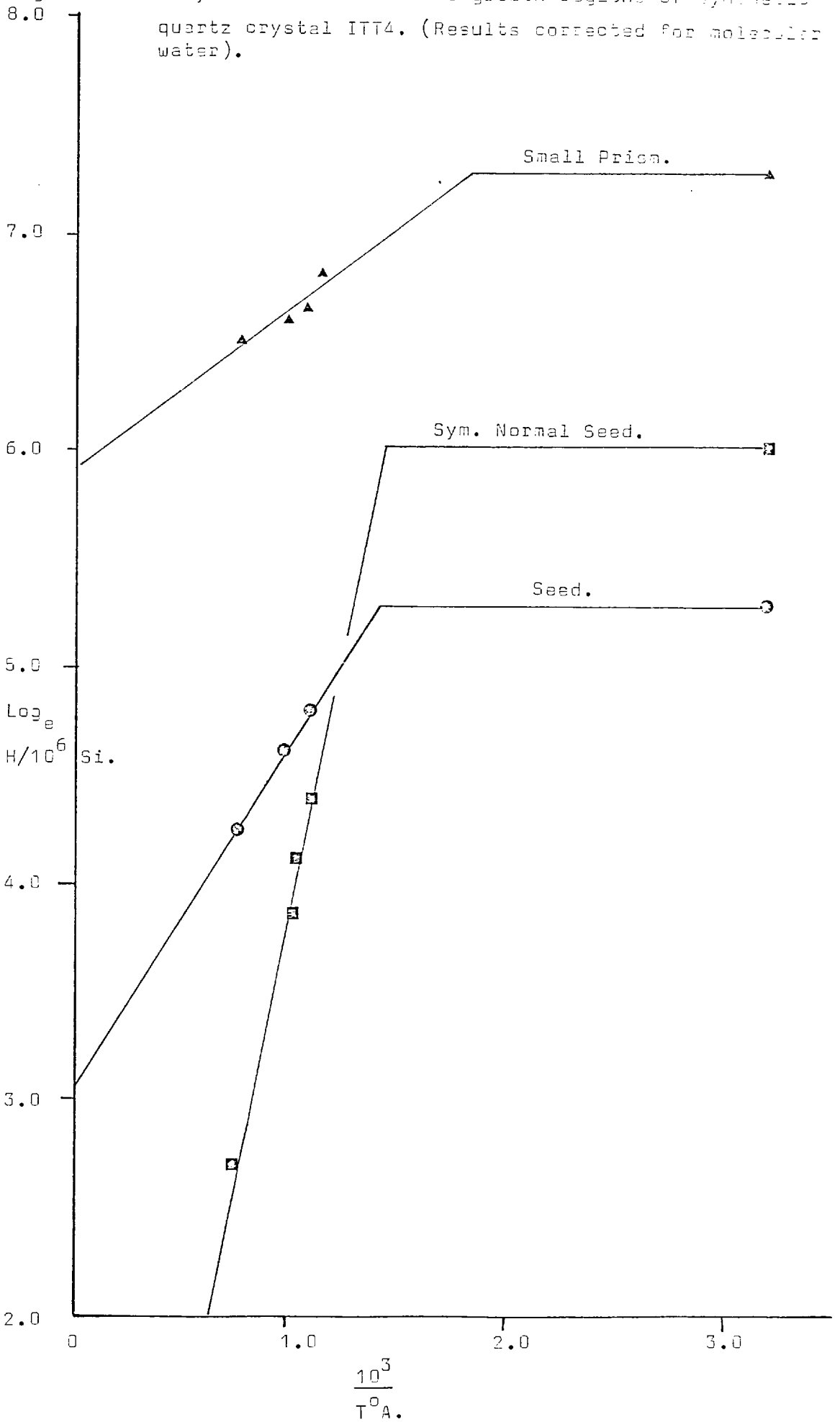

In the discussion on the microstructure of synthetic quartz presented later, some evidence is given which would seem to indicate that this is indeed the case.

5.4.2. Other Synthetic Crystals

Figure 5.6 shows the dehydration curves for the z growth regions of crystals AX1 and A2 which show the familiar form but again are both unique in detail. It is interesting to note that the threshold temperature is lower for crystal AX1 than for crystal A2 and it is crystal AX1 which has the largest hydroxyl concentration.

It would thus seem a reasonable proposition to suggest that the hydroxyl concentration in synthetic (and Brazilian type natural) quartz crystals is reduced by heating above a threshold value, but that this temperature at which the dehydration starts, and the temperature sensitivity is widely variable, being unique to each part of each crystal. Thus no simple method is available to predict the dehydration behaviour of a crystal from its room temperature hydroxyl concentration. The only satisfactory method being to determine the dehydration curve from experiments of the type described above.

5.4.3. Description of the Dehydration Curve for Synthetic Quartz

The dehydration curves for synthetic quartz have a similar shape to those recorded for Brazilian Type quartz, and are also described by equation 5.3. Table 5.2 records the values of Co and ΔH for the synthetic crystals studied.

A comparison of tables 5.1 and 5.2 shows that in laboratory deformation experiments, the dissolved hydroxyl in natural Brazilian quartz will be less stable than that in the synthetic crystals and hence the synthetic crystals will maintain proportionally higher concentrations of hydroxyl than will natural Brazilian Type quartz.

Figure 5.6a. The dehydration of synthetic crystal AX1. (Corrected for molecular water.

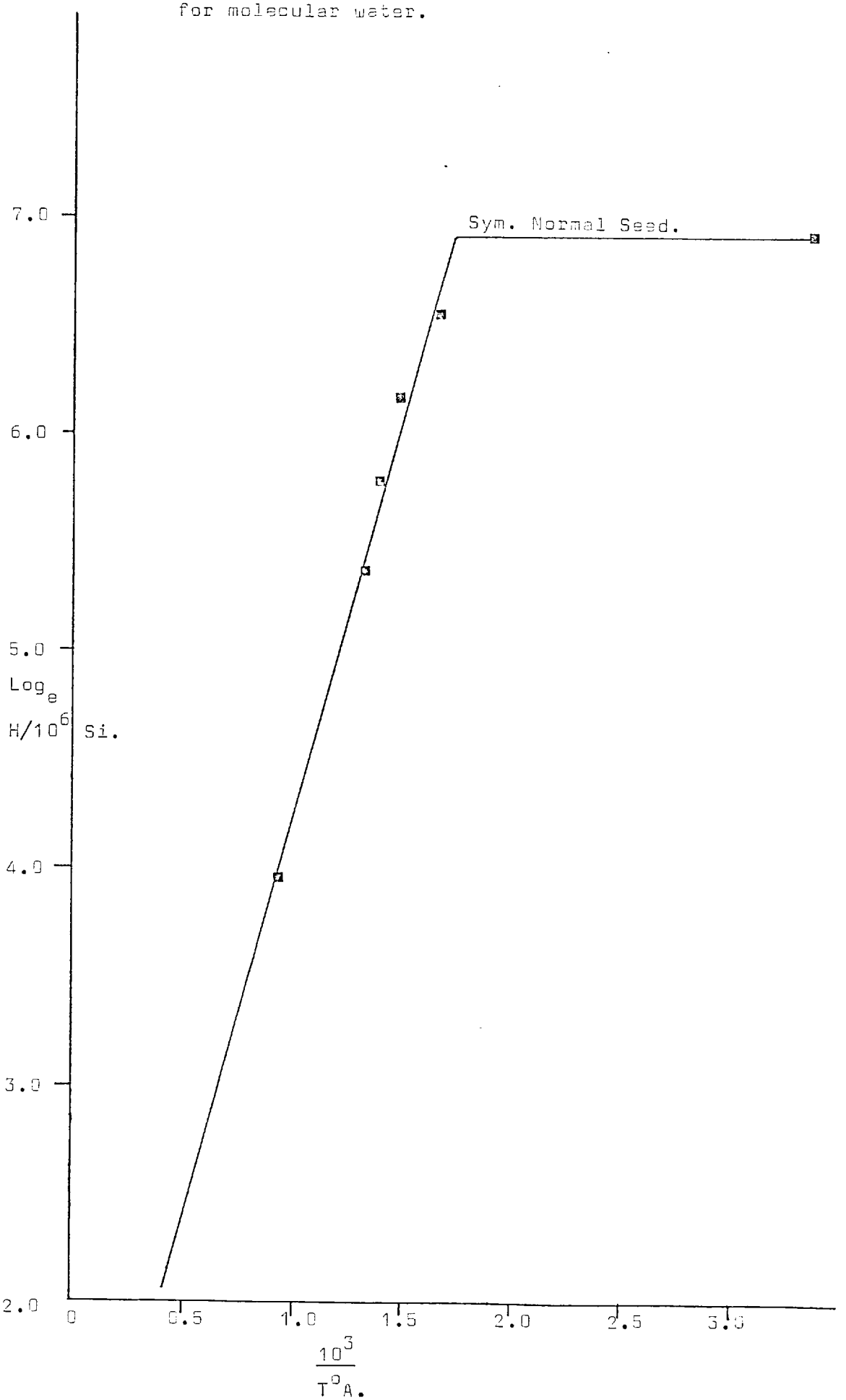

Figure 5.6b. Dehydration of synthetic crystal A2. (Corrected for molecular water).

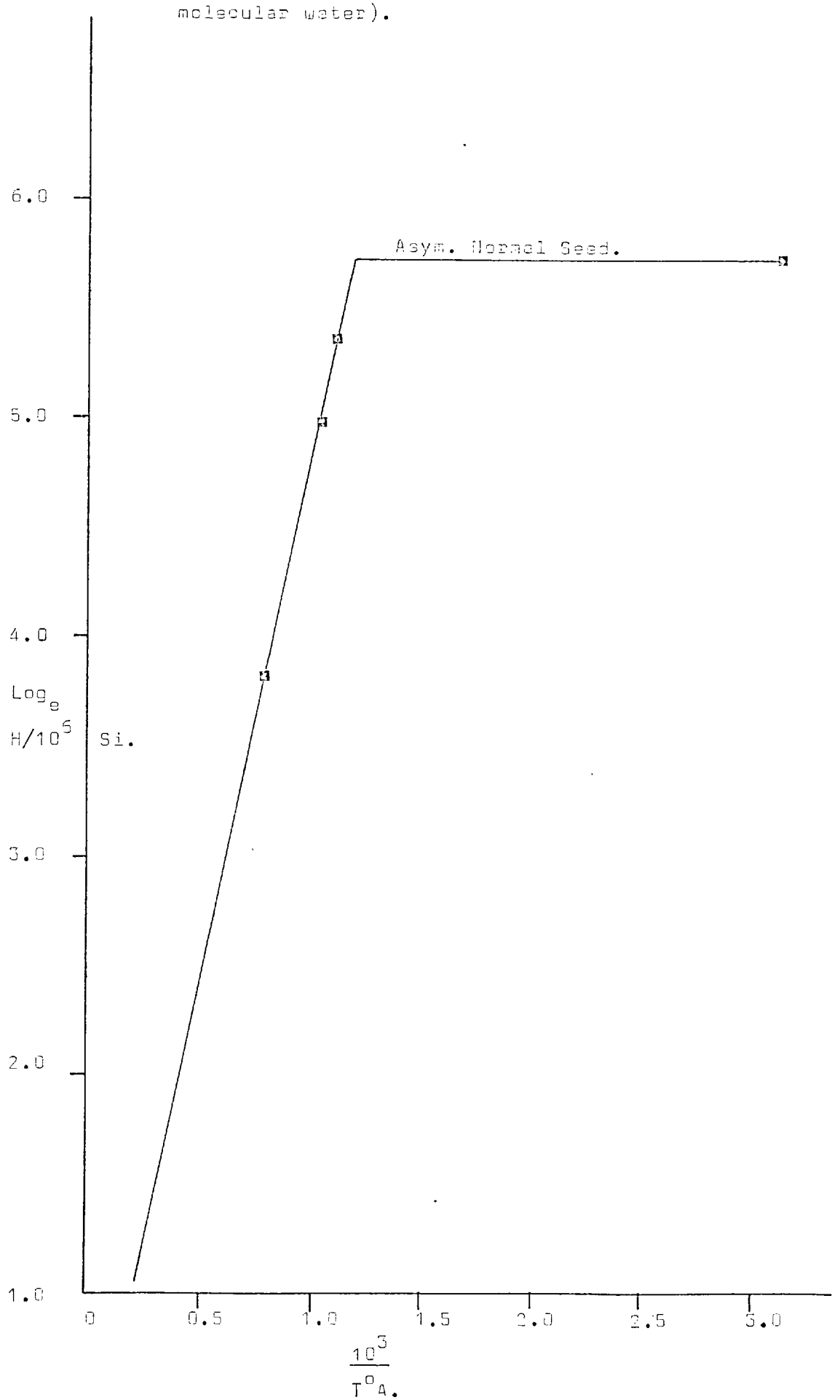

Table 5.2. Values of C_o and ΔH for the dehydration of synthetic quartz crystals. These values are calculated from the dehydration curves for these crystals.

Crystal	Orientation	C_o $H/10^6 Si$	ΔH cal $mole^{-1}$
ITT4	Sym.Norm.Seed.	0.55	8900
ITT4	Small Prism.	365	1600
ITT4	Seed.	21	3100
AX1	Sym.Norm.Seed.	1.65	7330
A2	Asym.Norm.Seed.	0.81	9700

5.5. THE EFFECT OF TIME

5.5.1. On the Laboratory Experiments

The curves in figure 5.7, which are plots of log concentration versus log heating time at constant temperature, show that when a sample is taken to some elevated temperature above the threshold temperature the concentration changes by a continually reducing rate, this rate of change being small after 5 to 10 hours heating time. This is important for it shows clearly that the greater part of the dehydration takes place shortly after the temperature rise and that only very prolonged heating at lower temperatures can be subsituted for a short heating time at high temperature in a laboratory experiment. Thus any great increase in the heating time used in the dehydration experiments (which was always between 1 and 7 days) will not affect greatly the slope or the shape of the dehydration curve.

The shape of these concentration versus time curves is obviously significant to the interpretation of deformation test results. Clearly, shortly after raising the specimen temperature to that of the test, the structure bound water concentration is being rapidly reduced and as the test proceeds this rate of change becomes less, with near equilibrium concentrations being obtained in tests conducted at slower strain rates ($10^{-5}sec^{-1}$). It will be shown later that the effect of hydrostatic pressure on this reaction is negligible up to at least 10 kilobars.

Clearly, if the mechanical properties are dependent on the concentration of water contained bound in the structure as inferred in current models of hydrolytic weakening (Griggs etc., loc cit) then these properties are continually varying throughout the test and this variation must be reflected in the shape of the stress-strain curve, and in any data involving a range of strain rates. Such an effect has not been reported

Figure 5.7. The effect of increasing time on the structural water concentration of crystal ITT 4 at elevated temperature. (Corrected for molecular water.)

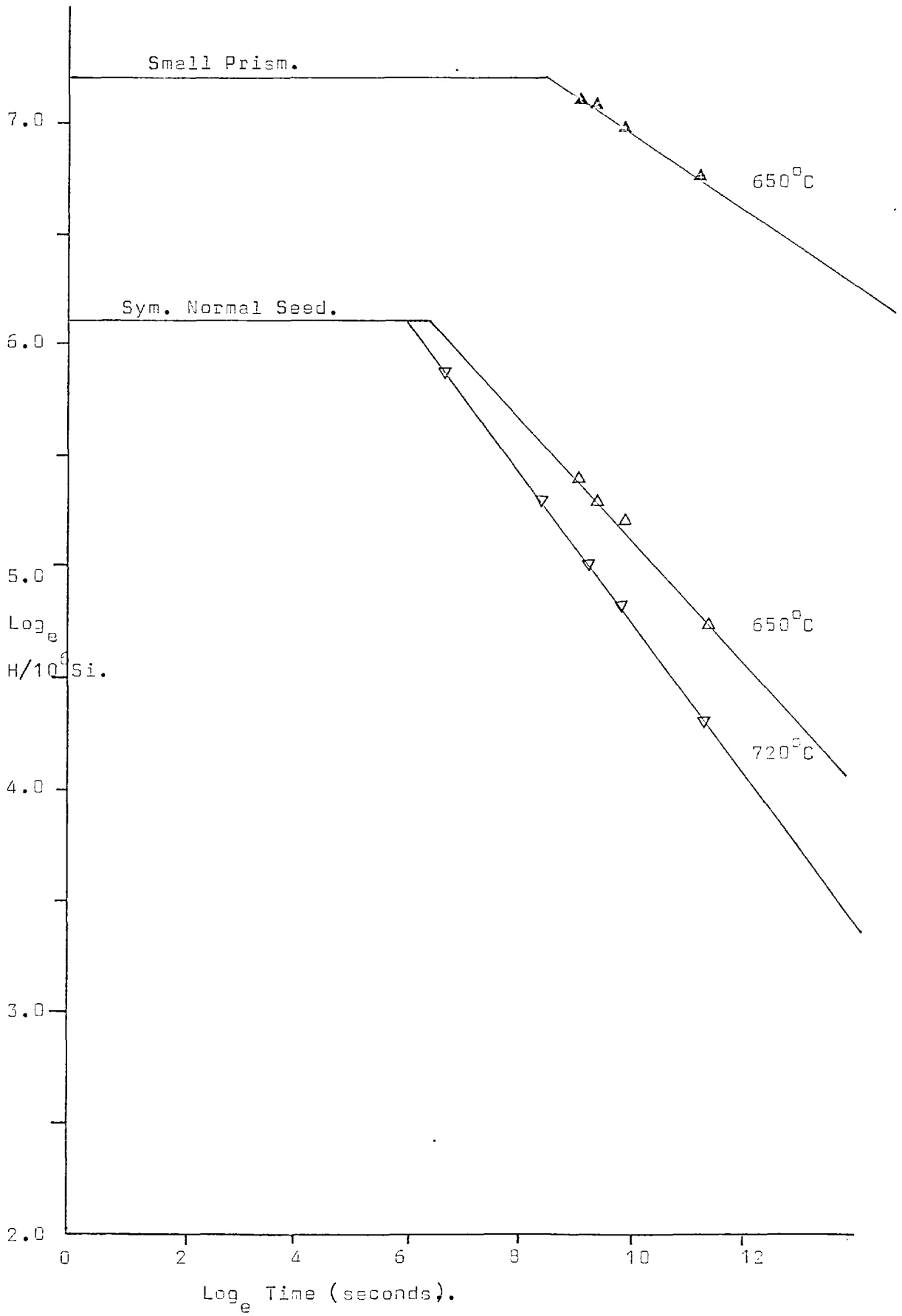

in the literature, but recently Mervyn Paterson (personal communication 1976) has noted an increase in strength associated with annealing his samples prior to deformation. In this study all the samples used in deformation tests were maintained under the conditions of the test for at least 24 hours before the start of loading, to establish a new equilibrium hydroxyl concentration at the test temperature. The only exception to this were the tests conducted on natural crystal P3 which were conducted in a manner identical to the experiments used by Griggs and Blacic (loc cit) to identify the weakening temperature so that the results of the experiments may be compared directly with the published data of Griggs and Blacic. Obviously the constants in the Griggs equation relating room temperature hydroxyl concentration with the weakening temperature (see Chapter 4, equation 4.1) have no simple physical interpretation, and until deformation tests are conducted on preheated samples from which the hydroxyl concentration is determined after the deformation, a true activation energy for hydrolytic weakening cannot be determined.

5.5.2. In Nature

Figure 5.8 is an extrapolation of the data for crystal ITT4 (small prism, at 650°C) shown in figure 5.7 to times of geological significance (10^7 years). Clearly after this time a considerable proportion of the structural water has been precipitated leaving only 20 H/10^6Si in the structure.

Figure 5.9 shows how the threshold temperature varies with the initial structure bound water concentration. This data shows some scatter presumably because pressure and chemistry of the growth solution as well as its temperature will affect the uptake of water by the growing crystal (these all having an influence on the rate of

Figure 5.8

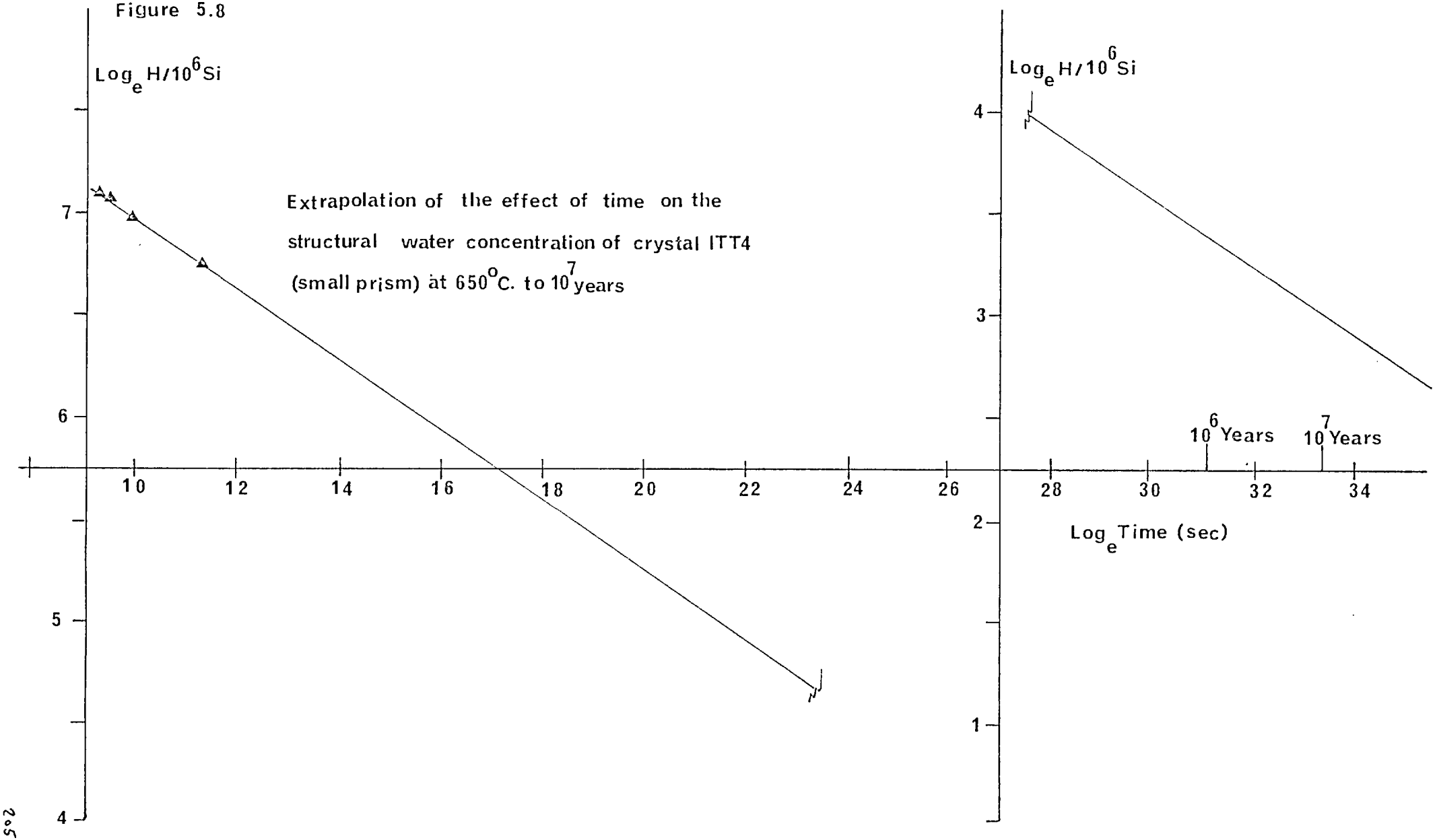
Log$_e$ H/10^{6}Si
Extrapolation of the effect of time on the structural water concentration of crystal ITT4 (small prism) at 650°C. to 10^7 years
7
6
5
4
10
12
14
16
18
20
22
24
26
Log$_e$ H/10^{6}Si
4
3
2
1
10^6 Years
10^7 Years
28
30
32
34
Log$_e$ Time (sec)

Figure 5.9. The aproximate correlation of the threshold temperature for dehydration and the grown in structural water concentration. Note that a value of 15000 $H/10^6Si$ gives a threshold temperature of only 152°C. This would indicate that much natural milky quartz started dehydration immediately upon crystallization.

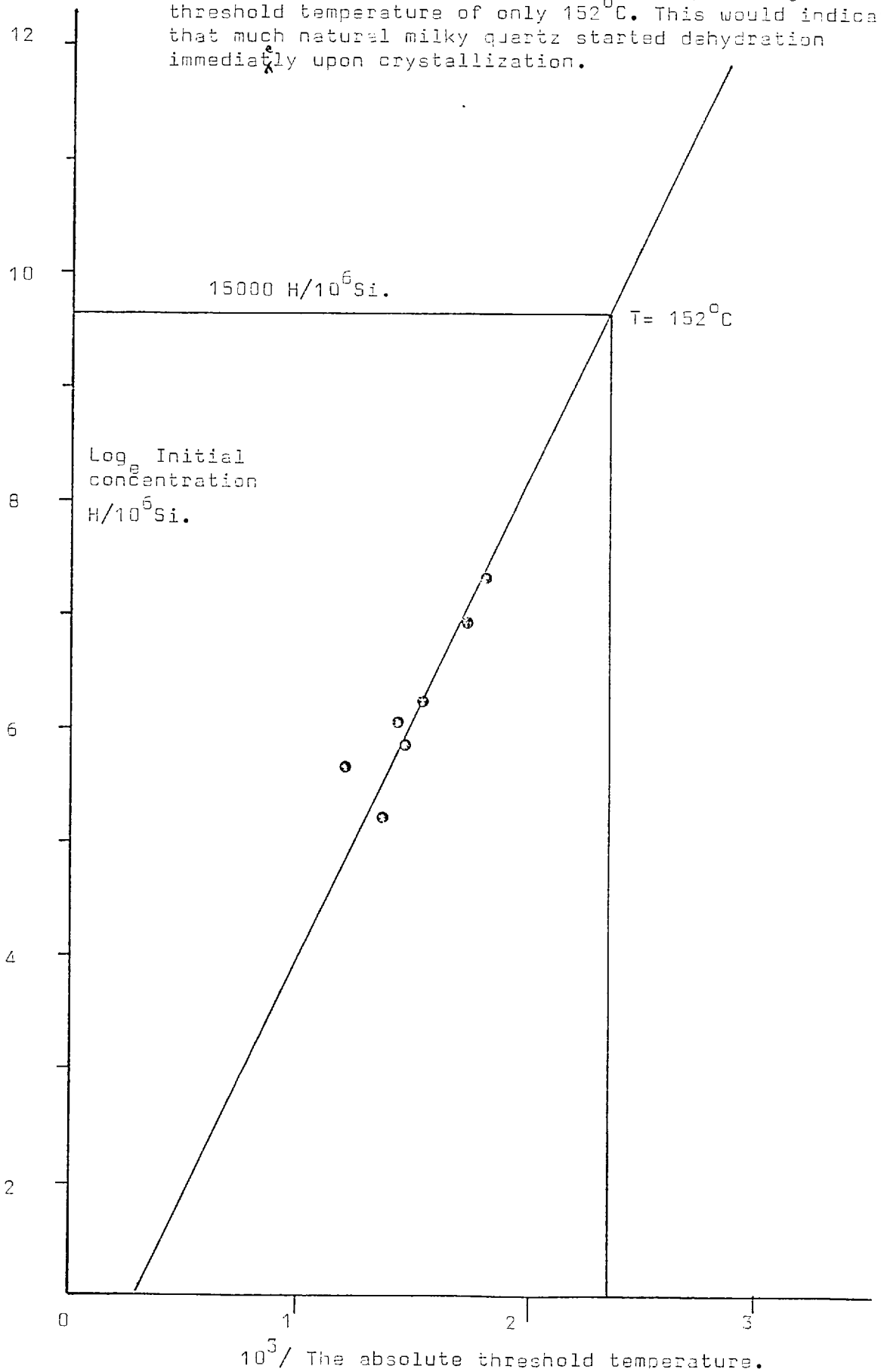

crystal growth which in turn influences the initial concentration (Dodd and Fraser 1967). However extrapolating the data shows that a natural crystal with 15000H/10^6Si (typical of much low grade natural quartz) will start to dehydrate at a temperature around 150°C. From fluid inclusion studies on quartz veins etc. (see Kerrich 1975 or Clarke 1972) much low grade quartz typically gives temperatures of formation of around 200°C. This quartz will thus start to precipitate its structural water at its temperature of formation or at temperatures only slightly above. Presumably at these low temperatures the rate of precipitation will be slow but will have proceeded to a significant extent in only a few years or tens of years. This may well explain why natural quartz which is free from bubbles but which contains a large structure bound water concentration is never encountered. Another consequence of this spontaneous dehydration is that this natural quartz will have a continuously increasing strength with age from the moment of its formation.

5.6. PRECIPITATION OF MOLECULAR WATER

So far the discussion in this chapter has been restricted to only half of the dehydration reaction.

$$2(\equiv Si\text{-}OH) \longrightarrow \equiv Si\text{-}O\text{-}Si \equiv + H_2O$$

without considering the form of the molecular water which is produced. Because the results of the dehydration experiments are independent of the size of the specimen it cannot be assumed that the water simply leaves the system. If it did, the time taken for the concentration to equilibrate would be dependent on the length of the diffusion path, i.e. the specimen size (predominantly thickness).

In this section then the second half of the reaction will be considered, and it will be from these results that a positive if qualitative statement about the influence of pressure on the dehydration reaction will be made. As a starting point for this analysis I considered the milkyness (opalescence) produced when 'wet' synthetic quartz is heat treated at some temperature above the threshold value.

5.6.1. The Precipitation of Molecular Water in Heat Treated Synthetic Quartz

The milkyness produced in wet synthetic quartz when heated has long been recognized (loc cit) and has been shown to be due to bubbles of molecular water (Dodd and Fraser 1965). I found as expected a similar milkyness in my heat treated samples of synthetic quartz, and as expected found that this milkyness was most intense in those regions of the crystal which showed the largest original structure bound water concentration. Plate 5.1 shows a series of electron micrographs from ion beam thinned samples (see appendix 1) of this heat treated synthetic quartz. These were recorded using a 100 KEV E.M.I. electron microscope. These pictures clearly show the distinct voids produced during the dehydration reaction, which presumably contained molecular water prior to thinning. They have densities in the region of 10^{13} to 10^{14} voids per cm^3, with diameters in the range 100 to 3000 $\mathring{A}$. These micrographs show the contrast typical of voids or bubbles in a crystalline solid. Those penetrating both sides of the foil appear clear and bright, whilst those penetrating only one side, or contained entirely within the foil may be light or dark depending on whether the thickness of foil remaining is an exact multiple of the extinction distance for the material. Larger voids may in fact show concentric rings around their largest diameter representing the change in extinction condition with changing

foil thickness across the void. The contrast is reversed if the dark area of a bend or thickness contour runs through the void position.

The second half of the dehydration reaction for synthetic quartz can be approximated by a diffusion process in which the precipiated molecules of water or the released OH^- and H^+ ions diffuse to discrete centres, which exist as an array throughout the structure, and coalesce forming voids filled with molecular water. As the dehydration reaction proceeds to equilibrium, and the supply of material to these growing voids becomes small the voids themselves start to equilibrate with the structure, becoming negative crystals (Mclaren 1966). This change to a lower surface energy configuration is accomplished by surface diffusion. The precipitation of molecular water by the dehydration reaction may then be regarded as a three stage process, involving the nucleation or seeding of the voids filled with water, their rapid growth in a disequilibrium shape, and their final shape change to an equilibrium configuration. Each of these stages will now be dealt with separately.

5.6.1.a. Nucleation

Nucleation of a new phase from a solution, melt, or within the structure of an existing crystal may be considered to occur either in a random spontaneous manner or as the result of some positive action (often termed seeding) which facilitates the growth of the new phase on implanted nuclei. In this latter respect, the appearance of a condensed fluid phase precipitated in the structure of a crystal may be considered as being a process identical to the growth of a crystal from its saturated solution or melt.

I will show later that the growth of bubbles in synthetic quartz is by a process akin to the seeding of crystals from a solution, but as

a starting point to this discussion it is worthwhile considering the nucleation as a random spontaneous process. Such a spontaneous process may well be important when the growth of bubbles in natural milky quartz is considered.

In this analysis the nucleating bubbles will be considered spherical, and it will be assumed that they remain spherical until the final stages of growth when they equilibrate with the crystal structure. Obviously for nucleation to be occurring at all, a specific free energy change of ΔFv must have occured and this must be negative and of magnitude,

$$-\frac{4}{3}\pi r^3 \Delta Fv \qquad 5.4$$

for a nucleus of radius r. However this nucleus will have a surface energy γ per unit area, so the total free energy change for a particle of radius r is given by,

$$\Delta f = 4\pi r^2\gamma - \frac{4}{3}\pi r^3 \Delta Fv \qquad 5.5$$

As the particle increases in size, its free energy also increases, until a radius r^* is reached. Once this radius is exceeded the particle will lower its free energy by growing. Thus a critical radius exists and particles with ($r < r^*$) will tend to react back whereas those with ($r > r^*$) will tend to grow. The former are called embryos and the latter nuclei. It follows from this that to form a nucleus the energy Δf^* must be added to the thermal activation for the reaction. It follows from equation 5.5 that r^* and Δf^* are given by,

$$r^* = \frac{-2\gamma}{\Delta Fv} \qquad 5.6$$

$$f^* = \frac{16\pi\gamma^3}{3(\Delta Fv)} \qquad 5.7$$

If the number of bubbles which appear is n_o then the number of nuclei (n^*) may be calculated from,

$$n^* = n_o \exp-(\Delta f^*/kT) \qquad 5.8$$

where k is Boltzmann's constant, and T the absolute temperature.

If nucleation proceeds simply as the result of random thermal fluctuations, then it may be expected that the reaction will proceed in all quartz crystals undergoing dehydration in which sufficient molecular water is locally produced to create a nucleus of radius greater r^*. However if the rate of arrival of ions at the site of the prospective nucleus is very slow then the rate of loss due to the back reaction may be faster and the nucleus will never grow beyond the embryonic stage, i.e. the crystal will not turn milky. The rate of nucleation $\dot{N}$ is the product of the frequency of motion of a single ion into the nucleus (V), the number of ions ($\overset{*}{m}$) that actually arrive there and the number of nuclei.

$$\dot{N} = \overset{*}{n}\, V\, \overset{*}{m} \qquad 5.9$$

If diffusion to the bubble is the rate controlling process then N (nuclei per second) is dependent on the diffusive motion of the ion, thus,

$$V \propto \exp-(\Delta f_D/kT) \qquad 5.10$$

where Δf_D is the activation energy for diffusion. $\overset{*}{m}$ is geometrical, being related to the shape of the nucleus at which the ions are arriving. $\overset{*}{N}$ is thus proportional to the product of the previous three equations,

$$\dot{N} \propto \overset{*}{m} \exp-(\Delta \overset{*}{f} + \Delta f_D)/kT \qquad 5.11$$

This expression satisfactorily explains the observed features of the dehydration and precipitation, namely that the bubble density is greatest in those parts of the crystal with the highest original structure bound water concentration, and that the higher the temperature the greater the bubble density. Equation 5.11 also implies that below a certain temperature or initial concentration no bubbles will form. This is observed in synthetic quartz crystals with small hydroxyl concentrations, in which bubbles only appear (if at all) at very high temperatures.

However it is clear from the comparison of infrared data and T.E.M. that the dehydration reaction proceeds in all crystals at temperatures lower than those which cause the first appearance of bubbles. There is thus a range of temperatures, between the threshold value and the temperature of first appearance of bubbles in which the precipitated molecular water remains dispersed throughout the structure.

5.6.1.b. The Growth of a Bubble

After a stable population of nuclei have developed bubble growth proceeds by diffusion of the precipitated water to these nucleating sites, i.e. is time dependent at any given temperature above the threshold temperature for nucleation (which I have shown to be greater than the threshold value for the dehydration). All diffusion reactions are paired and it is thus necessary to consider also the bulk diffusion of SiO_2 in the opposite direction away from the growing bubble. Movement of the precipitated water to the growing bubble may be accomplished by one of two possible processes, either as complete water molecules or as the independent ions H^+ and OH^- which reach the surface of the void

in the ionic state and react on that surface.

It must be considered that the interstitial H_2O molecule may be too large to be able to diffuse at a significant rate through the tetrahedral structure of crystalline silica. This has meant that independent H^+ and OH^- ions have often been assumed to be the diffusing species (White 1971). This however poses several problems. Firstly the H^+ ion has an extremely short lifetime in any system other than a vacuum ($10^{-13}sec^{-1}$)(Bell 1959) and almost certainly would combine by hydrogen bonding either with an oxygen in the structure, a water molecule (if any were available) to form the more stable H_3O^+ ion (the hydronium ion) or most probably with the hydroxyl group released simultaneously during the breakdown of a silanol bond to form a water molecule. If the silanol group migrated by hydrating successive Si-O-Si bridges until the edge of the void was reached these problems are overcome, and such a mechanism for the diffusion of silanol bonds has been considered (Griggs loc cit). But such a process would not cause any reduction in the intensity of the infrared absorption until the surface of the void were reached. I have shown above that the threshold temperature for the dehydration reaction as monitored by infrared spectroscopy is significantly lower than the threshold value for the nucleation of bubbles (monitored visually by T.E.M.), i.e. that the dehydration proceeds independently of the rate of bubble growth and although the latter is slower it is not the rate controlling process. From this data diffusion to the void surface (and probably to dislocations as well) cannot be accounted for by successive hydration of Si-O-Si bridges.

The Space Problem

In an attempt to overcome this problem I looked at the possible mechanisms for diffusion of $Si-O_4$ tetrahedra away from the surface of

the growing void. Clearly the diffusion of the complete tetrahedra away from the void surface is even more difficult than diffusing the H_2O molecule to the surface if size is considered as a criterion for ease of diffusion. However the diffusion of a complete SiO_4 tetrahedra away from the void may be considered as directly analogous to the diffusion of 4 oxygen and one silicon vacancies to the surface of the void. Using the diffusion of vacancies to the void to account for the removal of SiO_4 provides a possible solution to this whole problem.

At any given temperature the structure of a crystalline solid always contains an equilibrium number of vacancies, given by the relationship:-

$$\frac{N_v}{N_o - N_v} = \exp -E_v/kT \simeq \frac{N_v}{N_o} \text{ if } N_v << N_o \qquad 5.12$$

where N_v is the number of vacant sites

N_o is the number of sites (total)

and E_v is the energy required to make a single vacancy.

In crystalline silica some evidence is available to suggest that E_v oxygen is about $\frac{1}{4}$ of E_v silicon, although these numbers are still very unreliable (White, Personal Communication 1977).

Development of the void containing the water molecules requires that a proportion of the vacancies move to the distinct sites in the structure which are to become the bubbles and produce the silica free volume into which the molecular water passes. However the ordered grouping of vacancies in a crystalline solid will only occur in response to some externally applied force such as high energy ionizing radiation. Or to relieve internally produced strain fields in the microstructure resulting from the external application of a stress and consequent

deformation of the solid. But in response to neither of these are voids of the type shown in plate 5.1 produced.

The ordered grouping of the precipitated molecular water distributed uniformly throughout the structure of the dehydrating crystal is a similar problem requiring some potential to initiate and drive the diffusion reaction. The actual breakdown of the silanol bond is a thermally activated process, which increases the entropy, and presumably lowers the free energy of the system. However in synthetic quartz crystals in which bubbles appear during the dehydration there is presumably a further decrease in the free energy, accomplished by the moving of this widely distributed interstitial precipitate into the discrete sites which develop as bubbles. I have suggested above that the development of the void to contain this water results from vacancy diffusion to the partic--ular sites, but the void fills as it grows, i.e. the diameter would appear to be dependent on the water reaching the surface, not the removal of silica tetrahedra by vacancy diffusion.Thus the movement of the interstitial water molecules has to be linked to the vacancy diffusion and allowing for the size problem the water molecules are probably carried in some of the vacancies themselves. Thus the internal energy of the crystal can be minimized by utilizing the equilibrium vacancy concentration to maneouver precipitated molecular water to discrete sites and create voids at these sites to contain it. Details of the vacancy mechanism of diffusion are given in Manning (1968).

Theoretical Analysis of the Diffusion of Water into Bubbles.

A theoretical treatment of this diffusion of water into bubbles is complicated, so that an 'in depth' analysis was beyound

the scope of this project. These complications stem from difficulties in identifying the actual mechanism of diffusion. As stated above it would seem probable that the water is supplied to the bubble, and that the void containing the bubble developed, by the accumulation of water carrying vacancies at these points. This process in itself is not difficult to describe, but the bubbles appear to grow on strain fields (see section 5.6.3.) in the quartz structure and there is thus a driving force term which must be considered and this seriously complicates the solution. The flux of water carrying vacancies J may be written in the following form.

$$J = -D^{*}\frac{dc}{dx} + f_1\left[\frac{dc}{dx}\right] + f_2 x \qquad 5.13$$

in which $f_1\left[\frac{dc}{dx}\right]$ and $f_2 x$ are the driving forces for the diffusion at concentration c along the path x and D^{*} is a tracer diffusion coefficient. If the second term in 5.13 has the form $D\left[\frac{dc}{dx}\right]$ then the combination of this with the first term gives an intrinsic diffusion coefficient.

The tracer diffusion coefficient thus equates the flux with the rate of change of concentration along the diffusion path, whilst the intrinsic diffusion coefficient also includes the effect of driving forces such as potential gradients within the structure. For a full discussion on the types of diffusion coefficient and their application to problems, the reader is referred to Manning (1968).

Further problems are associated with the nature of this diffusion mechanism. At the temperatures of interest, the equilib-rium vacancy population is small so that if all the water is carried by these vacancies, then this will seriously restrict

the rate at which the bubble can grow. Taking the energy to produce one vacancy as 20 KCal $Mole^{-1}$ then at $600^{o}C$ there will be only 10 vacancies per 10^{6}Si atoms, this rising to 100 vacs./10^{6}Si. at $800^{o}C$.Unfortunately it is not possible to calculate a rate from these figures (to compare with that determined experimentally) this is because firstly the velocity of motion of the vacancy into the bubble is unknown and secondly because the magnitude of the extrinsic vacancy population is unknown. This extrinsic vacancy population will be related to the chemical breakdown of the silanol bonds within the crystal structure, and to the effect of temperature on the strain fields associated with any existing or newly introduced microstructure in the grain. The population of extrinsic vacancies may far out number the equilibrium popu--lation.

Because of this difficulty in specifying the constraints on the value of the diffusion coefficient in developing a theo--retical model for this diffusion reaction, I decided to tackle the problem only at its most simple level. To this end I used a solution to Ficks second law (equation 5.14) for radial diffusion in an infinite solid bounded internally by a sphere which acts as a sink. This is a standard solution to the equation of conduction (Carslaw and Jaeger 1959).

$$\frac{dCx}{dt} = \frac{d}{dx} D\left[\frac{dCx}{dx}\right] \qquad 5.14$$

where $\frac{dCx}{dx}$ is the concentration gradient

D is the diffusion coefficient

C is the concentration

and x is the linear distance from some origin.

This may be simplified to :-

$$\frac{dCx}{dt} = D\frac{d^2Cx}{dx^2} \qquad \text{in one dimension} \qquad 5.15$$

$$\frac{1}{D}\frac{dC}{dt} = \nabla^2 C \qquad \text{in three dimensions} \qquad 5.16$$

which gives solutions of the form

$$\frac{C_x - C_o}{C_s - C_o} = 1 - \text{erf}\left\{\frac{x}{2\sqrt{Dt}}\right\} \qquad 5.17$$

where C_s is the initial high concentration

C_o the initial low concentration

and erf the Gaussian error function.

The form of the required solutions to equation 5.17 are prescribed by the boundary conditions in the system, which in the instance of a single bubble may be considered to be an infinite volume bounded internally by a sphere.

Restricting the solution to radial diffusion (which is valid in this example) and assuming a constant diffusion coefficient and that all contributions to the driving force are proportional to the concentration gradient, equation 5.15 takes the form :- (Carslaw and Jaeger 1959).

$$\frac{\delta C}{\delta t} = D\left\{\frac{\delta^2 C}{\delta_r{}^2} + \frac{2}{r}\frac{\delta C}{\delta r}\right\} \qquad 5.18$$

writing

$$u = Cr \qquad 5.19$$

this becomes

$$\frac{\delta u}{\delta t} = D\frac{\delta^2 u}{\delta_r{}^2} \qquad 5.20$$

which is the equation for linear flow in one dimension. Thus for the infinite region bounded internally by the sphere $r = a$ and assuming that at all $r > a$ there is an initially uniform

concentration C_0, with the spherical surface $r = a$ maintained at concentration C_1 the solution becomes simply (Carslaw and Jaeger 1959)

$$C_{(r)} = C_0 - \left(\frac{aC_1}{r} \operatorname{erfc} \left(\frac{r - a}{2\sqrt{Dt}} \right) \right) \qquad 5.21$$

where $\operatorname{erfc} = 1 - \operatorname{erf}$ and $\operatorname{erf} z$ is defined as

$$\operatorname{erf} z = \frac{z}{\pi^{\frac{1}{2}}} \int_0^z e^{-n^2} \, dn \qquad 5.22$$

Values for both erf and erfc are tabulated in standard mathematical tables or are available from library routines in most Fortran compilers.

Equation 5.21 is a valid approximation because throughout most of their growth the bubbles remain approximately sphereical. Diffusion to the sphereical sink can be considered to be in an infinite volume providing values selected for r are maintained small with respect to the recorded interbubble distance in the dehydrating quartz crystals. Ideally solutions to equation 5.21 which give the observed reduction in concentration in the times recorded during laboratory experiments will yield a close approximation for the actual value of the diffusion coefficent for this reaction. However this model has one major failing in so much that it does not reproduce the continuous increase in the bubble diameter (a) which is seen to vary continuously until the reaction reaches equilibrium. This has been corrected in the numerical analysis, see appendix 2.

Numerical evaluation of this function was facilitated using a Fortran computer program (see appendix 2). This gave the expected distribution around the bubble for various times but gave the surprising result that the solutions are independent of the choosen diffusion coefficient for times, rates and radii of

Figure 5.10. Caption.

Figures 5.10 a,b,c show the influence of varying the diffus--ion coefficient on the concentration at differing times and diffusion radii. These curves show that at the radii and times of interest, the function is almost independent of the diffusion coefficient. The physical interpretation of this is probably that the entry of water into the bubble and the subsequent growth of the bubble are the rate controlling processes, or that the effect of D is apparent only at long times and large radii, compared with the inter-bubble distance.

Figure 5.10d shows the increase in bubble diameter with time for a diffusion coefficient of 10^{-6} and an initial concentration of 1000 $H/10^{6}Si$. This function is also independent of the diffusion coefficient over the range of conditions of interest, but shows an effect at much longer times.

Figure 5.10e gives the predicted distribution of hydroxyl around a growing bubble for a diffusion coefficient of 10^{-6}.

The data given in this figure are derived from a model for the growth of a bubble in an infinite crystal at a temperature of $1000^{o}A$. At lower temperatures the rate of bubble growth will be less, and as a result of this so will the change in hydroxyl concentration around the bubble. At higher temperatures, the rate of bubble growth and diffusion into the bubble will be faster, and thus the solution will be more sensitive to the diffusion coefficient for the hydroxyl in the crystal.

Figure 5.10a.

The effect of the diffusion coefficient on the concentration at different diffusion radii and at a time of 10^3 seconds.

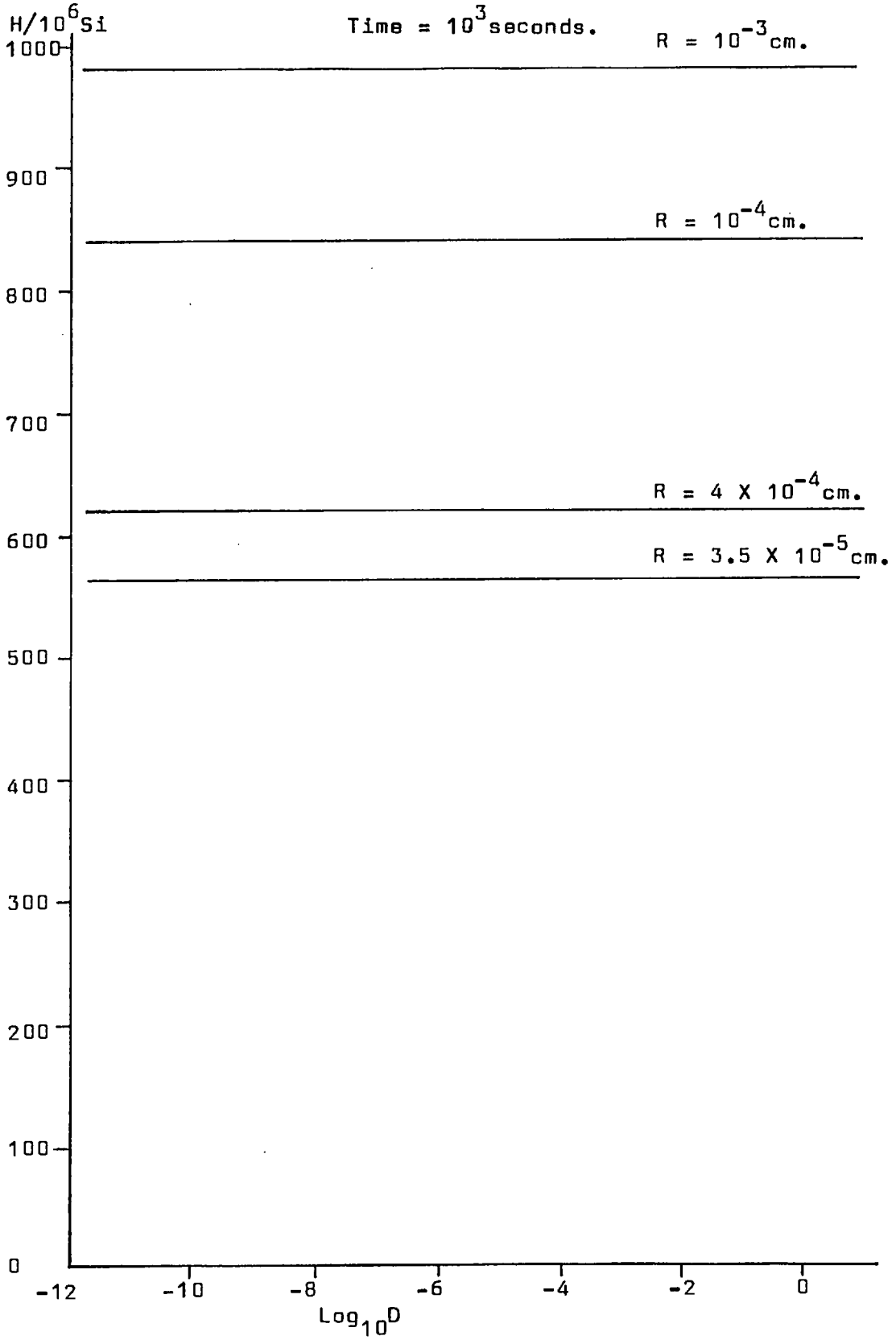

Figure 5.10b.

The effect of the diffusion coefficient on the concentration at different diffusion radii and at a time of 10^5 seconds.

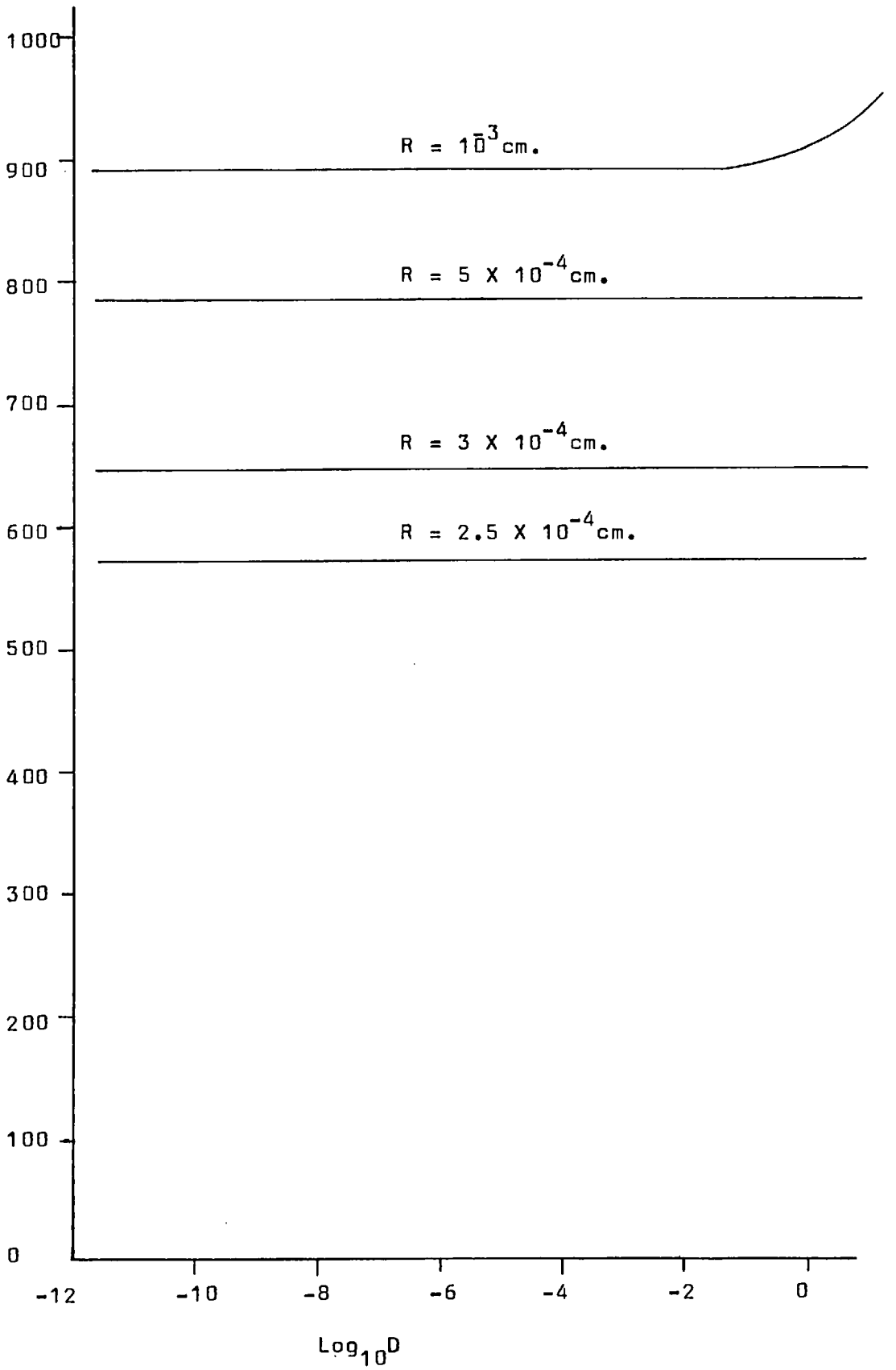

Figure 5.10c.

The effect of the diffusion coefficient on the concentration at different diffusion radii and at a time of 10^7 seconds.

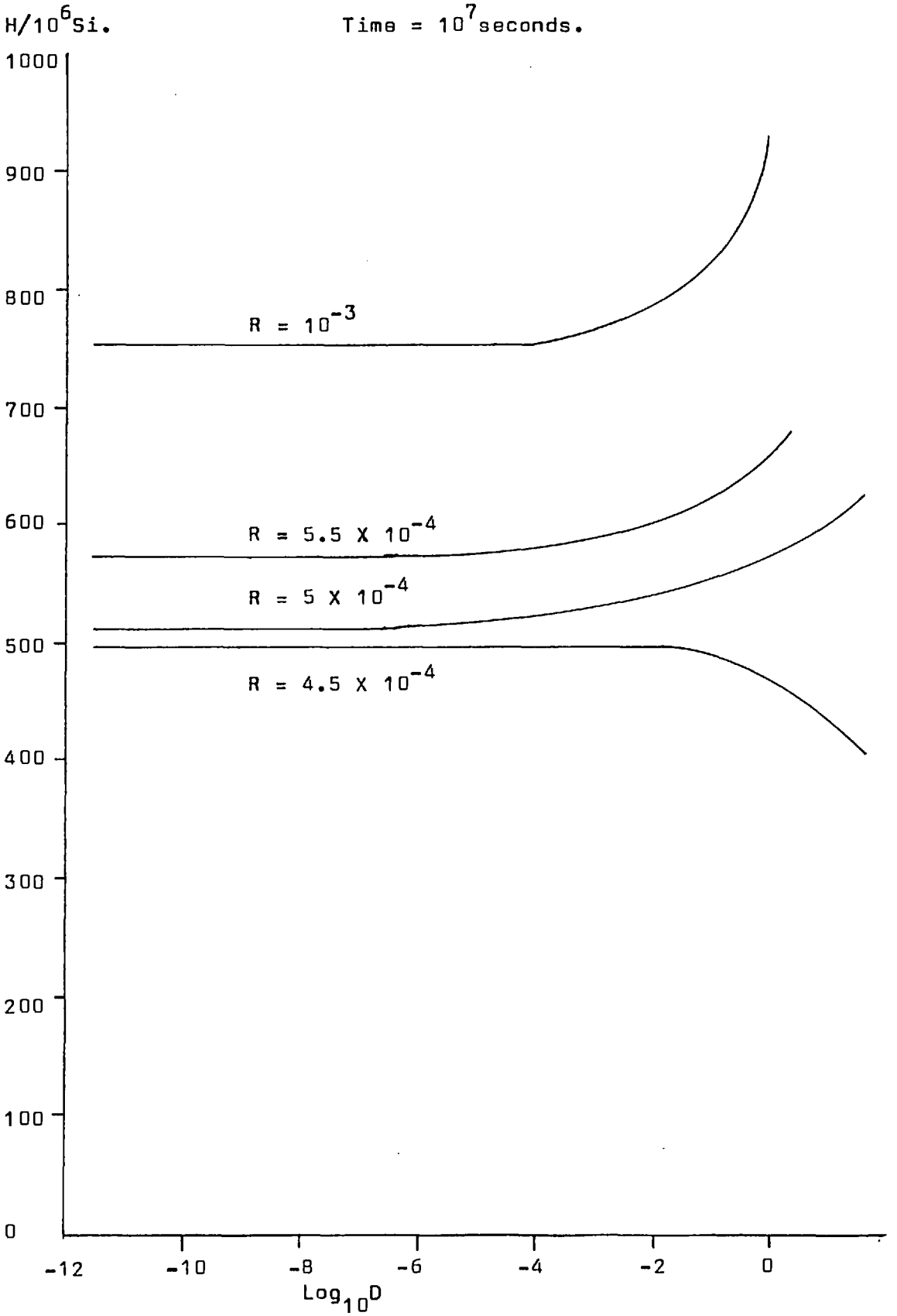

Figure 5.10d.

The change in bubble diameter with increasing time.

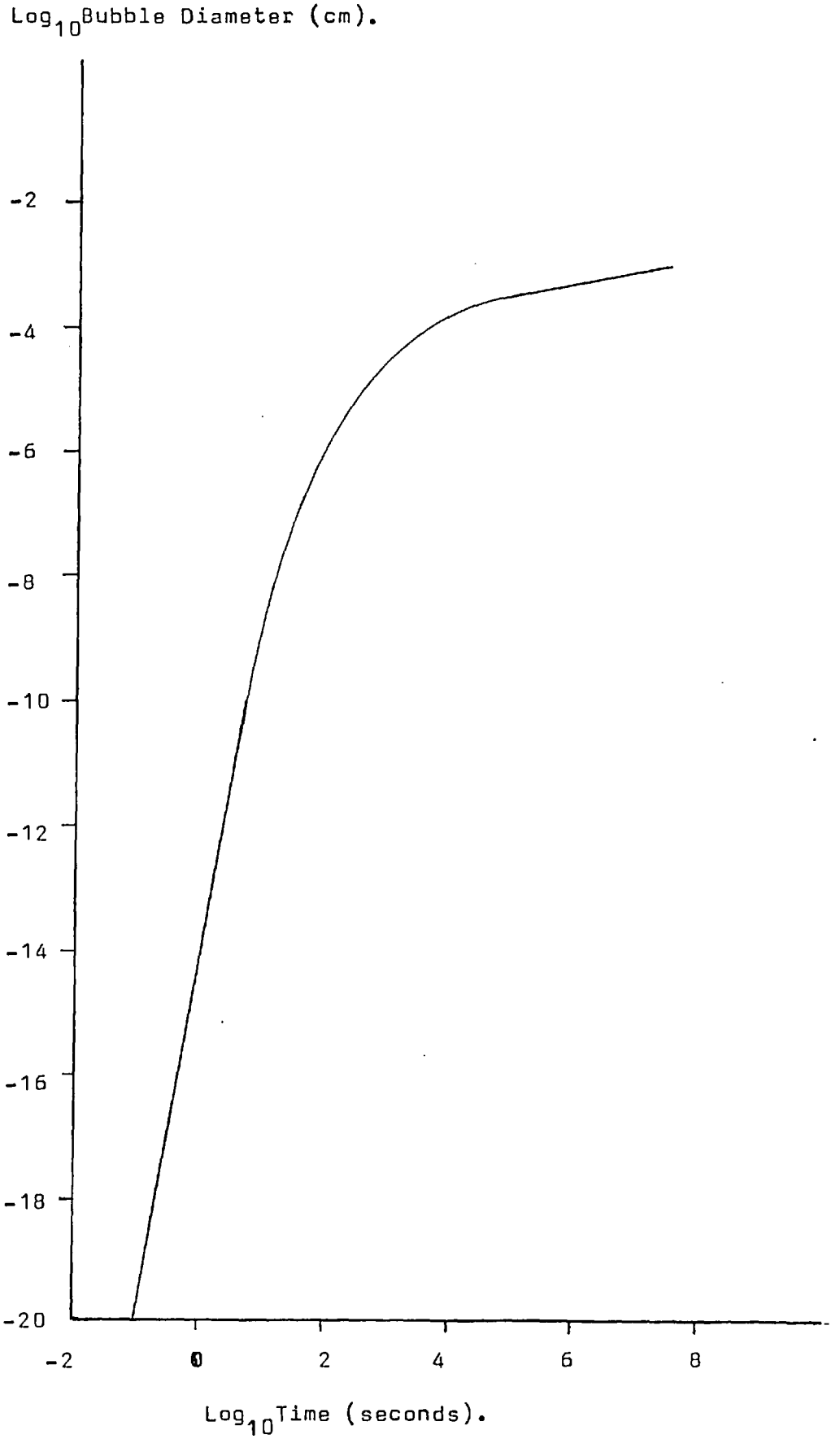

Figure 5.10e.

The distribution of water around the growing bubble at various times for an initial concentration of 1000 $H/10^6Si$, and a diff--usion coefficient of 1×10^{-6}.

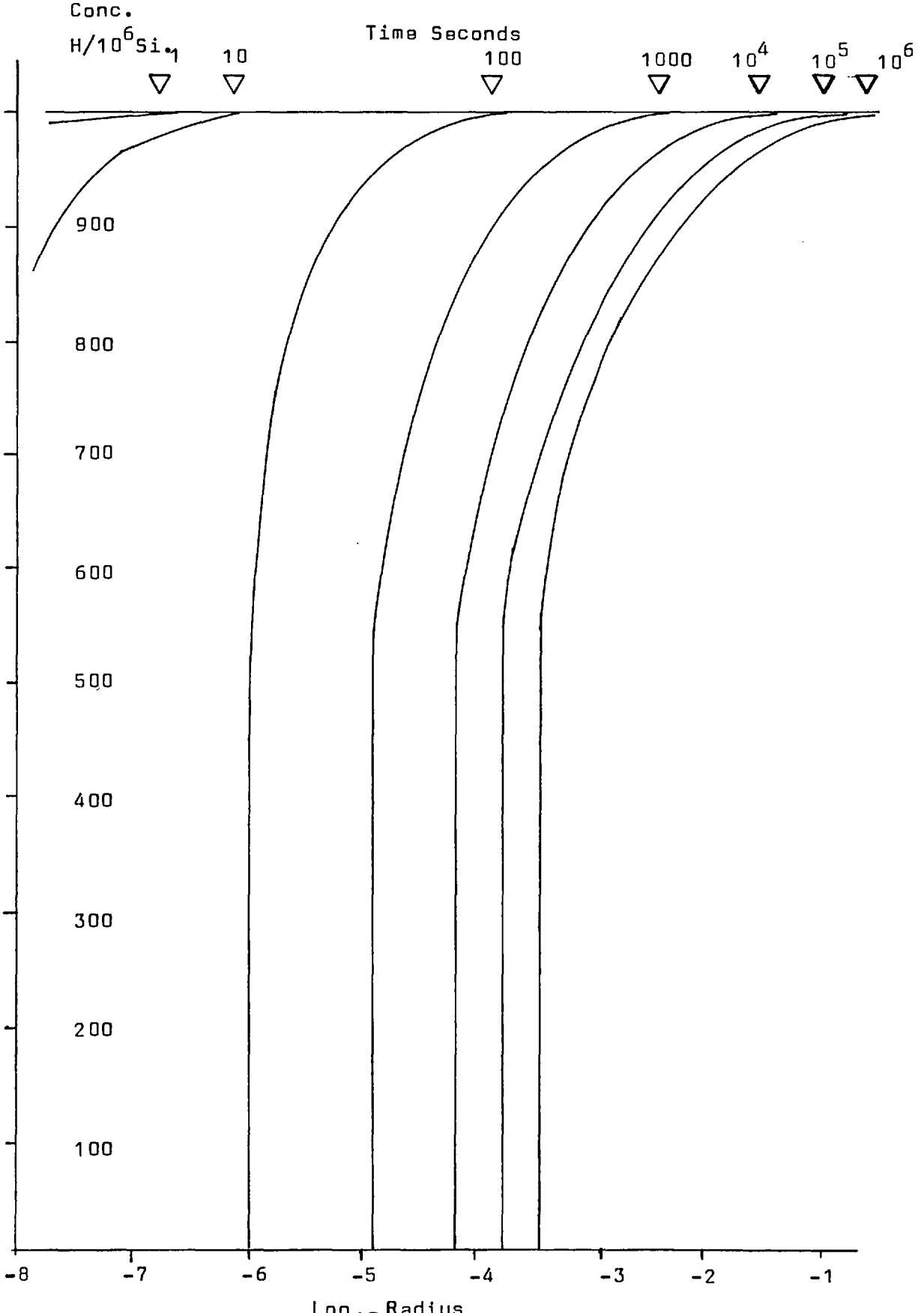

interest. Figure 5.10 shows the predictions of this model for the hydroxyl distribution around the bubble for different (in--creasing) times. The problem stated earlier of increasing the bubble size was overcome by calculating a new value for the bubble radius for each time increment in the solution using the relationship of Mclaren and Phakey(1966) (See Chapter 4). An attempt was made numerically to solve equation 5.21 for an array of bubbles but this gave very poor results and was abandoned, because of the very precise nature of the boundary conditions in this solution of equation 5.14.

In a more specific theoretical study, it should be possible to develop a satisfactory model for this diffusion reaction. Any such study will have to investigate the actual diffusion mechanism in depth, and evaluate fully the constraints on the value of the diffusion coefficient. The use of the electron microscope will be of the utmost importance in this respect. Unfortunately time did not permit such a detailled analysis to be undertaken during this study.

5.6.1.c. The Approach to Equilibrium.

Mclaren and Phakey (1966) noted that the bubbles precipitated in their amethyst samples became negative crystals after long periods of heating (50 hours at 900^{o}C). This shape change is caused by redist--ribution of the SiO_4 tetrahedra on the surface of the bubble(by solution and surface diffusion) to minimize the surface energy. A full mathemat--ical discussion of the equilibrium shape of gas bubbles and voids in crystalline solids (producing a minimum surface energy)is given by

Nelson, Mazey and Barns (1965) and will not be reproduced here.

The analysis used by Mclaren and Phakey (1966) based on that of Nelson et al (1965) is as follows. The total surface energy for a bubble in a crystalline solid is given by

$$E = \int \gamma dA = \sum_{hkil} A_{(hkil)} \gamma_{(khil)} \qquad 5.23$$

(where h,k,i,l are the miller indices of the crystal surface in question)

which for negative crystals in quartz is

$$6.a.b.\gamma_{(10\bar{1}0)} + (3\sqrt{3})a^2\phi\gamma_{(10\bar{1}1)} \qquad 5.24$$

where ϕ is the angle between (0001) and $\{10\bar{1}1\}$ and is approximately 52°. a and b are the dimensions of the $(10\bar{1}0)$ face.

The volume of the polyhedron is given by

$$V = \tfrac{1}{2}(3\sqrt{3})a^2b + (3/2)a^3\tan\phi \qquad 5.25$$

From Nelson et al (1965) the equilibrium shape is found by minimizing E as a function of a and b using the expression for V to prevent E from vanishing. This condition being

$$\frac{\partial E}{\partial a} + \lambda \frac{\partial V}{\partial a} = 0 \qquad 5.26$$

$$\frac{\partial E}{\partial b} + \lambda \frac{\partial V}{\partial b} = 0 \qquad 5.27$$

where λ is a Lagrangian multiplier.

This analysis is from Mclaren and Phakey (1966) and has been included for completeness, for it is the density and growth of the

bubbles together with the reduction in the structure bound water concentration which is important where hydrolytic weakening phenomena are concerned.

5.6.2. Precipitation of Molecular Water in Brazilian Quartz

Dehydration experiments, and other tests involving the heat treatment of Brazilian Type quartz crystals show quite conclusively that no visible precipitate is produced by the dehydration reaction, regardless of the temperature (up to 1350°C) and the initial hydroxyl concentration (up to 900H/10^6Si). This range of values overlaps widely the range of conditions and concentrations recorded for the appearance of bubbles of molecular water precipitated during the dehydration of synthetic quartz.

Two possible explanations are available to account for this difference in behaviour observed in these two quartz types. Firstly it can be suggested that the reactions being observed are not the same, or secondly, it can be suggested that the structure of Brazilian type quartz differs from that of synthetic quartz and does not provide the thermodynamic potential for the diffusion of the precipitated water (together with a vacancy) to particular isolated sites producing bubbles.

Considering the first of these possibilities, it is obvious that the "reaction" under discussion in fact refers to a range of possible chemical reactions of fairly similar type all of which occur to greater or lesser extent during the dehydration of every quartz crystal. The extent depending solely on the relative concentrations of Al^{3+}, Fe^{3+}, Na^{+} and Li^{+} in the structure of the dehydrating grain. The end product of all such reactions will however always be either molecular water or

a metal hydroxide and in almost every case the concentration of molecular water produced by reactions of the type:-

$$2(\equiv Si - OH) \quad = \quad \equiv Si - O - Si \equiv \quad + \quad H_2O$$

will far exceed the concentration of hydroxides produced by

$$(\equiv Si - OH..MO - Si \equiv) \quad = \quad \equiv Si - O - Si \equiv \quad + \quad M\text{-}OH$$

Because of the far greater proportion of water related solely to hydrogen bonded silanol groups than that involved in charge compensation with substitutional and interstitial metal impurities, simply to suggest that in Brazilian quartz the reaction will predominantly produce hydroxides which will not diffuse is insufficient. (Also, why shouldn't these hydroxides themselves diffuse by mechanisms similar to that for water diffusion (suggested here) and form crystalline precipitates in the structure). I thus dismiss differences in the detailed chemistry of the reaction as being insufficient to account for the observed behaviour.

The second alternative is at first examination no more attractive, the structure of pure Brazilian and pure synthetic quartz should be identical, and certainly the undeformed crystals barely differ when their dislocation microstructures (particularly densities) are compared. This leads to the conclusion that the bubbles which grow in dehydrating synthetic quartz cannot have formed simply from nucleation resulting from random thermal fluctuations (if they did they would also occur in Brazilian type quartz) and therefore it would seem that the structure of synthetic quartz must contain an impurity which acts as the seed on which these bubbles nucleate. (See the next section).

5.6.3. Impurity Seeding of Bubble Growth in Synthetic Quartz

If the bubbles which grow in the structure of dehydrating synthetic quartz are to be seeded, on the small grains of an impurity phase, or as the result of some other feature such as the strain fields associated with the microstructure. This seed must be found throughout the structure of all synthetic crystals and in all synthetic crystals its density must vary in direct proportion to the hydroxyl concentration reflecting the hydroxyl distribution, allowing the precipitated water in the bubbles to do likewise as is observed in heat treated crystals.

I found such a seed in the structure of synthetic quartz crystals by chance. Whilst setting up a sample cut from a synthetic quartz crystal in the heating stage of the High Voltage Electron Microscope (HVEM) it became apparent under certain (weak beam) diffracting conditions that the structure of this particular synthetic quartz crystal was packed with a finely dispersed crystalline impurity phase. (The importance and properties of these impurity particles together with the HVEM heating stage experiments are the topic of the next chapter). An example of this impurity is shown in plate 5.2. The density of these impurity particles was found to reflect the distribution of hydroxyl in the structure of the quartz sample (see next chapter) and when a foil containing these impurities is heated to a sufficiently high temperature in the electron microscope, the bubbles are seen to nucleate and grow around these particles. Plate 5.3 conclusively shows the role played by the impurity phase in acting as seed nuclei for the bubbles.

In the next chapter I will show that the number of impurity particles is reduced whilst their individual size increases with increasing temperature, and that this reaction proceeds more rapidly than the

growth of the bubbles of precipitated water. During this reaction the impurity particles maintain distinct strain fields which become extreme during cooling, and it is probable that it is the presence of these strain fields which drives the spontaneous migration of vacancies (together with the water molecules they are carrying) to the immediate area of each impurity particle. As the temperature of the crystal is increased more vacancies become available and move with increasing rapidity to the environs of the precipitate particles forming the void into which any water molecules carried in these vacancies are deposited. This model is supported by the electron microscope observations that at comparatively low temperatures the number of impurity particles decreases whilst their size increases but at higher temperatures those on which bubbles have nucleated seem to undergo little change as if separated from the host crystal by a screen (of molecular water). At these higher temperatures the bubbles grow very quickly and soon become many times the diameter of the seed particle. So at low temperature (low density of available vacancies) the impurity phase shows a diminishing density and increasing particle size with increasing time. At higher temperature (greater density of available vacancies) the diffusion processes leading to this minimization of the surface area of the impurity phase increases in rate and the first bubbles may start to form. At higher temperatures still (very high density of vacancies), the growth of bubbles of water around the precipitate particles becomes obvious and very rapid (more rapid than the growth of the impurity grains) and those grains contained within a bubble cease to enter into the diffusion processes connected with the reduction in number of impurity grains.

This section is concerned primarily with the seeding of nuclei for the growth of bubbles in the structure of dehydrating synthetic quartz,

I shall therefore save further discussion of the impurity phase and the complex diffusion processes connected with it until the next chapter which is devoted to this impurity and its role in the deformation of synthetic quartz.

The suggestion that bubbles of molecular water present in heat treated synthetic quartz have grown on crystalline impurity seeds poses the problem as to how the similar bubbles found in natural milky vein quartz and heat treated amethyst (Mclaren 1966) nucleated and grew. This is the topic of the next section.

5.6.4. Precipitated Molecular Water in Natural Quartz

Much of the quartz occurring in veins, or as a rock forming mineral in nature is seen to contain large numbers of small bubbles similar in size and shape to those produced during the dehydration of synthetic quartz. Plate 5.4 is an electron micrograph (100 KEV) of such a crystal from a north Devon (Culm Measures) tectonic vein. Amongst this natural quartz with high densities of bubbles, the highest densities are reported from low grade tectonic and hydrothermal veins, pegmatites and sedimentary overgrowths in quartzites (particularly those which have not been subjected to metamorphism above the lowest Greenschist facies grade).

White (1973) has suggested that all such small fluid inclusions may have developed in the solid crystal after crystallization had finished, and as such are not the primary growth imperfections which the body of geological opinion has generally considered them to be. This suggestion of White (1973) has been strongly supported by the work of Knipe (1977) in his study of low grade quartz shear zones. Similarly Mclaren and Phakey (1966) succeeded in growing bubbles by heating an amethyst crystal

which underwent a similar dehydration reaction to that reported here for synthetic quartz. They also found that citrine behaved in a similar fashion. Both these minerals and other colour variants such as Rose quartz may appear milky in nature. There is thus a reasonable body of evidence to suggest that the milkyness (or opalescence) often seen in natural quartz samples results from large densities of small fluid inclusions which grew in the solid crystal structure as the result of some dehydration reaction after crystallization was complete. (The reaction may of course have happened spontaneously immediately after the formation of the grain. If this is so (as I believe it to be) how did these bubbles grow in the natural quartz when from experimentation it is seen that some nuclei seed species is needed to initiate the bubble growth. What possible seed species is available in the structure of most commonly occurring quartz crystals which is not present in the structure of smokey or Brazilian type quartz? (Brazilian type quartz will not turn milky, whereas synthetic quartz turns milky as a result of precipitation of water around impurity particles).

This question has in part been answered by White (1973) who recognized that many of the bubbles found in natural quartz lie along individual dislocations, low angle dislocation walls, subgrain walls and grain boundaries, i.e. in crystals with an established microstructure, it is possible for the microstructure to become decorated with these bubbles of precipitated water. This decoration will presumably occur because of the strain fields associated with the defects attracting vacancies in the same manner as that suggested previously for the diffusion of hydroxyl filled vacancies to the strain fields associated with impurity particles in synthetic quartz. More recently however Knipe (1977) has shown that bubbles may also pin dislocations in the

quartz structure, so perhaps not all of the precipitated water in the grain that is associated with the microstructure need necessarily have been precipitated as a result of that microstructure. (See Knipe PhD London 1977). Mclaren and Phakey (1966) found in their heat treated amethyst and citrine samples that nearly all the bubbles were associated with dislocations. These dislocations were however generated during the same heat treatment as that which produced the bubbles. Mclaren and Phakey (1966) interpreted these dislocations as resulting from deformation produced by the stress field around the growing bubble, suggesting that the quartz was hydrolytically weakened in these tests. I suggest that the opposite is more probable, the dislocations developing in response to thermal stresses in the heat treated sample, which once established had their own strain fields reduced by local annihilation of a dislocation line segment by vacancy diffusion resulting in the precipitation of molecular water. It is important to note that at the high temperatures used in this study (normally between 100°C and 800°C) and allowing for the small strains that these dislocations are associated with (implying that they would have developed and moved only very slowly during the duration of the test, equivalent to a slow strain rate deformation) there would seem to be little need to evoke hydrolytic weakening at all.

Possibly then the development of milkyness in natural quartz results simply from vacancy diffusion to strain fields in the microstructure. This however cannot always be the case. Some natural milky quartz has only very small dislocation densities, as do some grain overgrowths in quartzites, and naturally milky amethysts. Futher, the milkyness in natural quartz often develops at comparatively low temperatures (200°C), when the equilibrium concentration of vacancies is small so that any process of hydroxyl diffusion associated with vacancy

migration will only proceed very slowly.

Thus some spontaneous mechanism for the development of bubbles in natural quartz crystals, which does not require the comparatively high temperatures associated with a large equilibrium vacancy population, will have to be sought, although long times may suffice.

Knipe (1977) has recorded bubbles in the grain overgrowths of some quartzites which may have developed at temperatures as low as 100°C and it is well known that most the quartz occurring in veins, saddle reefs and other structures associated with deformation or metamorphism in the low grade environments is invariably milky. I have shown (Section 5.5) that increasing the heating time greatly will have only minimal influence on the shape of the dehydration curve, and it would thus seem that such natural quartz must have had a very low threshold temperature for the dehydration. From the dehydration curves shown in figures 5.3, 5.4, 5.5 and 5.6 a qualitative statement may be made to the effect that a low threshold temperature is related to high concentrations of hydroxyl dissolved in the structure, so as a starting point in the search for a spontaneous precipitation mechanism it is worthwhile investigating exactly how large these concentrations might be.

In Chapter 4 I introduced the relationship

$$\pi d^2 n = 3NkT/2\gamma$$

which was used by Mclaren (1966) to predict the approximate number of H_2O molecules in equilibrium in the bubbles assuming that the H_2O molecules behave as a perfect gas and that the bubbles are in equilibrium. For a low temperature quartz vein with $T = 473^{\circ}A$, $d = 1000\times10^{-8}$, $n = 10^{14}cm^{-3}$ and $\gamma = 1000erg/cm^2$ (Brace and Walsh 1962, Mclaren 1966) then the concentration of hydroxyl groups originally dissolved in the

structure is of the order of 30000 to 35000 H/10^6Si. If the bubble density is $10^{15}cm^{-3}$ then this concentration is increased by an order of magnitude giving 300000 to 350000 H/10^6Si. Thus some natural quartz may have supported 2,3 or even 4 orders of magnitude more structural water shortly after its crystallization, than the synthetic quartz used in the laboratory dehydration experiments. If as suggested much natural quartz which crystallized in the zone of diagenesis or in low temperature hydrothermal veins contained these vast concentrations of structure bound water then the question must be asked as to whether this hydrous silica mineral can correctly be termed quartz? This problem has been studied by Knipe (1977) and I strongly support his view that it cannot, i.e. that the water now present in the bubble resulted from a distinct phase change and was precipitated during the associated major recrystallization from hydrous silica (silica gel?) to quartz together with molecular water.

The sudden release of a large quantity of molecular water into the structure, associated with what must be fairly major structural changes may account for the spontaneous formation of large numbers of bubbles at low temperatures. During the phase change very large strains will develop between the new and the old grains, and the area influenced by such strains will continually be changing. The release of so much molecular water into the structure will cause a drastic increase in the free energy of the grain associated with the large numbers interstitial water molecules and this will be reduced by the equilibrium vacancy populations absorbing these water interstitials. With so many water molecules present in the grain, it is probable that random thermal fluctuations will cause the nucleation of the bubbles. Any water molecule

reaching the bubble has a probability of leaving it which is inversely related to the bubble diameter. Thus as the bubbles grow, their potential as sinks for water molecules becomes greater and it is only the diminishing concentration in the structure (the number of random motions being proportional to the concentration) that eventually slows the growth rate to a negligible amount.

5.6.5. Precipitated Water in Quartz - Summary

From the dehydration experiments is it observed that synthetic quartz turns milky on heating whilst Brazilian quartz crystals do not. This distinction, which is related to the high densities of impurity particles in the synthetic quartz structure may be fundamentally important to the comparison of their mechanical properties (see the discussion at the end of Chapter 6) the impurities which act as nuclei in the synthetic quartz structure are absent in Brazilian type natural quartz which I suggest accounts for the absence of precipitated water in bubbles when such quartz undergoes a dehydration.

The migration of the molecular water to the bubble site poses a space problem which is most simply overcome by assuming that the water molecule is carried in a silica vacancy diffusing to the strain field around the impurity particle.

Natural milky quartz and amethyst also contain bubbles (or produce them when the crystals are heated) but appear not to contain the impurity phase which acts as the nuclei in synthetic quartz. In many of these cases the dislocation microstructure supplies the strain fields to which the water carrying vacancies diffuse whilst in other (low temperature hydrothermal vein quartz and grain overgrowths in quartzites) a distinct phase change and recrystallization from hydrous silica to quartz plus

water is probably the cause of the large quantities of precipiated molecular water which becomes organized into bubbles by one or more of the several processes outlined above.

Thus a further major distinction can be identified between the three classes of quartz (natural Brazilian, Synthetic, and Natural opalescent and other poor quality quartz). The recognition of these three distinct quartz types will be shown later to be of fundamental importance to the interpretation of deformation experiment results.

5.7. THE EFFECT OF PRESSURE ON THE DEHYDRATION REACTION

As stated at the beginning of the chapter, it has been suggested (Ayensu and Ashbee 1977) that the dehydration reaction is supressed by large hydrostatic pressures, and that at these pressures water will diffuse from bubbles and the external environment into the structure of the quartz crystal creating silanol groups (Griggs and Blacic loc cit). It it thus necessary to investigate the effect of pressure to substantiate the applicability of the preceeding discussion to experimental and natural quartz deformation under triaxial conditions.

This investigation was conducted using the solid pressure medium deformation machine operating under hydrostatic conditions to 10 kBar confining pressure and 850^{o}C using a talc confining medium. Unfortunately these experiments proved difficult to conduct and did not supply good quantitative information. The reasons for this were twofold, firstly the poor condition of the specimens recovered from the rig (they contained close spaced fractures parallel to the core ends) made them unsuitable for infrared analysis, and secondly operating difficulties with the rig meant that it was impossible to maintain constant conditions for long periods (maximum time 1 hour). Which meant that the time to equilibrium

(as determined at 1 atmosphere) could not be accomplished. However careful design of the experiment particularly as far as choice of sample was concerned provided positive (if qualitative) evidence that the dehydration is not insignificantly suppressed by large hydrostatic pressures and may even be enhanced by them.

5.7.1. The Experiment

Cores were cut from crystal ITT6, each containing the same set of growth bands whose plane was parallel to the core axis. The group of bands chosen were selected to give an easily recognizable pattern of bubbles when the sample was heat treated. The fresh cores were then heated in the solid medium rig at pressures of 5 or 10 kBar and at a temperature of 850°C for periods varying between 5 and 60 minutes. The samples were then recovered and their cross section at the middle of the core examined optically to see if the distinct pattern of growth bands was picked out by bubbles of precipitated water. In all cases it was. From some of these samples (10 kBar, 850°C, for 10 minutes) thin foils were prepared for electron microscopy, Plate 5.5 compares electron micrographs from this foil with those from a sample of the same crystal (same growth bands and orientation) heat treated, at atmospheric pressure, at 850°C. Table 5.3 compares the bubbles densities and sizes and shows that the dehydration has proceeded to a similar degree in each case.

5.7.2. Conclusion

From this experiment two very important conclusions may be drawn.

(1) The dehydration reaction proceeds in a manner not significantly changed by pressures up to 10 kBars.

(2) Water released by the dehydrating talc confining pressure medium does not enter the quartz structure, and is not responsible for forming the bubbles as suggested by Blacic (1975). (It was prevented from doing so by an Al_2SiO_5 jacket).

TABLE 5.3.

A comparison of the densities and size of fluid inclusions produced by the heat treatment of synthetic quartz crystal ITT6 at 850°C. and either atmospheric pressure or 10 Kilobars hydrostatic confining pressure. (From Jones 1978). The longer heating time for the 1 atmos. sample was selected so as to give a volume fraction of precipitated water which was generally within an order of magnitude of that recorded for heating for 10 minutes at 10 Kilobars. Heating at 850°C. and 1 atmos. for 10 minutes produced no detectable precipitation. The volume fraction of precipitated water was calculated on the assump-tion that the bubbles are of spherical form.

CONDITIONS.	DENSITY. Cm^{-3}.	DIAMETER. Å.	VOLUME FRACTION.
1 atmos. 850°C. 24 hours.	6.35×10^{12}	1000	3.3×10^{-3}
1 atmos. 850°C. 24 hours.	4.17×10^{12}	1200	3.7×10^{-3}
1 atmos. 850°C. 24 hours.	1.08×10^{12}	900	4.1×10^{-4}
10 Kbar. 850°C. 10 minutes.	5.12×10^{11}	1000	2.6×10^{-4}
10 Kbar. 850°C. 10 minutes.	2.1×10^{11}	1300	2.4×10^{-4}
10 Kbar. 850°C. 10 minutes.	6.8×10^{11}	900	1.8×10^{-4}

These two conclusions both follow from the observation that the same pattern of bubbles is produced in about the same time at similar temperatures irrespective of whether the sample is heat treated in the presence of dehydrating talc at 5 or 10 kBars or in the presence of dry air at atmospheric pressure. On the strength of this experiment I think that the original interpretation placed by Griggs and Blacic (loc cit) on their early experiments ("that the quartz was hydrated by the dehydrating talc and hence water weakened") is probably completely wrong, and that the observed mechanical properties should be attributed to the original impurity concentrations in the samples. At the temperature at which the talc dehydrates much quartz with the exception of only the very purest Brazilian type crystals will flow comparatively easily. If this is so then the original interpretation can be put down to the coincidence that the weakening temperature and the talc dehydration temperature were the same in the samples used in those particular experiments.

5.8. THE DEHYDRATION REACTION AND 'NATURAL' HYDROLYTIC WEAKENING

I have shown in this chapter that the structure bound water concentration in natural or synthetic quartz is reduced if the crystal is maintained at some elevated temperature above a threshold value given by the data in figure 5.9. I have also shown that this reaction is initially rapid but that its rate diminishes rapidly with increasing time by a log/log relationship. Using this data from Chapter 5 would thus indicate that much of the low metamorphic grade natural quartz will be precipitating water from its structure from the moment of its crystalization. At the low temperatures at which this natural dehydration

reaction will proceed (around 200°C) the rate of this reaction will be much slower than that recorded in the laboratory. Thus for some time after its formation the crystal will be in a position to be water weakened but this effect will be continually diminished with increasing time. This does however mean that any deformation attributed to hydrolytic weakening must occur during the first thermal event to which the quartz rock is subjected and this in the case of most vein quartz must be associated with the actual formation of the vein. After some time presumably measured at the most in years or tens of years the quartz will have dehydrated to the extent that it will become brittle or be undeformable by natural stresses (according to currently available mechanical data) as a result of the ongoing dehydration. It may be that the structural water concentration can be re-established by recrystalization of the cold worked structure but this has not been reported from laboratory experiments.

It must therefore be concluded that the absence of any satisfactory mechanism for the diffusion of molecular water into the structure of crystaline silica under natural geological conditions seriously restricts the importance of natural water weakening to possibly only one deformation event early in the history of any particular natural quartz crystal. Water weakening cannot then have the wide ranging significance originally suggested for the process unless some diffusion process for the movement of water into the quartz structure in rocks can be identified. It would seem that microstructural studies of low grade quartz rocks could be important here in identifying superimposed deformation widely spaced in time and not separated by a major period of recrystallization. Assuming that such a microstructure can be found then it will be necessary either

to identify the diffusion reaction or to look for a parallel or alternative weakening mechanism. Alternatively, although not recorded in laboratory experiments, the dehydration reaction may be reversed on cooling. The rate of this back reaction would have to be very slow for it to be undetectable in the laboratory, and as such its existence is only speculative. The existence of large numbers of fluid inclusions in natural quartz grains subjected to slow cooling ($1^{o}C$ per 10^{4} years may well occur in nature) certainly does not support the existence of this slow back reaction.

5.9. CONCLUSIONS

The major conclusions of this chapter may be summarized as follows.

(1) The concentration of structure bound hydroxyl groups in quartz crystals is reduced on heating above a threshold temperature, which may possibly be related in some way to the temperature and pressure at which the crystal grew.

(2) Natural Brazilian Type crystals dehydrate more rapidly than do synthetic quartz crystals.

(3) The dehydration reaction approached pseudo equilibrium in 5 to 10 hours after reaching the higher temperature in laboratory experiments.

(4) The molecular water produced by the dehydration reaction will be carried and precipitated by vacancies migrating to regions of lattice strain associated with the crystals microstructure. In natural Brazilian Type Quartz crystals, which have a comparatively pure structure with few dislocations such precipitation does not occur in the laboratory.

(5) The growth of bubbles of precipitated water can be modelled

by the diffusion equation, leading to constraints on the value of D for the movement of precipitated water into fluid filled voids.

(6) The sponteneity of the reaction is not significantly affected by changes in hydrostatic pressure in the range 1 atmosphere up to 10 kilobars.

(7) Water cannot be made to diffuse readily into the structure of quartz in the laboratory under hydrostatic conditions without the application of an external potential such as a high voltage electric field (Kats 1962). This is in conflict with the ideas of Griggs and Blacic (loc cit) who have suggested that water released from dehydrating talc in the deformation rig entered and weakened the structure of the quartz test specimen.

A detailed discussion of these conclusions will be deferred until the last chapter in which the conclusions of the microstructural studies still to be presented can be brought into the discussion as well.

Chapter 5.

ELECTRON MICROGRAPHS.

Plate 5.1. Caption.

5.1a, b, c). Bubbles produced by the heat treatment of a synthetic quartz specimen.

Plate 5.2. Caption.

5.2). The impurity phase found in the structure of all the synthetic quartz crystals examined during this study.

Plate 5.3. Caption.

5.3a, b, c). Bubbles nucleating on the impurity particles in the structure of synthetic quartz. These micrographs were recorded during an insitu heating experiment in the 1000 KeV microscope, at a temperature of about 900^{o}C. At these high temperatures, thermal fluctuations on the surface of the foil lead to a continual slow drift of the foil. This is shown in the micro--graphs in their slightly blurred appearence. This is unavoid--able.

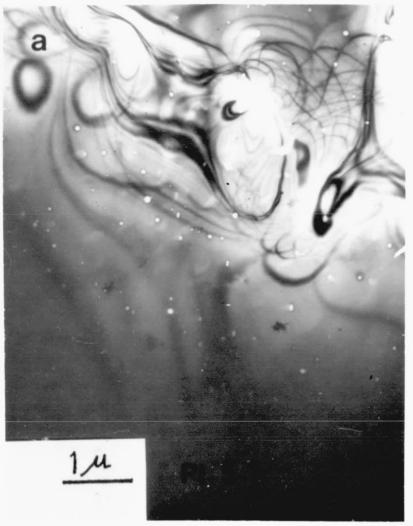
a
1μ

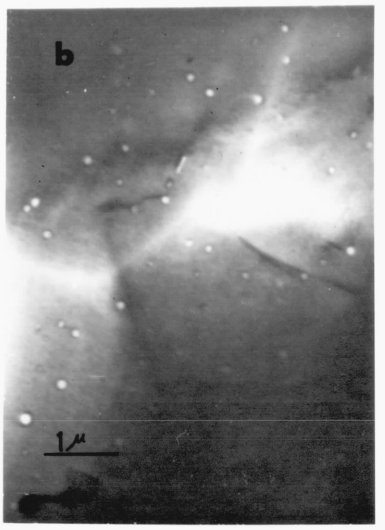
b
1μ

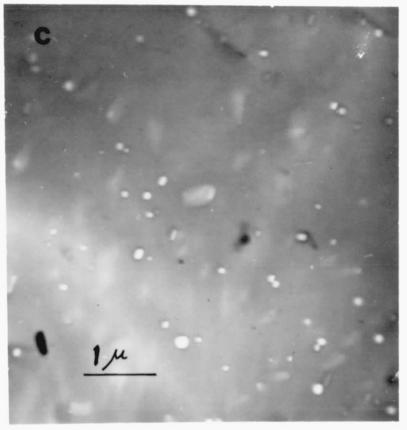
c
1μ

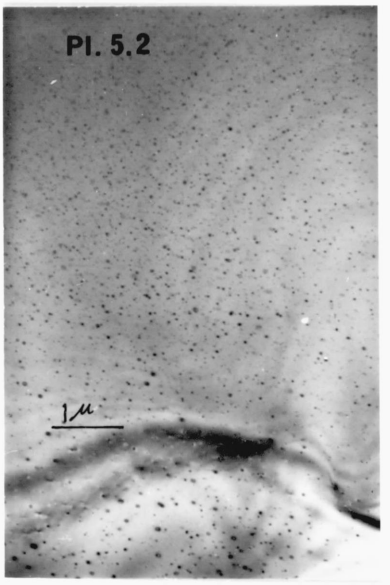
Pl. 5.2
1μ

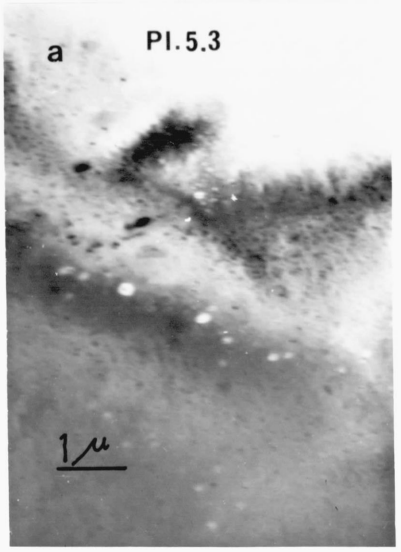
a
Pl. 5.3
1μ

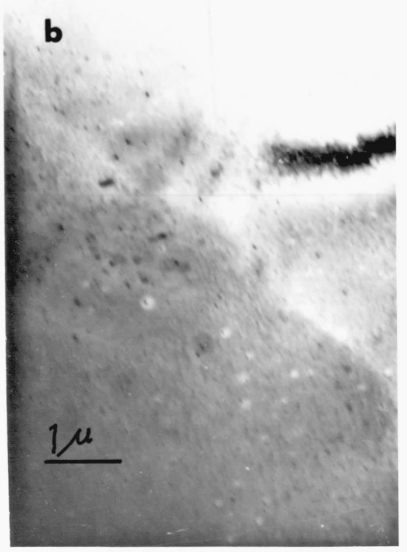
b
1μ

Plate 5.4. Caption.

5.4). The microstructure of a natural milky quartz crystal from a tectonic vein in the Culm, North Devon.

Plate 5.5. Caption.

5.5a, b). Typical bubble densities produced by the heat treatment of synthetic quartz at 850^{o}C and 10 Kbars for 10 minutes in the solid confining pressure medium deformation rig.

5.5c, d). The bubble densities produced by the heat treatment of the same synthetic quartz crystal (Same growth bands) at 850^{o}C. and atmospheric pressure for 24 hours.

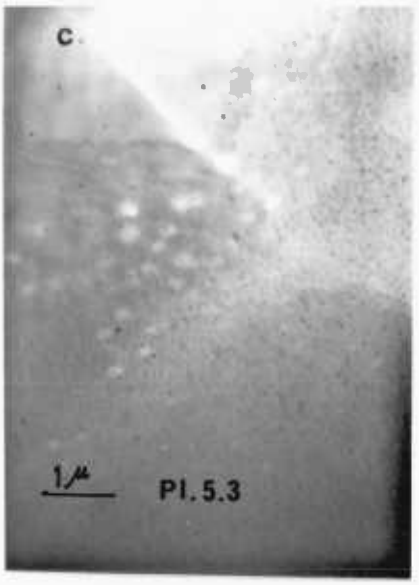
c
1μ
Pl. 5.3


Pl. 5.4
1μ

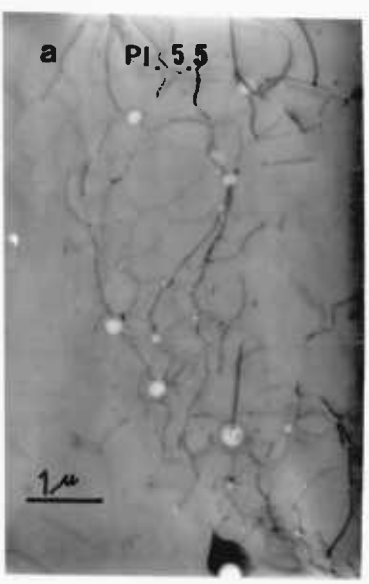
a
Pl. 5.5
1μ

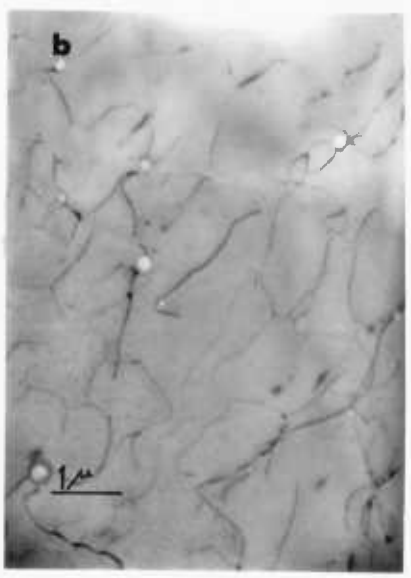
b
1μ


c
1μ


d
1μ

Chapter Six.

A COMPARISON OF THE MICROSTRUCTURE OF THE THREE QUARTZ TYPES.

Chapter 6. A COMPARISON OF THE MICROSTRUCTURE OF THE THREE QUARTZ TYPES.

6.1. Introduction.

6.2. Microstructure of Natural Quartz.

- 6.2.1. The Microstructure of Brazilian Type Quartz.
- 6.2.2. The Microstructure of Natural Opalescent and related quartz.

6.3. Microstructure of Undeformed Synthetic Quartz.

- 6.3.1. An Impurity Phase in the Structure of Synthetic Quartz.
- 6.3.2. Insitu Heating Experiments.

6.4. Mechanical Effects of the Impurities.

- 6.4.1. The Mechanical Effects of an Impurity Phase in the Structure of a Crystalline Material.
  - 6.4.1.a. Weakening Mechanisms.
  - 6.4.1.b. Hardening Mechanisms.
- 6.4.2. Observations of the Mechanical Effects of Impurity Particles in the Synthetic Quartz Structure.

6.5. Conclusion.

6.1. INTRODUCTION

In Chapter 4 I demonstrated that natural milky quartz crystals do not have the mechanical properties predicted (using the Griggs 1974 relationship) from their structure bound hydroxyl concentrations. From this I concluded that either natural milky quartz is stronger than predicted because of some other feature of its microstructure (or trace chemistry) or that molecular water as against structural hydroxyl cannot cause similar weakening to that reported for hydroxyl in synthetic quartz.

Before proceeding with the comparison of quartz microstructures in which I identify an alternative weakening mechanism in synthetic quartz, I shall briefly review the basic hypothesis of water weakening. Griggs and Blacic (loc cit) found in a series of perfectly reproducible deformation experiments that the temperature at which yield was first recognized, and the temperature at which the sample first became weak varied inversely with the structure bound hydroxyl concentration of the sample. Because of this apparent relationship, it was assumed that the hydroxyl ions were responsible for this weakening effect although no entirely satisfactory explanation for the relationship has been produced. At no stage in the development of the theory has the possibility that some third factor which varies in direct relation with the hydroxyl concentration may be important been considered. However the work of Kats (1962), Bambuer (1961), Cohen and Hodge (1958) and to a lesser extent this study, strongly suggest a direct relationship between the concentrations of Al^{3+} (also Fe^{3+}), Li^{+} and Na^{+} in the quartz structure and the hydroxyl concentration. Variations in the intensity of the infrared absorption will then not only be a measure of the concentration of hydroxyl in the structure but will also indicate the relative concentrations of these other impurities. The original assumption that the

weakening is due solely to the concentration of hydroxyl ions may then be in error, these other impurity ions also having a possible part to play.

In this chapter, I intend to examine the microstructure of the three classes of quartz (previously defined) and will show that the suggestion made above may well be true. I shall then discuss generally the mechanical effects of an impurity phase, dispersed as fine particles in the structure of a crystal, and review the observed mechanical effects of such an impurity in the structure of synthetic quartz. I shall suggest a reinterpretation of the mechanical data for synthetic quartz based on these observations in the final chapter.

6.2. MICROSTRUCTURE OF NATURAL QUARTZ

In this section I shall discuss the microstructure of undeformed or only slightly (naturally) deformed natural quartz.

6.2.1. The Microstructure of Brazilian Type Quartz

The microstructure of piezoelectric grade, Brazilian type, quartz is typically featureless. The density of grown in dislocations is small; around $10^2 cm^{-2}$ (Baeta and Ashbee,1970) and the structure is normally devoid of bubbles and twins. Occasionally such crystals contain planes of macroscopic fluid inclusions but these are normally along the lines of healed fractures and are obviously of a secondary nature.

The trace chemistry of these crystals is equally simple, the hydrogen concentration is always small (see Chapter 4) but the AL^{3+} (or Fe^{3+}) concentration may be fairly large if the sum of the Li^+, Na^+ and H^+ charges is sufficient to satisfy the charge deficit of the Al substituted for Si in the structure, (Bambuer 1961). Thus all the major trace impurities are involved in atomic substitution in the structure.

This is clearly seen in the spectrum, and predicted by the studies of Kats (1962). The low dislocation density provides few sites for hydroxyl silicon bonds of the type envisaged by Griggs (1967) in the water weakening model and there is little water present to form silanol bonds of the type suggested by Brunner (1961). Another consequence of the small 'grown in' dislocation density is that if no sources are available to produce dislocations at low stresses, the yield stress will be high. This is in keeping with experimental results which only report yield to occur at high temperatures and then normally at high stress except at the highest temperatures (1000°C). Mechanical tests on Brazilian type quartz will thus provide mechanical data which is close to the theoretical strength of the silica structure. This strength is not attainable by most testing machines except at the highest temperatures, and often at high pressures to prevent brittle failure of the sample. High temperature plastic deformation of this material has however been described by McLaren et al (1967).

6.2.2. The Microstructure of Opalescent and Related Natural Quartz

The types of quartz commonly encountered in nature have a more or less complex microstructure with variable densities of bubbles, dislocations and features related to subgrain production and recrystallization. Such quartz has normally undergone some degree of plastic deformation, even that from the lowest temperature environments.

I examined the microstructure of a milky vein quartz crystal from a North Devon tectonic vein. This crystal shows well developed arrays of dislocations with fluid precipitates developed in regions where large lattice strains would be expected. The micrographs in plate 6.1 are typical examples of this microstructure.

Crystals of this type have large concentrations of precipitated

molecular water, which are far in excess of the Al^{3+} concentration. Originally much of this water was either bound in the microstructure or was present in silanol groups.

If the present theory of water weakening is correct, some quartz of this type (that which retains fairly large structural water concentrations) should behave plastically at low stress and comparatively low temperatures in the laboratory. This is found not to be the case. However an examination of the microstructure shown in plate 6.1. shows no features commensurate with a large increase in the yield or flow stress. It may be argued that the fluid precipitates will pin the dislocations during plastic flow, but such an effect should only influence the flow stress after yielding has occurred, the yield stress being independent of any such effect. Another possibility is that the natural deformation may have significantly work hardened the crystal prior to laboratory deformation. The total hydroxyl concentration in these crystals gives weakening temperatures of around 450°C. No large drop in flow stress is found at this temperature although the slope of the flow stress versus temperature curve does change at around 500°C but still at high stresses. Experiments with synthetic quartz show that once the weakening temperature is passed the crystal ceases to work harden (loc cit), and may even show strain softening immediately after yield, to quite large strains. Any hardening effect of deformation below the weakening temperature should then be negated in deformation conducted above this temperature. Figure 6.1 demonstrates this effect. The dislocation densities in quartz of this type are normally about 10^9 to $10^{10} cm^{-2}$ (White, Personal Communication 1976) which are not particularly high. The densities of dislocations responsible for work hardened

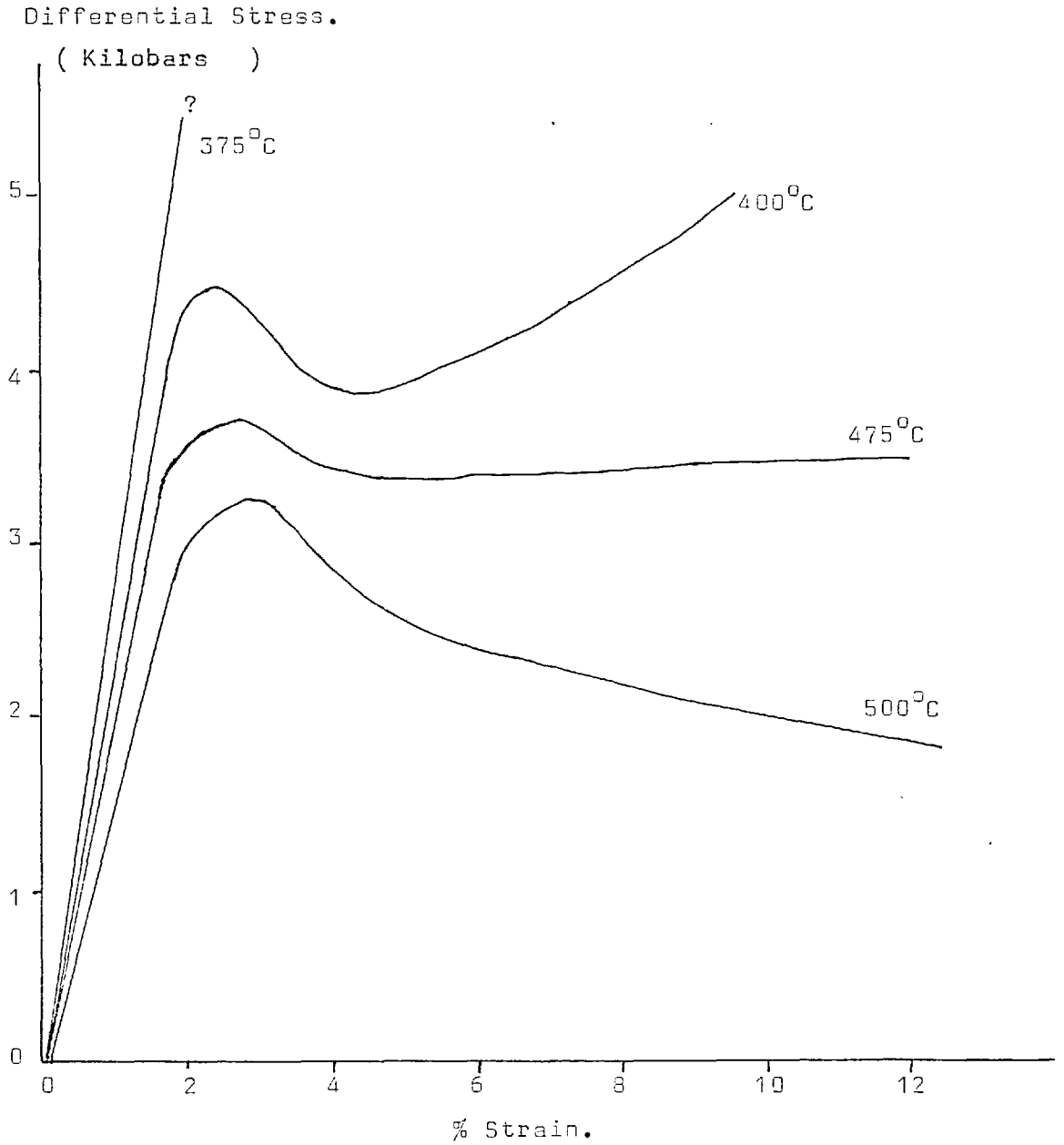

Figure 6.1. Stress/strain curves for crystal AX1 recorded as part of this study using a Heard style deformation apparatus. The specimens were heat treated at the test temperature and confining pressure (1 Kbar.in all cases) for 24 hours prior to loading. The average strain rate was 5 X 10^{-5} sec^{-1}. These four curves clearly show the abrupt change in the shape of the stress strain curves as the narrow range of temperature around the weakening temperature is crossed. In this particular crystal the deformation changes from a strain hardening regime through steady state creep to a strain softening regime in only 50°C

synthetic quartz are very high, $10^{12}cm^{-2}$ (Griggs 1974) so the microstructure of these natural crystals is not commensurate with any significant hardening by previous deformations.

If the dislocation microstructure in these natural quartz crystals is not pinned by the fluid precipitates or condensation of other impurity ions, then the large grown in dislocation density should have the effect of lowering the yield stress, compared with that of natural Brazilian quartz. Further reduction in yield stress should also be expected if the bubbles themselves act as dislocation sources. These two effects may well occur for some mechanical studies on quartzites have shown the material to be weaker than Brazilian quartz, although stronger than synthetic. Figure 6.2 shows line drawings of possible interactions between dislocations and bubbles in the microstructure.

There are several good published papers on the microstructure of natural quartz (White 1971, 1973a,b,c,d,e, 1975a,b) and McLaren 1965, 1966) to name but a few. Recent work by Knipe (1977) has concentrated on both the hardening and softening effects of the micro-fluid inclusions in natural quartz which deformed at low temperatures. It is on this work that the idea of dislocations being pinned by bubbles (figure 6.2) is based. Generally we appear to be in complete agreement on the role of these fluid inclusions in the deformation.

6.3. THE MICROSTRUCTURE OF UNDEFORMED SYNTHETIC QUARTZ

The microstructure of fresh undeformed synthetic quartz shows a very small dislocation density, less than $10^{4}cm^{-2}$ (see Baeta and Ashbee 1970, McLaren *et al* 1971, and this study). Obviously much of the large hydroxyl concentration reported for this material will be found then either as silanol bonds or in complexes with other impurity ions. Only

Figure 6.2. Possible interactions between dislocations and bubbles.

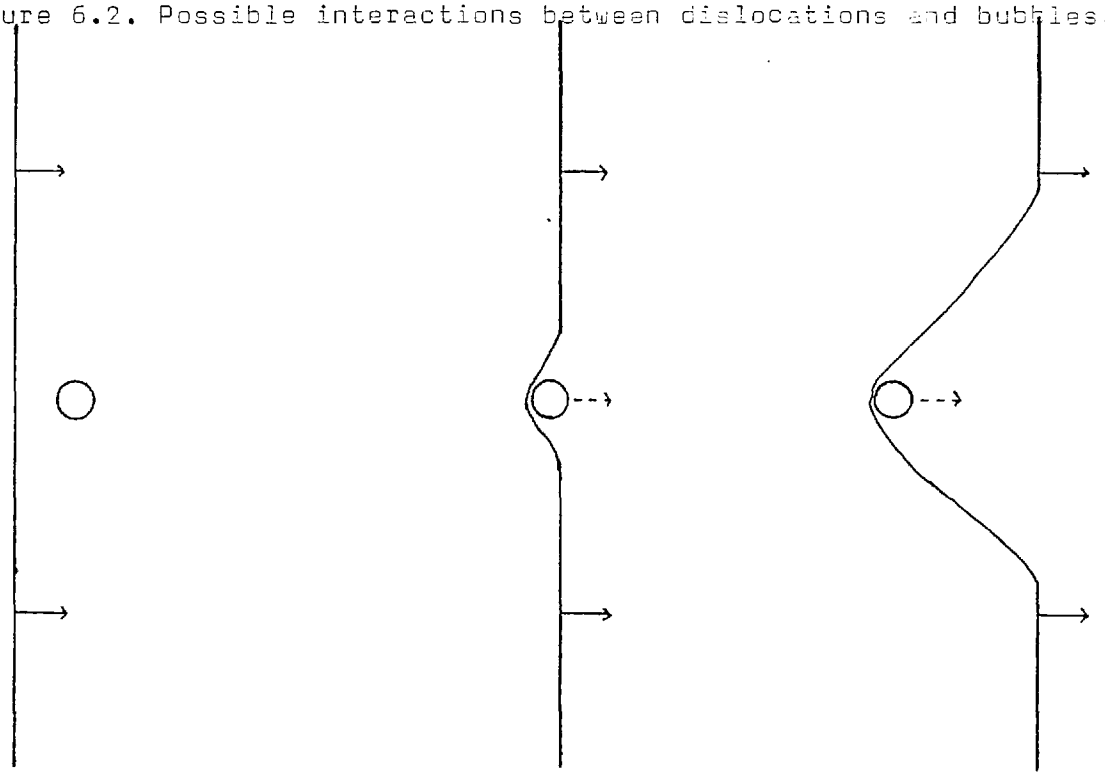

Soft Pinning. The dislocation approaches close to the bubble wall and is slowed by the bubble. The bubble is then pulled by the dislocation. Eventually the whole dislocation line will be slowed and pulled into a curve at which stage the dislocation will either break free from the bubble or become sessile.

Hard Pinning. In this case the bubble is immobile. The dislocation approaches close to the bubble wall and is stopped. The segments on either side of the bubble keep moving and the dislocation line length is increased. Eventually the dislocation will become sessile or will break away from the bubble leaving a sessile loop which will act as a further obstacle to dislocation movement.

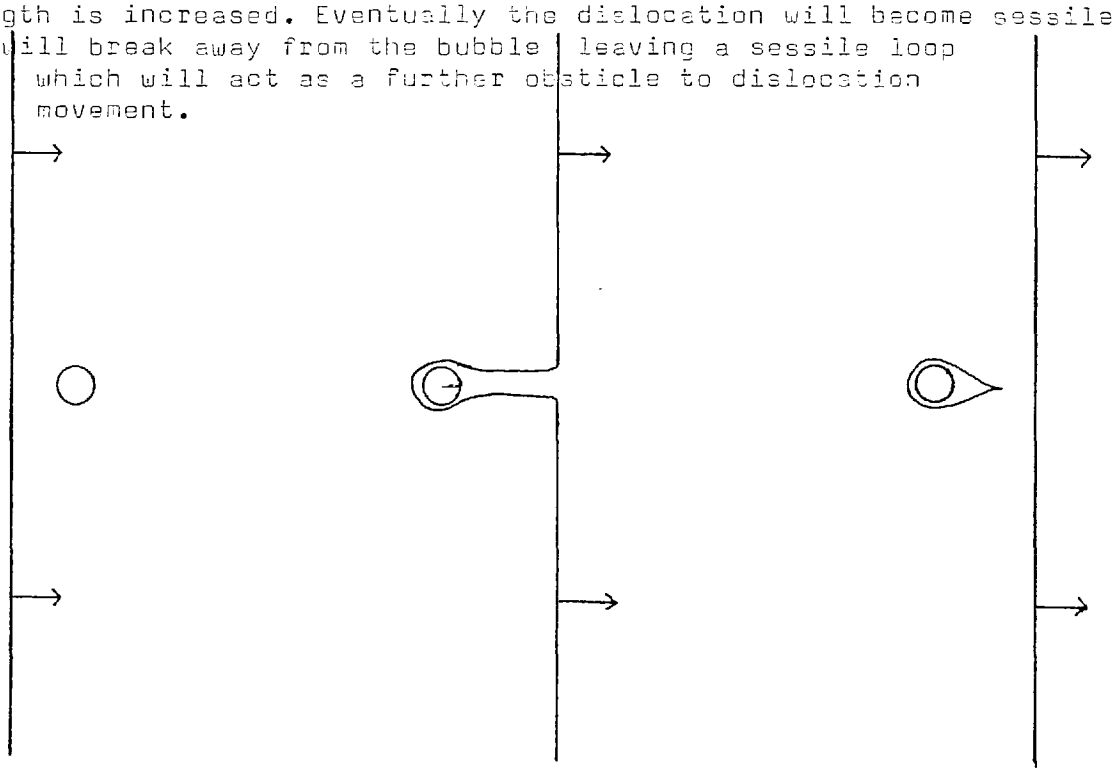

Figure 6.2 contin.

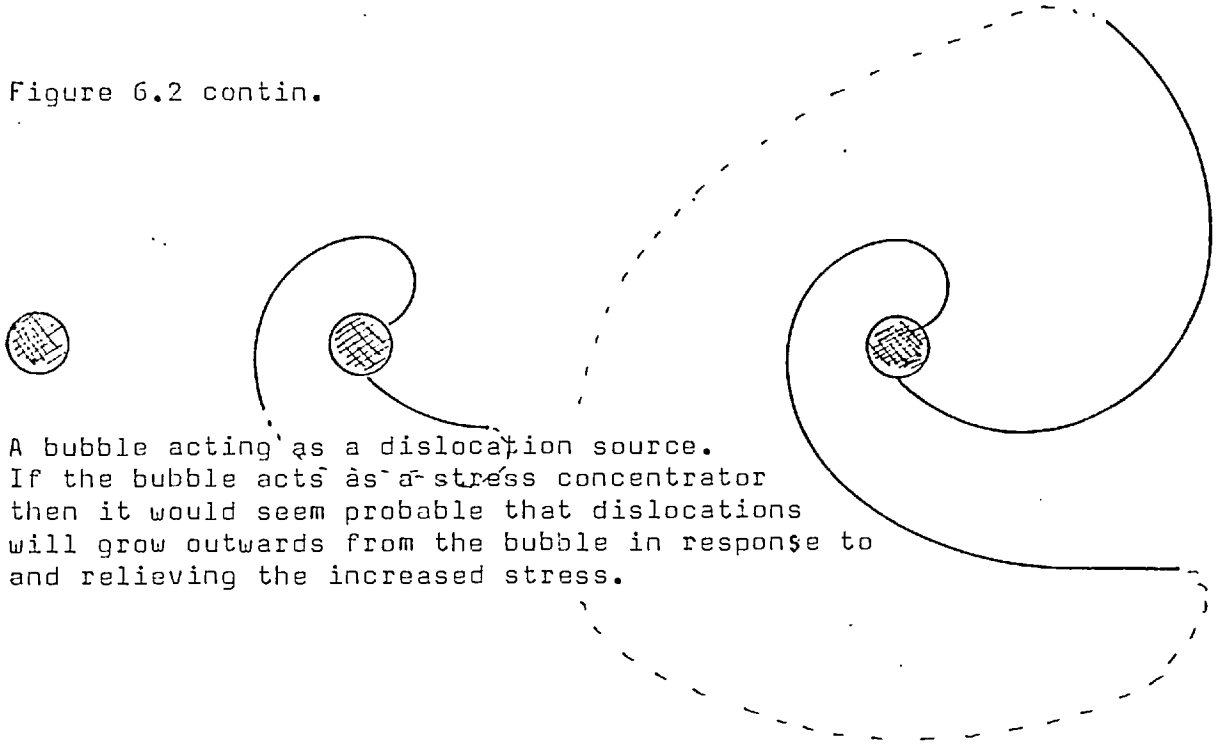

A bubble acting as a dislocation source.
If the bubble acts as a stress concentrator then it would seem probable that dislocations will grow outwards from the bubble in response to and relieving the increased stress.

Bubbles leaking into a dislocation and forming a wall structure. In this example, the dislocation interacts with the bubble wall rather than bending around it. This will enable the fluid in the bubble to diffuse into the dislocation core with comparative ease. The results of this process will be twofold. Firstly the bubble will become smaller (or its internal fluid pressure will be reduced) and may even completely disappear as its contents pass out into the dislocation. Secondly as the dislocation core becomes saturated with impurity ions, the ability for the dislocation to move will become impaired, as the core structure is broken down. It is probable that in many quartz dislocations, the core actually becomes a glass. The dislocation is thus rendered sessile. Other dislocations on the same glide plane will be stopped by this sessile dislocation, and may also be damaged by further impurity ions escaping from the bubble. Thus a stable wall structure is built up containing bubbles which have leaked into the close spaced dislocations.

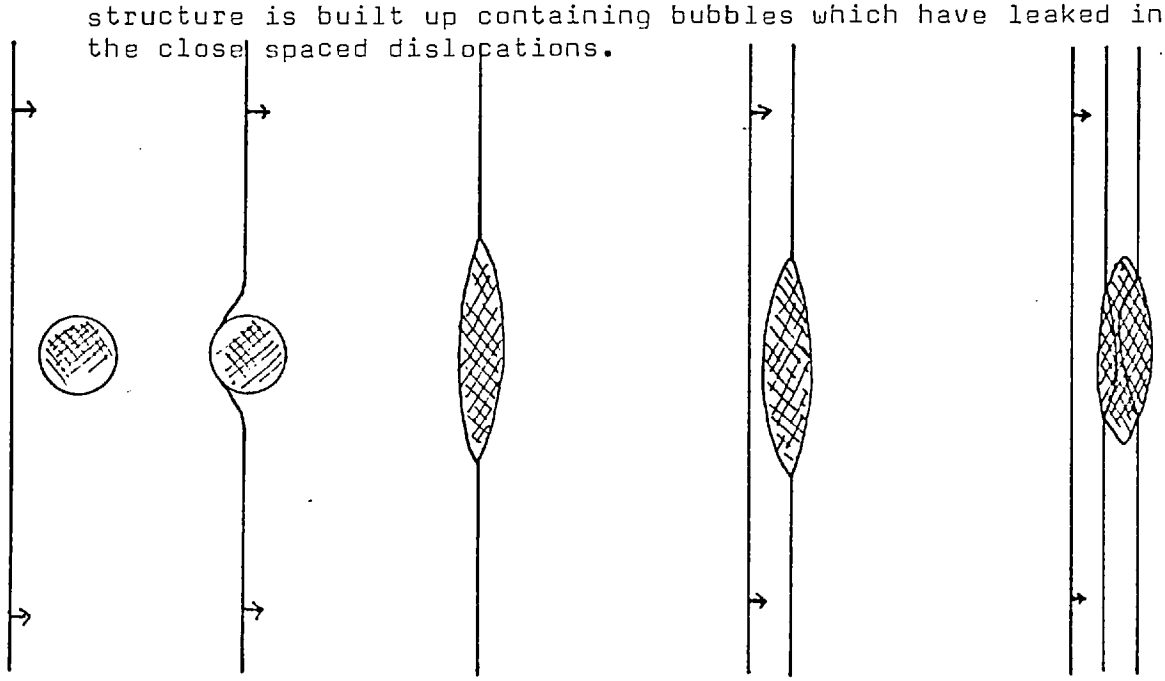

a very small proportion of the water being associated with this grown in microstructure. However the microstructure of these synthetic crystals contains another feature which is not present in the structures of either opalescent or Brazilian type quartz, an impurity phase dispersed through the structure on a very fine scale. This may be very significant.

6.3.1. An Impurity Phase in the Structure of Undeformed Synthetic Quartz

Plate 6.2 shows a series of electron micrographs of the structure of a synthetic quartz crystal which has been neither stressed nor heat tested in any way. These micrographs, clearly show the low dislocation density, and the high density of small impurity particles distributed throughout the structure.

These particles resemble radiation damage in the micrographs but can easily be shown not to be so. Firstly the micrographs were taken in the high voltage microscope using the 10^6 electron volt beam. The microscope had been recently conditioned to eliminate ion beams from the electron gun, so the possibility of beam damage is extremely small. Secondly, the particles were found throughout the thin area of the foil, and were visible as soon as an area of the foil was moved into the beam, radiation damage develops during a finite time of exposure and is never instantaneous. Thirdly it was possible by condensing the beam to a small diameter to produce a small area of damage on the foil, over these particles. If the particles were themselves damage centres they would be seen to grow or coalesce, this was not observed to happen. The damage centres developed between these grains. Thus it is possible to conclude that the microstructure shown in plate 6.2 is not the

superficial effect of beam damage. A micrograph of the damaged area is shown in plate 6.3.

A second possibility was that the particles were a surface effect, possibly related to the carbon coat on the specimen. This again was simply shown not to be so, firstly the effect is noticed in the microstructure of every foil of undeformed synthetic quartz that was studied, but not in foils of any other quartz type. It would certainly be a strange property of the material if it were impossible to carbon coat the surface of the synthetic crystals, in contrast to the natural ones. The second check against this was more positive, samples of the crystal were ion thinned and heated to a high temperature in the microscope (see section 6.3.2) and allowed to cool. As the temperature dropped, wide strain fields developed around the individual particles, showing that not only were they contained within the foil, but that they had very different physical properties to the quartz matrix. This effect is shown by the micrograph in plate 6.4.

Imaging the particles, as against their strain fields, proves to be difficult, except in the beta quartz stability field, requiring a weak beam diffracting condition. (See plate 6.5). Strangely however, finding the correct diffracting condition actually to image the strain fields can also be difficult (this is shown in plate 6.5) and it is perhaps not surprising that previous electron microscope studies on deformed synthetic quartz have often missed them. The studies of Morrison-Smith and Coworkers (published in 1975 and 1976) have commented on this impurity, and have reported some of its mehcanical effects. They report that the images of these particles that they found were not compatible with the images of dislocation loops, bubbles or ion and

electron beam damage, and conclude as I have done that such features are not responsible for the observed contrast. To date, I have failed to obtain a selected area diffraction pattern from these particles, and thus have not been able to identify them. Morrison-Smith et al. appear to have encountered similar problems but suggest that (after consultation with the manufacturers of their crystals) a sodium iron or sodium aluminium impurity with an acmite structure is responsible. I have found no evidence for an acmite structure, the particles being more spherical than platy, and because of the work of Cohen and Hodge (loc cit) and this study which show that Aluminium is often closely associated with sodium and hydrogen, assume that a large proportion of the structure water may be found in these particles. I suggest that the particles are a hydrous sodium aluminium silicate, which may be glassy or only partially crystallized rather than fully crystalline. Such an assumption, is compatible with their shape and the difficulty of obtaining a diffraction pattern showing any reflections which are not from the quartz structure.

The distribution of these particles within the structures is of interest, Morrison-Smith et al. report that they are either present in densities of the order of $10^{12}cm^{-3}$ to $10^{14}cm^{-3}$ or they are absent, with little or no gradation between these extremes. I suspect that this is not so, my observations being compatible with the idea that the density varies in direct proportion with the observed hydroxyl concentration. I record an upper limit of $10^{15}cm^{-3}$ (but I, like Morrison-Smith, have not allowed for overlap in the counting. As I worked at 1000 KEV and Morrison-Smith worked at 200 KEV, it is probable that the incidence of overlap in my micrographs is higher, accounting for my higher concentration), but I find a steep but obvious gradation from these high values

to low densities (often too small to count easily). The low density areas appeared to correspond to the dry areas of the crystal. Plate 6.6 shows a typical example of this. The foil was taken across the boundary of the Small Prism region (= large OH^- conc) and the Z-growth (= small OH^- conc) growth regions of crystal ITT4. Across the foil I found the linear feature where the high density of particles suddenly drops to the very small (but non-the-less real density shown in the micrograph). (The change in contrast is probably due to twinning). Other features seen in foils taken from entirely within the small prism region of this crystal appear to be commensurate with growth bands. Because of the difficulties of relating the small scale of the electron micrograph to the infrared absorption data (which is taken on a macroscopic scale), it is difficult to make such observations with confidence. However, two alternative lines of reasoning are available to support this supposition.

Firstly it has been shown by Dodd and Fraser (1967) and to a lesser extent in this study, that the density of bubbles of molecular water precipitated during heat treatment of synthetic quartz crystals can be used to reveal variations in the hydroxyl concentration on a fine scale within the structure, and this density would thus appear to be proportional to the hydroxyl concentration. Dodd and Fraser (1967) obtained exact correlation between their Infrared topographs taken at 3500 cm^{-1}, contrast in shileren photographs and the intensity of the light scattered by the microfluid inclusions produced by heat treatment. In chapter 5 of this thesis, I have shown that the bubbles of precipitated water nucleate on the strain fields associated with the particles in the synthetic quartz structures, and that when such

strain fields are absent, no bubbles grow. Knowing that the density of the particles acting as bubble nuclei varies greatly throughout the structure of any given synthetic crystals and between crystals, it would seem reasonable to suppose that the variation in particle density correlates with the variation in hydroxyl concentration. If this were not the case, precipitation of molecular water would not invariably reveal the true distribution of hydroxyl in the structure, which it does in all cases tested at present.

The second line of reasoning is, that if the distribution of water in the quartz structure follows the distribution of the other major impurities (as it has been shown to do), then the density of the particles containing the major impurities must vary in direct proportion to the measured hydroxyl concentration, assuming a uniform particle size, which appears to be the case in synthetic quartz. It is probable that the distribution of these particles is responsible for creating the contrast in the schileren photographs taken by Dodd and Fraser (1967).

If, within individual crystals, the density distribution of the impurity particles is identical to the variations in hydroxyl concentrations then presumably this can be taken a stage further, and we may suppose that those crystals shown to be relatively 'wet' by infrared spectroscopy will have relatively high densities of impurity particles. Likewise, those crystals shown to be relatively dry, will show small densities of these particles.

Thus in conclusion to this section, it can be shown that synthetic quartz has an impurity phase which varies in direct proportion to the hydroxyl concentration, as measured by infrared spectroscopy, and that this phase, being present as distinct impurity grains of a crystalline or glassy nature, may well affect the mechanical properties, which have

hitherto been related solely to the hydroxyl concentration by the infrared absorption. The mechanical effects of particles in two phase materials, and the mechanical effects of these particles on synthetic quartz will be discussed in a later section.

6.3.2. Insitu Heating Experiments

In an attempt to make accurate kinetic measurements on the growth of micro-fluid inclusions in the synthetic quartz structure, I set up (jointly with S. White) an insitu heating experiment in the 1000 KeV microscope. The object of this experiment was to heat up the quartz foil in a stepwise fashion to temperatures in the range 600 to 700°C and observe directly any interesting changes that may have occurred in the microstructure, particularly the growth of the microfluid inclusions. Following the successful result of this preliminary test, a series of more quantitative experiments were conducted.

The apparatus used in these experiments was a single tilt heating stage in which the foil was held between thin perforated platinium ribbons which were lightly tensed to prevent the foil from moving within the microscope. Power was supplied to this via a variable resistor and a digital ammeter (on the microscope control consol) from a 12 volt wet cell accumulator. The temperature was estimated from the current passed by the stage (measured on the ammeter), and could be varied by changing the resistance of the circuit with the variable resistor. The temperature/current calibration curves for this stage were constructed from observations of metals and alloys which underwent distinct structural changes at accurately known temperatures. As these calibration reactions were confined to metals, it was necessary to check this calibration for the non-metal quartz (which has a very different thermal conductivity to most metals). Fortunately the alpha/beta quartz phase

change at 573°C is very distinctive (see Tendeloo et al. 1975, 1976) and provides a check on the calibration during every experiment. In all but two cases, agreement between the temperature and the calibration curve was very good. In both of these exceptions, the platinium foil had recrystallized, and apparently reacted with some metal studied in it by some previous user, changing its resistance. For further details of this technique, the sample preparation procedure and suggestions for its application to other mineralogical reactions, see appendix 1.

It was whilst setting up the first of these experiments that the impurity phase was first recognized, and it was during this experiment that it became obvious that the size of some of the particles increased whilst the overall density decreased. Plate 6.7 is a series of micrographs which show this change in size and density as the temperature is increased.

In this first experiment, certain of the impurity grains grew very rapidly in the beta quartz field. These large grains lie along distinct lines in the foil, but are not linked by any resolvable feature. This may be a problem of diffraction conditions, the heating stage has only a single tilt, so that certain dislocations out of contrast would not be resolvable. It may be however that the particles do not lie along a dislocation but are concentrated along some small step like feature on the surface of the foil. The only objection to the latter being that the particles are not elongated along the step as might be expected. Plate 6.8 is particularly interesting, this shows a broad band of quartz on either side of the line of large particles which has been completely cleared of the small diameter impurity grains. More detailed studies of this phenomenon may provide very useful data on volume diffusion in quartz.

Plate 6.9 shows a number of micrographs taken as the foil passed through the α/β phase transition. On heating, the quartz twins repeatedly just below the inversion temperature (plate 6.9a and b) and then with the structural change, these twins vanish leaving a clear foil with few bend or thickness contours (plate 6.9c). On cooling the rather featureless image of beta quartz is preserved until the alpha phase field is entered, then the foil is again seen to twin repeatedly with the reappearance of bend and thickness contours (plate 6.9d). These cooling twins are preserved in the specimen on cooling to room temperature (plate 6.9a). During cooling, very large strains can be imaged in the quartz structure around the impurity particles (plate 6.10a). It is perhaps important to note that even the very large particles produced by diffusion of impurities in the beta quartz field develop these strains suggesting that they are within the foil, not on its surface, and hence associated with an out of contrast dislocation. (Plate 6.10b). Assuming this to be the case, dislocations in the quartz structure show a very strong affinity for impurity ions clearing areas of several microns diameter around their core. Although the experiment did not allow quantitative measurement of the rate of diffusion of the various impurity ions across this region, it must be concluded that the diffusivity of these ions is very great, the clear area taking only minutes to form. Equally however the potential driving this diffusion falls off rapidly with increasing distance from the dislocation core (assuming that it is a dislocation which provides the potential). Thus the clear band shown in plate 6.8 develops rapidly and quickly reaches a finite diameter after which further growth is either very slow or has stopped.

Following these preliminary qualitative experiments, I conducted a series of experiments in which the sample was held at constant temperature for comparatively long periods of time. The results of these tests show that the density of impurity grains decreases exponentially with increasing time producing a negative straight line on a natural log density versus linear time plot. Examples of these plots are given in figure 6.3 for experiments at 400°C, 600°C and 850°C. In these plots the curves for density recorded at 10000 and 25000 diameters magnification is given (the 850°C plot also gives a third curve for an area of abnormally high initial impurity grain density). It is unfortunate that as a result of the need to use diffraction contrast imaging together with the absence of any suitable microanalysis technique on the 1000 KEV microscope, that these data are plots of density versus time, and not grain diameter or composition versus time. It is thus difficult to calculate any of the parameters of this diffusion process without having to make assumptions as to the change in volume or composition of the individual grains. However a simple relationship of the Arrhenius type does exist between the slope of these change in density versus time curves and the temperature of the experiment. The physical interpretation of this relationship is not in any way apparent and because of this, I have omitted to plot the data in this way.

These insitu kinetic heating experiments thus show that not only does the density of these impurity grains show a distribution similar to that of the structure bound water in the sample but also that this density changes when the sample is heated in a manner similar to that recorded for the hydroxyl concentration. I have shown that these particles create lattice strains which act as nuclei for bubbles of precipitated molecular water, so the possibility that much of the structure bound

Figure 6.3. Variation of particle density at 400°C with time.

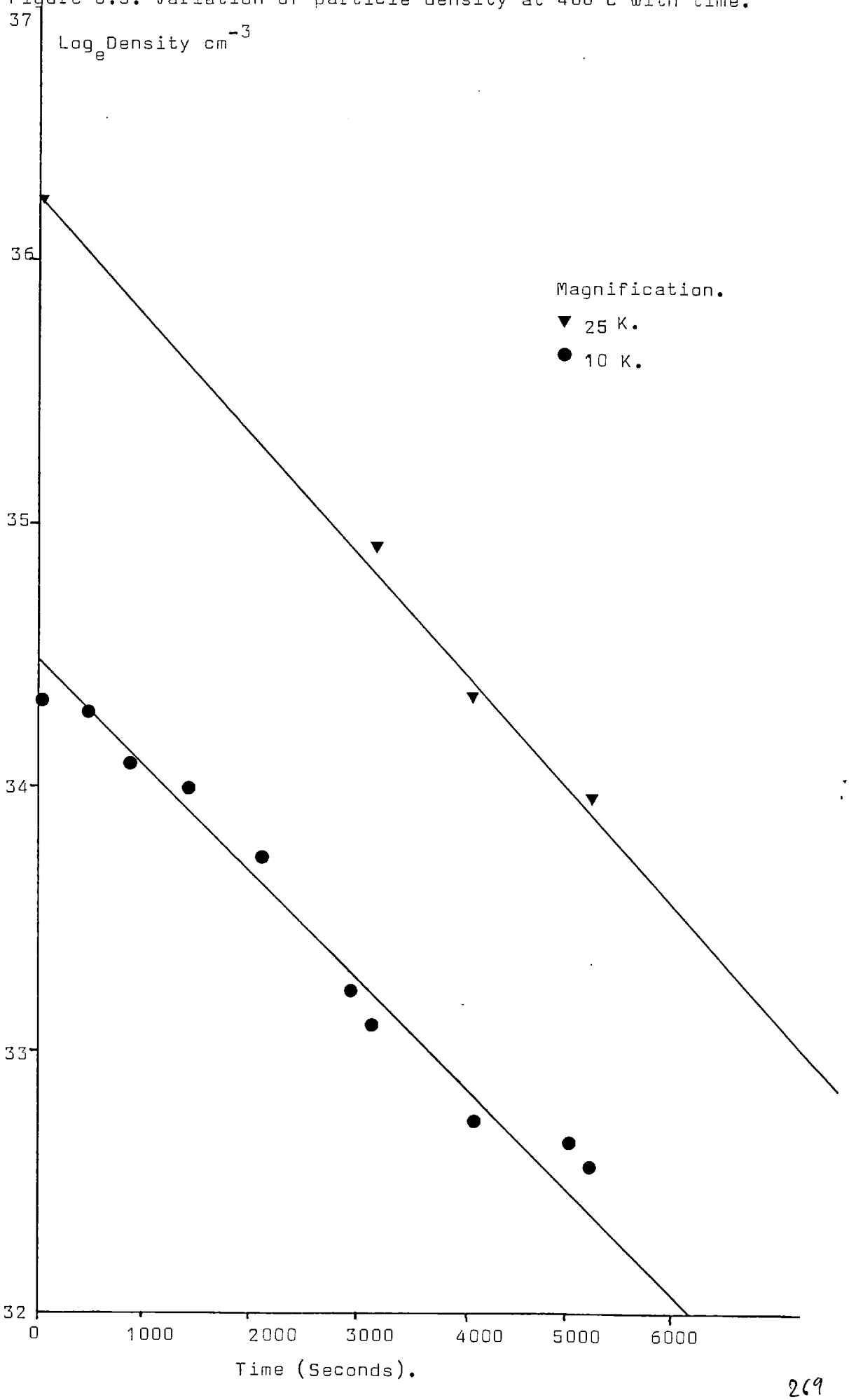

Figure 6.3 contin. Variation of particle density at 600°C with time.

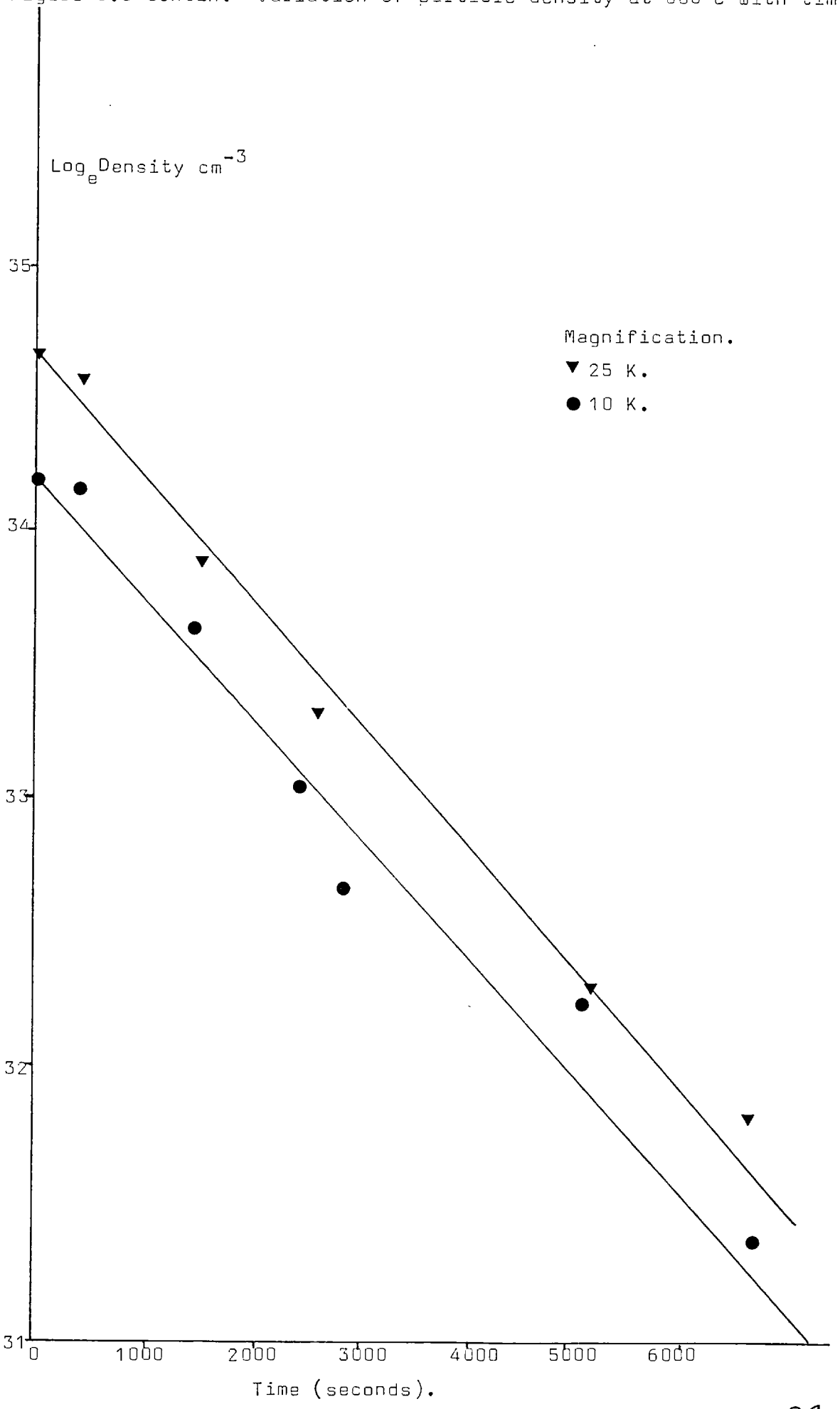

Figure 6.3. contin.
Variation of particle density at 850°C with time.

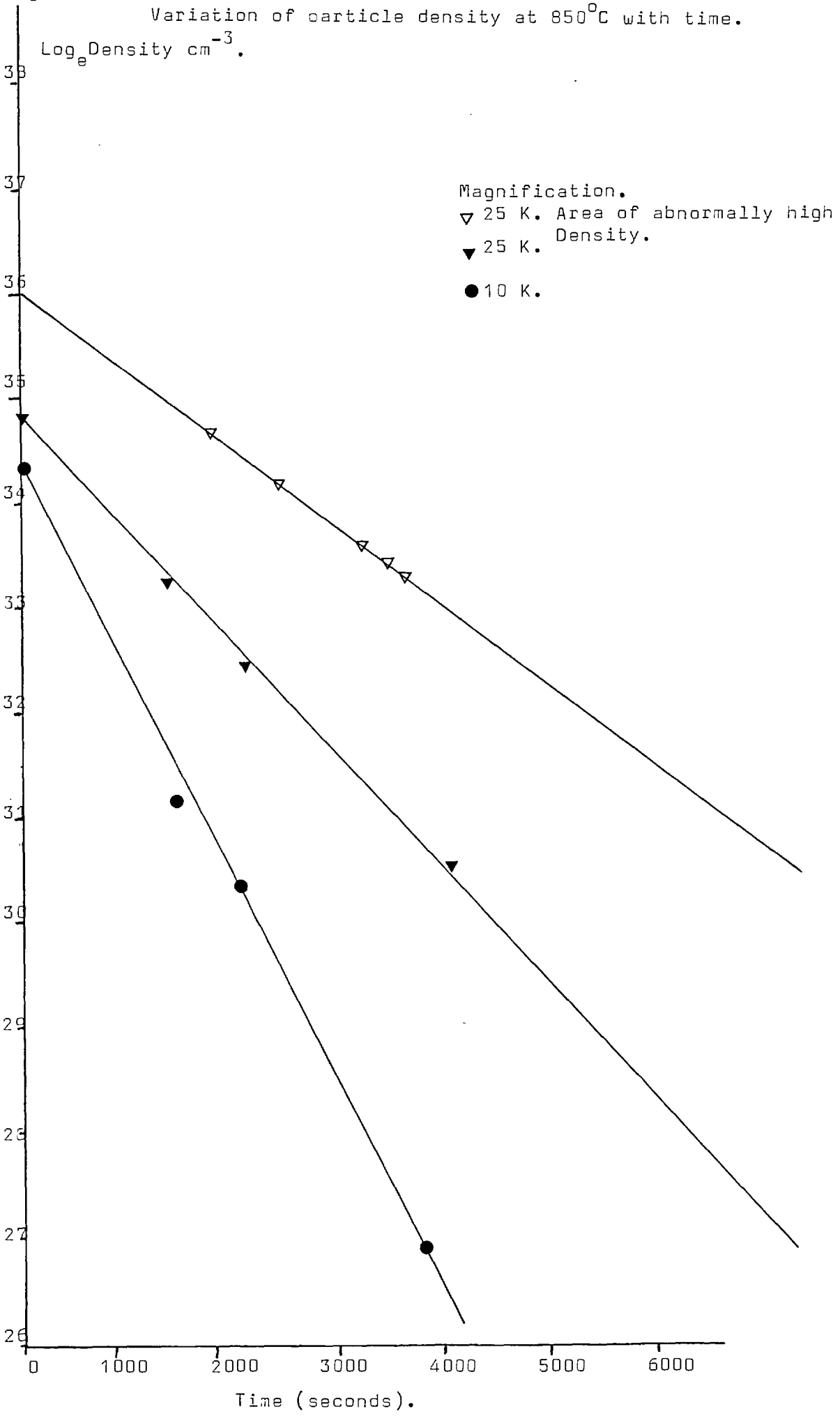

water in synthetic quartz crystals is bound up in this impurity phase and not in the quartz structure cannot be ignored.

In an attempt to cause some of these impurity grains to grow to a large size so that a selected area diffraction pattern can be recorded from them, I set up a long term laboratory heating experiment. In this a sample cut from synthetic quartz crystal ITT4 was heated in a furnace for two months at 850°C. On cooling the sample was found to be strongly milky due to bubbles of precipitated water. A specimen was cut from the small prism growth region which showed the most intense milkyness and this was thinned in the ion beam thinning machine for electron microscopy in the normal way. However when this foil was examined, it was found to show no trace of the impurity grains, only large bubbles showing a fairly typical density. (See plate 6.11). Close examination of the micrographs from this foil revealed that the majority of the bubbles contained a small solid precipitate. This may be quartz precipiated from solution in the bubble as the sample cooled (but if this is the case why didn't it precipitate on the bubble wall) or it may be the remains of the impurity phase which either coalesced and was then engulfed by the growing bubble or dissolved in the bubble and was precipitated on cooling, which ever of these alternatives proves correct, it was impossible to record a selected area diffraction pattern from the material.

A second interesting result of this long term experiment (which was also noticed in other heating tests) is that the specimen shows an obviously increased dislocation density when it is cooled. This is particularly interesting, suggesting the apparent ease with which these thermal dislocations nucleate to relieve the thermal strains. The production of these extra dislocations may be analogous to very slow

strain rate deformation of the natural type. Thus it may well be possible to exchange the high temperatures of these heating tests with lower temperatures and small applied stresses at very slow ($10^{-14}sec^{-1}$?) strain rates to produce a similar microstructure. It is interesting to note that the microstructure of the synthetic quartz used in this long term heating test is far more akin to that recorded from much naturally deformed low grade quartz than that developed in synthetic crystals deformed in compression at fast strain rates below the recorded weakening temperature for the grain. Normally however the natural quartz shows somewhat higher dislocation densities than those reported here but this is to be expected because of the larger strains being accommodated by the natural material.

6.4. THE MECHANICAL EFFECTS OF THE IMPURITIES

In the first part of this section I shall briefly review the mechanical effects of a second, impurity phase in a crystaline solid, as widely discussed and understood by metallurgists interested in the properties of alloys. At the present state of knowlege, any discussion about the actual mechanical effects of the impurity in synthetic quartz are speculative and because of this I shall not discuss the theory in great detail. In the second part of this section I shall discuss what data is available on the mechanical effects of this impurity. I will leave the formulation of a model combining the theory with the observed effects to the final concluding chapter (Chapter 7), in which I shall try to outline my ideas on the relative roles of structural water, bubbles and this impurity phase in the plastic deformation of quartz single crystals.

6.4.1. The Mechanical Effects of an Impurity Phase in a Crystalline Material

The role of an impurity phase in the deformation of a crystalline solid may be simply subdivided into weakening and strengthening mechanisms. I shall deal with these separately. Much of the discussion in these sections can be found in most standard textbooks of metallurgy. In this work I have found Honeycombe (the Plastic Deformation of Metals), and Smallman (Modern Physical Metallurgy), particularly useful as a starting point.

6.4.1.a. Weakening Mechanisms

If a strain field exists or is introduced into the crystalline matrix around an impurity particle, then this can become a source of dislocations. The methods by which such a source will operate is a combination of two complementary effects. Firstly if a strain field already exists around the particle, and the matrix is subjected to a further stress, the two will be additive in certain directions and may locally become great enough to cause the nucleation of dislocations. These will slow and possibly become stationary at some distance from the particle because of the decreasing stress field, but as more dislocations nucleate, the area of matrix subjected to high strains will increase and eventually the dislocations will break away from the particle. The particle then acts as a source. Secondly, even if no strain exists in the matrix around the particle, differences in the elastic properties of the particle and its matrix will lead to a local intensification of lattice strains in the matrix resulting from an externally applied stress. This can also lead to the nucleation of dislocations if the intensification is great enough. Honeycombe (1968, p194) shows a typical example of dislocations nucleating around large

particles of niobium carbide in an austenitic steel. The nucleation was caused by thermal stresses introduced during quenching.

Although the presence of an array of impurity grains in a crystal matrix may result in the softening of the matrix, by the nucleation of dislocations, this effect is secondary to the hardening effects of the complete array in most metal systems studied. This is because the array viewed as a whole drastically reduces the mean free path through which the dislocations nucleating on individual impurity grains can move.

6.4.1.b. Mechanisms of Hardening

The mechanisms of particle (or precipitate) hardening are well understood for many metal alloys and a number of different theories are available to explain the observed mechanical properties. In this section I shall summarize the discussions of hardening mechanisms presented in Honeycombe (1968, p178) and Smallman (1970, p405) with an emphasis on those mechanisms of possible importance in quartz deformation.

When a finely dispersed impurity phase is present in a crystalline matrix, an additional barrier to the movement of dislocations through the matrix is created. The impurity particles will lie across the slip planes, along which the dislocations move, so that the dislocations must act in one of two ways:

(1) Cut through the impurity;

(2) Take a path around the obstacle.

The former mechanism tends to apply in the case of finely dispersed coherent particles whilst the latter applies to coarser grained particles.

The first theoretical attempt to describe these interactions was that of Mott and Nabarro (1948) which considered an alloy containing spherical solute (or groups of solute), atoms. Applied to solid solutions, this theory defines the atomic radius of the solvent

atom as Rs and the atomic radius of the solute atom as Rs(1+θ) where θ is the misfit parameter defined as $\theta = \frac{1}{a}\frac{da}{dc}$ where a is the lattice parameter and c the atomic concentration of the solute. This concept can also be applied to groups of solute atoms such as occur in G.P. zones in precipitation hardened alloys. The elastic strain between a group of solute atoms and the matrix has an average spacing Δ which is the wavelength of the internal stress field (see figure 6.4). The shear strain ε in the internal stress field at a distance L from the center of a spherical particle of radius r_o when $L \geq r_o$ is given by:-

$$\varepsilon = \frac{\theta r_o^3}{L^3} \qquad 6.1$$

then defining L as $\frac{1}{2}\Delta$, a mean shear strain ε_m can be calculated. Defining L in terms of N, the number of particles per unit volume gives:-

$$L = \tfrac{1}{2}N^{-1/3} \qquad 6.2$$

which gives the mean shear strain as:-

$$\varepsilon_m = (\theta r_o^3)(2N^{1/3})^3 = 8\theta r_o^3 N \qquad 6.3$$

The concentration of solute C_o is given as:-

$$C_o = \frac{4}{3}\pi r_o^3 N \qquad 6.4$$

so that the critical shear stress of the alloy is defined in terms of mean elastic strain as follows.

Figure 6.4.

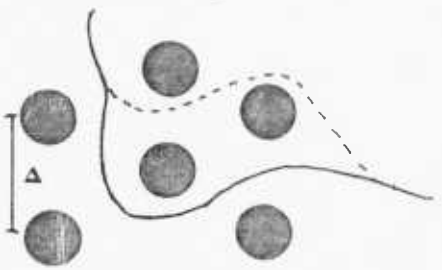

A Slip plane (plan).

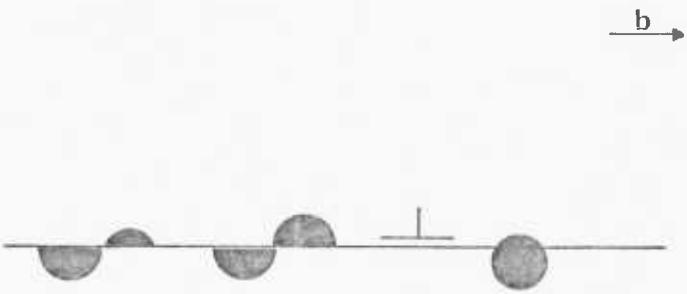

B Slip plane (edge-on)

The interaction of a dislocation line with impurity particles or precipitates in an alloy. A) Plan view. B) Edge-on to the slip plane.

From the Mott and Nabarro theory for aged alloys, based on the diagram in Honeycombe (1968,p179).

$$\tau_o = \varepsilon_m G \qquad 6.5$$

$$= 8G\theta r_o^3 N \simeq 2G\theta C_o \qquad 6.6$$

This expression is independent of the yield stress, this is not compatible with the experimental results on metals which have shown that for incoherent particles the yield stress is inversely related to the particle spacing.

This problem can be overcome if the dislocation line is assumed to be flexible and move locally in a manner independent of the line as a whole. This movement would then be dependent on the spacing between the centres, which is the wavelength Δ. Because a dislocation line always tends to lower its energy by shortening itself, the concept of a line tension T, analogous to the surface tension of a fluid has to be introduced. Mott and Nabarro (1948) have shown that

$$T \simeq Gb^3 \qquad 6.7$$

so that a curved dislocation is only in equilibrium if acted on by a stress. In the following analysis, assume that this stress needed to maintain a dislocation curvature of radius r is τ_o.

Consider a small arc δS of dislocation strength b (figure 6.5). The angle subtended by the arc at the center of curvature, O, is $\delta\phi = \delta S/r$. There is an actual force along OA due to the applied stress equal to τ_o b δS and an opposing inward force due to the line tension and given by

$$2T \sin \frac{\delta\phi}{2} \simeq TS\phi \qquad 6.8$$

at equilibrium

Figure 6.5. The limiting radius of a dislocation line.

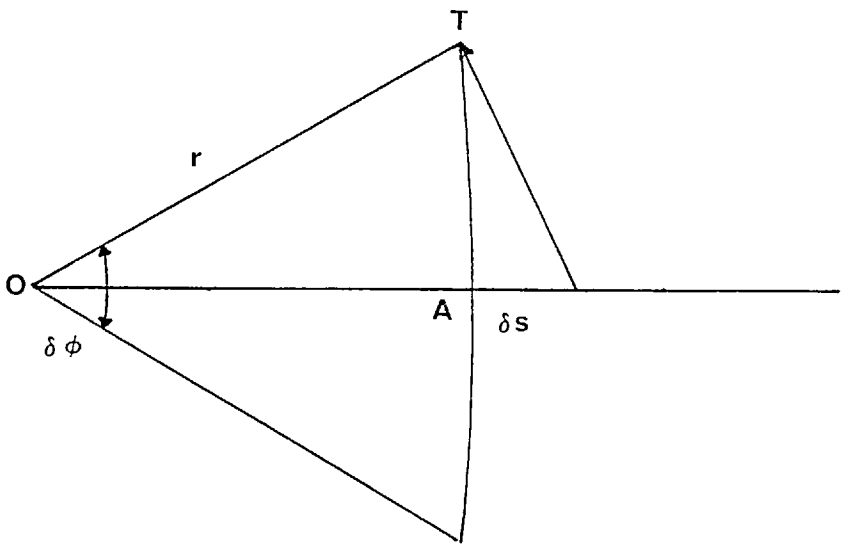

Figure 6.6. Interaction of a dislocation with particles. (After Orowan 1948).

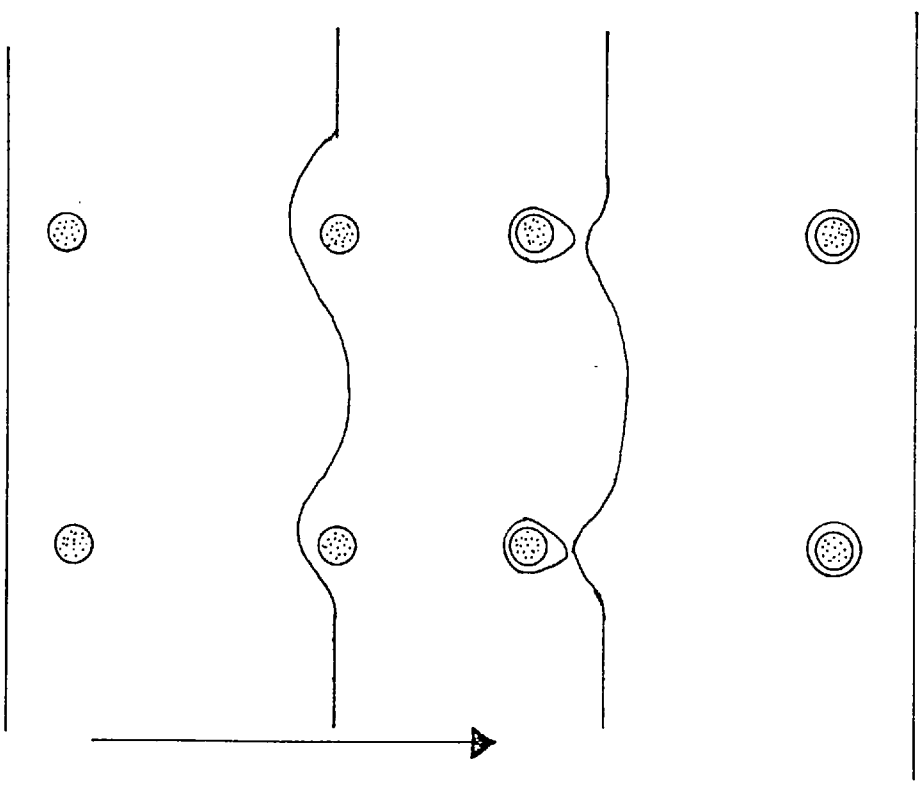

$$T\delta\phi = \tau_o b\, \delta S \qquad 6.9$$

so that

$$\tau_o = \frac{T\delta\phi}{b\delta S} = \frac{T}{br} = \frac{G\,b}{r} \qquad 6.10$$

Thus the radius of curvature is inversely proportional to the applied stress. In solid solutions $r \gtrsim \Delta$, but there are two other cases of importance for impurity dispersions.

(1) The case $r = \Delta$. This applies to the condition when a high stress is needed to force the dislocation loops between closely spaced impurity particles, e.g. G.P. zones in Al-Cu alloys.

For this case Mott and Nabarro (loc cit) have shown that the critical stress needed to force a loop to move was defined by equation 6.6. Now:-

$$\Delta = \frac{\alpha G b}{\tau_o} \qquad 6.11$$

So that the optimum dispersion size Δc is obtained by substituting

$$\Delta c = \frac{\alpha b}{2\theta} C_o \qquad 6.12$$

Which for G.P. zones in Cu-Al alloys gives spacings of 50-100Å and high yield stresses ($\sim 10^{-2} G$). Thus yielding will probably occur by dislocations shearing the particles rather than bending around them

(2) $r \lesssim \Delta$. This will correspond to the over aged condition in an alloy. The particles are further apart and the dislocation will find it easier to bend around them. This yield stress will then be lower, being that required to bend the dislocation line into loops of radius $\frac{1}{2}\Delta$ and thus:-

$$\tau_o = \frac{2\alpha Gb}{\Delta} \qquad 6.13$$

This situation is that of the Orowan model (Orowan 1948) (see figure 6.6) in which the particles are bypassed by the dislocations leaving residue dislocation loops around each particle. A simplified form of the flow stress given by this model is

$$\tau_o = \tau_s + \frac{T}{6\Delta/2} \qquad 6.14$$

where τ_s is the critical resolved shear stress and T the line tension of the dislocation.

The yield stress thus varies inversely as the spacing between the impurity particles and the material softens as the spacing between the particles increases. The relationship can only be properly applied to systems in which no coherency strain occurs between the particles and the matrix, i.e. systems in which no attempt is made to preserve lattice continuity. Consideration of the interaction of dislocations with coherent particles will probably not apply to the case of synthetic quartz where the micrographs of Morrison-Smith (1976) strongly suggest a large degree of incoherency between the particles and the matrix.

For incoherent particles, the Orowan model is taken a stage further by Fisher et al (1953). They emphasize the importance of the dislocation loops and each of the particles as each dislocation line bows around them. These dislocation loops exert stresses on the particles which are opposed by them. Likewise the stresses on the loops oppose further slip on the plane by acting as a back pressure on the dislocation sources. The result of this is an extremely rapid rate of work hardening at an early stage in the deformation. This is seen in overaged Cu-Al alloys.

The shear stress due to the loops is approximately

$$\frac{N G b}{r} \qquad 6.15$$

where N is the number of loops about each particle of radius r. The increment in flow stress τ_p due to work hardening resulting from the loops was found to be

$$\tau_p = a f^{3/2} \qquad 6.16$$

where $f = (r/\frac{1}{2}\Delta)^2$ = the volume fraction of precipitate when Δ = the particle spacing and a is a constant.

Thus the rate of work hardening increases both with increasing fineness of the dispersion and as the volume fraction of the impurity phase increases.

Ansell and Lenel (1960) have also looked at the Orowan model and came to the conclusion that appreciable plastic flow will only occur when the particles are fractured as a result of the stress concentration caused by dislocations piling up against them. These pile-ups must be in the form of multiple loops or rings of dislocations around the particles. The theory gives a relationship for the flow stress τ_o in terms of the volume fraction of the precipitate f.

$$\tau_o = \tau_s + \frac{G'}{4a}\left(\frac{f^{1/3}}{0.82-f^{1/3}}\right) \qquad 6.17$$

where τ_s is the yield stress of the particle free matrix, a is a constant and G' is the shear modulus of the particles. This theory however raises a number of problems, notably that it assumes that no plastic flow occurs prior to the fracture of the particles, which is demonstrably not the case in a number of systems.

6.4.2. Observations of the Mechanical Effects of Impurity Particles in Synthetic Quartz

Plate 6.12 shows a series of electron micrographs of an abnormally dense cluster of impurity particles in the structure of crystal ITT 4. These micrographs, which have been recorded with increasing temperature, show that as the temperature is increased dislocation loops nucleate on the particles. Dislocations appear at the lowest temperatures in those regions of the crystal with the highest density of impurity particles and at higher temperatures in areas of progressively lower particle density. If the spectroscopic data can be extrapolated down to this scale it could thus be interpreted that the dislocations nucleated at the lowest temperatures in those regions with the highest water concentration. Certainly in this case the role of the water is either complimentary to that of the impurity phase or is superfluous, the relationship being only apparent from the similar distributions of water and solid impurity particles. Thus those regions of the crystal showing the largest impurity particle density will be the first areas to generate dislocation loops as the temperature of a stressed crystal is increased and as the densities of dislocations in these regions become high, the first areas to show considerable work hardening. The actual dislocations nucleated in plate 6.12 are caused as a result of thermal stresses in the sample undergoing heat treatment.

Morrison-Smith et al (1976) found that these particles are responsible for the nucleation of dislocations at the onset of plastic deformation, and has recorded a sequence of micrographs showing the nucleation of dislocation loops, and the subsequent locking of these loops in dense tangles around the particles as the strain increases. Figure 6.7 is a series of line drawings based on these micrographs showing

Figure 6.7.

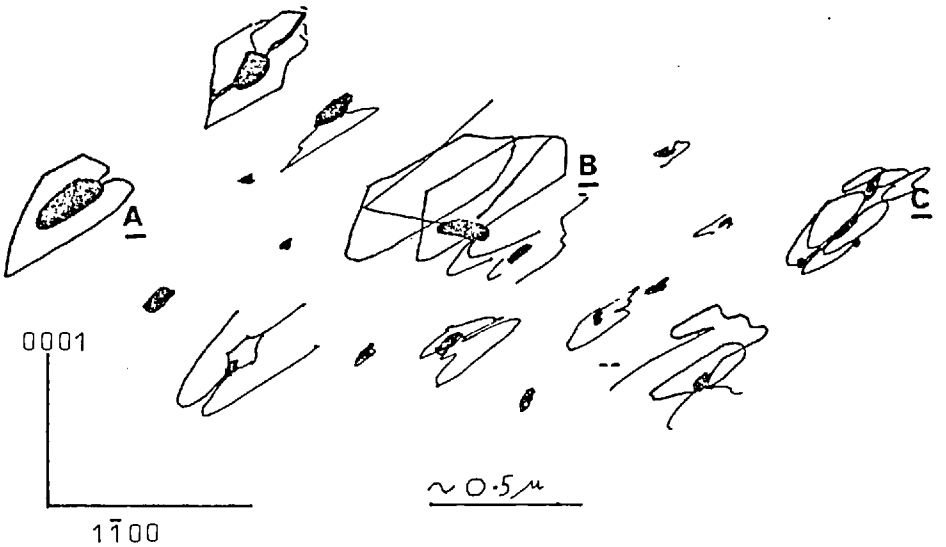

The three types of dislocation source identified by Morrison-Smith et al (1976) for dislocations nucleating on impurity particles in synthetic quartz. Type A are the simplest but like type B are less common than the more complex type C.

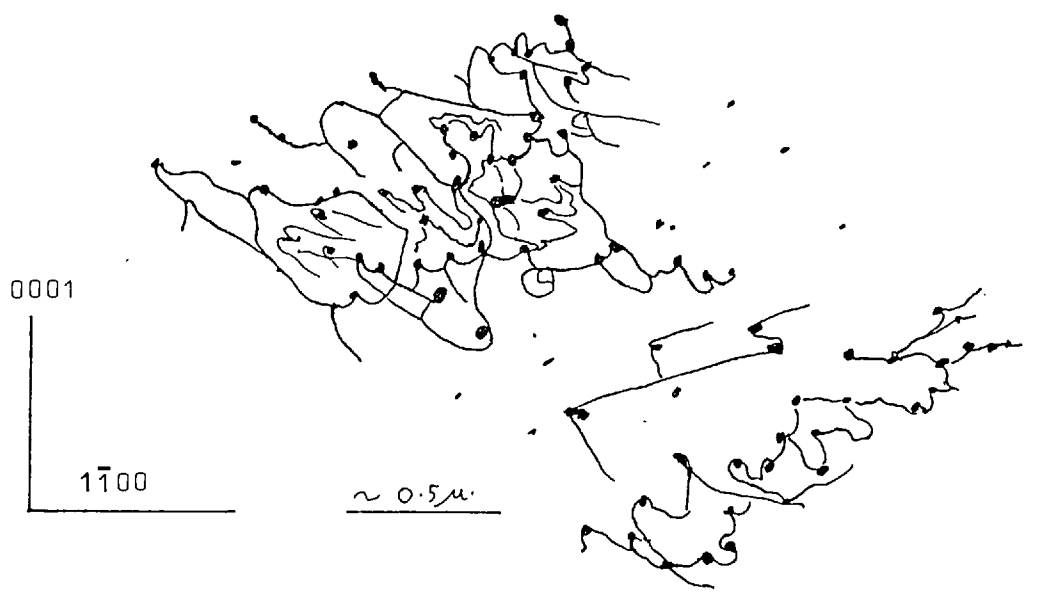

Typical particle/dislocation reactions occuring in the strain hardening regime of a synthetic quartz crystal being deformed below the hydrolytic weakening temperature. Based on a micro-graph by Morrison-Smith et al (1976).

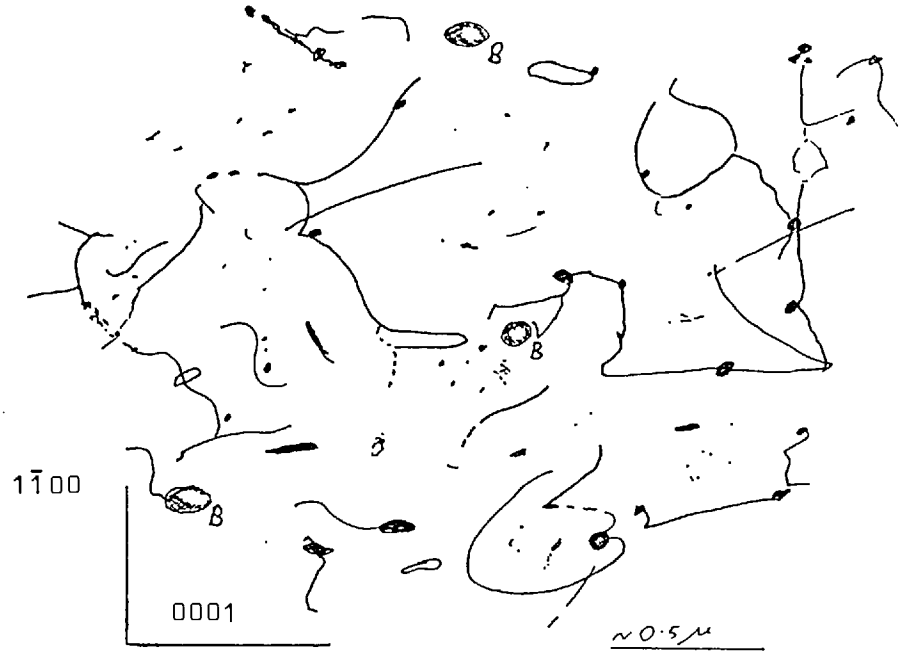

Figure 6.7 contin.

This is a sketch of the microstructure typical of a synthetic quartz crystal deformed above its weakening temperature. The dislocation density is reduced, interactions between the dislocations and the impurity particles are far less obvious, dislocation debris occurs and bubbles of molecular water have appeared (marked B).

The three sketches in this figure are based on electron micrographs recorded from specimens deformed 0.3% at 475°C, 2% at 550°C.and 4% at 900°C. respectively. These sketches and the micrographs on which they are based clearly show the importance of the impurity phase in controlling the deformation behaviour of synthetic quartz crystals at temperatures below the weakening temperature.

the effects of nucleation and locking with increasing strain.

6.5. CONCLUSION

In this chapter I have briefly examined and reviewed the literature on the microstructure of Brazilian and Opalescent natural quartz, and I have compared this to observations of the microstructure of undeformed or slightly deformed synthetic quartz made by Morrison-Smith et al (1976) and as part of this study. From this it may be deduced that the microstructure of most undeformed synthetic quartz is fundamentally different from the microstructures most commonly recorded for the various types of natural quartz. I suggest that this difference may at least in part account for the abnormal mechanical properties of synthetic quartz and that the effect of structural water on the shape of the stress strain curve may be nothing like as great as suggested by the present theory. The discussion of the mechanical effects of dispersions of impurity particles in a crystalline matrix shows that the existing metallurgical models may be applied qualitatively to the synthetic quartz data with some success. This is supported by observations of interaction between the impurity and the dislocation microstructures reported by Morrison-Smith et al (1976) and as part of this study.

In the next chapter I shall outline a qualitative model for the mechanical properties of synthetic quartz based on this limited amount of experimental data and the metallurgical theory. This model is a qualitative first attempt to include this new data into the mechanical model for synthetic quartz and should be taken as a suggestion for further work and a speculation rather than an absolute conclusion.

Chapter 6.

ELECTRON MICROGRAPHS.

Plate 6.1. Caption.

6.1a). An area from a natural milky quartz crystal showing a low density of bubbles and dislocations. Specimen from the Culm, North Devon.

6.1b). A different area of the same foil showing a low density of straight dislocations and occasional bubbles. The spotting on the micrograph is caused by radiation damage to the foil.

6.1c). A foil prepared from a more intensely deformed milky quartz specimen from the Culm, North Devon. Note the higher density of dislocations, and the wall structure. This foil shows a higher density of bubbles than that shown in a and b above.

Plate 6.2. Caption.

6.2a, b, c). Initial densities of the impurity grains in three different synthetic quartz crystals.


a
Pl. 6.1
0.5μ

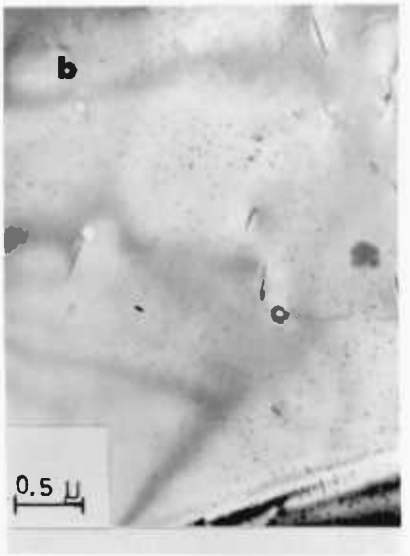
b
0.5 μ

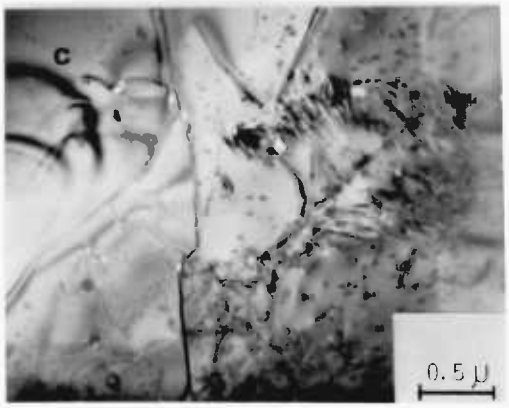
c
0.5 μ

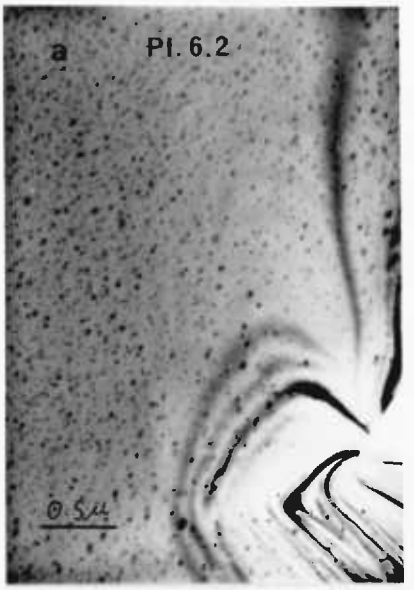
a
Pl. 6.2
0.5μ

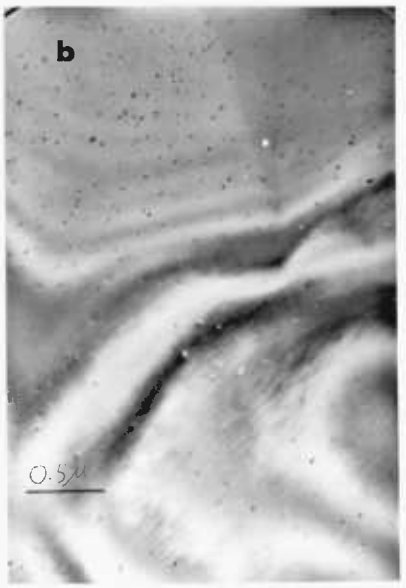
b
0.5μ

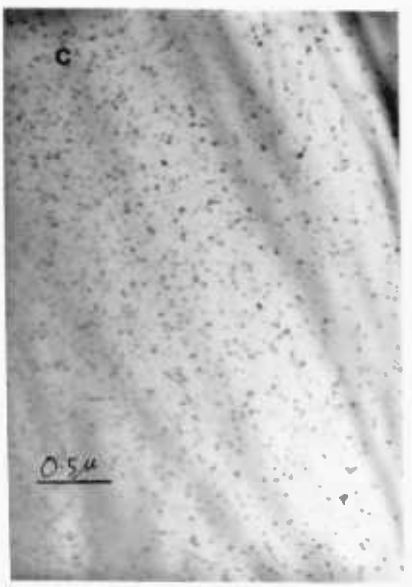
c
0.5μ

Plate 6.3. Caption.

6.3). The effect of beam damage superimposed on the particles in a synthetic quartz foil.

Plate 6.4. Caption.

6.4). The strain fields around the precipitate particles.

Plate 6.5. Caption.

6.5). The weak beam diffracting condition used to image the particles.

Plate 6.6. Caption.

6.6). The change in particle density across a growth band.

Plate 6.7. Caption.

The effect of temperature on the particle density. The series of micrographs are of the same foil, taken at different stages during an insitu heating test.

6.7a). The initial density of particles.

6.7b). At 300^{o}C.

6.7c). At 400^{o}C.

6.7d). At 500^{o}C.

6.7e). At the alpha/beta transition (573^{o}C.).

6.7f). At 650^{o}C.

6.7g). At 850^{o}C.

The specimen was allowed to equilibrate for 15 minutes at each temperature during this experiment.


Pl. 6.3
1μ

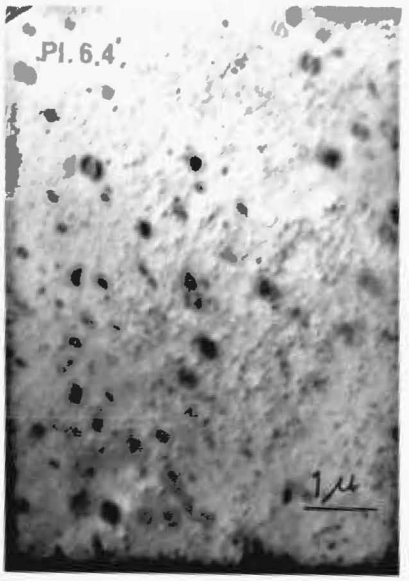
Pl. 6.4
1μ


Pl. 6.5
D P

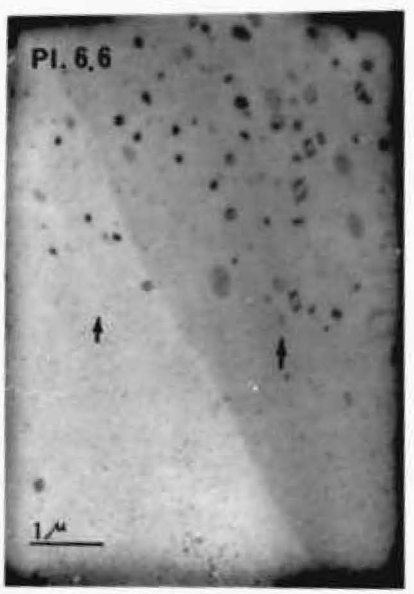
Pl. 6.6
1μ

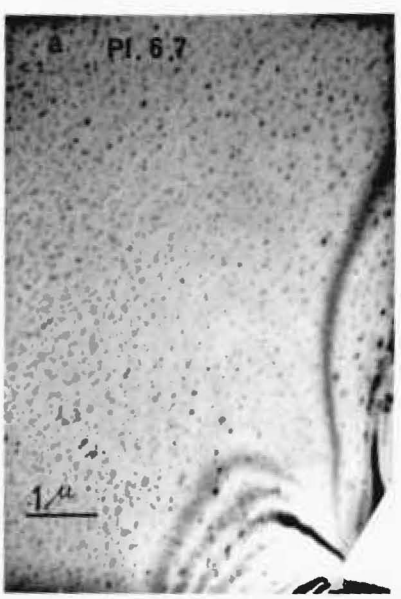
a
Pl. 6.7
1μ

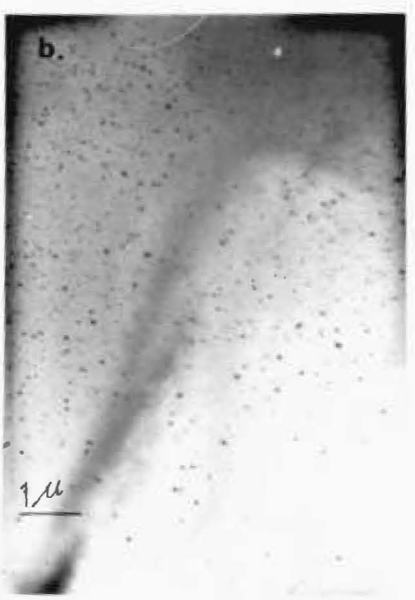
b.
1μ

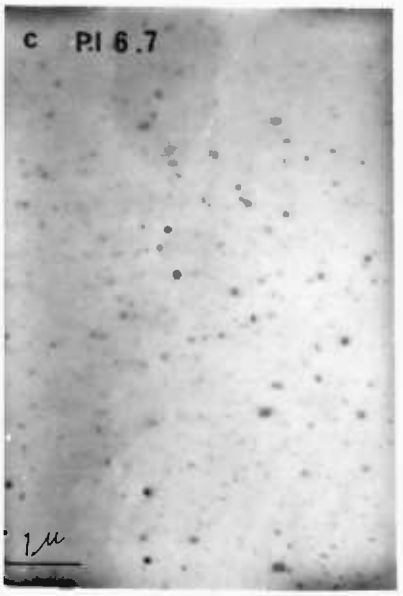
c Pl 6.7
1μ

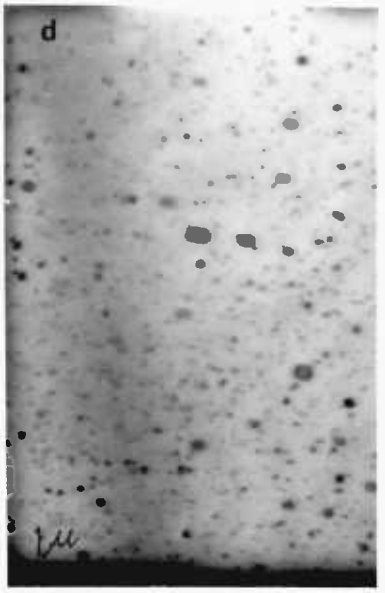
d
1μ

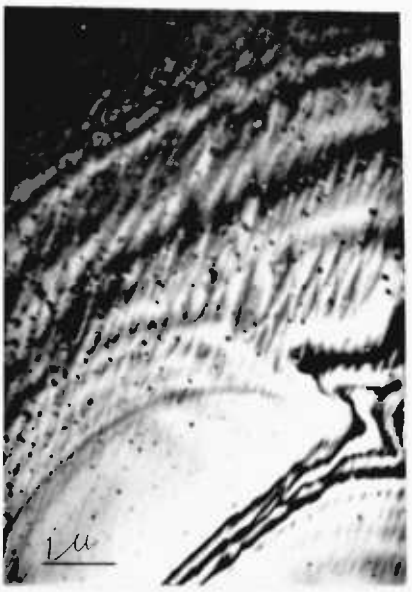
1μ

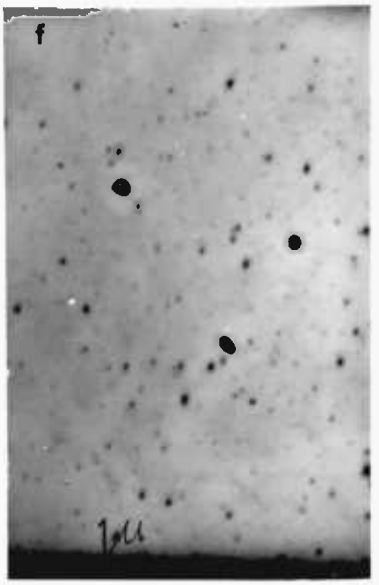
f
1μ

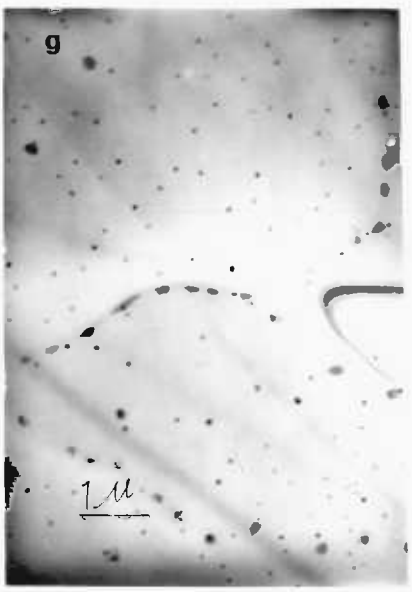
g
1μ


Pl: 6.8
1μ

Plate 6.8 Caption.

6.8). The alignment of enlarged impurity grains and the clear area left by this alignment.

Plate 6.9 Caption.

The alpha/beta transition.

6.9a, b). Close spaced twinning developing in the foil as the alpha/beta inversion temperature is approached.

6.9c). The structure of synthetic beta quartz showing the impurity particles (large spots) and some beam damage (small spots).

6.9d). Cooling to the inversion temperature. The reappearence of diffraction contrast in the specimen indicates that part of the foil has inverted to alpha quartz. These streaky areas of diffraction contrast eventually develop into twins similar to those formed in the 500 to 573^{o}C range on heating. Further cooling leads to shrinkage of these twins but as the rate of cooling in the microscope is fast, the majority remain frozen into the foil.

6.9e). The strain fields developed around the particles during cooling. Note that the areas of radiation damage do not develop strain fields in this way.

Plate 6.10. Caption.

6.10a). The strain fields developed around the impurity particles on cooling to room temperature. Note that in this micrograph no strain fields are visible around the beam damage centres.

6.10b). A more slowly cooled specimen of synthetic quartz. The impurity particles show large strain fields and have themselves shrunk on cooling. In this foil the diffracting condition also resolves strain fields around the damage centres.


a
1 μ
Pl.6.9

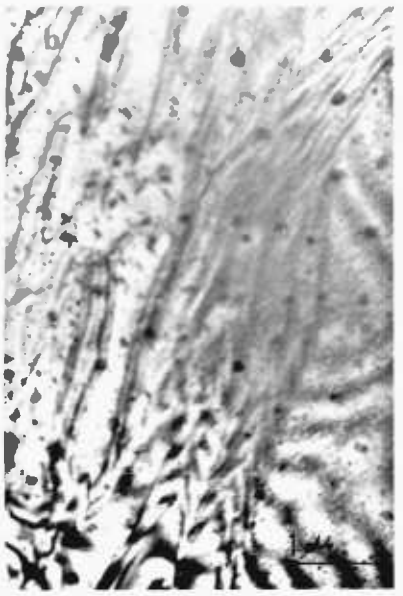
b
1 μ

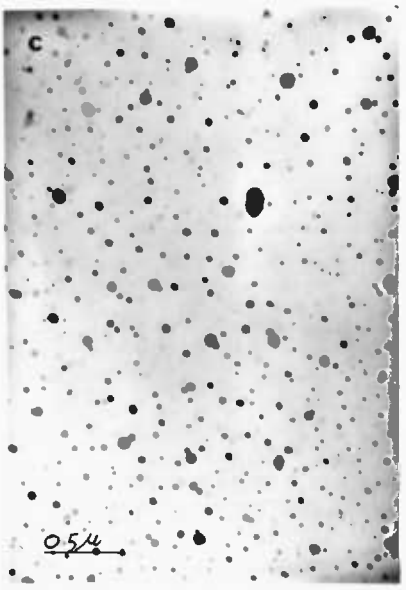
c
0.5 μ

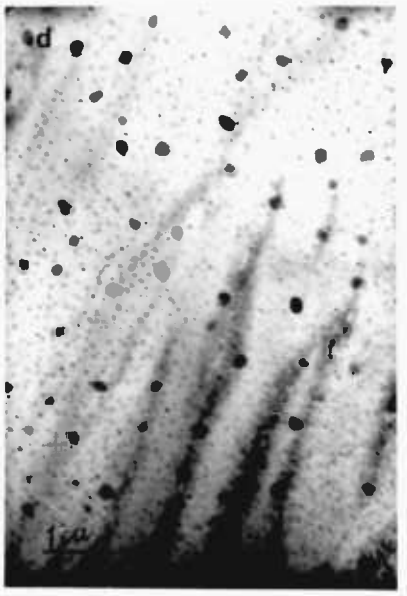
d
1 μ

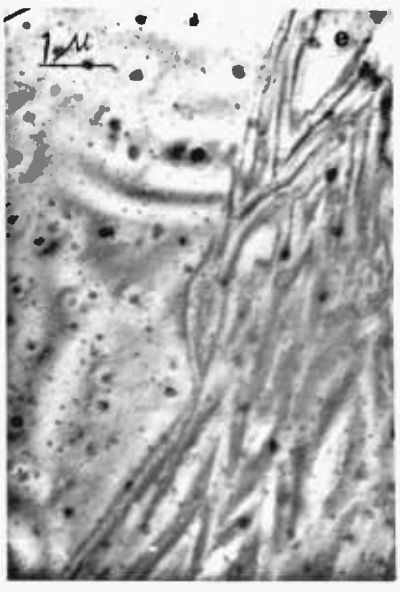
1 μ
e

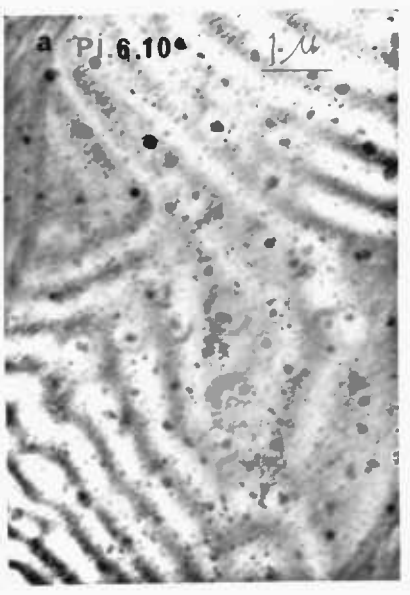
a
Pl.6.10
1 μ

Plate 6.11. Caption.

The effect of long term heating on a synthetic quartz crystal. 6.11a, b, c, d, e, f). These micrographs are all from a foil pre-pared from a sample of synthetic quartz which had been heat treated at 850°C and atmospheric pressure for two months. The micrographs show that a large population of fluid inclusions have developed, and that a number of dislocations have appeared in response to thermal stresses in the specimen. These dislocations show inter-actions with the bubbles. Of interest is the fact that the pop-ulation of impurity particles has nearly entirely disappeared, those particles which remain being very small and indistinguishable from beam damage centres. A close examination of the dislocations and the bubbles shows that the bubbles appear to contain a second phase and that the dislocations are decorated in many instances. It would thus appear that the bubbles nucleated on the strain fields associated with the particles and as they grew, eventually engulfed them. Similarly, the impurity phase which collected along dislocations, see plate 6.8., spread out along the dislocation line, producing the decoration and presumably rendering the dislocations sessile.

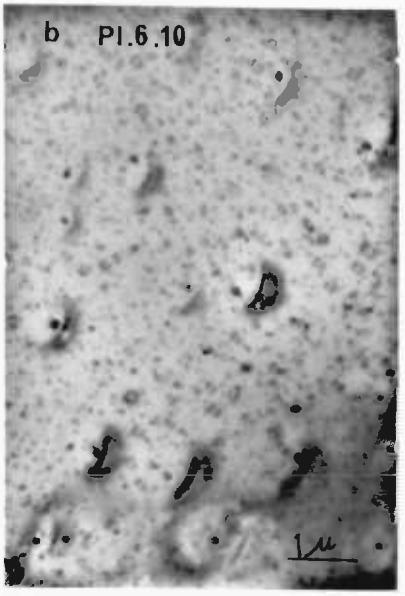
b Pl.6.10
1μ


a Pl 6.11
1μ

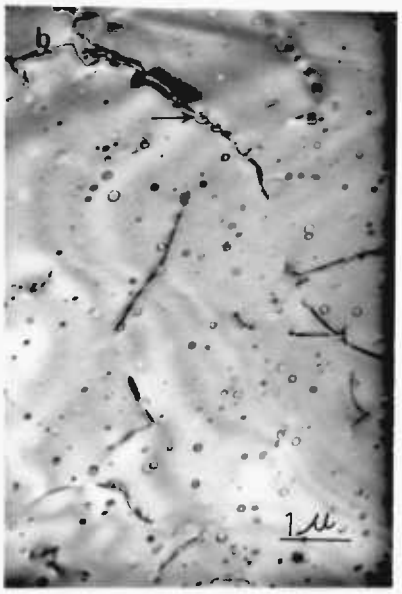
b
1μ

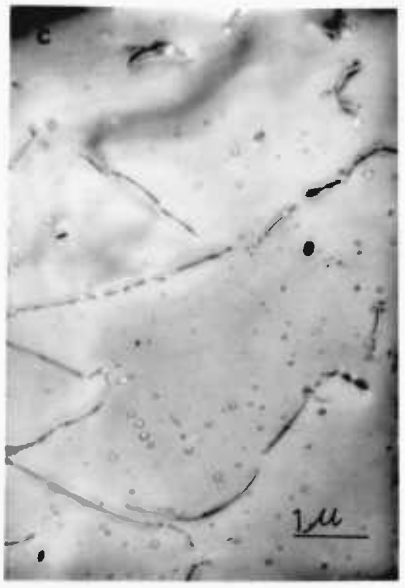
c
1μ

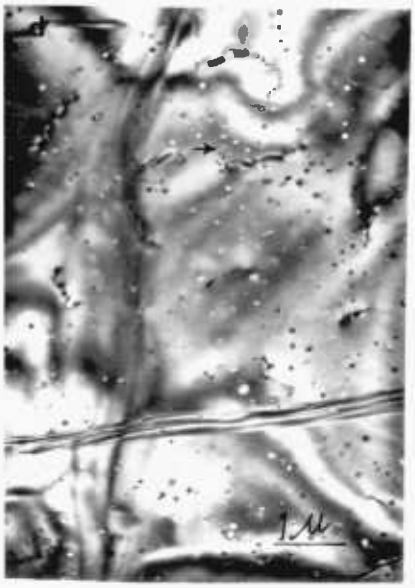
d
1μ

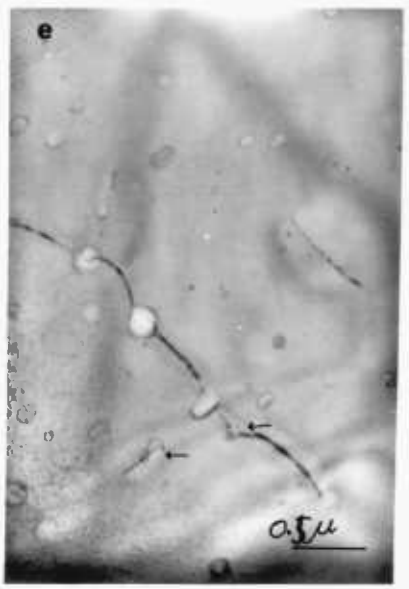
e
0.5μ

Plate 6.12. Caption.

The nucleation of dislocations on a cluster of impurity particles at 850°C. and increasing times.

6.12a). The cluster of impurity particles at room temperature.

6.12b). 850°C. and 20 minutes.

6.12c). 850°C. and 40 minutes.

6.12d). 850°C. and 60 minutes.

6.12e). 850°C. and 80 minutes.

6.12f). 850°C. and 100 minutes.

6.12g). 850°C. and 120 minutes.

6.12h). 850°C. and 140 minutes.

Pl. 6 .11

f

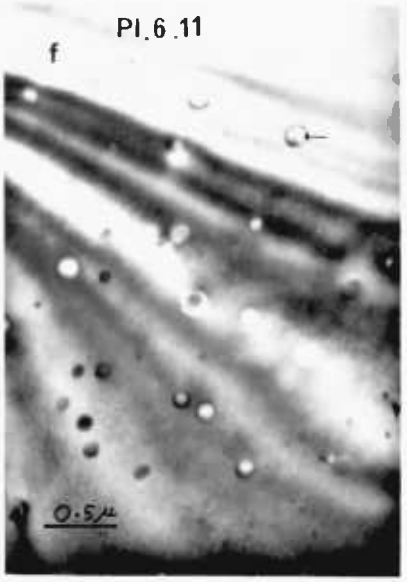

Pl. 6 .12

a

b

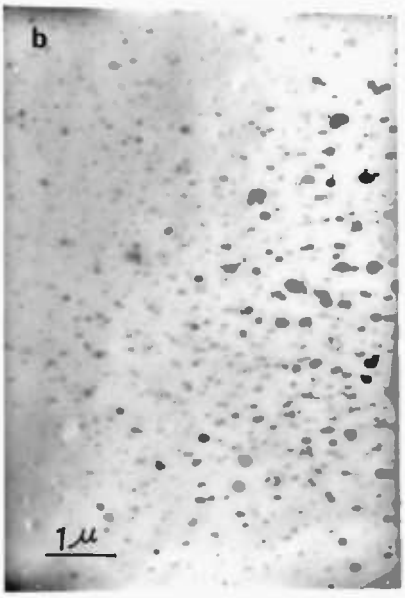

c

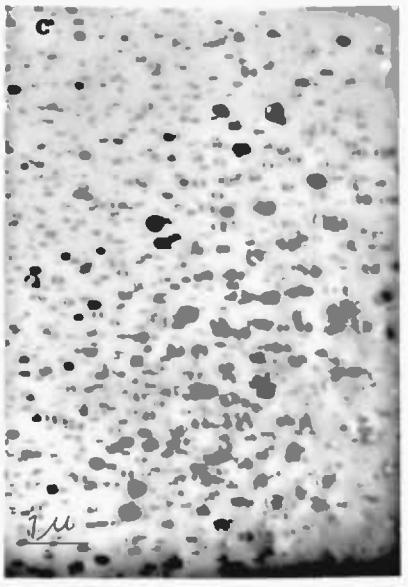

d

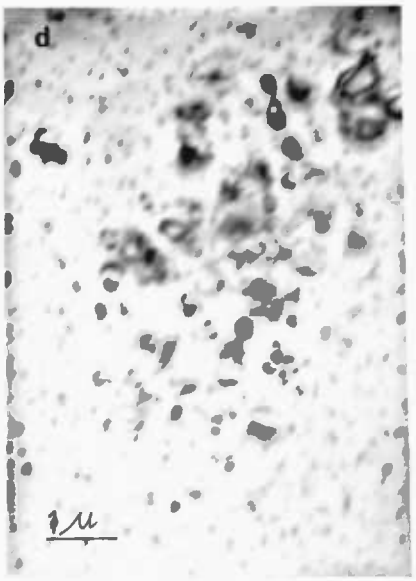

e

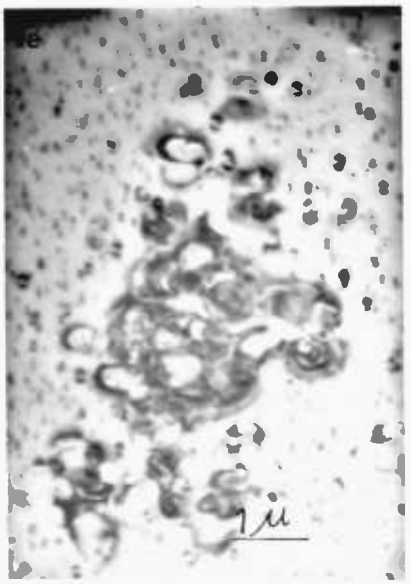


f
Pl. 6.12
1μ

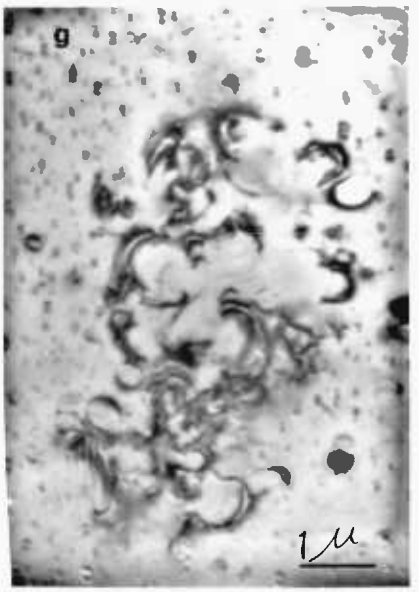
g
1μ

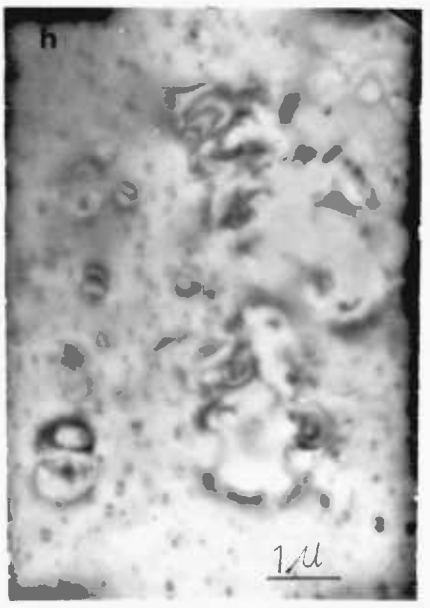
h
1μ

Chapter Seven.

DISCUSSION, CONCLUSIONS AND SPECULATIONS.

Chapter 7. DISCUSSION , CONCLUSIONS AND SPECULATIONS.

7.1. INTRODUCTORY COMMENT

To write a conclusion to this work at its present stage would be to assume the outcome of many experiments still to be conducted. Because of this I am writing this final chapter not so much as a summary of the results and discussions presented earlier but as a proposal for further work based on a synthesis of these ideas. The model I am going to present is based as much on supposition as on fact, but I feel that it goes some of the way to accounting for the anomalies in the mechanical properties of synthetic quartz. I hope that this will be taken as the basis for further electron microscope and mechanical studies which will refine, negate or collaborate these ideas. Most of what I am to say should be ammenable to experimentation.

7.2. A NEW MODEL FOR THE ABNORMAL MECHANICAL PROPERTIES OF SYNTHETIC QUARTZ

In the following sections, I shall try to relate systematically

the various phenomena recorded from mechanical tests on synthetic quartz to the roles of Impurity particles, structural water or some combination of the two.

7.2.1. The Depression of the Yield Point

Synthetic quartz crystals with large concentrations of structural water show a pronounced yield point in stress/strain curves recorded at temperatures at which no yield is recorded for drier crystals. This yield occurs at high stress, but has been recorded at temperatures as low as 310°C (Griggs loc cit). With increasing temperatures this yield stress is reduced until the weakening temperature is reached. Figure 7.1a shows the lowest temperature stress strain curve for synthetic crystals of differing water content and figures 7.1 b and c show the effect of increasing the temperature on these curves, up to the weakening temperature (see also Chapter 2).

Depression of the yield stress, at any given temperature, is not a phenomenon normally associated with an impurity phase such as the hydroxyl or with a high density of incoherent particles in the structure, but with a high grown in dislocation density, or density of dislocation sources (Honeycombe 1968, Smallman 1970). Synthetic quartz is known not to have a large in grown dislocation density so it must be assumed that the incoherent particles act as dislocation sources giving an apparently large ingrown dislocation density. This supposition is strongly supported by the work of Morrison-Smith (1976), and this study (Chapter 6). I demonstrated in Chapter 6 that the applied stress for the formation of dislocation loops around the impurity particles varies inversely with the particle density at constant temperature, presumably because of increased local stress concentrations in regions of high impurity particle density. Thus it might be expected that both the

Figure 7.1a.

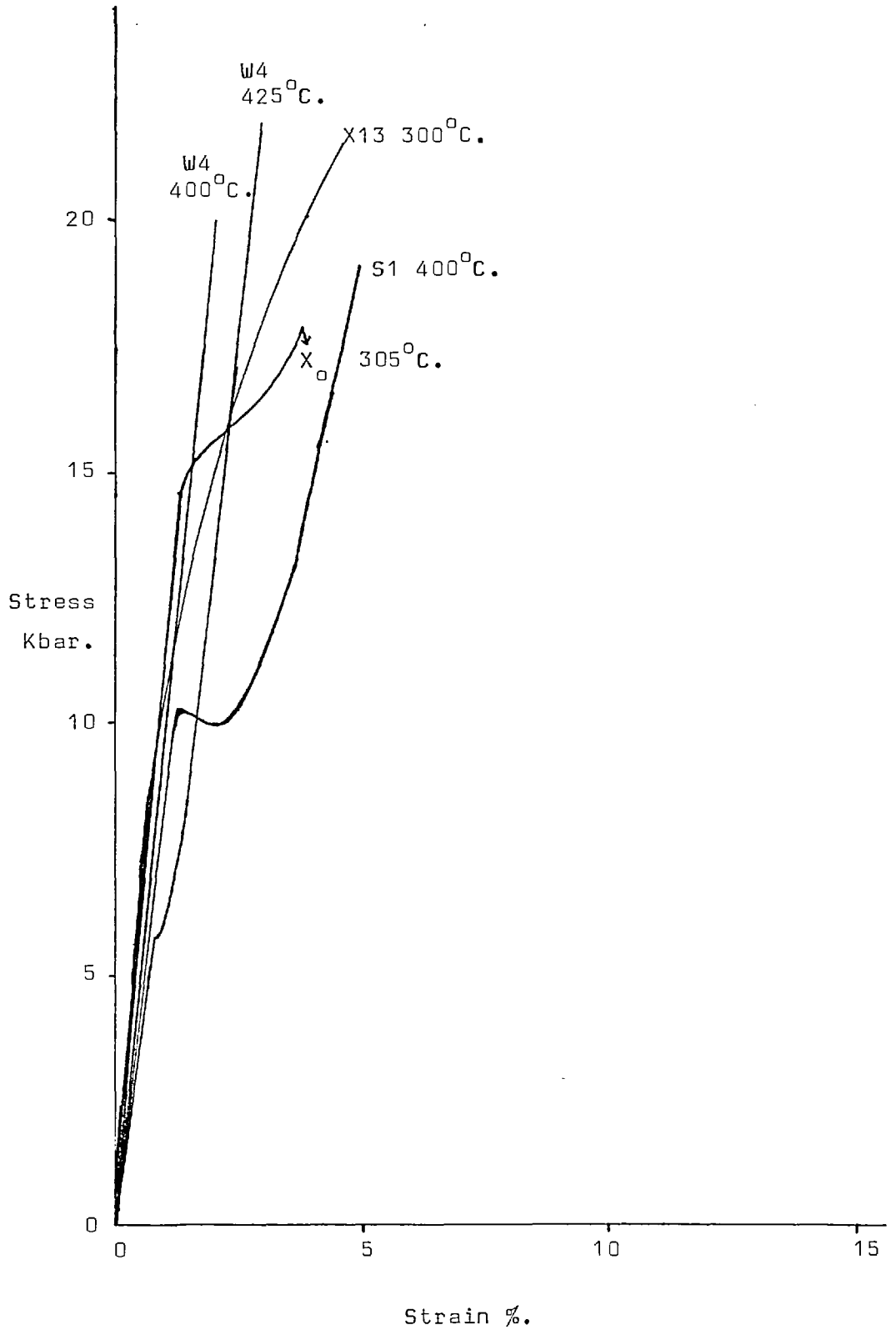

The lowest recorded temperature stress/strain curves for synthetic quartz which show yield points.

Figure 7.1b.

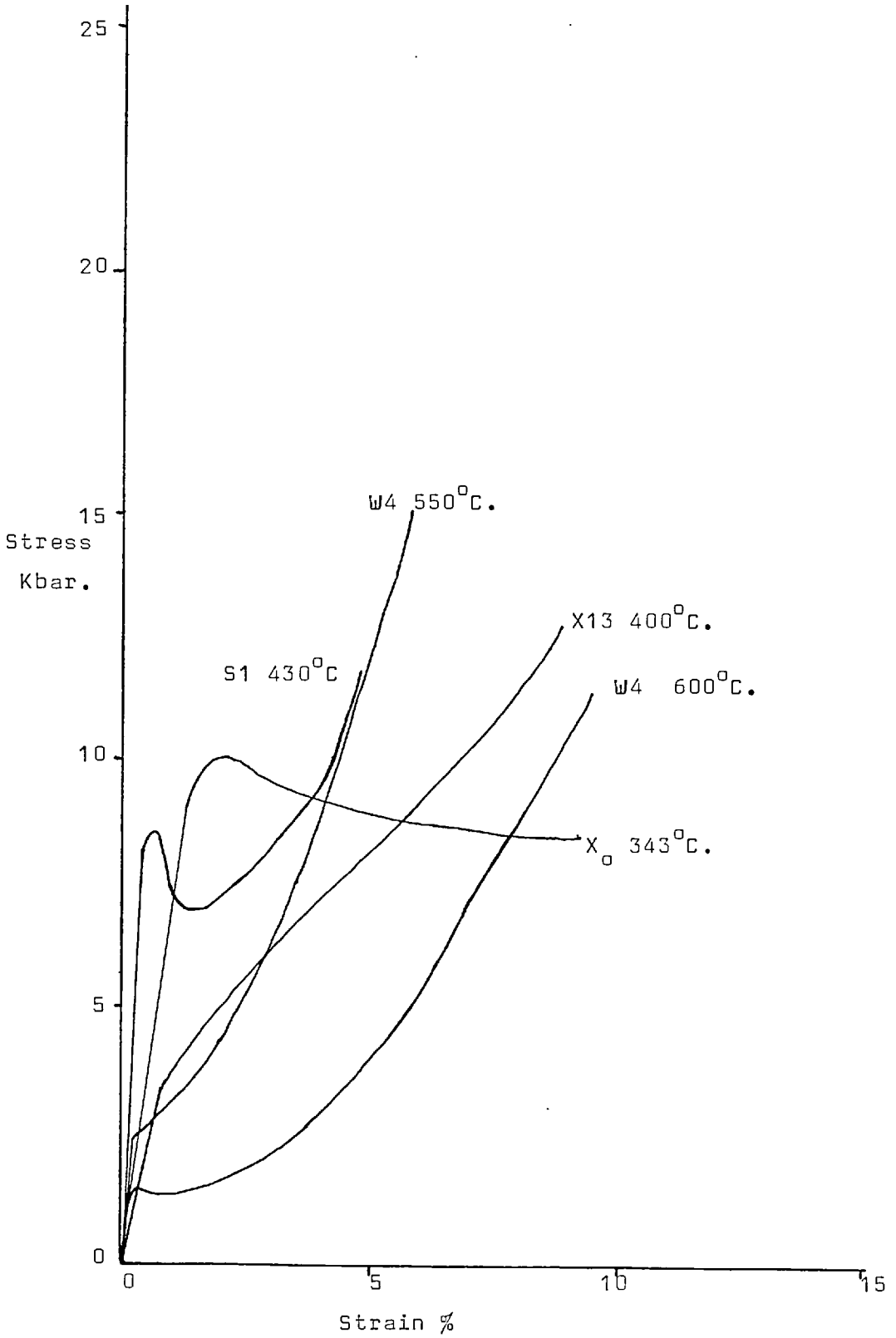

Stress/Strain curves for quartz crystals in the temperature range below the weakening temperature, but above the lowest recorded yield temperatures.

Figure 7.1c.

The large change in stress as the weakening temperature is approached.

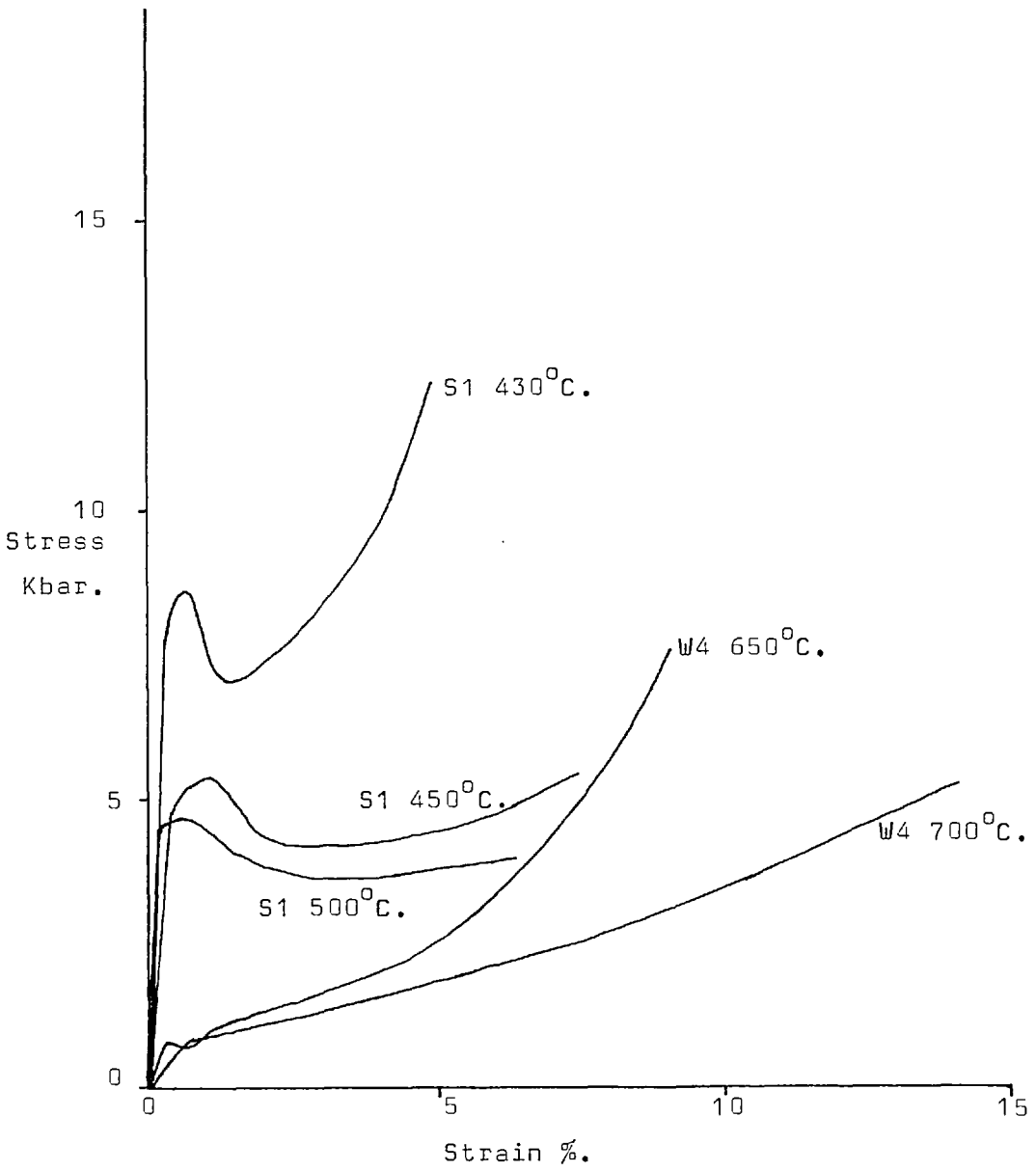

The stress strain curves in this figure are taken from Hobbs (1968), Hobbs et al (1972) and Griggs (1974) which I hope will indicate how widely the temperature dependence of the synthetic quartz stress/strain curves has been investigated and how similar these investigations are.

applied stress and the thermal activation energy required to produce dislocations will be reduced in those crystals with the highest impurity particle density. From Chapter 5 it is seen that these are also the crystals with the largest structural water concentration.

7.2.2. Low Temperature Work Hardening

The stress strain curves in figures 7.1 b,c and in figure 7.2 show that immediately after the yield point in the lowest temperature tests, the crystals work harden at a very rapid rate. This rate of work hardening is highest in those crystals with the lowest recorded yield points (which are those crystals with the largest structural water and impurity particle concentrations) and is seen to decrease in all crystals with increasing temperature until the weakening temperature is reached. At and above the weakening temperature, the rate of work hardening is negligible. This work hardening behaviour below the weakening temperature is compatible with the theory of Fisher et al (1953) which predicts strong work hardening, becoming more severe with increasing particle density. The observations of Morrison-Smith (1976) are compatible with this suggestion, showing strong dislocation /particle interactions, and showing that the degree of tangling and the total dislocation density increases with increasing strain. The mechanism must differ in detail from that of Fisher et al because the dislocations are nucleating on the particles in this case and it will not be until some significant strain has accumulated that the situation described by Fisher's theory will be attained fully. At an early stage in the deformation at low temperatures it is probable that the dislocations will slow or stop as they move outwards into regions of decreasing local stress from the sources. Subsequent loops will then feel the back pressure from these stationary dislocations and will themselves exert

Figure 7.2.

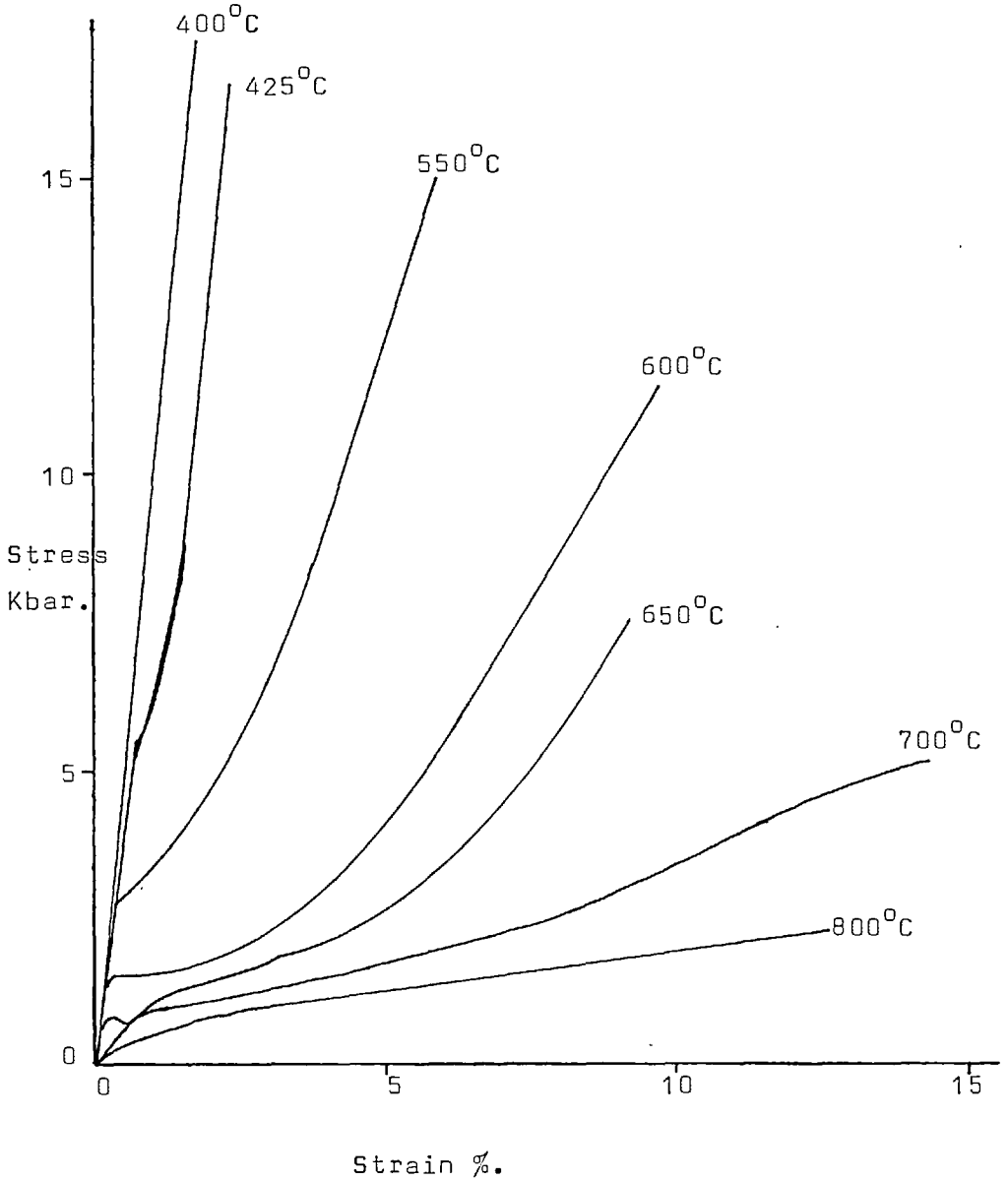

The stress strain curves for crystal W4 from Hobbs et al (1972). These curves demonstrate the extreme work hardening and its strong temperature sensitivity which characterize the low temperature deformation of synthetic quartz.

a similar backpressure on the source which will have to be overcome either by an increase in the applied stress or the temperature. Thus at the yield point and during subsequent low temperature deformation, the role of structural hydroxyl ions may be insignificant. Obviously this area is open to easy experimental investigation, particularly deformation to small strains at low temperatures and high stresses, followed by the necessary electron microscopy. Unfortunately a solid medium testing machine is completely unsuitable for this kind of experimentation.

The decrease in rate of work hardening with increasing temperature is a commonly observed feature of the deformation of matrix/incoherent particle systems. (See the stress strain curves on page 188 in Honeycombe 1968). The decrease in the rate of work hardening at small-strains (see figure 7.3) is presumably associated with the dislocation loops moving into the hitherto dislocation free areas between sources as the temperature is increased (Morrison-Smith et al 1976), this giving greater accommodation of strain at constant stress before the dislocations slow and exert the back pressure on the source as mentioned above. The limit to this reduction in rate at small strains will in all cases be when dislocations from adjacent sources interfere with each other. Also, with increasing temperature, the numbers of dislocations leaving the sources by the mechanism predicted in the Orowan theory of work hardening will increase and this will lead to a significant reduction in the rate of work hardening as the temperature is raised.

7.2.3. The Weakening Temperature

The basic concept behind all of the present theories of water weakening is that above a certain temperature the stress supported at all values of strain beyond the yield point becomes small. Figure 7.4

Figure 7.3.

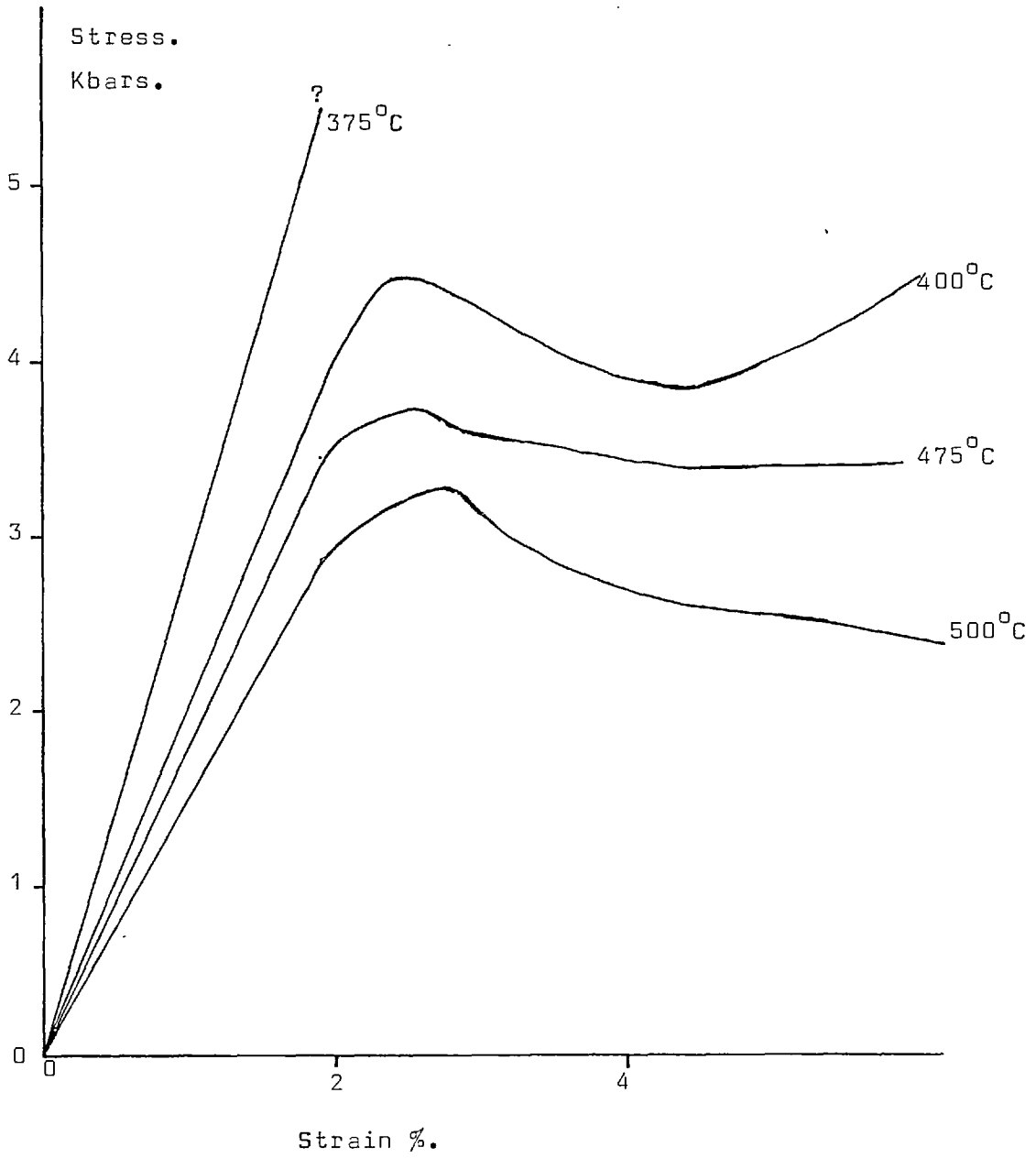

The shape of the yield point at various temperatures near to the weakening temperature for crystal AX1. (See also figure 6.1).

Figure 7.4.

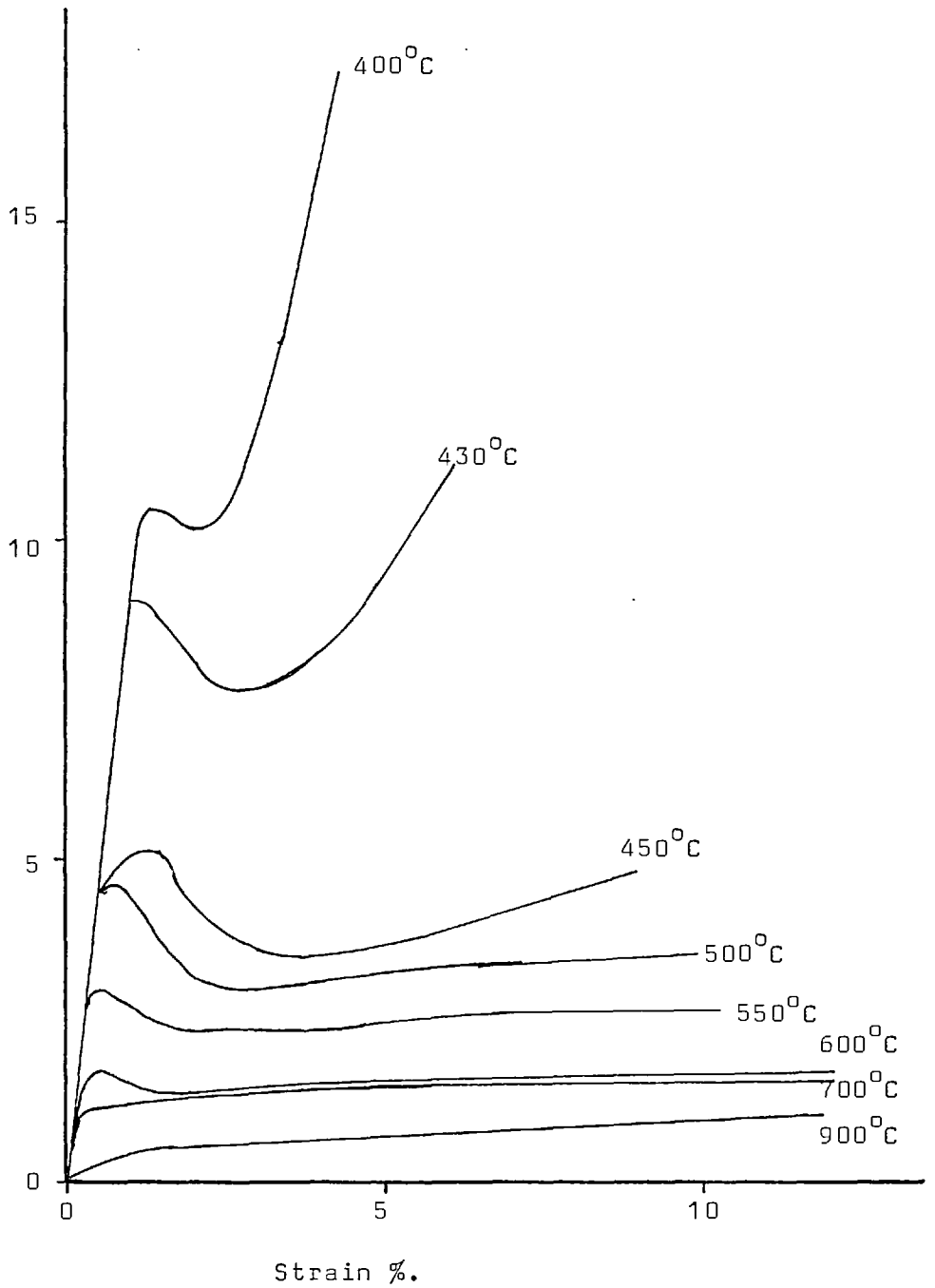

Stress/strain curves for crystal S4 (from Hobbs et al 1972) which clearly show the change in shape of the stress/strain curves as the weakening temperature is passed.

shows the change in shape of the stress strain curves for crystals of differing structural water concentration as the weakening temperature is passed. To define the weakening temperature, Hobbs et al (1972) plotted the stress supported at 2% strain against temperature for four different crystals and defined the weakening temperatures from the resulting curves. These curves reproduced in figure 7.5 show a linear decrease in strength with increasing temperature until at some temperature when the stress becomes small the curves flatten out. The temperature at which the flattening occurs being apparently related to the structural water concentration. At the low temperature end of these curves, it would appear that they could be extrapolated to very high stresses at low temperatures, the exception being the one point for crystal W4 at about 400°C. It has always been assumed that the deformation of synthetic quartz can be divided into a high stress low temperature region and a low stress high temperature region, both with slight temperature sensitivities, with a strongly temperature dependent region between. The strongly temperature dependent region corresponding to the weakening temperature (or the change in deformation mechanism at this temperature). The data of Hobbs, with only one point in the low temperature high stress low temperature sensitivity regime does not support this three-fold subdivision of the mechanical data if this point is ignored. Replotting the Hobbs data without the point for W4 at 400°C produces a set of curves for the temperature dependence of the flow stress which are typical of many aged alloy systems though somewhat more severe. Thus it may be possible to reinterpret the hydrolytic weakening temperature not as a sharply definable temperature at which the deformation mechanism changes but as the end point of the continually diminishing effects of the array of impurity particles in the quartz matrix.

Figure 7.5.

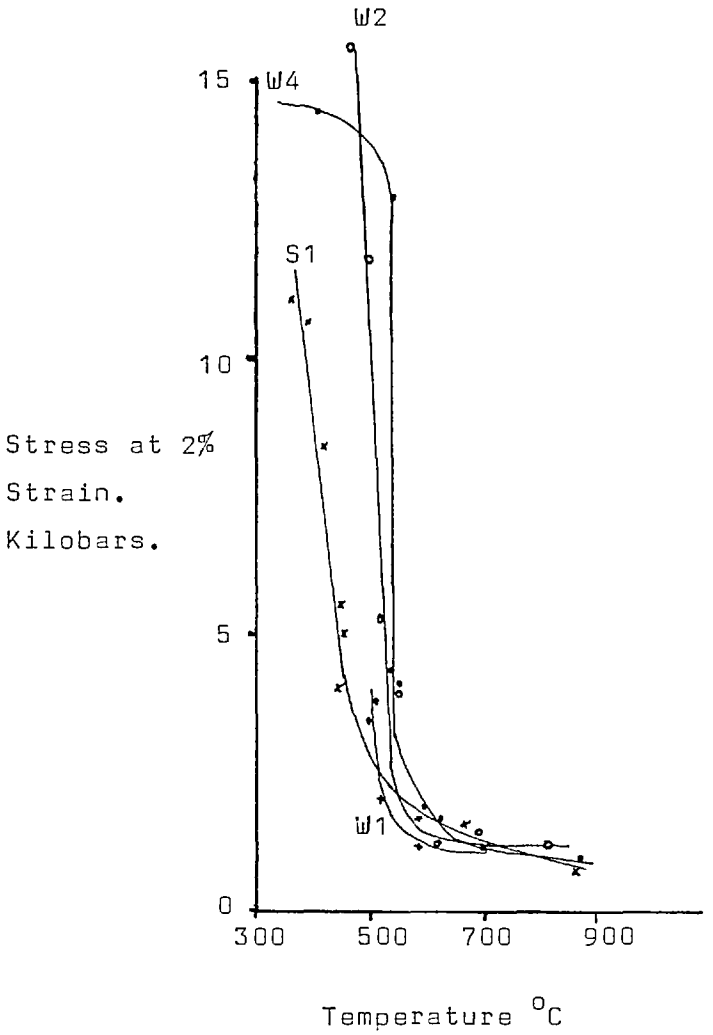

Plot of flow stress at 2% strain for crystals S1 (×), W1 (+), W2 (o) and W4 (•) as a function of temperature. From Hobbs et al (1972). This data (with the exception of the 14.5 Kbar, 400°C point for crystal W4) indicates an extreme example of the temp--erature dependence of the flow stress for a two phase material such as any precipitation hardened alloy.

Hobbs et al (1972) plotted the 'inflexion point' of the temperature sensitivity of the flow stress curves against the water concentration for their synthetic crystals and produced the graph reproduced in figure 7.6. In view of the foregoing discussion and the fact that the structural water concentration varies in apparent direct relationship with the impurity particle density it may well be possible to interpret this data not in terms of water weakening but in terms of the effect of differing densities of particles on the mechanical properties of the quartz matrix.

From the earlier chapters, three important aspects of diffusion of impurities in the quartz structure can be introduced here. Firstly (from Chapter 5) hydroxyl ions diffuse to the vicinity of impurity grains and may eventually envelope them in a bubble of water. Secondly that the temperature at which this process starts is inversely proportional to the initial structural water concentration. Thirdly that the impurity particles do themselves diffuse to or along dislocation lines, or in the absence of a dislocation coalesce as the temperature is raised.

The theory of Orowan (loc cit) requires that a material softens as the spacing between the particles is increased. So diffusion processes leading to a reduction in the number of impurity grains will reduce the rate of work hardening, and because diffusion is temperature dependent will lead to a temperature dependent flow stress. The diffusion of water to particles causing them to become completely encased in a bubble will also help this softening process. Firstly by relieving the stress concentrations around grains by hydrolyzing Si-O-Si bridges, causing the particles to become less efficient dislocation sources, and secondly by isolating the particles from the stress system in the

Figure 7.6.

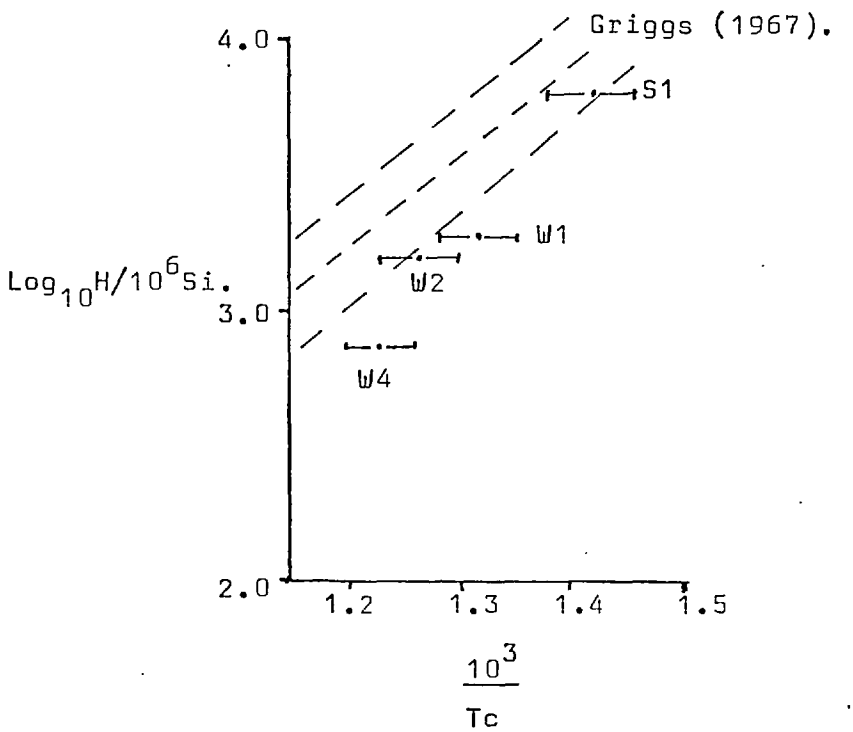

The relationship between the hydroxyl concentration and the critical temperature of hydrolytic weakening for the data of Griggs (1967) and Hobbs et al. (1972). After Hobbs et al. (1972).

matrix by forming a water bubble around them. Knipe (1977) suggests that although bubbles will pin dislocations, they are 'soft' and will still allow that dislocation segment to move although at a slower rate than the unpinned sections of the dislocation line. If this is correct then bubbles pinning dislocations can easily by pulled by the dislocations in the wall structures.

The three diffusion processes mentioned above will all serve to clear the quartz matrix of impurity particles and water, serving to release pinned dislocations and eventually to allow the dislocations, dislocation debris and impurity ions to be swept clear of areas of the matrix and accommodated in some low energy configuration (subgrain walls or deformation lamellae?). A further process must also occur however, namely cross slip. With increasing temperature pinned dislocations will be able to leave their glide plane at pinning points by the formation of jogs and will thus free themselves from the pinning obstacle. Thus more dislocations will be moving either into wall structures or into configurations where those of opposite sign will be able to annihilate one another.

Morrison-Smith et al (loc cit) report that in the temperature range associated with the weakening, the dislocation tangles become larger and more open but with areas of clear matrix between them. Large numbers of loops and other dislocation debris are present at these temperatures. Once the weakening temperature is passed the density of debris and loops is greatly reduced, dislocations are seen to lie in more than one plane, indicative of recovery, and the dislocations adopt a form typical of that reported for the microstructure in natural milky quartz (White 1973a). In his study Morrison-Smith (loc cit) does not report the formation of subgrain walls or recrystallization textures,

but this may be the result of disregarding those samples which have recrystallized (a common practice in deformation studies when interest is in unravelling dislocation based deformation mechanisms). The work of Hobbs (1968) has shown that the formation of sub-grains or a completely recrystallized texture is the common result of the deformation of synthetic quartz to and beyond the weakening temperature. These observations are thus consistent with the discussion given above.

Thus it may be possible to relate the mechanical effects reported at the weakening temperature to the impurity particle density and suggest that synthetic quartz behaves in a manner similar to over aged alloys in many metal systems. In the case of synthetic quartz the behaviour is exaggerated by several diffusion processes which affect both the matrix and the particles. It is probably concentration/temperature dependent controls on these diffusion processes which cause the rapid weakening in synthetic quartz to be temperature/concentration dependent. The supposition presented here should be open to experimental investigation for, if diffusion processes are responsible for the pronounced stress drop then the temperature at which this occurs should be strain rate dependent. Following from this, high temperature annealing or simply heating the sample prior to deformation should alter the mechanical properties. Recent experiments by Paterson (Personal Communication 1976) and by Kirby (Personal communication after experiments following this suggestion 1975) seem to support this view.

7.2.4. Flow Above the Weakening Temperature

At temperatures above the weakening temperature, synthetic quartz deforms by dislocation glide but with climb, cross slip and recrystallization becoming important as the temperature is raised. (Stress/strain curves for synthetic quartz crystals at temperatures above their weakening

temperature are given in figure 7.7).

In this high temperature flow regime the role of impurity ions and particles is minimised by the deformation process itself and as a result of other diffusion reactions (see Chapters 5 and 6). The structure bound water concentration is being rapidly reduced and molecular water is deposited in bubbles, many of which will be in the growing dislocation wall structures of newly formed sub grains (or grains) and thus will not interfere with dislocation slip in these grains. The impurity particle density is small by this stage and will only exert an influence when particles are arranged so as to cause a build up of dislocations leading to a new grain wall. Impurity particles away from grain walls presumably dissolve in the quartz structure (e.g. along dislocation lines) and are eventually precipitated in sub-grain walls or around new grains in recrystallized material. The dislocation pinning ability of any remaining impurity particles will be greatly reduced by the action of climb and cross slip which are important processes accompanying deformation at these high temperatures.

Morrison-Smith et al (1976) reports that in this regime above the weakening temperature the microstructure becomes cleaner with a decrease in debris type features and clear evidence of recovery features with dislocations lying in more than one plane. These dislocations form open tangles and as such are typical of the microstructure of naturally deformed milky quartz. This would be in keeping with the observations made in Chapters 5 and 6 and repeated in this chapter which show that with increasing temperature the structure bound water and impurity particle densities in synthetic quartz crystals are reduced. These being replaced by an array of micro-fluid inclusions which are very similar to the fluid inclusions in the milky quartz microstructure.

Figure 7.7.

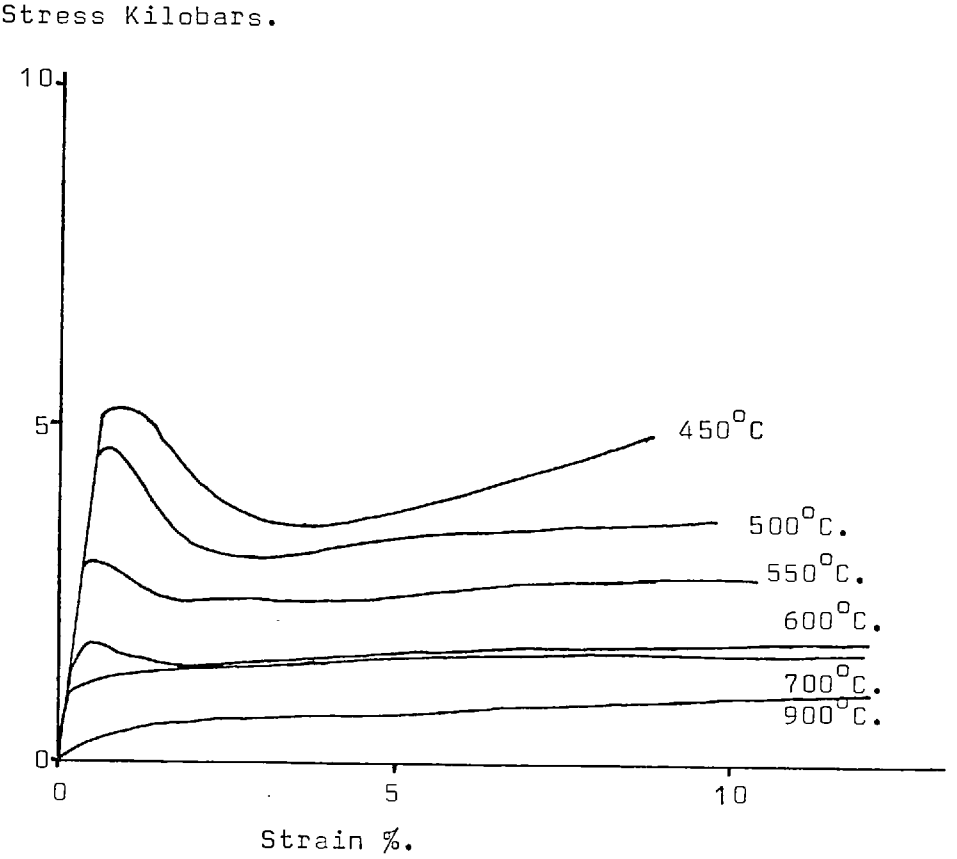

Stress/strain curves for crystal S1 at temperatures above the weakening temperature. From Hobbs et al (1972). These curves are typical for those of synthetic crystals deforming above the weakening temperature showing little or no work hardening and a characteristically low flow stress with little temperature sensitivity.

Thus the behaviour of synthetic quartz crystals at temperatures well above the weakening temperature or after a long period of aging at temperatures above the weakening temperature prior to the deformation, will be akin to that observed in naturally deformed milky quartz.

7.2.5. Conclusion

The model presented in the preceding pages equates the mechanical properties of synthetic quartz with those of an aged two phase alloy containing incoherent precipitate particles. In the quartz however, the particles are responsible not only for its cold worked textures (particularly the features leading to the rapid rate of work hardening) but also for creating the initial high dislocation density. In this respect synthetic quartz may be unique. Temperature sensitive diffusion processes, particularly those involving the mobility of structure bound hydroxyl groups and the impurity particles are responsible for the large drop in flow stress at constant strain as the temperature is increased. This drop in the flow stress is itself temperature sensitive because the larger the initial hydroxyl concentration the lower the temperature at which water becomes mobile in the system.

The yield weakening phenomena is thus only dependent on the hydroxyl concentration through their mutual dependence on the impurity particle density. If these impurity particles were not present to depress the yield point then the weakening phenomena would be recorded at a higher temperature (or possibly only at slower strain rates) in synthetic quartz crystals). In view of this I would suggest that synthetic quartz is of only limited use as a model for the mechanical behaviour of natural quartz except at the highest temperatures when it will deform by mechanisms akin to those which occurred in natural milky quartz at lower deformation temperatures.

7.3. BUBBLES AND WATER

Most natural quartz deformation will be dominated by the effect of bubbles of molecular water and/or the effect of structural water. From Chapters 4 and 5 it can be seen that natural quartz crystals will show significant weakening for only a limited period after their crystallization. In this section the role of the bubbles will be summarized followed by a discussion on the role of the initial structural water concentration. As a study of the deformation mechanisms of natural low temperature deformed quartz is the topic of another thesis being prepared concurrently with this work (see R. Knipe, Ph.D., Univ. of Lond. 1977) I will not presume to discuss the behaviour of natural quartz beyond that arising directly from this work or which is of importance to the completeness of this work.

7.3.1. The Role of Bubbles

As stated in Chapter 5, the microstructure of natural milky quartz becomes dominated by bubbles at some finite time after crystallization and the structure becomes effectively dry as a result of this precipitation of water. Knipe (1977) has suggested that these bubbles may act both as the source of dislocations and as 'soft' impurity particles pinning dislocations within the structure. Assuming this to be correct, then these bubbles are acting in a similar (but presumably much slower and less spectacular) manner to the grown in impurity phase in synthetic quartz crystals. From laboratory experiments (see Chapter 4) it would seem that at fast strain rates ($10^{-5}sec^{-1}$) the bubbles do not cause yielding at attainable stresses and laboratory strain rates so that presumably any weakening attributable to a high density of bubbles in a dry quartz crystal structure will only appear at very slow strain rates. Alternatively the weakening effect (and work hardening) of the

bubbles only proceeds whilst some structural water remains unprecipitated.

7.3.2. The Role of Structural Water

From this study I think that it must be concluded that grown in microfluid inclusions in natural milky quartz are the exception rather than the rule. Thus it follows that nearly all naturally occurring hydrothermal quartz has undergone a period immediately after its crystallization when an initially large structural water concentration is reduced, accompanied by the growth of microfluid inclusions. The strength of this natural quartz, which may be initially very low thus increases with time after the initial crystallization thus any deformation will proceed with decreasing strain rate and will eventually cease.

This leads to a very interesting possibility for natural quartz deformation. Consider a newly formed tectonic vein. The quartz fill in this vein will initially deform plastically, but with increasing time will harden as the water in the vein quartz crystals is precipitated. The strain rate for the quartz veins will then decrease whilst the stress increases. Deformation may proceed in surrounding softer material (other mineral phases etc.) relieving the stress build up and as a result the dominant rock deformation mechanism may pass, for example, into pressure solution/coble creep on the quartz deformation map (Rutter 1975, White 1975). Chemical removal of the grain by boundary diffusion or solution will lead to the deposition of the quartz in overgrowths or as new grains in low stress areas. This newly deposited quartz will have a similar high initial structural water concentration and thus if subjected to stress of sufficient magnitude will again deform plastically. With increasing age it again hardens and so the process goes on in a cyclic fashion. The close spaced

filled fractures which are common in many low metamorphic grade quartz rocks may owe their origin to a similar process of alternating deformation mechanisms depending on whether the strain is being acommodated by newly deposited or aged quartz.

7.4. CONCLUDING STATEMENT

Perhaps the most important product of this study is the realization that the whole area of quartz deformation needs many more detailed physical studies. The combined use of the Electron Microscope and the deformation rig are not enough. Detailed diffusion experiments both on the macroscopic scale on the laboratory bench and using insitu techniques in the electron microscope must be combined with accurate chemical studies. There is scope for detailed experimental projects on such aspects as bubble growth, impurity ion diffusion, quartz crystallization and the incorporation of impurity ions, and the chemical and physical properties of the impurity particles in synthetic quartz. I think that studies of this type, preferably in addition to the traditional deformation study approach, will greatly benefit this area of work and eventually add considerably to our knowledge of the deformation behaviour of both natural and synthetic quartz. In this study I have touched on many areas where detailed work is necessary. At least some of these areas have never been considered previously and this has led to what I think are interesting speculations. Hopefully, further studies will go far in either proving or disproving these ideas.

FINIS

Appendices.

Appendix 1. SAMPLE PREPARATION TECHNIQUES.

A1.1. Preparation of crystal plate samples for infrared spectroscopy.

A1.2. Preparation of pressed disc samples for infrared spectroscopy.

A1.3. Preparation of the specimens for the rock deformation experiments.

A1.4. Preparation of thin foils for the T.E.M. heating stage.

* * * * *

A1.1. Preparation of Crystal Plate Samples for Infrared Spectroscopy.

Samples for infrared spectroscopy, prepared from quartz single crystals, or coarsely crystalline vein quartz specimens, were in the form of crystal plates. These were cut in the desired orientation with a rotary diamond saw. The plates were originally cut to 0.75cm. thick and were then ground on successively finer carborundum pastes to a final thickness of between 0.08 cm. and 0.5 cm. but were not polished to prevent reflection from the surfaces. (The thicker crystal slices were necessary to produce reasonable spectra from the drier quartz specimens). When a specimen of unknown water concentration was being analyzed for the first time, a specimen thickness of 0.1 cm. was used and the result of this initial analysis then used to indicate whether a thick or a thin crystal plate should be used in subsequent analysis.

Where the variation in hydroxyl concentration across the crystal or vein being studied, the plate was held in a movable clamp which could be positioned to enable analysis of any part of the specimen. Where the specimens were prepared from, for example, a sample of natural vein quartz it is essential to

consider the path that the infrared beam will take. It is obviously necessary to position the plate so that the beam is contained entirely with in one grain to avoid determining the absorption due to hydrous silicate phases in the grain boundaries.

If only a single analysis is required from one part of a crystal then a core 1.25 cm. in diameter was taken from the plate using a diamond drill, this circular plate was then fitted into one of the standard sample holders for the spectrometer.

A1.2. Preparation of Pressed Disc Samples for Infrared Spectroscopy.

Tuddenham and Lyon (1960) describe a method for preparing pressed discs of powdered silicate minerals in potassium bromide. They emphasise the importance of accurately reproducing the grinding technique, if the optical properties of the resulting discs are to be similar. The grinding procedure adopted in this study is based on that of Tuddenham and Lyon (1960) and is as follows. Firstly, the sample was mechanically crushed in absolute alcohol to produce a coarse powder with an average grain size of 0.1 cm. This was then dried by evaporation and ground in a pulverizing mill for 10 minutes. The resulting powder was then mixed with KBr in the ratio 5 parts KBr to 1 part silica by weight and finely ground by hand to ensure thorough mixing.

A quantity of the mixture (between 1 and 2 grams) was then placed in a 1.25 cm. diameter die and pressed under vacuum using a load of 20 tons applied for 10 minutes. The resulting discs gen--erally gave good spectra, which were reproducible and compared favourably with spectra recorded from single crystal plates of the same material. After the first analysis the discs were dried in an oven for 48 hours at 150^{o}C. to drive off any absorbed water. The specimens were then analyzed again and the spectra compared,

in no case was any significant change in the absorption recorded, indicating that the powdered quartz had not absorbed any significant quantity of water on to the surface of its grains.

Contamination of any quartz powder by iron or water will seriously influence the infrared absorption and must be eliminated. To this extent, the following precautions were taken. All hand grinding of the silica was conducted in 99.998% pure ethanol, and the pulverizing was conducted in a tungsten carbide mill, using a tungsten carbide ball, thus preventing iron contamination. All the apparatus used in the crushing and pressing technique was wash--ed before and after use in the pure ethanol, to remove traces of quartz powder and absorbed water from the vessal walls, and to dehydrate the atmosphere in the vessel.

Moore and Rose (1973) discuss the absorption of water by quartz powders during grinding, they quote Hillebrand (1908) who identified two classes of absorbed moisture, loosely held water, liberated at temperatures below 105^{o}C. and firmly held water liberated above 105^{o}C. Hillebrand (1908) ground samples of quartz for 3 hours, and reported that the loosely held moisture increased from 0 to 0.35%, and that the firmly held water increased from 0.06% to 0.45% by weight. Moore and Rose (1973) ground their samples for periods of between 10 and 400 hours and determined the degree of water absorption. Extrapolating their data back to the short grinding times used in this work, indicates that no measurable water absorption should have occured in my quartz powders during grinding.

A1.3. Preparation of the Specimens for the Rock Deformation Experiments.

Both the solid confining medium and the Hugh Heard fluid confining medium deformation machines were operated with the

same sized specimens. These were of circular section with a dia-
-meter of 0.25 inches and were 0.5 inches long. This size was choosen so that comparatively high stresses could be applied to the specimens without overloading the deformation machines.

The specimens were cored from the single crystal, or vein quartz samples, using a 0.25 inch. internal diameter diamond coring tool lubricated with water. These cores were then cut on a rotary diamond saw into 0.75 inch. lengths. Each length of core was then mounted in a steel V block and the ends lapped flat and parallel on a miniture lathe fitted with a rotating grindstone. After lappping the specimens had a length of 0.5 inches. These were then accurately measured before use, (to within $\pm$ 0·00025cm.).

A1.4. Preparation of Thin Foils for the T.E.M. Heating Stage.

In preparing these thin foils, it proved to be impossible to use the copper support discs normally used in the preparation of thin foils from microscope slides of silicates. These was because no suitable adhesive was found to attach the disc to the silicate slide which would remain stable under high vacuum at elevated temperatures.

This problem was overcome by using thicker slices of quartz as a starting material, relying on the mechanical strength of this alone to support and protect the thinned area.

The procedure was as follows. Firstly, thin sections of the specimen 40 to 60 microns thick were prepared, mounted in Lakeside, not araldite, without a cover slip. After normal micro-
-scopic examination, the slide was divided into a number of sections by breaking along scored lines. The sample was then floated off the glass slide by soaking in ethanol and transferred to the sample holder of the Edwards Ion Beam Machining Apparatus. Penetration of the specimen by the beam was acheived in about 60 hours. Keeping the

film in this sample holder, it was transferred to a carbon coating machine and coated in the normal manner, after which it was kept in the sample holder until it was required to be transferred to the heating stage for examination and experimentation. Unfortunately, it was not normally possible to recover the intact foil from the heating stage after use.

* * * * * *

Appendix 2. COMPUTER PROGRAMS.

A2.1. Introduction.

A2.2. Evaluation of the Water Concentration from the Infrared Spectra.

A2.3. The Model for the Growth of a Bubble in an Infinite Quartz Crystal.

A2.1. Introduction.

In this section, the two main computer programs written as part of this study are listed together with documentation. The first of these was used in the analysis of all the infrared spectra, whilst the second was used in the numerical evaluation of the bubble growth model presented in chapter 5. The language in both cases is Fortran 4, but in the second case the program calls on the NAG5F library which may not be available on the Fortran 4 compiliers at other institutions.

A2.2. Evaluation of the Water Concentration from the Infrared Spectra.

The program listed below will read in values for the absorption, and baseline at constant frequency for a number of points in the absorption band, and from this data will calculate the concentration in $H/10^6Si$, and replot the absorption band as extinction coeff--icient (Brunner 1961) versus frequency. Documentation is in the form of comment cards inserted into the program listing.

```
1.      PROGRAM SPECTRA(INPUT,OUTPUT,TAPE5=INPUT,TAPE6=OUTPUT)
C
C       PROGRAM FOR THE ANALYSIS OF INFRARED SPECTRA
C
C                       OF QUARTZ.
C
C       BY MERVYN EDWARD JONES. RM242. STRUCTURAL GEOLOGY
C
2.      DIMENSION LINE(100)
3.      DIMENSION NAME(30)
4.      DIMENSION STORE(50)
5.      COMMON SPACE(50,3)
```

```
      COMMON N
      COMMON AFREQ,BFREQ,ORDER
      COMMON TINT,SINT
      COMMON F
      INTEGER EX,BLANK
      DATA EX/'X'/
      DATA CONVRT/0.926/
      DATA BLANK/' '/
C
C       I = TOTAL NUMBER OF SPECTRA IN THE BATCH TO BE
C
C           ANALYZED.
C
      READ(5,1000) I
 1000 FORMAT(I3)
C
C       SET UP LOOP FOR TOTAL NUMBER OF SPECTRA IN BATCH.
C
      DO 100 ISPEC = 1,I
C
C       BLANK DIMENSION NAME.
C
      DO 200 INAME = 1,30
      NAME(INAME)  = BLANK
  200 CONTINUE
C
C     LOAD NAME WITH SAMPLE IDENTIFIER.
C
      READ(5,2000)(NAME(IN),IN=1,30)
 2000 FORMAT(30A1)
C
C     WRITE SAMPLE   IDENTIFIER
C
      WRITE(6,3000) NAME
 3000 FORMAT(1X,////,10X,'SAMPLE IDENTIFIER IS',30A1,///)
C
C  N IS THE NUMBER OF UNITS OF SUMATION USED TO DETERMINE
C
C  THE NUMERICAL VALUE OF THE INTEGRAL FOR THE SAMPLE.
C
      READ (5,4000) N
 4000 FORMAT(I2)
C
C READ IN THE PARAMETERS OF THE SPECTRUM AND ITS BASELINE
C
C AND CONVERT THEM INTO THE CORRECT FORM FOR EVALUATING THE
C
C INTEGRAL ACCORDING TO THE BEER LAMBERT LAW. TMIN = IO
C
C TMAX = I
C
      DO 300 ITEM = 1,N
      READ(5,5000)TMIN,TMAX
 5000 FORMAT(F5.2,F5.2)
      SPACE(ITEM,1) = TMIN
      SPACE(ITEM,2) = TMAX
      E = TMIN/TMAX
      IF(E.LE.0.0)GOTO299
      F = ALOG10(E)
      STORE(ITEM) = F
      SPACE(ITEM,3) = F
```

```
      GO TO 300
  299 WRITE(6,5001)
 5001 FORMAT(20X,'ERROR******ERROR******E NEGATIVE')
  300 CONTINUE
C
C  DETERMINATION OF THE INTEGRAL INTENSITY USING SIMPSONS RULE.
C
      M = N/2
      J = 1
      SUM = 0.0
      DO 400 ISORT = 1,M
      SUM = SUM + STORE(J)
      J = J + 2
  400 CONTINUE
      M = (N/2)-1
      J = 2
      SUMN = 0.0
      DO 500 JSORT = 1,M
      SUMN = SUMN + STORE(J)
      J = J + 2
  500 CONTINUE
C
C  TINT AND SINT CORRESPOND TO TMIN AND TMAX AT THE START OF
C
C  THE ABSORPTION BAND.
C
      READ(5,6000) TINT,SINT
 6000 FORMAT(F5.2,F5.2)
      E = TINT/SINT
      IF(E.LE.0.0)GOTO501
      F = ALOG10(E)
      GO TO 502
  501 WRITE(6,6001)
 6001 FORMAT(20X,'ERROR******ERROR******E NEGATIVE***')
C
C  ADD TERMS OF SIMPSONS EQUATION
C
  502 XINT = SUM * 4.0
      YINT = SUMN * 2.0
      ADD = XINT + YINT
      ADD1 = ADD + F
      ADD2 = ADD1 + STORE(N)
C
C  READ IN THE FREQUENCY PARAMETERS. THE PROGRAM IS WRITTEN
C
C  TO ACCEPT THESE AS MICRONS * 4.0 AND THEN CONVERTS THEM
C
C  TO RECIPROCAL CENTIMETERS. THIS IS TO MAKE IT COMPATIBLE
C
C  WITH THE NUMERICAL FREQUENCY SCALE ON THE GRUBB PARSONS
C
C  SPECTROMASTER. OMITTING CARDS 69 AND 70 CONVERTS THE
C  INPUT TO MICRONS.
      READ (5,7000) AWAVE,BWAVE
 7000 FORMAT(F6.3,F6.3)
      AMICON = AWAVE/4.0
      BMICON = BWAVE/4.0
      AFREQ  = 10000.0/AMICON
      BFREQ  = 10000.0/BMICON
```

```
C
C  DETERMINE THE FIRST TERM OF SIMPSONS EQUATION.
C
      Z  =  FLOAT(N)
      DIFF = AFREQ - BFREQ
      ORDER = DIFF/Z
      DIVID = ORDER/3.0
      CALL DATSTOR
      SOLUT = ADD2 * DIVID
C
C  DIVIDE THE NUMERICAL VALUE OF THE INTEGRAL BY THE CELL
C
C  WIDTH. DCELL = THE CELL WIDTH IN THOU.
C
      READ(5,8000) DCELL
 8000 FORMAT(F6.1)
      CELL = DCELL * 0.0254
      DECLL = CELL/10.0
      RPCELL = 1.0/DECLL
      SOLUT1 = SOLUT * RPCELL
C
C  WRITE VALUE OF INTEGRAL
C
C  WRITE VALUE OF INTEGRAL/CELL WIDTH
C
C  WRITE VALUE OF 1/CELL WIDTH.
C
      WRITE(6,9000)SOLUT
 9000 FORMAT(10X,'NUMERICAL VALUE OF INTEGRAL =',F10.0,/)
      WRITE(6,1111)SOLUT1,RPCELL
 1111 FORMAT(10X,'INTEGRAL ABSORPTION = ',F10.0,
     1'     RECIPRICAL CELL WIDTH = ',F6.0,/)
C
C  COMPLETE SOLUTION OF THE EQUATION.
C
      SOLUT3 = SOLUT2/CONVRT
C
C     WRITE CONCENTRATION
C
      WRITE(6,2222) SOLUT3
 2222 FORMAT(1X,//,30X,'TOTAL NUMBER OF PROTONS IS ',
     1F12.6,'PER 10E6 SI')
C
C  CALL PLOTTING ROUTINE.
C
      DO 600 IFILL = 1,100
      LINE(IFILL)  = EX
  600 CONTINUE
      WRITE(6,3333) LINE
 3333 FORMAT(1X,///,15X,100A1)
      CALL GRAPHIC
      WRITE(6,3333) LINE
      WRITE(6,3333) LINE
  100 CONTINUE
C
C
      STOP
      END
```

```
104.        SUBROUTINE DATSTOR
      C
      C  SUBROUTINE TO LIST AND PRINT THE DATA USED IN EVALUATING
      C
      C  THE INTEGRAL AND IN PLOTTING THE ABSORPTION PEAK.
      C
105.        DIMENSION MYNAM(51,2)
106.        COMMON SPACE (50,3)
107.        COMMON N
108.        COMMON AFREQ,BFREQ,ORDER
109.        COMMON TINT,SINT
110.        COMMON F
111.        INTEGER FX
112.        DATA FX/'F'/
      C
      C
113.        NPLUS = N + 1
114.        K = 0
115.        DO 10 MY = 1,NPLUS
116.        MYNAM(MY,1) = FX
117.        MYNAM(MY,2) = K
118.        K = K+1
119.     10 CONTINUE
120.        WRITE(6,100)
121.    100 FORMAT(6X,'FUNCTION NAME =',6X,'IO',15X,'I',
122.       115X,'FREQUENCY',12X,'F',/)
123.        WRITE(6,200)MYNAM(1,1),MYNAM(1,2),TINT,SINT,AFREQ,F
124.    200 FORMAT(6X,A1,I2,17X,F5.2,12X,F5.2,15X,F6.1,10X,F6.4)
125.        CFREQ = AFREQ - ORDER
126.        MY = 2
127.        DO 20 NY = 1,N
128.        CFREQ = CFREQ - ORDER
129.        IF(CFREQ.LT.BFREQ) CFREQ = BFREQ
130.        WRITE(6,200)MYNAM(MY,1),MYNAM(MY,2),SPACE(NY,2),CFREQ,
131.       1SPACE(NY,3)
132.        MY = MY + 1
133.     20 CONTINUE
      C
      C
133.        RETURN
134.        END


135.        SUBROUTINE GRAPHIC
      C                                                      T
      C SUBROUTINE TO PLOT THE ABSORPTION BAND AS ABSORPIVITY AGAINST
      C                                                      ^
      C THE FREQUENCY. THE OUTPUT OF THIS SUBPROGRAM IS STRONGLY
      C
      C DEPENDENT ON THE VALUE OF N IN THE MAIN PROGRAM, AND IS
      C
      C BEST WHEN N IS LARGE.

136.        DIMENSION ISTORE(50)
137.        DIMENSION ILINE(100)
138.        COMMON SPACE(50,3)
139.        COMMON N
140.        COMMON AFREQ,BFREQ,ORDER
```

```
      COMMON TINT,SINT
      COMMON F
      INTEGER BLANK,EX,DOT,STAR
      INTEGER ONE,TWO,THREE,FOUR
      INTEGER FIVE,SIX,SEVEN
      INTEGER EIGHT,NINE,ZERO
      DATA BLANK/' '/
      DATA EX/'X'/
      DATA DOT/'.'/
      DATA STAR/'*'/
      DATA ONE,TWO,THREE,FOUR/'1','2','3','4'/
      DATA FIVE,SIX,SEVEN/'5','6','7'/
      DATA EIGHT,NINE,ZERO/'8','9','0'/
C
C  DATA FOR PLOT LOADED.
C
C  CLEAR LINE
C
      DO 10 ICLEAR = 1,N
      ILINE(ICLEAR) = BLANK
   10 CONTINUE
C
C  CONVERT SPACE TO INTEGER
C
      DO 20 M = 1,N
      POINT = SPACE(M,3)*1000.0
      ISTORE(M) = IFIX(POINT)
   20 CONTINUE
C
      WRITE(6,100)
  100 FORMAT(1X,////,10X,'GRAPHICAL REPRESENTATION OF
     1 ABSORPTION BAND',///)
      WRITE(6,200)
  200 FORMAT(10X,'SCALE * 10E-2 FOR STAR (*)',/,10X,
     1 'SCALE * 10E-3 FOR X')
C
C    PUT ON Y AXIS.
C
      ILINE(  1) = ONE
      ILINE( 24) = TWO
      ILINE( 25) = DOT
      ILINE( 26) = FIVE
      ILINE( 50) = FIVE
      ILINE( 74) = SEVEN
      ILINE( 75) = DOT
      ILINE( 76) = FIVE
      ILINE( 98) = ONE
      ILINE( 99) = ZERO
      ILINE(100) = ZERO
      WRITE(6,300) ILINE
  300 FORMAT(12X,100A1)
      DO 30 J = 1,100
      ILINE(J) = BLANK
   30 CONTINUE
      ILINE(  1) = DOT
      ILINE( 25) = DOT
      ILINE( 50) = DOT
      ILINE( 75) = DOT
      ILINE(100) = DOT
      WRITE(6,300) ILINE
      DO 40 K = 1,100
```

```
190.       ILINE(K) = DOT
191.    40 CONTINUE
192.       WRITE(6,300) ILINE
193.       DO 70 K = 1,100
194.       ILINE(K) = BLANK
195.    70 CONTINUE
       C
       C      PLOT DATA
       C
196.      FREQ = AFREQ-ORDER
197.      IFREQ = IFIX(FREQ)
198.      JFREQ = IFIX(BFREQ)
199.      DO 50 L = 1,N
200.      IF( IFREQ.LT.JFREQ) IFREQ = BLANK
201.      I = ISTORE(L)
202.      IF(I.LE.1)I=1
203.      IF(I.GE.101)M=I/10
204.      IF(M.GE.101)J=M/10
205.      IF(M.GE.101)GOTO102
206.      IF(I.GE.101)GOTO101
207.      IF(I.EQ.0)I=1
208.      ILINE(I) = STAR
209.      GO TO 111
210.   101 ILINE(M) = EX
211.       GO TO 111
212.   102 ILINE(J) = ZERO
213.   111 ILINE(1) = DOT
214.       WRITE(6,600) IFREQ,ILINE
215.   600 FORMAT(6X,I4,2X,100A1)
216.       IF = IFIX(ORDER)
217.       IFREQ = IFREQ-IF
218.       DO 60 IJ = 1,100
219.       ILINE(IJ) = BLANK
220.    60 CONTINUE
221.    50 CONTINUE
222.       RETURN
223.       END
```

The above program should run on any FORTRAN compiler with the following control cards, those given being of the correct form for the I.C.C.C. Network Operating System. The categories given being for the largest possible job size on this system.

```
JOB(_______ ,J13,SP4,CM50000,T600,LC5120)   (Insert jobnumber)
PASSWORD(__________________)                (Insert password)
MNF(T,D)
MAP(P)
```

A2.3. The Model for the Growth of a Bubble in an Infinite Quartz Crystal.

This program provides a numerical evaluation of the solution to the diffusion equation discussed in chapter 5. The program first solves the equation for a number of different radii with an extremely small bubble nuclei. After this first solution for a very short time, the actual amount of water in the bubble is calculated and this then used to give a new bubble diameter for the next time increment. The time increments, initial bubble radius, diffusion radii, diffusion coefficient, temperature of bubble growth and the starting hydroxyl concentration in the crystal are all prescribed in the program, so the only data input is one integer value which increases the initial concentration by a factor of ten for the given number of times, and similarly reduces the diffusion coefficient by a factor of ten for a similar number of times. The program functions as a number of nested do loops which modify these values, and create solutions for the dif-ferent radii at each of the different times. The solution at each radius calls on the Library subroutine S15ADF(X,IFAIL) from the NAG5F program library at Imperial College. This sub-routine gives solutions to the function erfc X, the complement to the Gaussian Error Function. Documentation is again in the form of comment cards.

```
1.      PROGRAM DIFFUSE(INPUT,OUTPUT,TAPE5=INPUT,TAPE6=OUTPUT)
C
C       PROGRAM TO MODEL THE GROWTH OF A FLUID INCLUSION
C
C       IN A QUARTZ CRYSTAL.  BY MERVYN EWARD JONES
C
C       ROOM 242    STRUCTURAL GEOLOGY
C
2.      DIMENSION T(10),R(10)
3.      DIMENSION STORE(10),SAVE(10)
4.      COMMON /BLK1/ T,R
5.      COMMON /BLK2/ DIFF,CONC,A
```

```
C
C   READ IN VALUE FOR THE NUMBER OF TIMES THE LOOP FOR
C
C   VARYING THE INITIAL CONCENTRATION AND THE DIFFUSION
C
C   COEFFICIENT IS TO OPERATE.
      READ(5,1000) IC
 1000 FORMAT(I2)
      D = DIFF
      CONCO = CONC
C
C   READ VALUES FOR INITIAL CONCENTRATION AND DIFFUSION
C
C   COEFFICIENT FROM THE BLOCK DATA STATEMENT
C
C   SET UP LOOPS TO MODIFY THE DIFFUSION COEFFICIENT AND
C
C   THE INITIAL CONCENTRATION AT THE END OF EACH CYCLE.
C
      DO 200 MIN = 1,IC
      DO 300 NIN = 1,IC
C
C  WRITE VALUES FOR THE DIFFUSION COEFFICIENT AND THE
C
C  INITIAL CONCENTRATION.
      WRITE(6,2000) D,CONCO
 2000 FORMAT(30X,E12.5,30X,E12.5)
      C1 = CONCO
      AA = A
C
C  READ THE INITIAL BUBBLE DIAMETER FROM THE BLOCK DATA
C
C  STATEMENT
C
      SUM = 0.0
C
C   SET UP LOOP TO READ VALUES OF TIME FROM THE BLOCK
C
C   DATA STATEMENT.
C
      DO 100 J = 1,10
      RSAVE = 0.0
      TT = T(J)
C
C   SET UP LOOP TO READ VALUES OF THE DIFFUSION RADIUS
C
C   FROM THE BLOCK DATA STATEMENT.
      DO 500 K = 1,10
      RR = R(K)
      IF(RR.LE.AA)RR = RR + AA
C
C   SOLVE THE DIFFUSION EQUATION
C
      CAD = (C1*AA)/RR
      SAD = (RR-AA)/2.0*SQRT(D*TT)
C
C  EVALUATE THE ERROR FUNCTION
C
      IFAIL = 1
      PAD = S15ADF(SAD,IFAIL)
```

```
C
C  CALCULATE THE CONCENTRATION AT RADIUS RR AND TIME TT
C
      YSOL = CAD*PAD
      C2 = CONCO - YSOL
      SAVE(K) = C2
C
C  WRITE THE TIME,THE RADIUS, THE BUBBLE DIAMETER AND THE
C
C  CONCENTRATION AT THIS TIME AND RADIUS.
C
      WRITE(6,3000) TT,RR,AA,C2
 3000 FORMAT(10X,E12.5,10X,E12.5,10X,E12.5,10X,E20.10)
C
C  CALCULATE THE VOLUME OF THE DEHYDRATING AREA
C
      IF(K.EQ.1)GOTO10
      VOL = (((RR - RSAVE)**3.0) *3.14*3.0)/4.0
      GO TO 20
   10 VOL = (((RR - AA)**3.0)*3.14*3.0)/4.0
   20 STORE(K) = (CONCO - C2) * VOL
      RSAVE = 0.0
      SUM = SUM + STORE(K)
      RSAVE = RR
C
C  END OF CYCLE OF RADII
C
  500 CONTINUE
C
C  CALCULATE THE BUBBLE DIAMETER FOR THE NEXT CYCLE
C
      C1 = SAVE(1)
      IF(SUM.LE.0.0) GOTO30
      AB = SQRT((SUM*4.14E-13)/6283.1854)
      AA = AB/2.0
      GO TO 100
   30 WRITE(6,4000) SUM
 4000 FORMAT(10X,'ERROR',10X,E12.5)
C
C  END OF COMPLETE TIME CYCLE
C
  100 CONTINUE
C
C  DIVIDE DIFFUSION COEFFICIENT BY 10 FOR THE NEXT TIME CYCLE
C
      D = D/10.0
C
C  END OF DIFFUSION COEFFICIENT CYCLE
C
  300 CONTINUE
C
C   MULTIPLY THE INITIAL CONCENTRATION BY 10
C
      CONCO = CONCO * 10.0
C
C   END OF INITIAL CONCENTRATION CYCLE, END OF PROGRAM
C
  200 CONTINUE
      STOP
      END
```

```
      BLOCK DATA
C
C     THIS BLOCK DATA SUBPROGRAM CONTAINS THE VALUES OF TIME
C
C     AND THE INITIAL VALUES OF THE DIFFUSION RADIUS, THE
C
C     BUBBLE NUCLEI RADIUS, THE DIFFUSION COEFFICIENT, AND
C
C     THE HYDROXYL CONCENTRATION.
C
      DIMENSION T(10),R(10)
      COMMON /BLK1/T,R
      DATA T/0.1,1.0,10.0,1.E2,1.E3,1.E4,1.E5,1.E6,1.E7,1.E8/,
     1R/1.5E-8,1.E-7,5.E-7,1.E-6,5.E-6,1.E-5,5.E-5,1.E-4,5.E-4,
     21.E-3/
      COMMON /BLK2/DIFF,CONC,A
      DATA DIFF/1.E-4/,CONC/1.E18/,A/1.E-20/
      END
```

This program gives solutions for a single bubble in an infinite crystal. Obviously solutions which give diffusion paths exceeding the mean interbubble distance in heat treated synthetic quartz crystals should be ignored. Equally bubble diameters exceeding those typically recorded for bubbles in heat treated synthetic quartz crystals indicate solutions which should be ignored. From heating experiments, and T.E.M. observations this restricts the correct solution for the diffusion coefficient to that value which will give a bubble diameter in the range 900 to 1500 $\mathring{A}$ in 24 hours with mean diffusion paths of the order of 1 micron and an initial concentration of the order of 10^{20}H atoms Cm^{-3}. The effect of hydrostatic pressure on this diffusion coefficient would be indi--cated by repeating the above solution for a time of 10 minutes instead of 24 hours but satisfying the other parameters.

Solutions of this program for the conditions of interest are given in chapter 5 figure 5.10.

The following control cards are necessary to run this program on the Imperial College computers. The program will run on the minimum category (J1) but this will not give the full output. With IC = 10, J13 is necessary to get the full output.

```
JOB(_______,J13,SP4,CM50000,T600,LC5120)     (Insert jobnumber)
PASSWORD(____________________)                (Insert password)
MNF(T,D,8=DIFFUSE)
MAP(P)
PROC(N=NAG5F)
LIBRARY(NAG5F)
DIFFUSE.
```

* * * * * *

Appendix 3. THE SOLID CONFINING PRESSURE MEDIUM DEFORMATION MACHINE.

A3.1 INTRODUCTION

Experimental studies of the mechanical properties of quartz single crystals and quartzites, necessitates the use of apparatus capable of applying large loads and confining pressures at high temperatures. The development of a machine capable of safely meeting these conditions is difficult, and in all cases only two basic designs have proved successful. The first is a steel vessel pressurized with a chemically inert gas (such as nitrogen) which contains an internal furnace to heat the sample. Apparatus of this type has been successfully developed and used by Mervyn Paterson and has provided all of the more reliable and useful mechanical data for quartz (Hobbs et al 1972, Morrison Smith et al 1976). The second alternative is to use an internally heated steel vessel using a soft crystalline solid to apply the confining pressure. This is the Solid Confining Pressure Medium Deformation Machine which was developed and used by Griggs and Co-workers in America. This apparatus is a triaxial modification of the solid medium pressure machines used in experimental petrology. Unfortunately

the solid confining medium machine has proved to be vastly inferior to the gas confining medium machines on all counts except for that of safety and the pressures attainable. High pressure gas systems are potentially very dangerous because of the large strain energy of the compressed gas, thus gas pressure vessels have to be large (thick walled), and housed in an explosion proof shelter. The pressure seals on such apparatus also tend to be difficult to construct, and if a suitable design is not developed are a source of continuous problems. The development of a gas confining pressure machine is therefore time consuming and because of this I settled for second best and concentrated on developing an improved version of the Griggs type solid confining pressure machine. The inherent problems in the Griggs design are, 1). the specimen is subjected to a large temperature gradient, 2). it is difficult to be certain of the actual hydrostatic pressure on the vessel, and 3). the system requires an external load cell so that the friction in the system is measured together with the sample strength and has to be calibrated out of the results, creating a large area of uncertainty. It only proved possible to tackle the first of these problems in this design, by increasing the furnace length and insulating it from the sample. However this was itself not without problems and further development is necessary.

A3.2 THE PRESSURE VESSEL

The pressure vessel is a thick walled cylinder with an inter-nal diameter of one inch. To calculate the necessary wall thick-ness of this cylinder for it to withstand an internal pressure of 10 or 20 kilobars, the thick cylinder formula must be applied. Solutions of this formula indicate that the stress decreases only slowly with increasing radius so that the cylinder would

require a disproportionately large diameter to support the internal pressure. This problem can be largely overcome by producing a compound vessel in which two coaxial thick walled cylinders are shrink fitted together producing a compressive hoop stress in the inner cylinder. (See figure A3.1). The magnitude of this hoop stress depends on the isothermal misfit of the two cylinders, the larger this overlap, the greater this stress and hence the greater the internal pressure that can be supported by the vessel. These formula are available in many books on mechanics, for instance "The Strength of Materials" by G.H.Ryder (1961). It was the anal-ysis given in this book which was used in the construction of the pressure vessel for the solid medium deformation machine. From these equations it was calculated that an inner tube of approximately 3 inches outside diameter with a bore of 1 inch, and an outer tube of 6 inches outside diameter with an approximate inside diameter of 3 inches, with an actual interference between the tubes of 0.0198 inches before shrinkage, would support an internal hydrostatic pressure of 20 Kilobars. Both tubes were constructed in H50 steel which maintains a high strength at temperatures up to 500°C.

Figure A3.1

Cross section of the pressure vessel.

Scale 2cm on the drawing = 1 inch on the actual vessel.

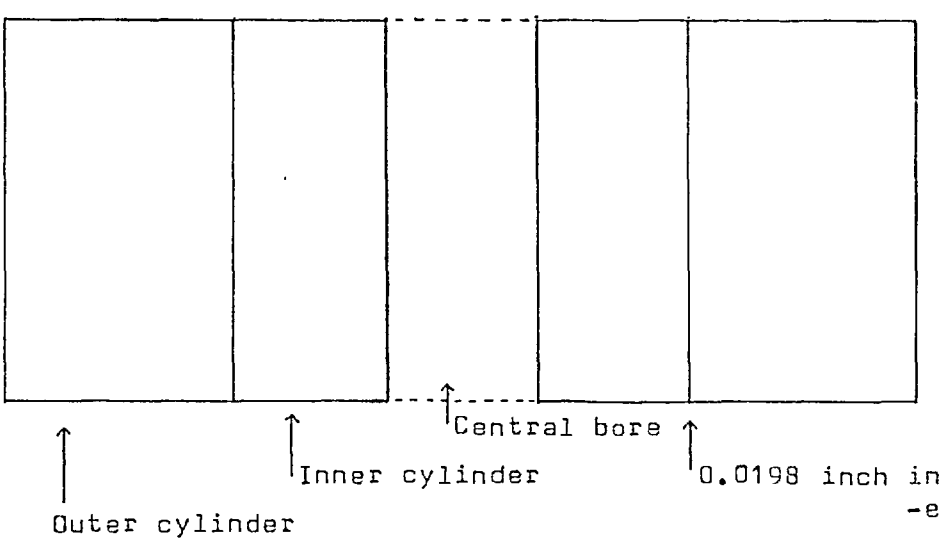

A3.3 THE DOUBLE YOKE AND PRESSURE ASSEMBLY.

The confining pressure is applied by loading a soft solid inside the pressure vessel. This load is applied by a hydraulic jack, acting on the mobile portion of a special double yoke which hangs in the loading frame. The principle of operation of this assembly is shown in figure A3.2.

Figure A3.2 (Not to scale).

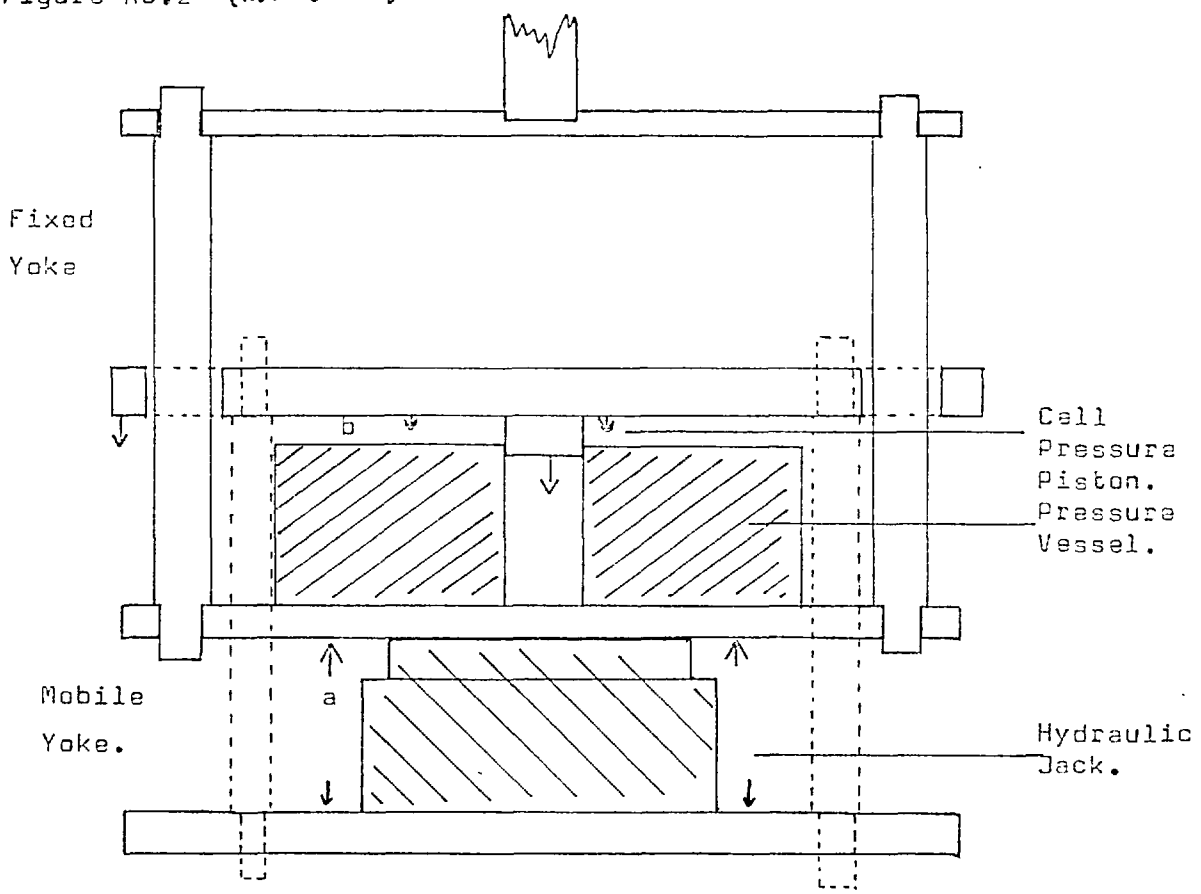

When the jack is pressurized, the distance a is increased as the mobile yoke is pushed down, and at the same time the distance b decreases. As a result of this, all the load is applied to the cell pressure piston which strains the soft solid confining medium. The cell pressure attained is related directly to the cross sectional area of the cell pressure piston (= the internal diameter of the pressure vessel) and to the fluid pressure applied to the ram. Drawings of the yoke plates are given in figure A3.3.

Fig A3·3.

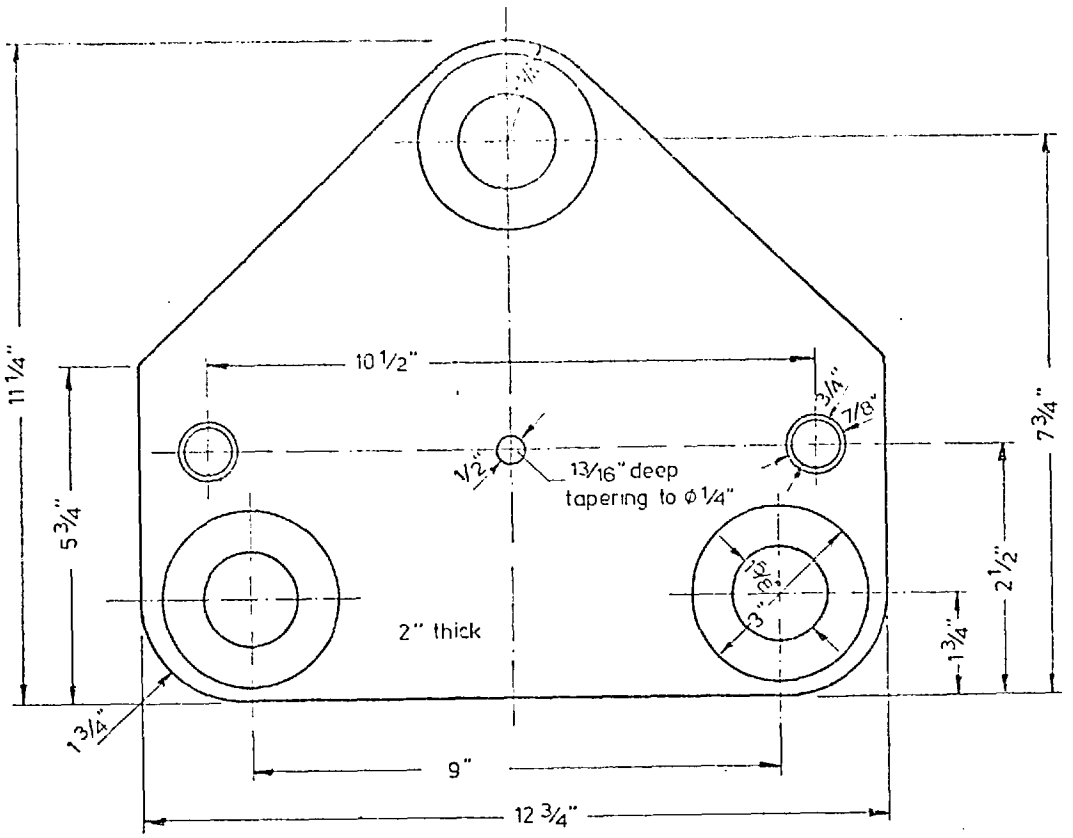

Mobile yoke top

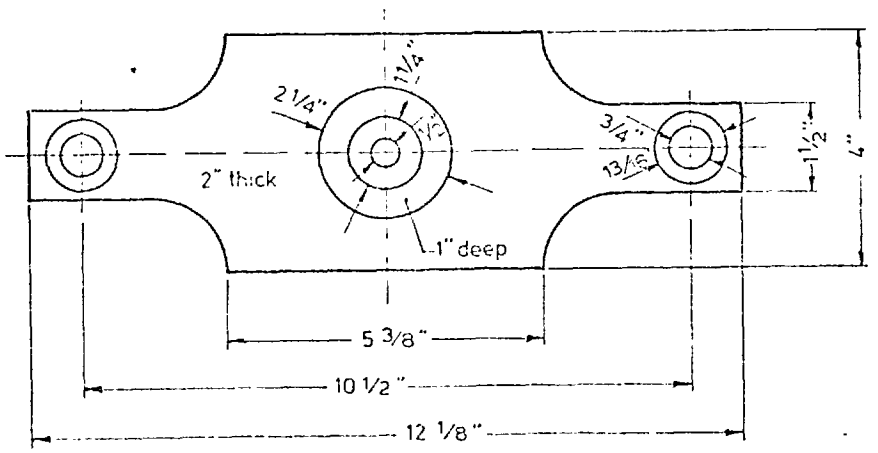

Fixed yoke top

Fig A3·3

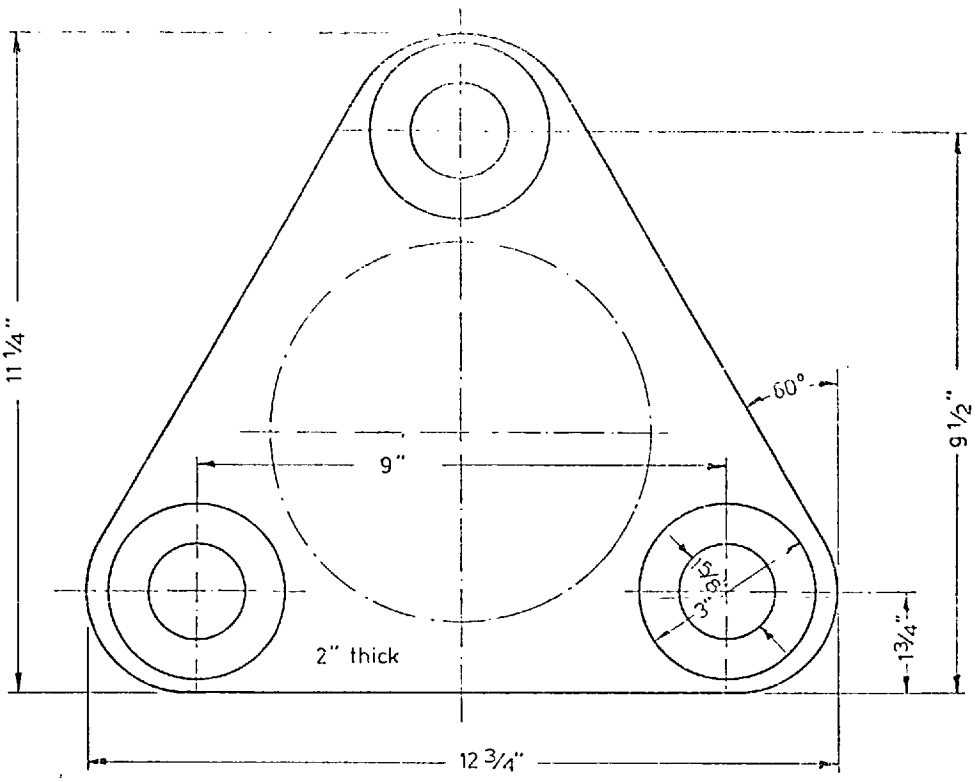

Mobile yoke bottom

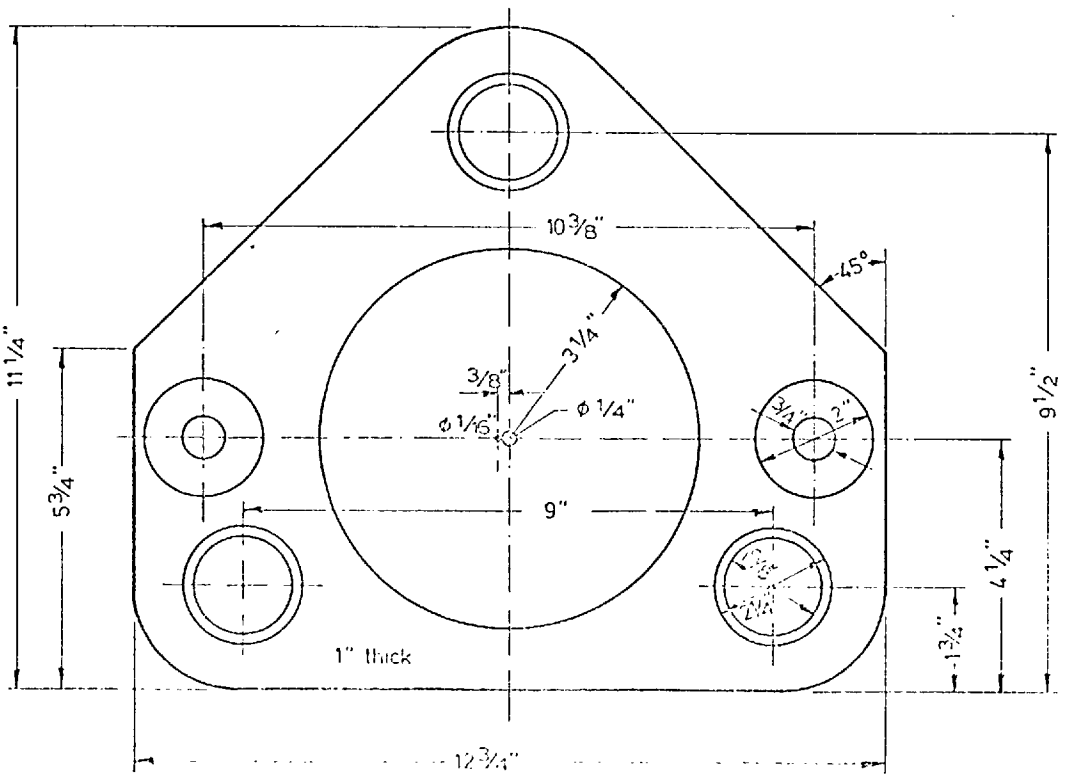

Fixed yoke bottom

A3.4 THE INTERNAL FEATURES OF THE PRESSURE VESSEL.

The design of the components which function inside the pressure vessel is by far the most important aspect in the development of a solid confining pressure medium deformation machine. Within the small volume of the pressure vessel it is necessary to arrange the carefully machined blosks of confining medium material, a furnace, a thermocouple, the power supply to the furnace and a system for the axial loading of the specimen. It is necessary for these components to function properly at temperatures of up to 1100^{o}C. and cell pressures of 20Kbars. The pistons used to apply the axial load have to withstand this load plus the vertical component of the cell pressure which in total may be as much as 50 Kbars. Details of the internal layout of the pressure vessel developed for this machine, together with the materials used and their function are given in figure A3.4.

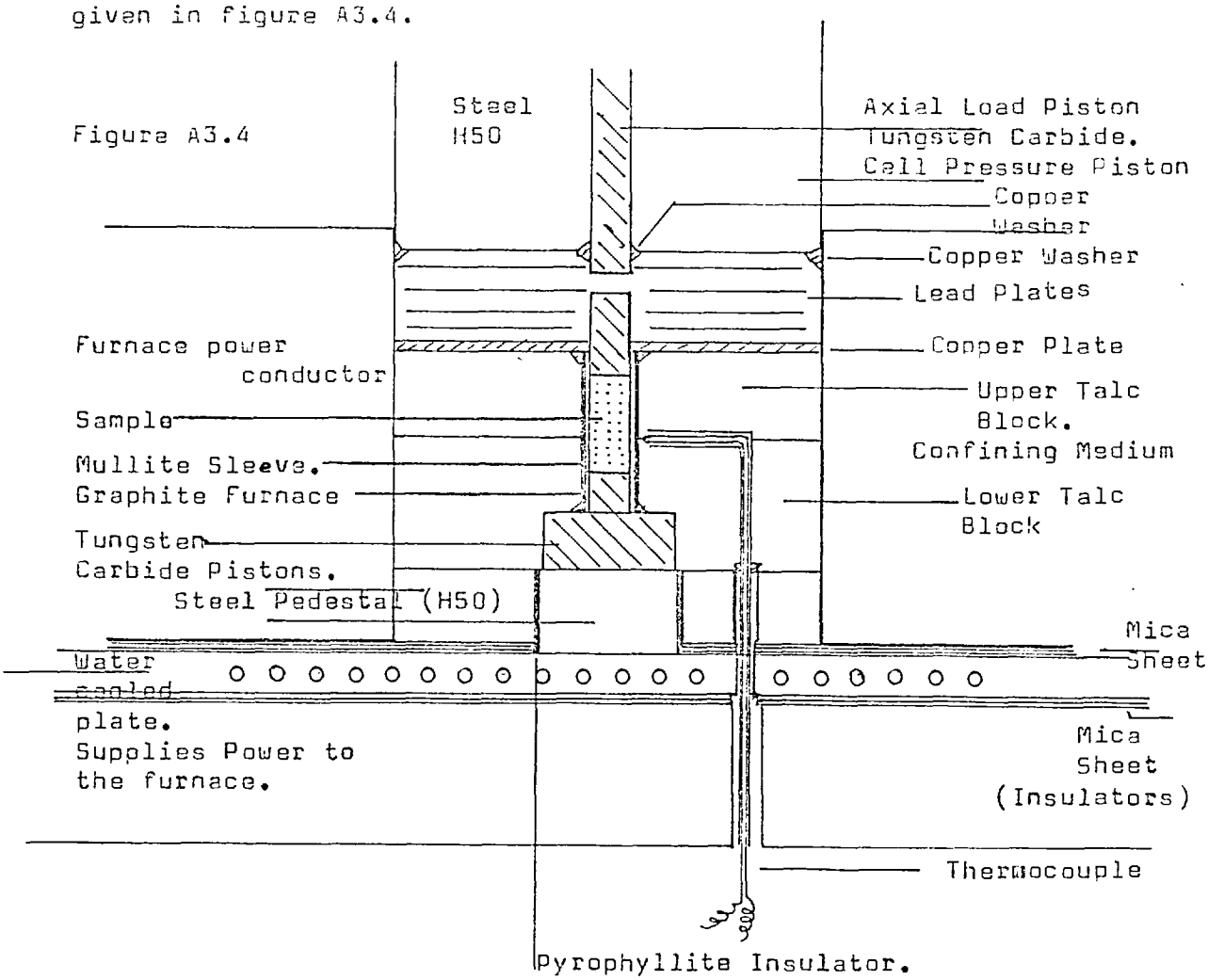

Figure A3.4

A3.5 THE COMPLETELY ASSEMBLED MACHINE.

Figure A3.5 shows the completely assembled double yoke with the pressure vessel, confining pressure ram and the axial loading column in place. This whole unit hangs in a Heard type loading (Rutter 1970) frame with specially extended tie bars, and utilizes the normal motor, gear train and ball screw arrangement used in the standard Heard deformation machines (at Imperial College) for applying the axial load. The axial load is measured using a load cell specially constructed for this task which is placed between the base of the ball screw and the top of the axial loading column. This load cell is a strong but elastic steel column fitted with strain gauges connected in the normal bridge arrangement, and energized with a stabilized 12 Volt d.c. supply.

Plate A3.1 is a photograph of the fully assembled machine.

A3.6 THE ELECTRONICS.

1) Axial Loading. The axial load was applied by a 240volt geared motor with forward and reverse drive selected by a switch adjacent to the motor housing. Power was supplied directly from the 240 volt main.

2) Force Measurement. As stated in section A3.5, the force acting along the axial column was measured with a load cell which was basically a strain gauged steel block. The strain gauges were connected in a standard bridge circuit and were continuously energized using a stabilized 12 volt d.c. supply. The output was displayed on a digital volt meter and/or a flat bed chart recorder. On the output side, a second stabilized d.c. supply was used to give a variable bias voltage. This could be set using a potential divider incorporating a variable potentiometer to give

Fig. A3·5·

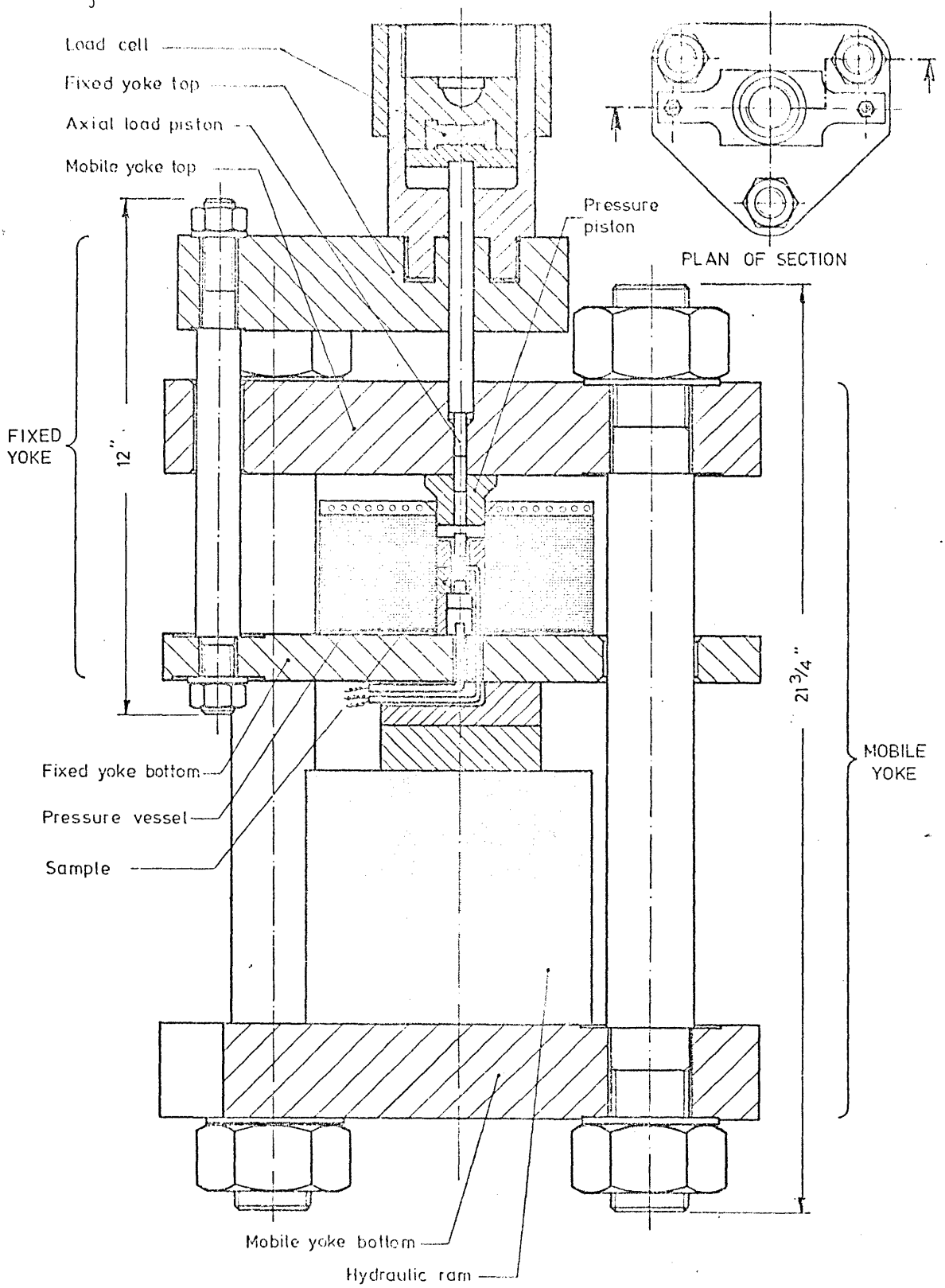

Solid confining pressure medium deformation machine

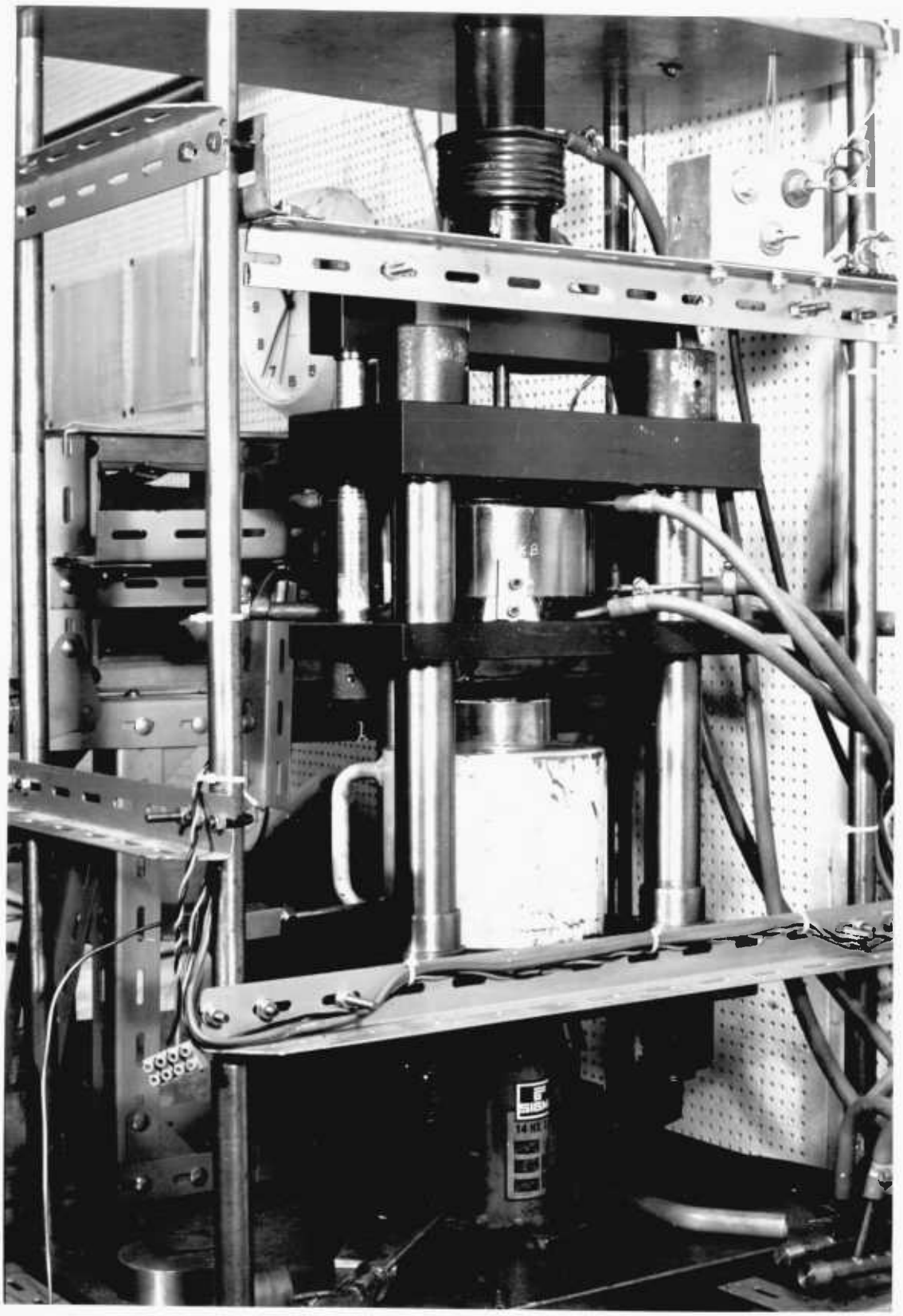

Plate A3.1

THE SOLID CONFINING PRESSURE MEDIUM DEFORMATION MACHINE.

zero volts output from the load cell when the system was under no load.

3) Temperature measurement. The temperature at the centre of the pressure vessel was measured using a Pt/Pt13%Rh. thermocouple cased in a crystallized alumina insulator. This was connected by compensating cable to a cold junction at 20°C. and to the furnace temperature controller. A digital volt meter was used to display the value of this output.

4) The furnace power supply and temperature control. The graphite furnace tube[1] operated at low voltages (less than 10 volts) and very high currents (up to 500amps.). This was achieved using three large transformers, which were operated in phase with their outputs connected in series. Stabilized 240volt mains was supplied via a Variac variable transformer directly to two of these trans-formers which had their inputs wired in parallel, and through a thyristor gate operated by an Eurotherm phase angle type proportional temperature controller to the other.

The output current of the transformer bank was measured using a current transformer and displayed on an ammeter, the voltage across the output stage was also monitored on a conventional voltmeter.

The high current supply was carried using 0.5inch diameter copper bar, but even with conductors of this thickness, some energy was lost in heating the bar, and it was necessary to minimize the length of these conductors if high temperatures (over 1100°C.) were to be obtained.

Figure A3.6 is an idealized wiring diagram for this apparatus.

Footnote 1. The furnace tube was longer than that used in the Griggs machines, extending 0.25 inches beyound the sample at each end and insulated from the loading pistons, except at its ends.This greatly improved the temperature gradients on the specimen.

Figure A3.6

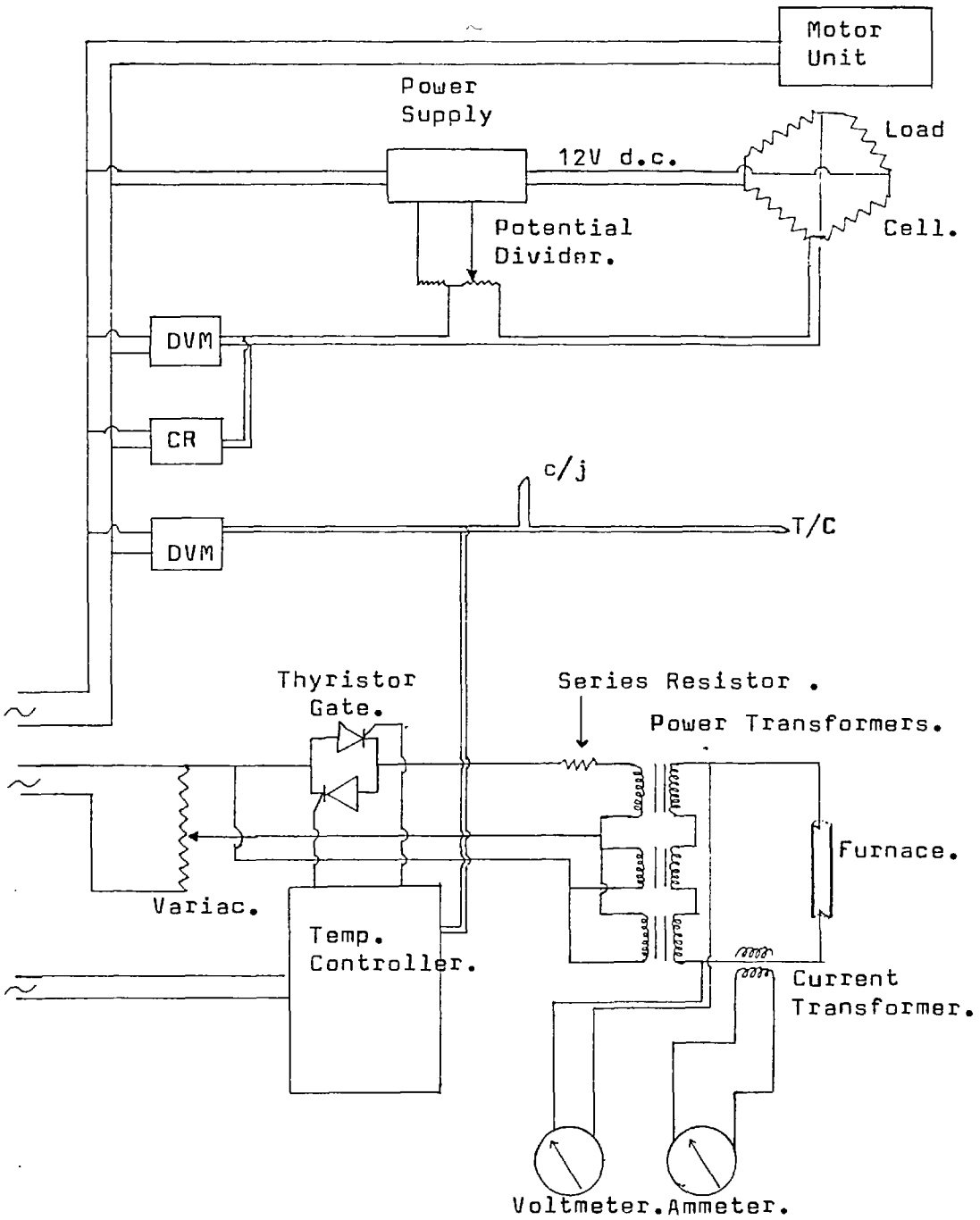

Idealized and simplified wiring diagram of the solid confining pressure medium deformation machine.

A3.7 CALIBRATION.

In this section the various calibration curves for the solid medium deformation machine are given, in most cases these curves are self explanatory, and details will be given in the figure captions, not as a separate text.

Figure A3.7

20 Ton Load Cell Calibration.
Load Applied With a 15 Ton Denison Creep Machine.

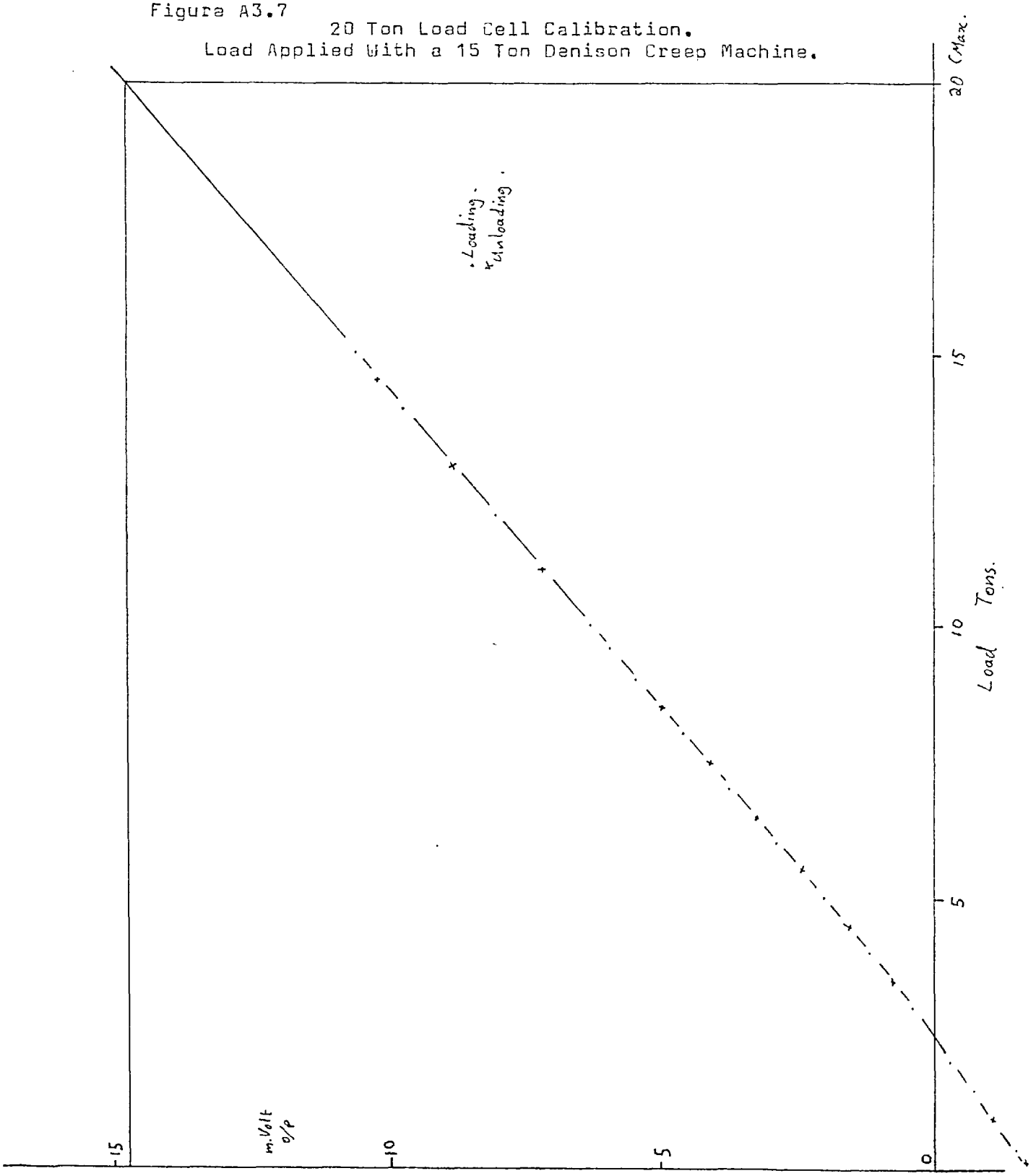

Figure A3.8. Furnace Temperature Produced by Different Applied Voltages.

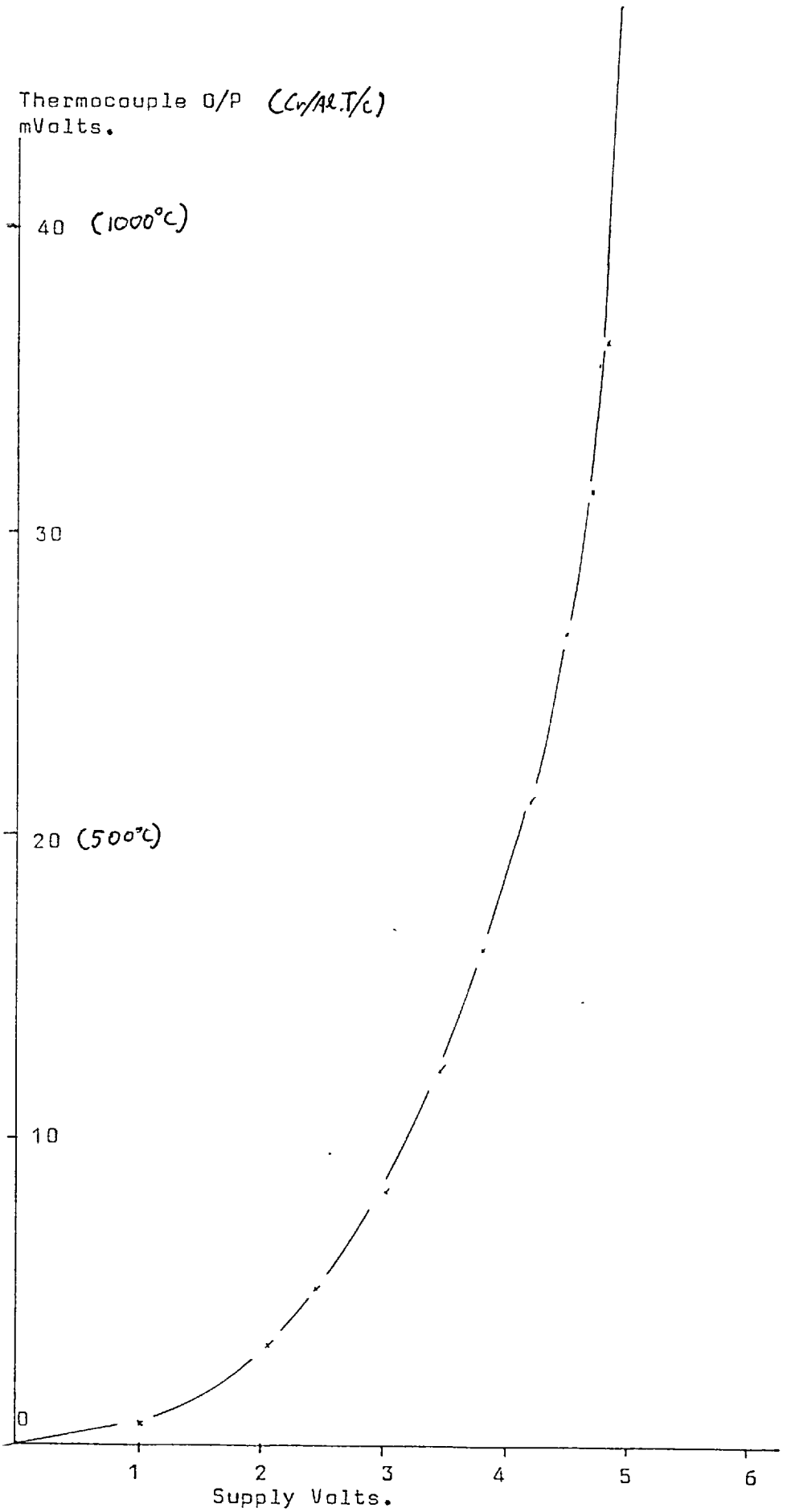

Figure A3.9. Furnace Temperatures produced in Response to Different Applied Currents.

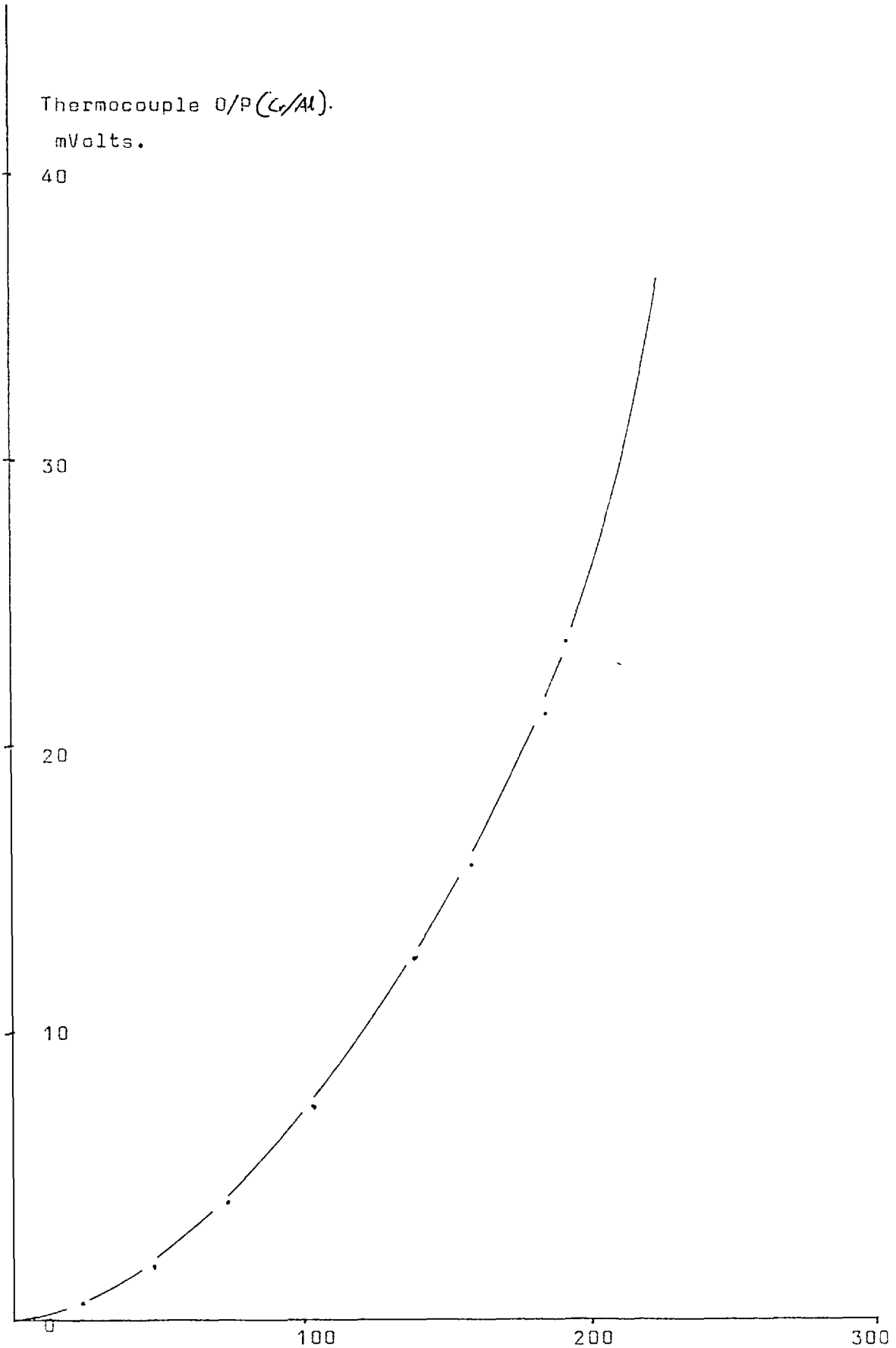

Figure A3.10 Furnace Temperature versus Furnace Input Power.

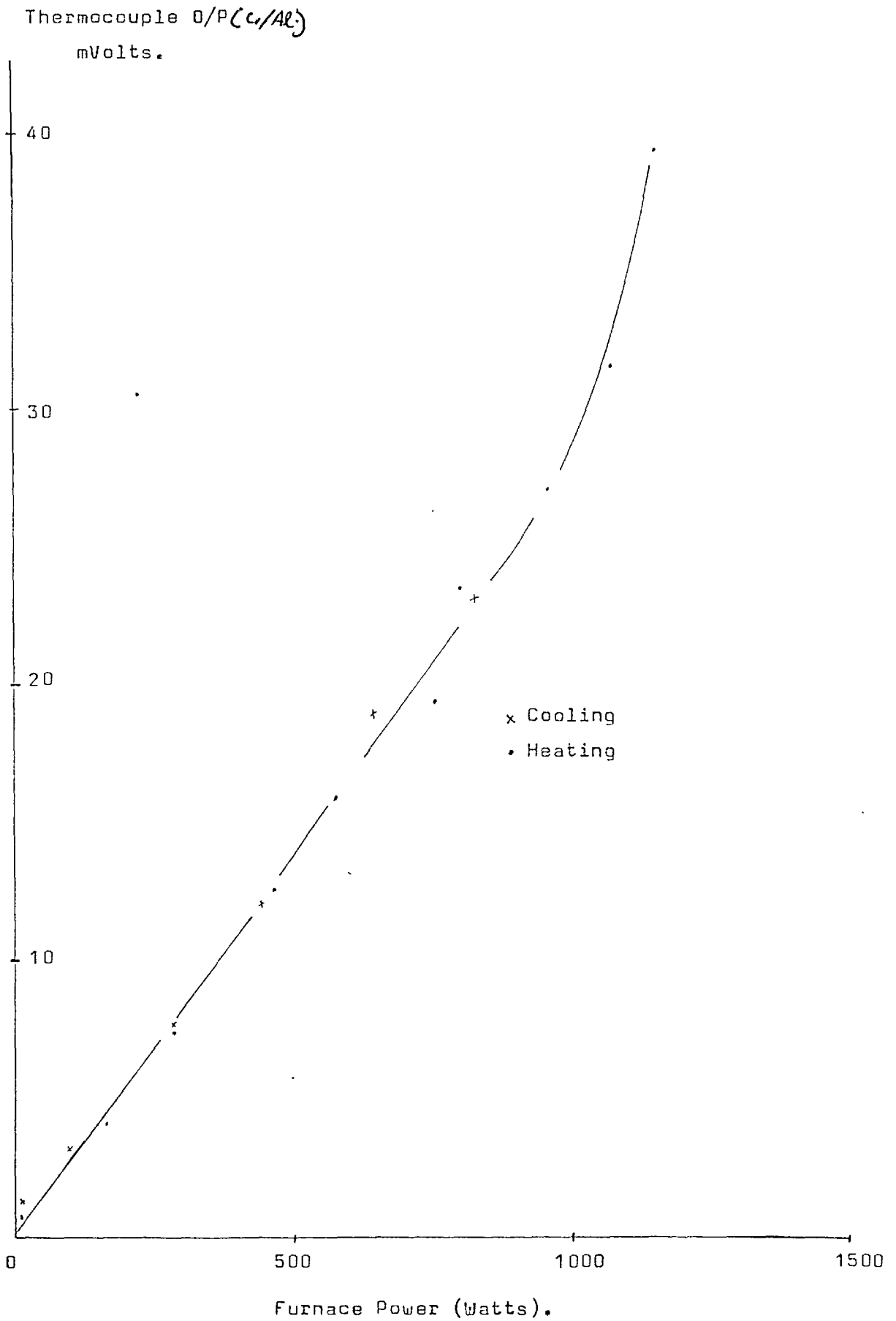

Figure A3.11.

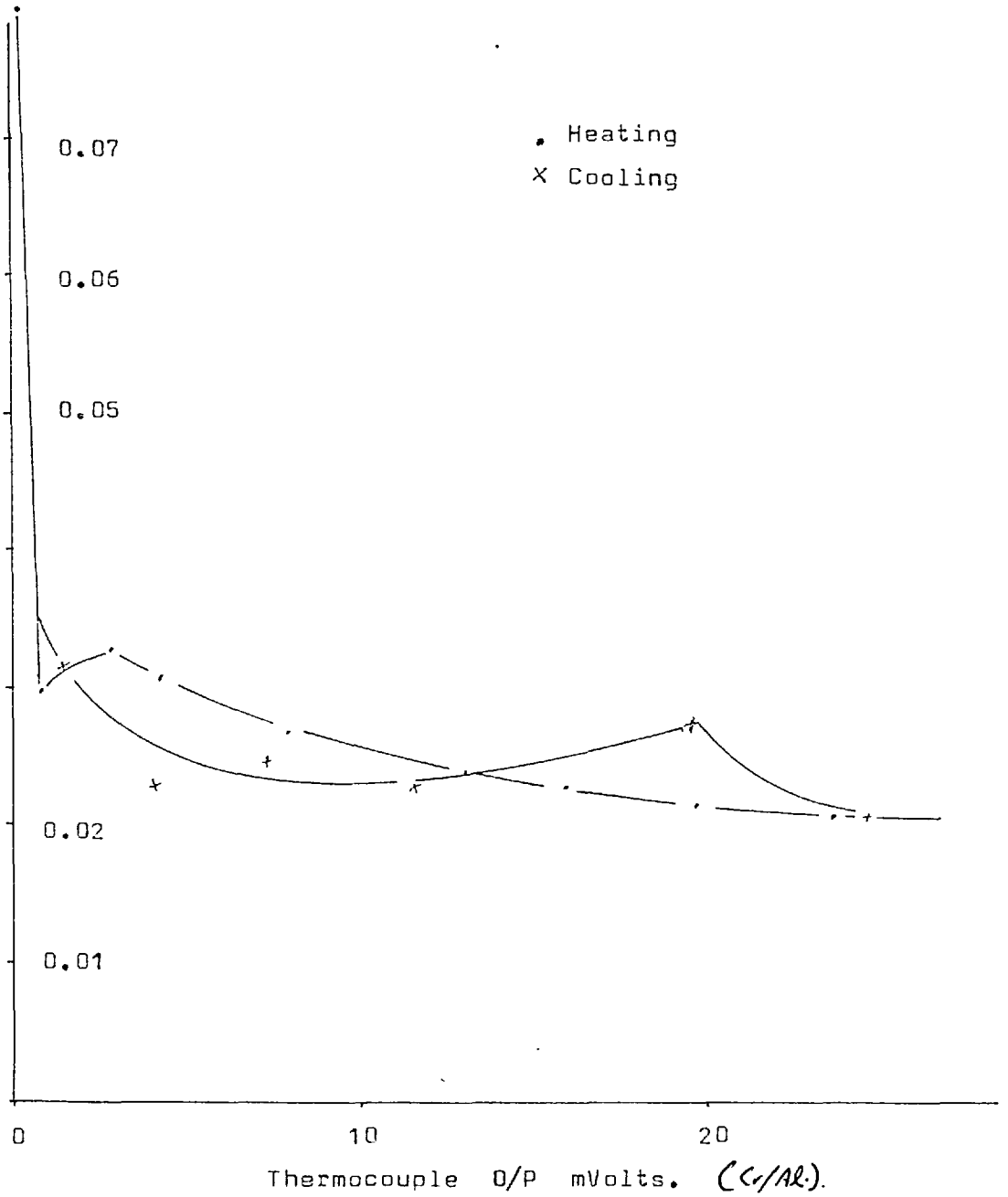

The change in resistance of the graphite furnace tube with temperature during one cycle of heating and cooling.

Figure A3.12 The Pressure Increase Caused by an Increase in Furnace Temperature.

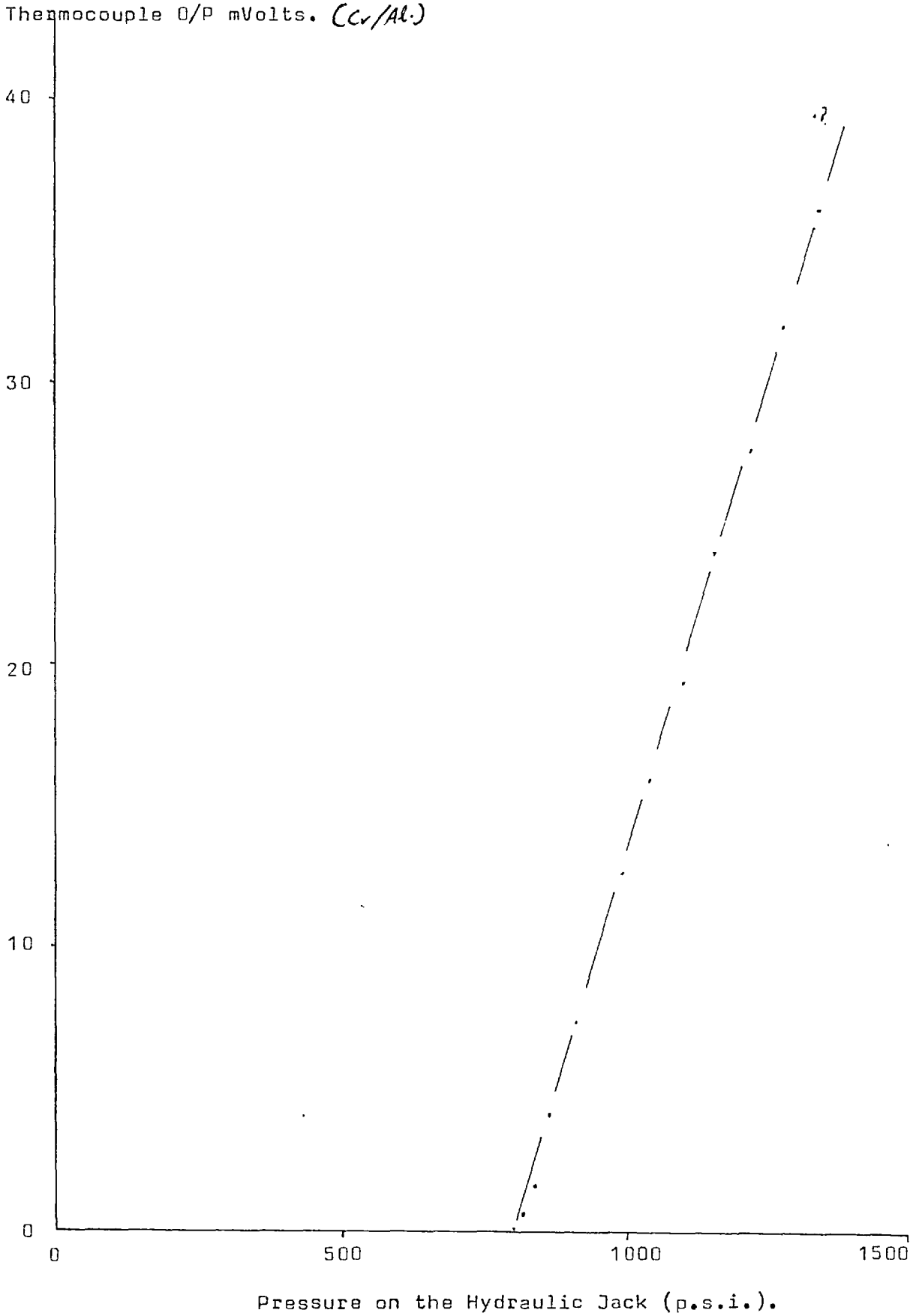

The large number of different but related calibration curves for the furnace are necessary because the thermocouple which measures the furnace temperature and operates the proport--ional controller is very susceptable to damage inside the pressure vessel. If the behaviour of the furnace is well known, it is often possible to save a test in the event of thermocouple failure. This is accomplished by bypassing the proportional controller and providing power to the furnace transformers directly from the variac. By carefully monitoring the supply volts, and amps,to the furnace from these transformers, and comparing these with the calibration curves, it is possible to maintain a fairly constant temperature manually and have a good idea as to what that temperature is.

* * * *

Bibliography.

Bibliography.

Alexander H. and Haasen P., 1968, Dislocations and Plastic Flow in the Diamond Structure., Solid State Physics,V22,pp27-158.

Ansell G.A. and Lenel F.V.,1960, Criteria for Yielding of Dispersion -Strengthened Alloys.,Acta Metall., V8, pp612-616.

Arnold G.W.(Jr.),1960, Defects in Natural and Synthetic Quartz, J.Phys.Chem.Solids., V13, pp306-320.

Augustine F. and Hale D.R., 1960, Topography and Etch Patterns of Synthetic Quartz . J.Phys.Chem.Solids, V13,pp344-346.

Ayensu A. and Ashbee K.H.G., 1977, The Creep of Quartz Single Crystals with Special Reference to the Mechanism by which Water Accommodates Dislocation Glide. Phil. Mag., V36, pp713-723.

Baeta R.D. and Ashbee K.H.G., 1968, Evidence of Plastic Deform--ation in Quartz at Atmosphereic Pressure (Abs). 4thEuropean Regional Conference on Electron Microscopy. Rome,Bocciarelli D.S.(ed). p427.

Baeta R.D. and Ashbee K.H.G., 1969a, Slip Systems in Quartz 1. Experiments. Am.Mineral., V54, pp1574-1582.

Baeta R.D. and Ashbee K.H.G., 1969b, Slip Systems in Quartz 2. Interpretation. Am. Mineral., V54 , pp1574-1582.

Baeta R.D. and Ashbee K.H.G., 1970a, Mechanical Deformation of Quartz. 1. Constant Strain Rate Compression Experiments. Phil. Mag., V22, pp601-623.

Baeta R.D. and Ashbee K.H.G., 1970b, Mechanical Deformation of Quartz. 2. Stress Relaxation and Thermal Activation Parameters. Phil.Mag., V22, pp624-635.

Baeta R.D. and Ashbee K.H.G., 1973, Transmission Electron Microscopy Studies of Plastically Deformed Quartz. Phys.Stat.Sol., (a), V18, pp155-170.

Baldermann M.A., 1974, The Effect of Strain Rate and Temperature on the Yield Point of Hydrolytically Weakened Synthetic Quartz. J. Geophys. Res., V79, pp1647-1652.

Ballmann A.A., Laudise R.A. and Rudd D.W., 1966, Synthetic Quartz with a Mechanical Q Equivalent to Natural Quartz. Appl. Phys. Letts., V8, pp53-54.

Bambuer H.U., 1961, Spurenelementgehalte und γ - Farbzentren in Quarzen aus Zerrkluften der Schweizen Alpine. Schweiz. Mineral. Petrog. Mitt., V41, pp335-369.

Barker C. and Sommer M.A., 1974, Potential Method of Geobarometry using Synthetic Quartz. Nature, V250, pp402-404.

Bell R.P., 1959, The Proton in Chemistry. Methuen,London.

Biggs A., 1975a, Hydroxyl Impurities and the Formation and Distribution of Cavities in Melt Grown MgO Crystals. J.Materials Sci., V10,pp729-736.

Biggs A., 1975b, The Formation of Hydrogen Filled Cavities in MgO Crystals Annealed in Reducing Atmospheres.
J. Materials Sci., V10, pp737-746.

Blacic J.D., 1975, Plastic Deformation Mechanisms in Quartz: The Effect of Water.
Tectonophysics, V27, pp271-294.

Bonner O.D. and Curry J.D., 1970, Infrared Spectra of Liquid H_2O and D_2O.
Infrared Physics. V10, pp 91-94.

Brace W.F. and Walsh J.B., 1962, Some Direct Measurements of the Surface Energy of Quartz and Orthoclas.
Am. Mineral., V47, pp1111-1122.

Brown C.S. and Thomas L.A., 1960, The Effect of Impurities on the Growth of Synthetic Quartz. J.Phys.Chem.Solids, V13,pp337-343.

Brunner G.O., Wondratschek H. and Laves F., 1959, Uber die Ultrarotabsorption des Quarzes im 3μ-Gehiet.
Naturwiss, V24, p664.

Brunner G.O., Wondratschek H. and Laves F., 1961, Ultrarotuntersuchungen uber den Einbau von H in Naturlichen Quarz.
Z.Elektrochem., V65, pp735-750.

Campbell J.A., 1970, Chemical Systems, Energetics, Dynamics and Structure. W.H.Freeman and Co., San Francisco.

Carslaw H.S. and Jaeger J.C., 1959, Heat Conduction in Solids. Oxford University Press, London.

Christie J.M., 1977, A paper read at the Royal Society Meeting on Creep of Engineering Materials and of the Earth, held on 24th and 25th Feb. 1977 in London. This article was however not includ--ed in the written volume on this meeting. Phil. Trans. R. Soc. Lond.(A), V288, pp1-236, 1978.

Clarke K.J., 1972, Fluid Inclusions as Geothermometers in Structural Geology.
M.Sc. Dissertation, Univ. of Lond. Unpublished.

Cohen A.J. and Hodge F.S., 1958, Zonal Specificity and non--Specificity of Certain Impurities During Growth of Synthetic Alpha Quartz.
J.Phys.Chem.Solids, V7, pp361-362.

Cohen A.J., 1960, Substitutional and Intersubstitutional Aluminium Impurity in Quartz, Structure and Colour Centre Interrelationships.
J.Phys.Chem.Solids, V13, pp321-325.

Cohen B.L., Fink C.L. and Deynam J.H., 1972, Non-destructive Analysis for trace Amounts of Hydrogen.
J.Appl.Phys., V43, pp19-25.

Crawford B.L. and Dinsmore J., 1950, Vibrational Intensities, 1. Theory of Diatomic Infrared Bands.
J.Chem.Phys., V18, pp983-987.

Dodd D.M. and Fraser D.B., 1965, The 3000 - 3900cm^{-1} Absorption Bands and Anelasticity in Crystalline Alpha Quartz.
J.Phys.Chem.Solids, V26, pp673-686.

Dodd D.M. and Fraser D.B., 1967, Infrared Studies of the Variation of Hydrogen Bonded OH in Synthetic Alpha Quartz.
Am. Mineral., V52, pp149-160.

Fisher J.C., Hart E.W. and Pry R.R., 1953, The Hardening of Metal Crystals by Precipitate Particles.
Acta Metall., V1, pp336-339.

Griggs D.T. and Blacic J.D., 1964, The Strength of Quartz in the Ductile Regime (abs).
Trans.Am.Geophys.Union., V45, pp102-103.

Griggs D.T. and Blacic J.D., 1965, Quartz, Anomalous Weakness of Synthetic Crystals.
Science, V14, pp292-295.

Griggs D.T., 1967, Hydrolytic Weakening of Quartz and Other Silicates.
Geophys.J.R.Astro.Soc., V14, pp19-31.

Griggs D.T., 1974, A Model of Hydrolytic Weakening in Quartz. J. Geophys. Res., V79, pp353-401.

Grubb Parsons Spectromaster Instruction Manual. Grubb Parsons, Walkergate, Newcastle Upon Tyne 6.

Heard H.C. and Carter N.L., 1968, Experimentally Induced "Natural" Intragranular Flow in Quartz and Quartzites. Am.J.Sci., V266, pp1-42.

Hillebrand W.F.J., 1908, The Influence of Fine Grinding on the Water and Ferrous Iron Content of Minerals and Rocks. J. Amer. Chem. Soc., V30, pp1120-1131.

Hinthorne J.R. and Anderson C.A., 1975, Microanalysis for flourine and Hydrogen in Silicates with the Ion Microprobe Mass Analyzer. Am. Mineral., V60, pp143-147.

Hobbs B.E., Blacic J.D. and Griggs D.T., 1966, Planar Deformation Features in Water Weakened Quartz (abs). Trans.Am.Geophys.Union., V47, p494.

Hobbs B.E., 1968, Recrystallization of Quartz Single Crystals, Tectonophysics, V6, pp 353-401.

Hobbs B.C., Mclaren A.C. and Paterson M.S.,1972, Plasticity of Single Crystals of Synthetic Quartz. In. Flow and Fracture of Rocks, Geophys.Monogr.Ser., V16. Edited by H.C.Heard,I.Y.Borg, N.L.Carter and C.B.Raleigh.,pp29-53, A.G.U. Washington D.C.

Honeycombe R.W.K., 1968, The Plastic Deformation of Metals. Arnold, London.

Jones M.E.,1975, Water Weakening of Quartz and its Application to Natural Rock Deformation. J.Geol.Soc.Lond. V131, pp429-432.

Jones M.E.,1976, Discussion. Phil. Trans. R. Soc. Lond. A. V283, pp171-172.

Jones M.E., 1978, The Influence of Hydrostatic Pressure on the Precipitation of Structure Bound Water into Micro-fluid Inclusions in Quartz. Phil. Mag. (In Press).

Kats A. and Haven Y., 1960, Infrared Absorption Bands in α- quartz in the 3 Micron Region. Phys. Chem. Glasses, V1, pp99-102.

Kats A., Haven Y. and Stevels J.M., 1962, Hydroxyl Groups in α-quartz. Phys. Chem. Glasses, V3, pp69-75.

Kats A., 1962, Hydrogen in Alpha Quartz. Phillips Res. Rep., V17, pp133-195, and pp201-279.

Kerrich R., 1974, Aspects of Pressure Solution as a Mechanism in Rock Deformation. Ph.D. Thesis, Univ. of Lond., Unpublished.

Knipe R., 1977, Ph.D Thesis, Univ. of Lond., Unpublished.

Knipe R. and White S., 1978, J.Geol.Soc.Lond., in Press.

Kostkowski H.J. and Bass A.M., 1956, Slit Function Effects in the Direct Measurement of Absorption Line Half Widths and Intensities. J.Opt.Soc.Am., V46, p1060.

Krauskopf K.B., 1967, Introduction to Geochemistry, Mcgraw Hill New York.

Lang A.R. and Miuscov V.F., 1967, Dislocations and Fault Surfaces in Synthetic Quartz. J.Applied Phys., V38, p2477.

Leich D.A. and Tombrello T.A., 1973, A Technique for Measuring Hydrogen Concentration Versus Depth in Solid Samples. Nucl. Instrum. Meth. V108, pp67-71.

Levy P.W., 1960, Reactor and Gamma - Ray Induced Colouring of Corning Fused Silica. J.Phys.Chem.Solids,V13, pp287-295.

Ligeon E. and Guivarch A., 1974, A New Utilization of ^{11}B ion Beams in Hydrogen Analysis by $^{1}H(^{11}B,\alpha)\alpha\alpha$ nuclear reaction. Rad. Effects, V22, pp101-105.

Manning J.R., 1968. Diffusion kinetics for Atoms in Crystals, Nostrand, Toronto.

Mclaren A.C. and Phakey P.P., 1965a, Dislocations in Quartz Observed by Transmission Electron Microscopy. J.Appl.Phys., V36, pp3244-3246.

Mclaren A.C. and Phakey P.P., 1965b, A Transmission Electron Microscope Study of Amethyst and Citrine. Aust.J.Phys., V18 pp135-141.

Mclaren A.C. and Phakey P.P.,1966a, Transmission Electron Microscope Study of Bubbles and Dislocations in Amethyst and Citrine Quartz. Aust.J.Phys., V19, pp19-24.

Mclaren A.C. and Phakey P.P., 1966b, Electron Microscope Study of Brazil Twin Boundaries in Amethyst Quartz. Phys.Stat.Sol., V13, pp413-422.

Mclaren A.C.,Retchford J.A.,Griggs D.T. and Christie S.M., 1967, Transmission Electron Microscope Study of Brazil Twins and Dislocations Experimentally Produced in Natural Quartz. Phys.Stat. Sol., V19, pp631-644.

Mclaren A.C. and Retchford J.A., 1969, Transmission Electron Microscope Study of Dislocations in Plastically Deformed Synthetic Quartz. Phys.Stat.Sol., V33, pp657-668.

Mclaren A.C., Turner R.G. and Boland J.N., 1970, Dislocation Structure of the Deformation Lamellae in Synthetic Quartz: a Study by Electron and Optical Microscopy. Contrib. Mineral. and Petrol. V29, pp104-115.

Mclaren A.C., Osborne C.F. and Saunders L.A.,1971, X-Ray Topographic Study of Dislocations in Synthetic Quartz. Phys.Stat.Sol. (a), V4, pp235-247.

Mclaren A.C. and Hobbs B.E., 1972, Transmission Electron Microscope Investigation of Some Naturally Deformed Quartzites. In. Flow and Fracture of Rocks. Geophys. Monogr. Ser. V16. Edited by H.C.Heard, I.Y.Borg,N.L.Carter and C.B.Raleigh. A.G.U. Washington D.C.

Moore G.S.M. and Rose H.E., 1973, The Structure of Powdered Quartz. Nature, V242, pp187-190.

Morrison-Smith D.J., Paterson M.S. and Hobbs B.E., 1976, An Electron Microscope Study of Plastic Deformation in Single Crystals of Synthetic Quartz.
Tectonophysics,V33, pp43-79.

Mott N.F. and Nabarro F.R.N., 1948. Report on the Strength of Solids, The Physical Society, London. p1.

Nelson C.M. and Crawford J.H., 1960, Optical Absorption in Irradiated Quartz and Fused Silica. J.Phys.Chem.Solids, V13, pp296-305.

Nelson R.S., Mazey D.J. and Barnes R.S., 1965, The Thermal Equilibrium Shape and Size of Holes in Solids.
Phil.Mag., V11, pp91-111.

Orowan E., 1948, Symposium on Internal Stresses in Metals.
The Institute of Metals, London, p451.

Potts W.J., 1963, Chemical Infrared Spectroscopy. Wiley, New York.

Primak W., 1960, A Review of the Gross Structural Effects of Energetic Atomic Particles on Vitreous and Crystaline Silica.
J.Phys.Chem.Solids, V13,pp279-286.

Rutter E.H., 1970, Ph.D. Univ. of Lond., Unpublished.

Rutter E.H., 1976, The Kinetics of Rock Deformation by Pressure Solution. Phil.Trans.R.Soc.Lond.(a), V283, pp203-219.

Ryder G.H., 1961, The Strength of Materials. Cleaver-Hume Press Ltd., London.

Scholze H., 1960, Uber die Quantitative U.R. Spektroskopische Wasserbestimmung in Silikates.
Fortscher. Mineral., V38, pp122-123.

Smallman R.E., 1970, Modern Physical Metallurgy. Butterworth, London.

Tendeloo G.van, Landuyt J.van and Amelinckx S., 1975, Correspondence Phys.Stat.Sol.(a), V30,pK11.

Tendeloo G.van, Landuyt J.van and Amelinckx S., 1976, The Alpha/ /Beta Phase Transition in Quartz and $AlPO_4$ as Studied by Electron Microscopy and Diffraction.
Phys.Stat.Sol.(a), V33, pp723-735.

Tsong I.S.T., Mclaren A.C. and Hobbs B.E., 1976, The Determination of Hydrogen in Silicates using the Ion Beam Spectrochemical Analyzer: Application to Hydrolytic Weakening.
Am.Mineral., V61, pp921-926.

Tuddenham W.M. and Lyon R.J.P., 1960, Infrared Techniques in the Identification and Measurement of Minerals.
Analytical Chemistry, V32, pp1630-1634.

Tullis J.A., Christie J.M. and Griggs D.T., 1973, Microstructures and Preferred Orientations of Experimentally Deformed Quartzites.
Geol.Soc.Amer.Bull.,V84, pp297-314.

Waldron D.H., 1955, Infrared Spectra of Ferrites.
Phys.Rev., V99, pp1727-1734.

Weertman J., 1970, The Creep Strength of the Earths Mantle.
Rev.Geophys.Space.Phys., V8, pp145-168.

White S.,1968, Decorated Diffusion Paths in Quartz.
Nature Phys. Sci., V219,pp1248-1249.

White S.,1970, Ionic Diffusion in Quartz.
Nature Phys.Sci., V225, pp375-376.

White S.,1971a, Hydroxyl Ion Diffusion in Quartz.
Nature Phys.Sci., V230, p162.

White S.,1971b, Reply to Doremus.
Nature Phys.Sci., V233, pp63-64.

White S.,1971c, Natural Creep Deformation of Quartzites.
Nature Phys.Sci., V234, pp175-177.

White S., Crosby A. and Evans P.E., 1971,
Dislocations in Naturally Deformed Quartzite. Nature Phys.Sci.,
V231, pp85-86.

White S., 1973a, The Dislocation Structures Responsible for the
Optical Effects in some Naturally Deformed Quartzites.
J.Materials Sci., V8, pp490-499.

White S.,1973b, Dislocations and Bubbles in Vein Quartz. Nature Phys.Sci., V243, pp11-14.

White S.,1973c, Syntectonic Recrystallization and Texture Development in Quartz. Nature Phys.Sci.,V244, pp276-278.

White S.,1973d, Deformation Lamellae in Naturally Deformed Quartz. Nature Phys.Sci., V245, pp26-28.

White S.,1973e, Application of High Voltage Electron Microscopy to Metamorphic and Structural Geology. Proc. third inst. HVEM Conf. Academic Press.

White S.,1975, The Effects of Polyphase Deformation on the Intracrystalline Defect Structures of Quartz . 1. The Defect Structures. N.Jb.Miner,Abh.. V123, pp219-316.

White S.,1975, The Effects of Polyphase Deformation on the Intracrystalline Defect Structures of Quartz.2. Origin of the Defect Structures. N.Jb.Miner.Abh., V123,pp237-252.

White S.,1976, The Effects of Strain on the Microstructures, Fabrics and Deformation Mechanisms in Quartzites. Phil.Trans.R.Soc.Lond.(A), V283, pp69-86.

Wood D.L., 1960, Infrared Absorption of Defects in Quartz. J.Phys.Chem.Solids, V13, pp326-336.

Wood D.L. and Ballmann A.A., 1966, Blue Synthetic Quartz. Am.Mineral.,V51, pp 216-220.

Water weakening of quartz, and its application to natural rock deformation

MERVYN E. JONES

Reprinted from the
JOURNAL OF THE GEOLOGICAL SOCIETY
vol. 131, pp. 429–432
(published July 1975)

Water weakening of quartz, and its application to natural rock deformation

MERVYN E. JONES

SUMMARY

New experimental data show that the weakening effect of structure-bound water in the quartz lattice occurs at hydroxyl concentrations lower than those previously considered. This is used, along with analyses of the hydroxyl concentrations of naturally deformed quartz, to show that water weakening can explain low temperature plastic flow in quartz from low grade metamorphic environments.

IT IS WELL KNOWN that trace quantities of hydroxyl ions in the quartz structure (Kats 1962), greatly reduce its mechanical strength (Griggs 1967, 1974, Baeta & Ashbee 1970) enabling plastic deformation and recrystallization to occur at temperatures below 500°C. The concentration of these hydroxyl groups is measured by infrared spectroscopy, the vibrational frequencies of the hydroxyl groups being around 3450 cm^{-1} (Dodd & Fraser 1965, 1967). Several bond types have been isolated of which the most important is the Silanol bond, first introduced by Brunner (1961). This has the formula Si–OH HO–Si. Various methods are available for the reduction of the infrared data (Kats 1962, Bambuer 1961, Dodd & Fraser 1967), the most widely used being that of Bambuer which expresses the concentration in the units $H/10^6Si$. Crystals with a low concentration of hydroxyl ions, such as Brazilian quartz, show a high strength at temperatures up to 700°C. The extent of this weakening phenomenon is apparently dependent on the concentration of the hydroxyl impurity, so that, with a sufficiently high concentration, plastic flow should become possible in the range 200–300°C. That quartz deforms plastically at this temperature in nature is clearly seen in any low grade metamorphic terrain. Deformation experiments conducted to demonstrate this weakening effect have been performed on synthetic quartz crystals with hydroxyl concentrations in the range 2000 to 8000 $H/10^6$ Si (Griggs 1967, Hobbs 1968). However no report has appeared indicating that natural quartz has such high concentrations, the reported values varying between 10 and 900 $H/10^6Si$ (Kats 1962, Bambuer 1961). Thus a dilemma exists as to whether this water weakening process is of importance in nature.

My experimental work has shown that the equilibrium concentration of hydroxyl ions in the quartz structure is extremely sensitive to temperature, and falls rapidly at temperatures greater than 300°C. This dehydration effect obeys an Arrhenius type relationship. The new equilibrium concentration is established in about 12 hours for a given temperature. It was found that for a synthetic crystal with an initial concentration of 2500 $H/10^6Si$, the concentration fell to 832 $H/10^6Si$, at 475°C which was established as the weakening temperature by deformation tests. At 500°C the sample showed plastic flow to 12% strain without work hardening and at low stress. The stress fell continuously after yield due to

Jl geol. Soc. Lond. vol. **131**, 1975, pp. 429–432. Printed in Northern Ireland

rapid recovery in the sample. In this experiment the sample was heated for 24 hours under test conditions, prior to loading, to ensure that the hydroxyl concentration had equilibrated at the test temperature. This period of heating prior to loading is essential if equilibrium is to be established during the early parts of the test, and has been ignored by previous workers (Griggs 1967, Hobbs 1968, Baldermann 1974). Many of the short term deformation tests reported in the literature were thus conducted under disequilibrium conditions, which cannot possibly be expected to occur in nature. This continual dehydration during the early stages of a test will cause a progressive increase in the mechanical strength, possibly accounting for the high rates of work hardening reported by some workers (Griggs 1974, Baldermann 1974). Under equilibrium conditions in a deformation test, water weakened synthetic quartz possesses hydroxyl ion concentrations commensurate with those of some natural specimens.

It is probable that the hydroxyl ion concentration is extremely sensitive to the number and type of defects in the quartz structure. This, plus the fact that there are many possible structural types for the hydroxyl bond (Dodd & Fraser 1965), explains why the dehydration of different crystals occurs at different rates. The different bond types themselves dehydrate at different rates, and the relative concentration of these will have a profound influence on the shape of the dehydration curve. It is thus impossible to generalize as to the concentration at the weakening temperature, and it is necessary to investigate fully the hydroxyl equilibrium curve for each crystal used in experimental deformation tests before the experimental results can be properly interpreted. Previous workers have overlooked this fact, and consequently current models for the water weakening process have only a qualitative significance.

Brazilian and Madagascan quartz of the type used in some deformation experiments also shows this dehydration effect, so that a crystal with an initial concentration of 800 H/10^6Si, will have its concentration significantly reduced under test conditions. The yield temperature then becomes very high and it is understandable that such quartz has never been recorded as showing significant water weakening.

Some evidence is available which suggests that if the partial pressure of water is high in the environment of deformation, the sample will not dehydrate and may even absorb hydroxyl ions becoming weakened (Griggs 1967). This has never been fully investigated, but could be of extreme importance to the deformation of quartz in nature, possibly providing a mechanism for the strain softening observed in some shear zones although by no means the only mechanism.

I have measured the hydroxyl concentrations of samples of natural quartz which are known to have deformed plastically at low temperatures. These crystals have very high concentrations, in many cases higher than the initial concentrations reported for weak synthetic crystals. The samples chosen for analysis were collected from tectonic veins in North Devon and North Wales, the evidence of plastic deformation being in the form of bent fibres, sub-grain growth and recrystallization. Fluid inclusion temperatures for these veins range from 200 to 275°C (Clark 1972, Kerrich 1974) showing that they deformed plastically at temperatures well below those at which even the weakest synthetic crystal has

shown significant plastic flow (Griggs 1967). The hydroxyl concentrations measured from this material are in the range 5 000 to 12 000 H/10^6Si, which are likely to be very similar to the concentrations at the time of deformation, these crystals having been subjected only to the low temperatures at which they were deformed. Such quartz is typical of that found in tectonic and pegmatite veins in a host of different geological environments. Crystals of the Brazilian type, often quoted as having hydroxyl concentrations typical of natural quartz, are rare and will grow only under very specific conditions. This material, often used in experimental deformation work, is atypical of much natural quartz.

It is concluded that investigations of water weakening of quartz have failed to consider the physical controls on the hydroxyl ion concentration, which has led to the idea that much higher hydroxyl concentrations are required to induce weakening than those found in nature. Further, material regarded as representative of natural quartz is seen to be atypical of the quartz found in the low grade metamorphic environments which contains very high concentrations of hydroxyl ions. Many of the deformation experiments designed to investigate water weakenmg of quartz may have been conducted under dis-equilibrium conditions. This may lead to abnormally high rates of work hardening making extrapolation of results to slower strain rates unreliable. It is suggested that water weakening is probably a very important feature in the plastic deformation of quartz in the low grade environment, enabling quartz to act in the ductile manner so often observed, yet only partially accounted for by existing interpretation of experimental deformation results.

Full details of the author's experimental work on the dehydration of quartz, and the analyses of the natural crystals are in preparation for publication.

Acknowledgments. I thank my supervisor Dr. E. H. Rutter for criticism and N.E.R.C. for a grant financing this research.

References

Baeta R. D. & Ashbee K. H. G. 1970. Mechanical deformation of quartz. 1. Constant strain rate compression experiments. *Philos. Mag.* **22**, 601–23.

Baldermann M. A. 1974. The effect of strain rate and temperature on the yield point of hydrolytically weakened synthetic quartz. *J. geophys. Res.* **79**, 1647–52.

Bambuer H. U. 1961. Spurenelementgehalte und γ-Farbzentren in Quarzen aus Zerrkluften der Schweizen Alpen. *Schweiz. Mineral. Petrog. Mitt.* **41**, 335–69.

Brunner G. O., Wondratschek H. & Laves F. 1961. Ultrarotuntersuchungen über den Einbau von H in naturlichen Quarz. *Z. Elektrochem.* **65**, 735–50.

Clarke K. J. 1972. Fluid inclusions as geothermometers in structural geology. *M.Sc. dissertation Univ. London* (unpubl.)

Dodd D. M. & Fraser D. B. 1965. The 3000–3900 cm^{-1} absorption bands and anelasticity in crystalline α-quartz. *J. Phys. Chem. Solids* **26**, 673–86.

—— 1967. Infrared studies of the variation of hydrogen bonded OH in synthetic α-quartz. *Am. Mineral.* **52**, 149–60.

Griggs D. T. 1967. Hydrolytic weakening of quartz and other silicates. *Geophys. J. R. astr. Soc.* **14**, 19–31.

—— 1974. A model of hydrolytic weakening in quartz. *J. geophys. Res.* **79**, 1655–61.

Hobbs B. E. 1968. Recrystallization of quartz single crystals. *Tectonophysics* **6**, 353–401.

KATS A. 1962. Hydrogen in alpha-quartz. *Phillips Res. Rep.* **17**, 133–95, 201–79.
KERRICH R. 1974. Aspects of pressure solution as a mechanism in rock deformation. *Ph.D thesis Univ. London* (unpubl.)

Received 24 March 1975.

MERVYN EDWARD JONES, Geology Department, Imperial College of Science & Technology, London SW7

The Journal of the Geological Society

Vol. 131, Part 4, July 1975

Published for
THE GEOLOGICAL SOCIETY OF LONDON
by
SCOTTISH ACADEMIC PRESS LTD
25 PERTH STREET
EDINBURGH, 3

and printed by
THE UNIVERSITIES PRESS
ALANBROOKE ROAD, BELFAST BT6 9HF, NORTHERN IRELAND